AFCRL-65-787

Nondestructive Analyses of Irradiated MITR Fuel By Gamma-Ray Spectroscopy

Jerry A. Sovka
Norman C. Rasmussen

Massachusetts Institute of Technology
77 Massachusetts Avenue
Cambridge, Massachusetts

Contract No. AF19(604)-7492
Project No. 5620
Task No. 562002
Scientific Report No. 4

MITNE-64

October 1965

Prepared for

Air Force Cambridge Research Laboratories
Office of Aerospace Research
United States Air Force
Bedford, Massachusetts

Requests for additional copies by Agencies of the Department of Defense, their contractors, and other government agencies should be directed to the:

DEFENSE DOCUMENTATION CENTER
CAMERON STATION
ALEXANDRIA, VIRGINIA

Department of Defense contractors must be established for DDC services, or have their "need-to-know" certified by the cognizant military agency of their project or contract.

All other persons and organizations should apply to the:

Clearinghouse for Federal Scientific
and Technical Information (CFSTI)
Sills Building
5285 Port Royal Road
Springfield, Virginia 22151

AFCRL-65-787

Nondestructive Analyses of Irradiated MITR Fuel By Gamma-Ray Spectroscopy

Jerry A. Sovka
Norman C. Rasmussen

Massachusetts Institute of Technology
77 Massachusetts Avenue
Cambridge, Massachusetts

Contract No. AF19(604)-7492

Project No. 5620

Task No. 562002

Scientific Report No. 4

MITNE-64

October 1965

Prepared for

Air Force Cambridge Research Laboratories
Office of Aerospace Research
United States Air Force
Bedford, Massachusetts

NONDESTRUCTIVE ANALYSES OF IRRADIATED MITR FUEL BY GAMMA-RAY SPECTROSCOPY

by

J.A. Sovka

Submitted to the Department of Nuclear Engineering
on 23 September, 1965
in partial fulfillment of the requirement for the
degree of Doctor of Science

ABSTRACT

Nondestructive analyses have been made of irradiated MITR fuel elements with a lithium-ion drift germanium gamma-ray spectrometer. Techniques for the preparation of Ge(Li) detectors were developed and are described in detail. Included are descriptions of the apparatus required for satisfactory performance of the spectrometers. Equipment used for scanning irradiated fuel elements in the MITR spent fuel storage tank is described. Gamma-ray spectra from fuel elements having different cooling periods show peaks attributed to the fission products Zr-95, Nb-95, Rh-106, Cs-134, Cs-137, Ba-140, La-140, Ce-144 and Pr-144. Fission product activities were determined from calculations of the intensities of the gamma-rays in the spectra. Spatial variations of fission product content in the elements are shown.

A method for interpreting the experimental results, requiring theoretical predictions of fission product activities in the fuel, is presented. The results of the application of this method include spatial distributions of absolute neutron flux, neutron exposure and total U-235 burnup and irradiation time of the fuel. The operating pattern of each element and the time since its removal from the reactor could also be inferred. Comparison of the results of the present investigations with independent determinations of these quantities showed that the agreement was within the 10% error assigned. Some of the problems and limitations of the method are discussed and suggestions are made for improving the accuracy and precision of the results. Other areas of possible use in reactor physics measurements are indicated.

Thesis Supervisor: Norman C. Rasmussen
Title: Professor of Nuclear Engineering

TABLE OF CONTENTS

LIST OF FIGURES

LIST OF TABLES

ACKNOWLEDGEMENTS

During the course of this research, many people have made valuable contributions, without which much of the work would not have been possible. In particular, I would especially like to thank Professor Norman C. Rasmussen for his enthusiastic assistance, advice and guidance throughout all phases of the research. His continuing interest and encouragement were in great part responsible for the achievements made. Special thanks are also offered to Dr. H.W. Kraner of the Radioactivity Center for providing research facilities and for his guidance and help during the development of germanium detectors.

The generous assistance and advice of Mr. F.L. Woodworth and the Reactor Machine Shop personnel are gratefully acknowledged. Thanks are extended for help received from the Reactor Operations staff. Also, thanks are offered to Mrs. B.R. Hites for help with handling and processing of the experimental data. I wish also to thank Professor T.J. Thompson for acting as thesis reader, and for his advice and constructive criticism of the manuscript.

Acknowledgement is made to the U.S. Air Force for providing the funds for this project, and for the research assistantship held during 1964-65. The research assistantship on the Fuel Cycles Project (1962-64) provided by the U.S.A.E.C. is also acknowledged.

Thanks are due to the staff of the M.I.T. Computation Center for providing the computing services required in these investigations.

My most special thanks go to my wife Lynn; first for her typing of the manuscript, but more especially for her patience and cheerful forbearance during the past three years at M.I.T.

NONDESTRUCTIVE ANALYSES OF IRRADIATED MITR FUEL BY GAMMA-RAY SPECTROSCOPY

I. INTRODUCTION

Quantitative data on the irradiation history of a reactor fuel element is often difficult to obtain. Flux distributions are generally determined from foil and/or wire measurements, usually made only at low power prior to initial startup. Furthermore, these foil results may not give the same spatial behavior as seen by the fuel because of different variations of reaction rates with neutron energy and with reactor conditions. Neutron spectral parameters are obtained by similar techniques using cadmium or indium covered foils. Interpretation of these results to ascertain conditions within the fuel itself is often difficult and subject to considerable error. Similarly, determinations of fissile fuel burnup usually include the use of flux distributions and depletion studies based upon computer codes of varying degrees of sophistication. Experimentally, fuel burnup is determined by a number of techniques, nearly all of which require the disassembly of the fuel element and subsequent radiochemical and mass spectroscopic analyses. These latter methods are lengthy, tedious and costly and, in addition, have often not given agreement amongst themselves. A long-term check on the average burnup sustained by a fuel charge can be made with a thermodynamic balance for the reactor system. This, although being nondestructive, is usually too crude to provide satisfactory

burnup values for individual fuel elements.

Because of the disadvantages of the above destructive methods, nondestructive techniques have often been investigated in order to obtain information about the irradiation performance of fuel elements. It has been recognized that the techniques of gamma-ray spectroscopy can supply such information. Various instruments have been used to measure total gamma-activity emitted by the fission products within the fuel. Good agreement was obtained between calculated power distribution and measured gamma-activity for some cores (B2, B10, E1). However, work done on Yankee fuel (N1) reported a 10-15% discrepancy between results of total gamma-activity and results of mass spectroscopy upon samples of fuel. This difference was attributed to the presence of cobalt impurities in the stainless steel fuel element cladding.

Rasmussen and Cohan (R1) described the use of a 6-meter bent quartz crystal spectrometer in studies of the fission product gamma-ray spectrum in which about 35 fission product gamma-rays were identified. In 1964, Mayman (M3) used the instrument to obtain spatial distributions of certain fission products within the fuel element. However, no definitive results on experimental burnup determinations were possible at that time. An outline of the usefulness of the bent crystal spectrometer in such investigations is included in Rasmussen, Sovka and Mayman (R2). Groshev and Demidov (G2) reported the use of a magnetic spectrometer to study the 2.186 MeV gamma-ray of Ce^{144} and quoted burnup values on fuel accurate to $\pm 10\%$.

Investigations with NaI scintillation crystals to resolve the gamma-ray spectrum of spent fuel were made by Kristiansen and Røgeberg (K5), but they were able to obtain results of only ±30% accuracy. More recently, Diggle and Blackadder (D2) reported results obtained with a NaI crystal of gamma-ray spectra of irradiated fuel showing variations in relative fission product activities with burnup and cooling time. They pointed out that, to obtain absolute estimates of burnup, careful calibrations of the experimental system were required.

Weinzierl (W5) first reported the use of a semiconductor detector in the study of gamma-ray spectra from irradiated fuel elements. A lithium-drift silicon detector, operating in coincidence with a NaI crystal to detect backscattered gamma-rays, was used to resolve the Cs^{137} gamma-ray at 662 keV and thereby infer the total uranium burnup.

However, in the above techniques, the total fuel burnup can be accurately determined only if the spectrometer and fuel element have been properly calibrated. It will be shown by the results of the present investigation that even without absolute calibration, considerable additional information can be extracted from the fission product gamma-ray spectra if the gamma-rays can be sufficiently resolved and their intensities measured.

The following study describes the use of a lithium-ion drift germanium gamma-ray spectrometer to obtain the energy spectra of fission product gamma-rays from irradiated MITR fuel elements. Analysis of these results has yielded determinations of the irradiation history of the fuel, including total neutron exposure,

absolute neutron flux distributions, irradiation time, operating mode of reactor and cooling time. Included are detailed descriptions of the techniques of preparation of Ge(Li) detectors and of the development of associated equipment necessary for satisfactory performance of the detectors. Gamma-ray spectra of well-known calibration gamma-ray sources are given, along with the spectra of several fission products of interest. The experimental apparatus required for the scanning of MITR fuel elements is described and results of investigations of several elements are presented. Interpretation of the results has required the writing of several computer codes to facilitate data handling and processing. Concluding remarks summarize the results and indicate other possible areas of use of the present methods.

II. LITHIUM-ION DRIFT GERMANIUM SPECTROMETERS

A. INTRODUCTION

In order to resolve the many gamma-rays emitted by the fission products in a fuel element, gamma-ray spectrometers of relatively high energy resolution are required. The equipment associated with the 6-meter bent quartz crystal spectrometer, built by Kazi, Rasmussen and Mark (K1), can obtain the necessary resolution at energies up to several MeV. However, because of very low efficiencies, no gamma-ray lines were detected above 500 keV (M3). Since the long-lived fission product considered most useful for burnup determinations, Cs^{137}, emits a gamma-ray at 662 keV, the use of this spectrometer was not considered further. Instead, development was begun of a solid state detector and of the associated equipment required for its operation. Lithium-ion drift germanium detectors have the necessary characteristics for use as gamma-ray detectors and, as will be shown later, offer a number of advantages over other types. Thus, development of suitable techniques for their preparation was begun in February, 1962.

This section includes a brief background and historical review of solid state detectors and outlines the reasons for using germanium as the semiconductor material for the detectors. The principles of the lithium-ion drift method are described, along with abridged recipes of techniques used in the present work. More detailed descriptions are presented in Appendix A. The equipment required for the proper preparation and use of the

detectors is described. A discussion of the operating characteristics of germanium gamma-ray spectrometers is presented along with results of gamma-ray spectra of calibration sources.

B. BACKGROUND INFORMATION

In recent years, semiconductors have been frequently used instead of detecting systems such as scintillation crystals and gas counters. The primary reason for this trend is the fact that semiconductors have an improved efficiency for converting the particle energy into an electrical signal. The absorption of a given amount of energy results in a charge about 10 times larger in such a detector than in a gas counter. In scintillators, inefficiencies in converting light to an electrical pulse result in a signal only $^{1}/_{100}$ of that from a semiconductor. Since the energy resolution of a system is dependent upon the ratio of signal-to-noise, the semiconductor detector can yield a resolution about a factor of 10 better than NaI and about a factor of 3 better than gas counters. To date, only silicon and germanium have been applied with reasonable success to nuclear radiation spectroscopy. Some of their relevant properties are given in Table 1.

The first attempt to use semiconductors as radiation detectors was reported by McKay in 1949 (M5) who tried to detect ionizing particles with point contact rectifiers and p-n junctions. However, because of impure crystals, his results were not encouraging. Now, as a result of improvements in transistor technology, many different types of semiconductor detectors are available (D1, I1, M6, T4).

TABLE 1

PROPERTIES OF SILICON AND GERMANIUM (a, b, c, d)

	Silicon	Germanium
Atomic Number	14	32
Atomic Weight	28	72.6
Density (gm/cm^3)	2.33	4.32
Dielectric Constant	12	16
Energy Gap (eV)	1.09	0.79
Energy/Electron-Hole Pair (eV)	3.6	2.8
Electron Mobility at 25°C ($cm^2/v/sec$)	1,350	3,900
Hole Mobility at 25°C ($cm^2/v/sec$)	480	1,900

References

(a) R.A. Smith, "Semiconductors", Cambridge University Press, New York (1959).

(b) R.A. Smith, "The Wave Mechanics of Crystalline Solids", Chapman and Hall, New York (1961).

(c) C. Kittel, "Introduction to Solid State Physics", J. Wiley and Sons, Inc., New York (1956).

(d) N.B. Hannay, ed., "Semiconductors", Reinhold, New York (1959).

The principles of operation of each is essentially similar to a parallel plate ionization chamber and will be exemplified by a silicon p-n junction detector as shown in Fig. 1. Between the n and p type silicon there exists a highly compensated region, called the "depletion region", of width w, having a resistivity corresponding to intrinsic silicon. Ionizing particles striking the depletion region create electrons and holes which drift under the action of the applied field. As the carriers move they induce charge on the n and p regions proportional to the potential difference they traverse, thus giving rise to an external signal. The latter is then usually amplified and subsequently processed to determine the amount of energy deposited in the depleted region by the particle. Particles striking the detector away from the depletion zone create carriers which tend to recombine before diffusing to the junction and therefore give rise to no external charge signal.

The thickness of the depletion layer in p-n junctions can be increased by applying a reverse bias and is given approximately by (M10)

$$w = \frac{\sqrt{\rho V}}{5} \qquad \text{(B.1)}$$

where w is the width in microns, ρ is the resistivity of the lightly doped region in ohm-cms, and V is the applied reverse bias voltage. The depletion region thickness determines the maximum particle energy that will be absorbed.

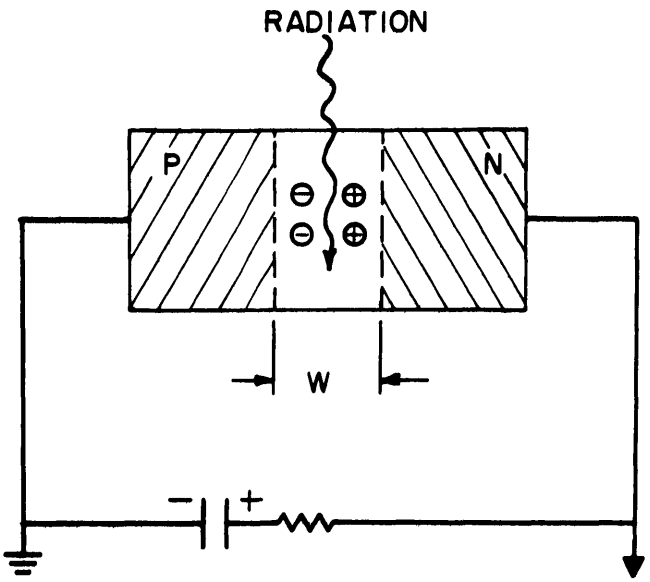

FIGURE 1 SCHEMATIC DIAGRAM OF A P-N JUNCTION DETECTOR.

For a typical silicon detector at 400 V bias, w is about 700 microns, which is sufficient to stop a 10 MeV proton.

Increasing the thickness of the depletion region also reduces the detector capacitance, resulting in improved signal-to-noise ratios. The other main factor influencing the signal-to-noise ratio is the detector reverse leakage current which is determined mainly by the resistivity of the intrinsic region, which in turn is inversely dependent upon the operating temperature. Much larger depletion layer thicknesses are required for complete absorption of photons; consequently, p-n junction counters are seldom used for gamma-ray spectroscopy. The production of relatively large intrinsic depletion volumes was first accomplished by Pell in 1960 with the lithium-ion drift technique (P1) outlined in the next section.

C. LITHIUM-ION DRIFT DETECTORS

An intrinsic region can be achieved by the ion drift technique by which donor and/or acceptor ions are drifted in the field of a reverse-biased n-p junction. The drift temperature must be sufficient to make either the donor or acceptor ions mobile but low enough to retain the n-p junction. Donor-acceptor ion pairing results in almost complete compensation of each other.

In the present method, Li^+ ions, which are donors, are drifted in p-type silicon or germanium, uniformly doped with acceptor atoms such as boron, gallium or zinc, to a level of N_A acceptors per cc. Lithium is then diffused into the

crystal to give a surface concentration of N_o donors per cc where $N_o \gg N_A$. The donor concentration, N_D as a function of distance into the crystal as shown in Fig. 2, is equal to the acceptor concentration at position x = c, thus creating an n-p junction.

Applying a reverse bias to this n-p junction, thereby creating an electrostatic field near c, causes the positively charged Li^+ ions to move from the Li-rich side of the junction to the Li-deficient side. Thus, the donor concentration N_D decreases for $x < c$ and increases for $x > c$, approaching the acceptor concentration N_A, thereby producing an intrinsic region of width w as illustrated in Fig. 3. The resulting structure is known as a p-i-n diode. An extensive theoretical treatment of the ion-drift method, along with experimental verification of the above model is given by Pell (P1).

The techniques of the lithium-ion drift method were successfully applied to the preparation of thick silicon detectors at a number of different laboratories (B4, M1, M2, G1, E1). Improvements in techniques resulted in decreased drift times and depletion layer thicknesses in silicon of up to 1 cm (M7).

Most applications of silicon p-i-n detectors were for the detection of charged particles, although some measurements were made of gamma-ray spectra (E2, K3). However, these detectors were of limited usefulness at energies above a few hundred keV because the ratio of photopeak area to the area under the Compton distribution was so small. The use of germanium,

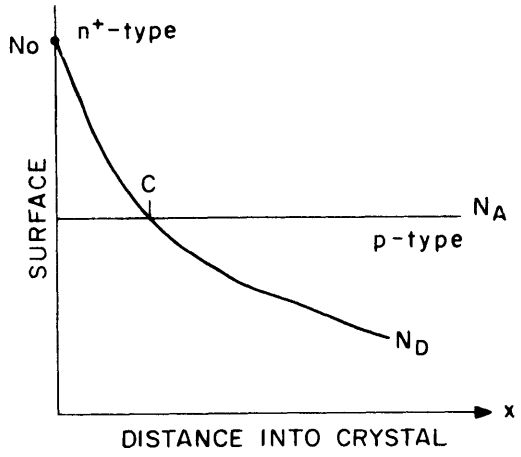

FIGURE 2 IMPURITY DISTRIBUTION IN CRYSTAL AFTER LITHIUM DIFFUSION

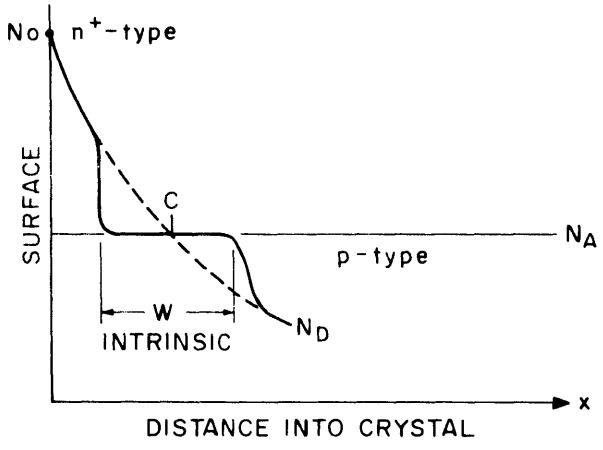

FIGURE 3 IMPURITY DISTRIBUTION IN CRYSTAL AFTER DRIFT

which has a Z of 32, compared with 14 for silicon, offers a great improvement since its photoelectric cross-section is about 40 times that of silicon. A comparison between the two for the photon interactions of photoelectric absorption, Compton scattering and pair production is shown in Fig. 4.

Successful germanium gamma-ray detectors prepared by the lithium-ion drift process, now known as Ge(Li) detectors, were first reported by Freck and Wakefield in 1962 (F3), followed shortly by Webb and Williams in 1963 (W3). The construction of Ge(Li) of sufficiently large volumes (up to 5 cm^2 x 8 mm thick) for use as practical gamma-ray spectrometers was first carried out by Tavendale in 1963 (T1, T2, T3). These devices obtained photopeak efficiencies of about 0.1% to 1% at 1 MeV while yielding energy resolutions about 10 times better than is possible with the best NaI scintillation spectrometer. Soon after Tavendale's results were reported, a number of other laboratories, including this one, have prepared successful Ge(Li) gamma-ray detectors (G1, H2).

Although the same general procedure is applied to the construction of Ge(Li) detectors, there is considerable variation in specific drifting techniques. Various methods of lithium diffusion are used as well as different drifting ambient conditions. Likewise, final detector completion procedures are dissimilar. In addition, fabrication of good detectors requires many finely detailed techniques which are not reported in the literature and without which extreme difficulties are encountered. For this reason, detailed descript-

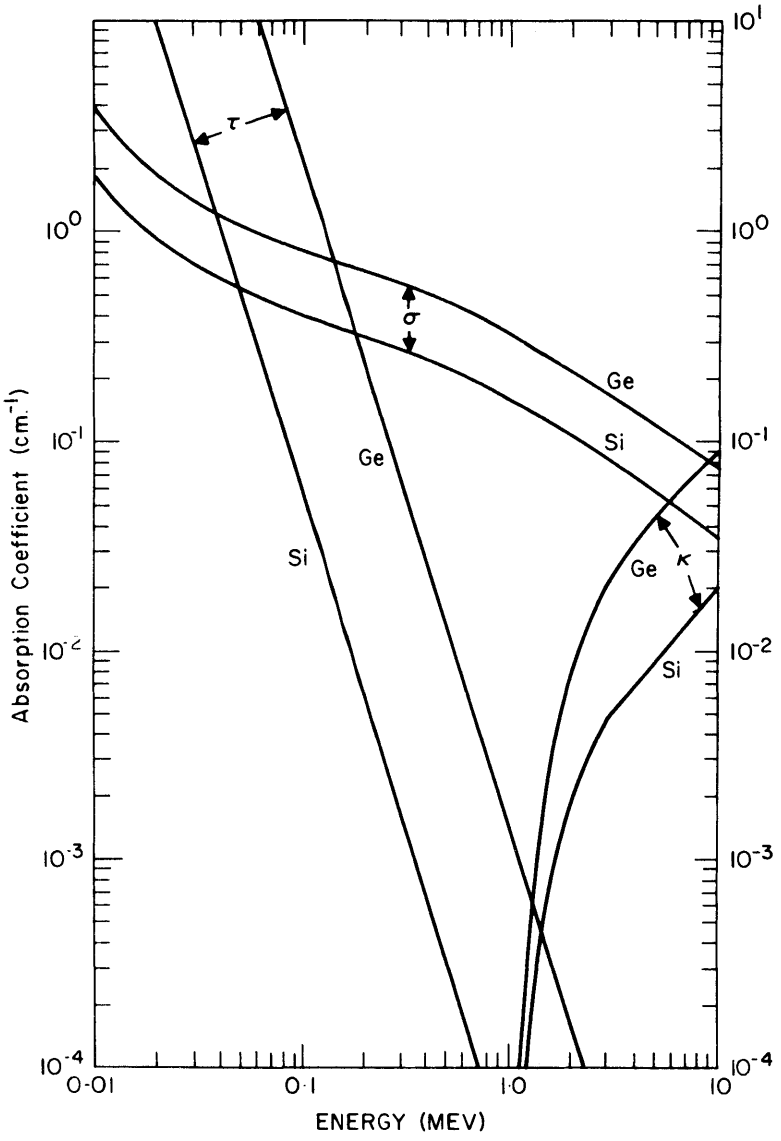

FIGURE 4 PHOTON ABSORPTION COEFFICIENTS FOR PHOTOELECTRIC EFFECT (τ), COMPTON SCATTERING (σ) AND PAIR PRODUCTION (κ) FOR SILICON AND GERMANIUM.

ions of the methods developed in this laboratory are presented in Appendix A, while a brief outline is given in the next section.

D. PREPARATION OF LITHIUM-ION DRIFT GERMANIUM DETECTORS

The germanium used for the fabrication of detectors was supplied by Sylvania Electric Products in the form of p-type, gallium doped, zone-levelled crystals with resistivities between 8 and 44 ohm-cms. Minority carrier lifetimes were greater than 100 μsec. and dislocation densities were less than 2000/cm^2. The crystals were cut with a diamond saw to give thicknesses of 5 to 15 mm and cross-sectional areas between 1 and 8 cm^2. Surfaces were lapped and etched, and a lithium-in-oil suspension was applied to one face. The lithium was then diffused into the crystal in an argon atmosphere at 400-450°C for 10 minutes. Nickel contacts were applied by the electroless plating method (B8, S3), the crystal etched and the resulting n^+-p diode was tested for resistance characteristics. Satisfactory diodes were then drifted in the apparatus shown schematically in Fig. 5 at approximately 50 to 55°C with DC reverse bias voltages from 200 volts at initial stages down to 30 volts at final stages of drift. The joule heating generated by the diode during the drift was dissipated by boiling of a fluorocarbon liquid (FX78 supplied by the 3M Company) and the heat of the fluorocarbon removed by cooling water in the condenser coils. Depletion depths of 1 1/2 to 3 mm were obtained after 1 1/2 to 4 days of drift. Several detectors 4 cm^2 in area and 1 cm depletion thickness have been prepared with a drift time

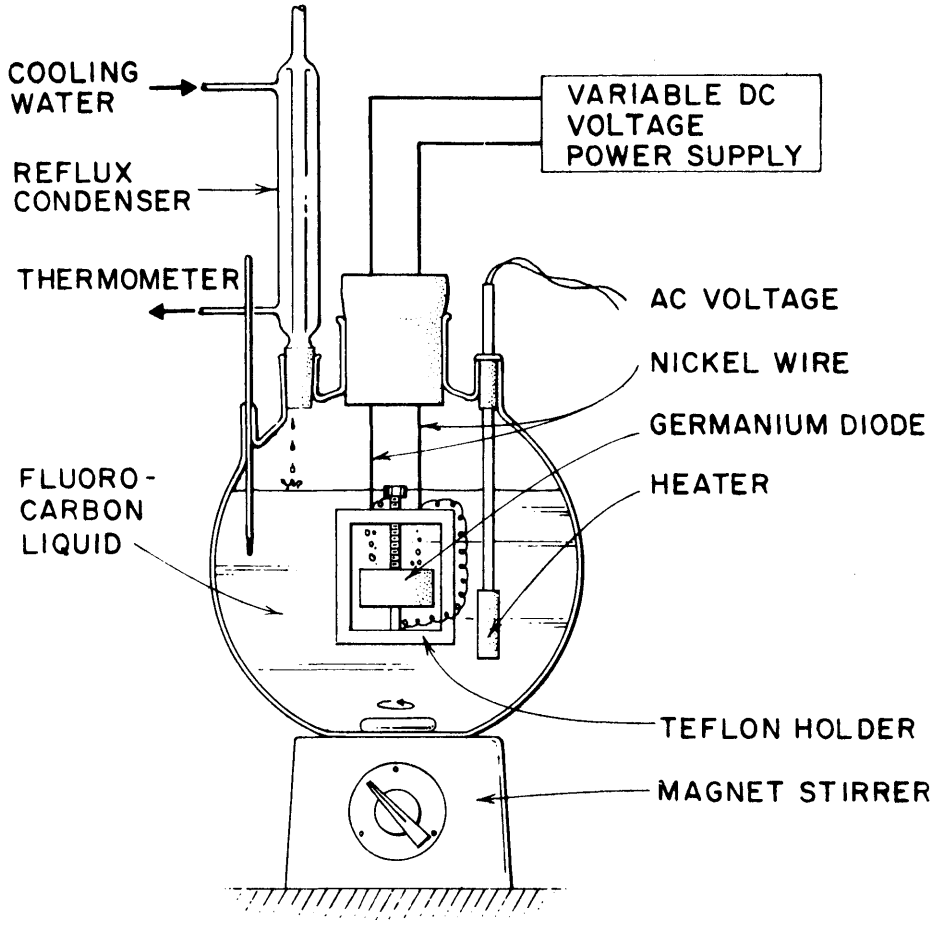

FIGURE 5 SKETCH OF APPARATUS FOR LITHIUM-DRIFT PROCESS FOR GERMANIUM DETECTORS

of approximately one month. The depth of diffusion and drift were checked with a number of different staining techniques. The p-i-n diode was then etched and tested in vacuo at liquid nitrogen temperatures in the cryostat shown schematically in Fig. 6. Reverse bias currents for satisfactory detectors were between 10^{-8} and 10^{-10} amp. at 100 to 300 volts. Currents higher than 10^{-8} amp. led to excessive noise during operation and thus poor energy resolution. In these cases, the diode was re-etched until the current-voltage characteristics were satisfactory.

E. DESCRIPTION OF ASSOCIATED EQUIPMENT

In order to prepare, test and use Ge(Li) detectors, it was necessary to have available considerable associated equipment. This included a small vacuum system, detector dewars, and various electronic equipment. In this section are described the types of apparatus used in the present work.

1. Vacuum System

Although the detector dewars were kept evacuated when at liquid nitrogen temperatures by a small ion pump, the latter did not have the capability to pump the dewars down from atmospheric pressure to the operating range of 10^{-6} to 10^{-5} mm Hg. Therefore, a small portable vacuum system was constructed for this purpose. A schematic diagram of the system is shown in Fig. 7, while Fig. 8 shows a photograph of the system in operation.

The mechanical pump (CENCO Model HYVAC 14) was shock-mounted to reduce vibration. The remaining components were

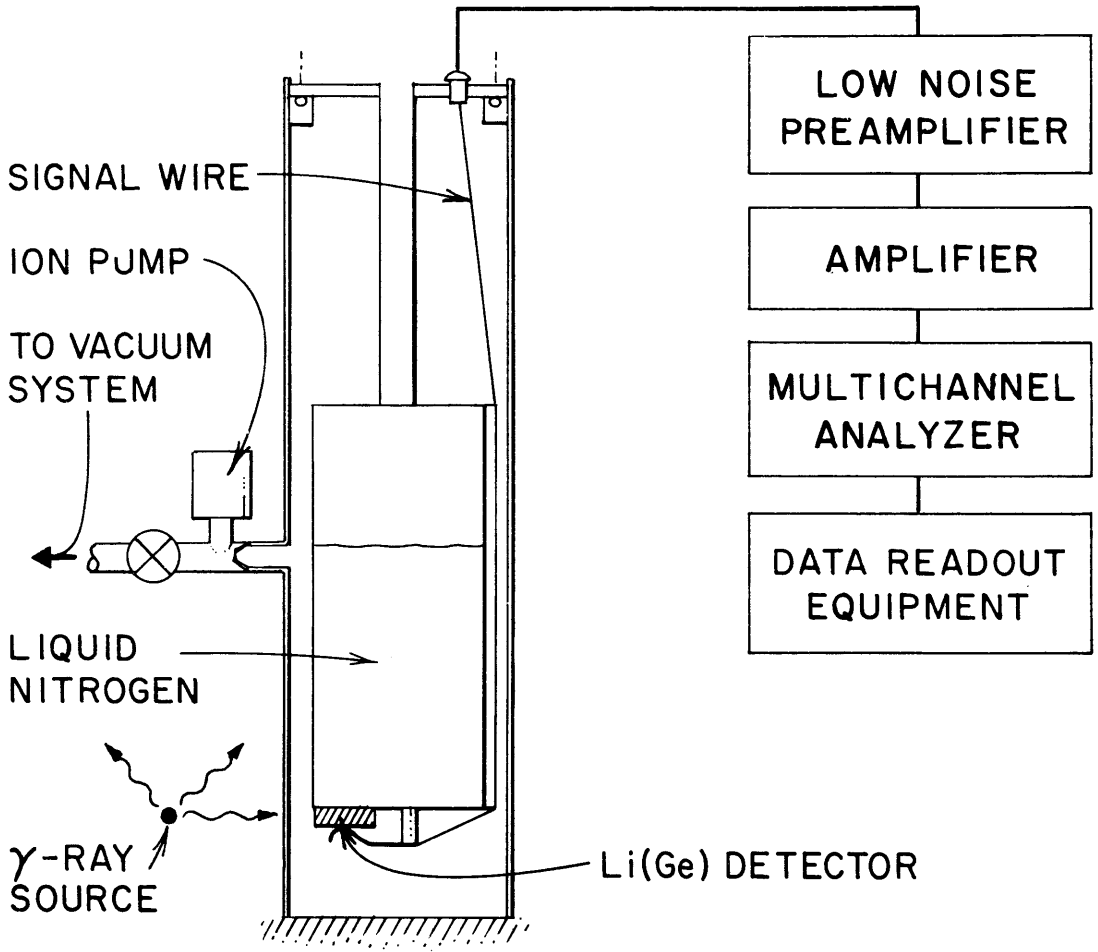

FIGURE 6 SCHEMATIC DIAGRAM OF VACUUM CHAMBER AND ELECTRONICS FOR USE WITH Li-DRIFTED GERMANIUM γ-RAY DETECTORS

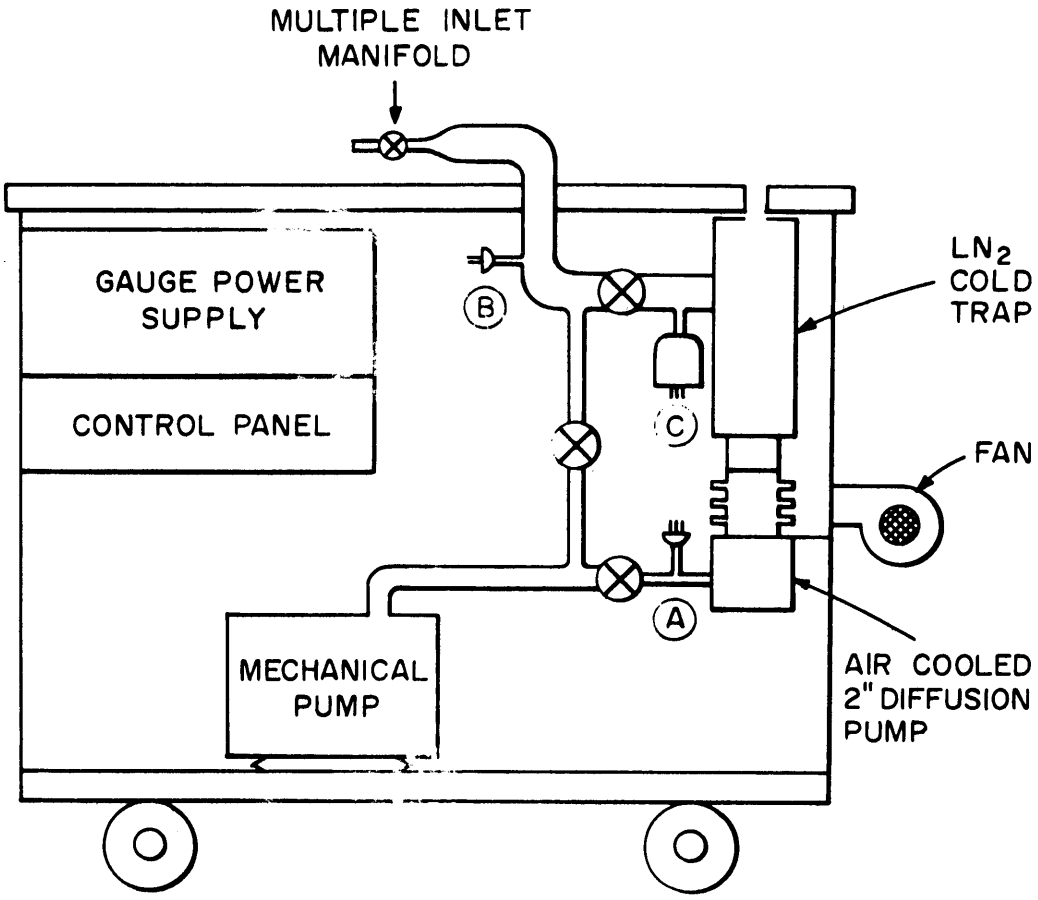

FIGURE 7 SCHEMATIC DIAGRAM OF PORTABLE VACUUM SYSTEM

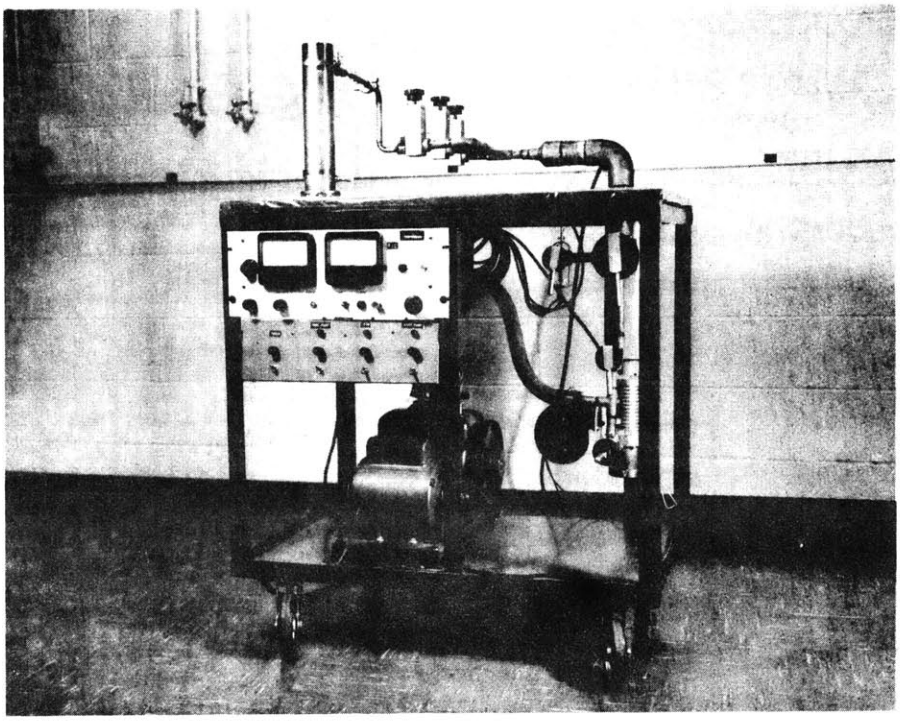

FIGURE 8 PHOTOGRAPH OF PORTABLE VACUUM SYSTEM

supplied by Vacuum Instruments Corp. (V.I.C.). The 2 in., air-cooled diffusion pump was rated at 150 liters/sec. A liquid nitrogen cold trap was installed to prevent backstreaming of diffusion oil into the dewars. Pressure measurements from atmospheric pressure down to about 1 micron (10^{-3} mm Hg.) were made at positions (A) and (B) with a thermocouple gauge, while system pressures below 1 micron were measured with a Bayard-Alpert type ionization gauge positioned at the outlet from the cold trap (C). A power supply and control panel actuated the gauges. Pressures down to 2 to 5 x 10^{-7} mm Hg. were readily attained for pump-down volumes of several liters.

2. Detector Dewars

Considerable time and effort were expended in the development and construction of satisfactory dewars or cryostats required for operating Ge(Li) detectors. The germanium diode must be operated at less than 150°K in order to reduce the reverse bias leakage currents during operation to acceptable levels (less than 10^{-8} amp.). For convenience, liquid nitrogen was used as the coolant and therefore the operating temperature was near 77°K. At the same time, to prevent possible deterioration of detector characteristics due to condensation and frosting of the detector from atmospheric water vapor, it was also kept in a vacuum. These two requirements were met simultaneously with the arrangement in Fig. 6 above.

This design consisted of a 1.3 liter capacity inner vessel suspended by 1 in. diameter, 0.010 in. thick, stainless steel tube, 8 in. long. These dimensions were chosen to minimize

heat conduction losses along the tube to the top plate. Surrounding this was a 5 in. diameter, 0.030 in. thick cylinder of stainless steel. A connecting tube was welded on the side and fitted with a 3/8 in. NRC Bellows-type vacuum valve. The dewar could be disassembled at both the top and the bottom to allow ease of mounting the detector and easy disassembly for cleaning. Although the stainless steel surfaces were electropolished to reduce radiative losses, an increase in liquid nitrogen hold-time of a factor of 2 could be attained by covering the stainless steel surfaces with highly reflective aluminum foil. The latter has an emissivity of 0.023 compared with 0.110 of stainless steel.

Because of internal outgassing of surfaces and small leakages through the hermitic feed-throughs, it was found necessary to use some means of maintaining the vacuum after removal from the diffusion vacuum system. Small (0.2 to 1 liter per sec.) ion pumps (supplied by Varian Associates) were found to perform this task very adequately, maintaining vacuums of 10^{-6} to 10^{-7} mm Hg. for several months while requiring almost no maintenance. Liquid nitrogen hold times for such conditions were up to 95 hours for 1.3 liters. Average values were about 60-70 hours.

In the earlier models of this design, the electrical feedthrough carrying the signal from the detector was positioned at the top. This required a fairly long ($\sim$12 in.) connection to the detector at the bottom of the inner vessel, resulting in a high input capacitance to the preamplifier, and thus decreased energy resolution. In the latest models, the

connectors were placed at the bottom, thus requiring only a short lead ($\sim$ 3 in. long) from the detector to the preamplifier.

The dewars, which are now available from A.D. Little, Inc., Cambridge, Mass., are described in considerable detail in (K4). Figure 9 is a photograph of a disassembled dewar showing the Ge(Li) detector in position, while Fig. 10 shows the assembled dewar with the ion pump power supply.

During development of suitable cryostats, a number of different designs were tried, and although not as generally useful as the design described above, may be useful in other types of experiments. The simplest of these consisted of a small chamber surrounding a copper rod. The detector was placed upon the rod, the chamber evacuated and the rod inserted into a glass dewar filled with liquid nitrogen. The main disadvantages of such a system were the frosting up of the leads and the relatively short liquid nitrogen hold time of the dewar. Further, because of air leaks, the detector itself also became frosted over after a lengthy run of several days without re-evacuation. However, in the use of this type of detector arrangement, it was found that the detectors could be satisfactorily operated in a dry argon or nitrogen gas atmosphere. This, however, increased the gas conduction heat leak, consequently reducing the hold time. However, it may be possible to use this arrangement in other situations.

For testing of detectors prior to placing in the larger dewars, smaller dewars with rapid evacuation and cool-down times

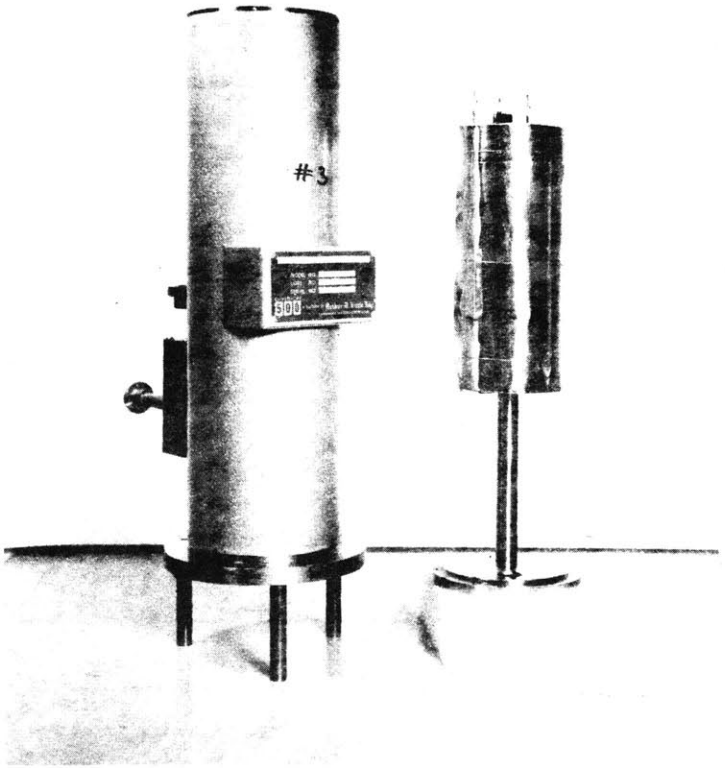

FIGURE 9 PHOTOGRAPH OF DISASSEMBLED DEWAR

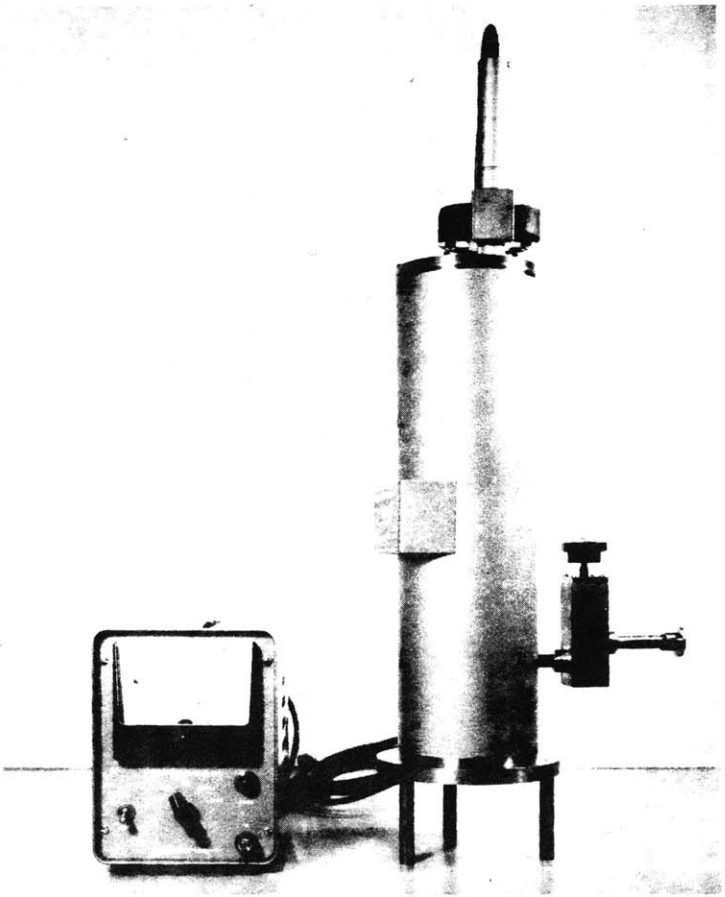

FIGURE 10 PHOTOGRAPH OF ASSEMBLED DEWAR AND ION PUMP POWER SUPPLY

were used. The design was basically the same with the detectors positioned on the bottom of the inner vessel in the evacuated space. These chambers were kept evacuated with the vacuum system and were capable of a hold-time of 3-4 hours. One such dewar is shown in Fig. 8 on the portable vacuum system platform.

3. Electronics

Realization of the high energy resolution possible with lithium-ion drift germanium detectors necessitates the use of high quality electronic apparatus to process the signal produced by the detector. In the present work, commercially available units were used. The schematic arrangement of the electronic apparatus was shown in Fig. 6. The signal from the detector was fed to a low noise type preamplifier (ORTEC 103, or 103XL, TENNELEC 110) then to a biased main amplifier (ORTEC 203) and analyzed in a multi-channel pulse height analyzer (Nuclear Data 1024 channels, Model 160; TMC 256, Model CN-110A).

F. OPERATING CHARACTERISTICS OF Ge(Li) GAMMA-RAY SPECTROMETERS

A detailed description of the general characteristics of Ge(Li) detectors is presented by Ewan and Tavendale (T3). Some of their results are included in the following summary.

1. Properties of Ge(Li) Detectors

(a) Temperature Characteristics

To reduce leakage currents, the detectors must be operated at low temperatures. Above 170°K the detector leakage current limits the resolution. Liquid nitrogen provides a convenient temperature (77°K); consequently nearly all Ge(Li) detectors

are operated at this temperature.

(b) Linearity of Response

Reference (T3) found that Ge(Li) detectors were linear to within $\pm 0.3\%$. In the present work, the combination of detector-amplifier-analyzer gave rise to a small differential non-linearity of about 1 to 3%. However, no measurements were made to determine the source of this non-linearity.

(c) Response Time of Detectors

The pulse-rise time of a 3.5 mm diode operated at optimum bias is less than 30 μsec, although the spectrum contains components with both slow and fast rise time, presumably due to trapping of the carriers.

(d) Bias

Although Tavendale reports measurements of good resolution for reverse bias voltages from 150 to 1000 v., voltages greater than about 300 were seldom required and generally resulted in poor resolution. Typical bias values were $\sim$ 200 v., although some detectors operated best at lower voltages. The optimum bias for a detector was located by determining the voltage that resulted in the best energy resolution for a gamma-ray such as the 662 keV photon from Cs^{137}.

(e) Stability of Detector with Time

Germanium detectors that were kept at liquid nitrogen temperatures and in vacuo retained their characteristics with no deterioration in performance after six months. For detectors that had warmed to room temperature, it was necessary to apply an etch treatment to provide clean junction surfaces.

Otherwise, cooling to liquid nitrogen temperature without etching resulted in leakage currents of 10^{-6} amp. or higher.

Even drifted diodes stored at room temperature for several months have been made to operate satisfactorily following a room temperature drift of $\sim$1 day and an etch treatment.

2. Energy Spectra of Calibration Gamma-Rays

In this section the use of Ge(Li) detectors to study the gamma-ray spectra of well-known energy calibration standard sources is discussed. The values of the gamma-ray energies are presented in Table B.1 of Appendix B. The detector used for these measurements (no. 9-19.1) had a depletion depth of 3.5 mm and a cross-sectional area of 1.6 cm^2. Results were punched on paper tape then on to IBM computer cards which then served as the input data for a curve-plotting program.

(a) Cobalt-57

Figure 11 shows the gamma-spectrum obtained from Co^{57} which emits two gamma-rays at 122.0 and 136.4 keV. The full width at half maximum (FWHM) was measured to be 3.59 keV (2.9%) for the 122 keV peak.

(b) Sodium-22

Figure 12 gives the gamma-spectrum of Na^{22} with gamma-rays at 511 and 1277 keV and illustrates the intense Compton electron background in addition to the peaks due to photoelectric absorption. This Compton distribution introduces a complication to the use of the Ge(Li) detectors for complex spectra with many gamma-rays, because of the possibility of misinterpretation of a sharp Compton edge for a low-yield gamma-ray. Also, because

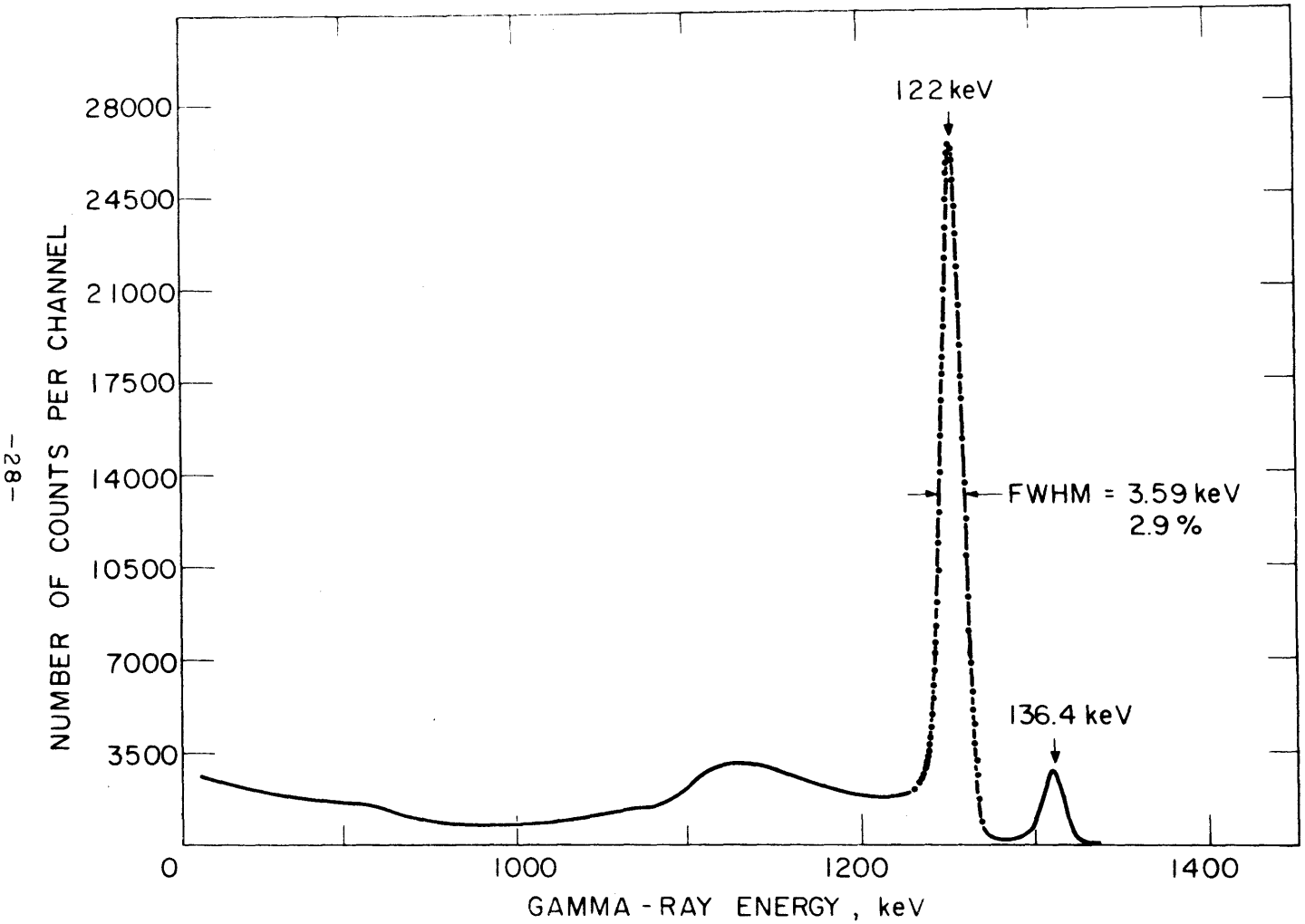

FIGURE 11 Co^{57} GAMMA - SPECTRUM GERMANIUM LITHIUM DRIFT DETECTOR No. 9 - 19.1
3.5 mm Depletion Depth, 1.6 cm^2 200 VOLTS BIAS, 77 °K

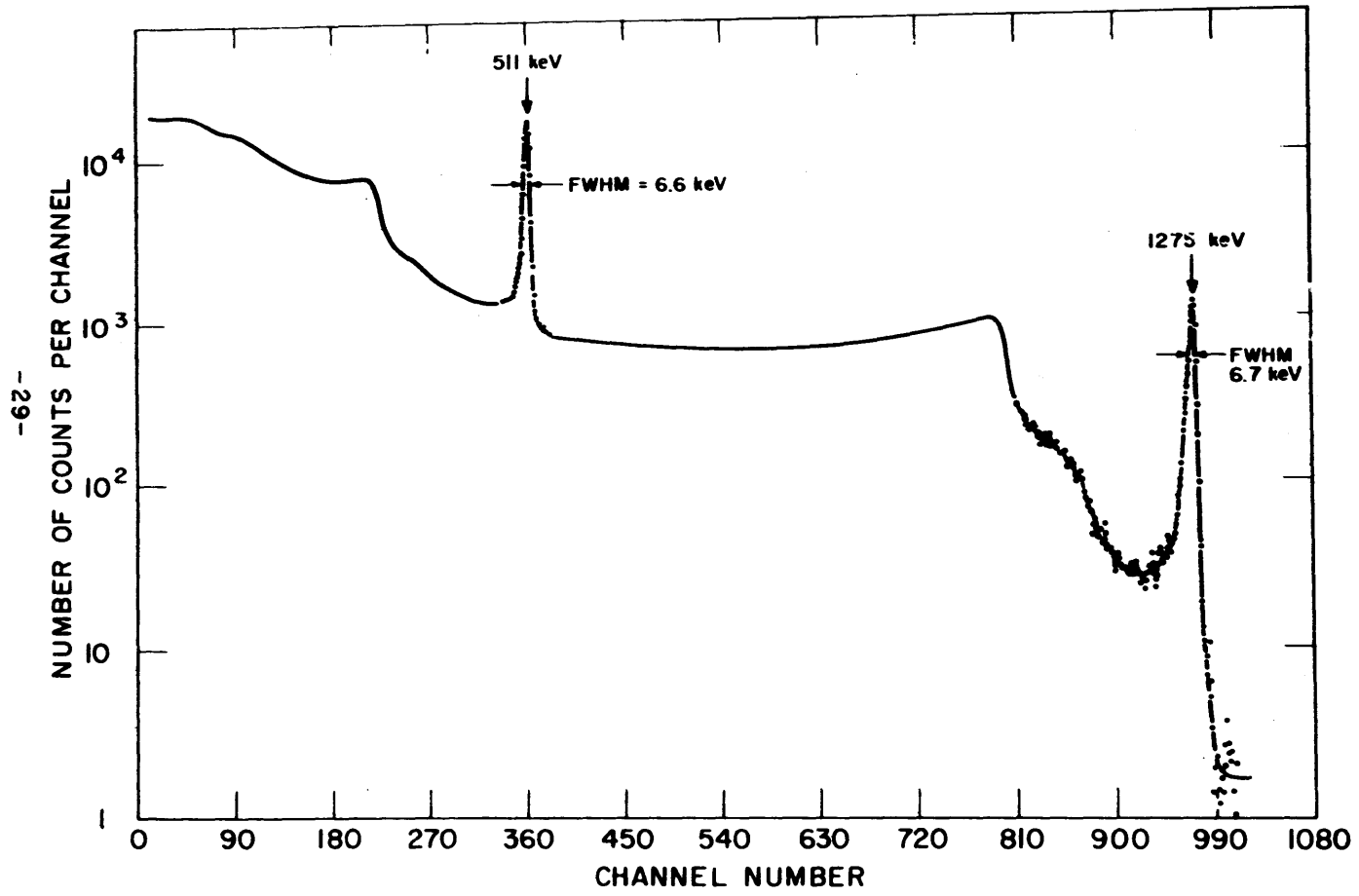

FIGURE 12 - Na^{22} GAMMA - RAY SPECTRUM

GERMANIUM LITHIUM DRIFT DETECTOR No. 9-19.1, 3.5 MM DEPLETION DEPTH, 1.6 CM^2 AREA, 170 VOLTS BIAS, 77°K

the resolution deteriorates for high count rates, and since the Compton distribution provides the greatest share of the counts, it limits the count rate useable in an experiment. The energy resolution was 6.6 keV at 511 keV and 6.7 keV at 1275 keV.

(c) Cesium-137

The well-calibrated gamma-ray of Cs^{137} at 661.6 keV gives rise to the spectrum shown in Fig. 13. The FWHM obtained was 4.7 keV.

(d) Manganese-54

The spectrum for the 835 keV gamma-ray of Mn^{54} is shown in Fig. 14. A value of 5.1 keV was calculated for the FWHM.

(e) Cobalt-60

The complete energy spectrum of Co^{60} is shown in Fig. 15, while an enlarged view of the region near the two gamma-rays at 1173 and 1333 keV is shown in Fig. 16.

(f) Thorium (B+C+C")

Figure 17 shows the high energy portion of the gamma-spectrum of Th(B+C+C") where the 2614 keV gamma-ray is due to decay of Tl^{228}. The double escape peak shown in the spectrum at 1592 keV is the result of pair production interactions in which both annihilation photons escape. Because the detector is small, the escape probability for the photons is large. Thus, this peak is considerably larger than either the total absorption or the single escape peak at 2103 keV. The FWHM for the photopeak at 2614 keV was 8 keV.

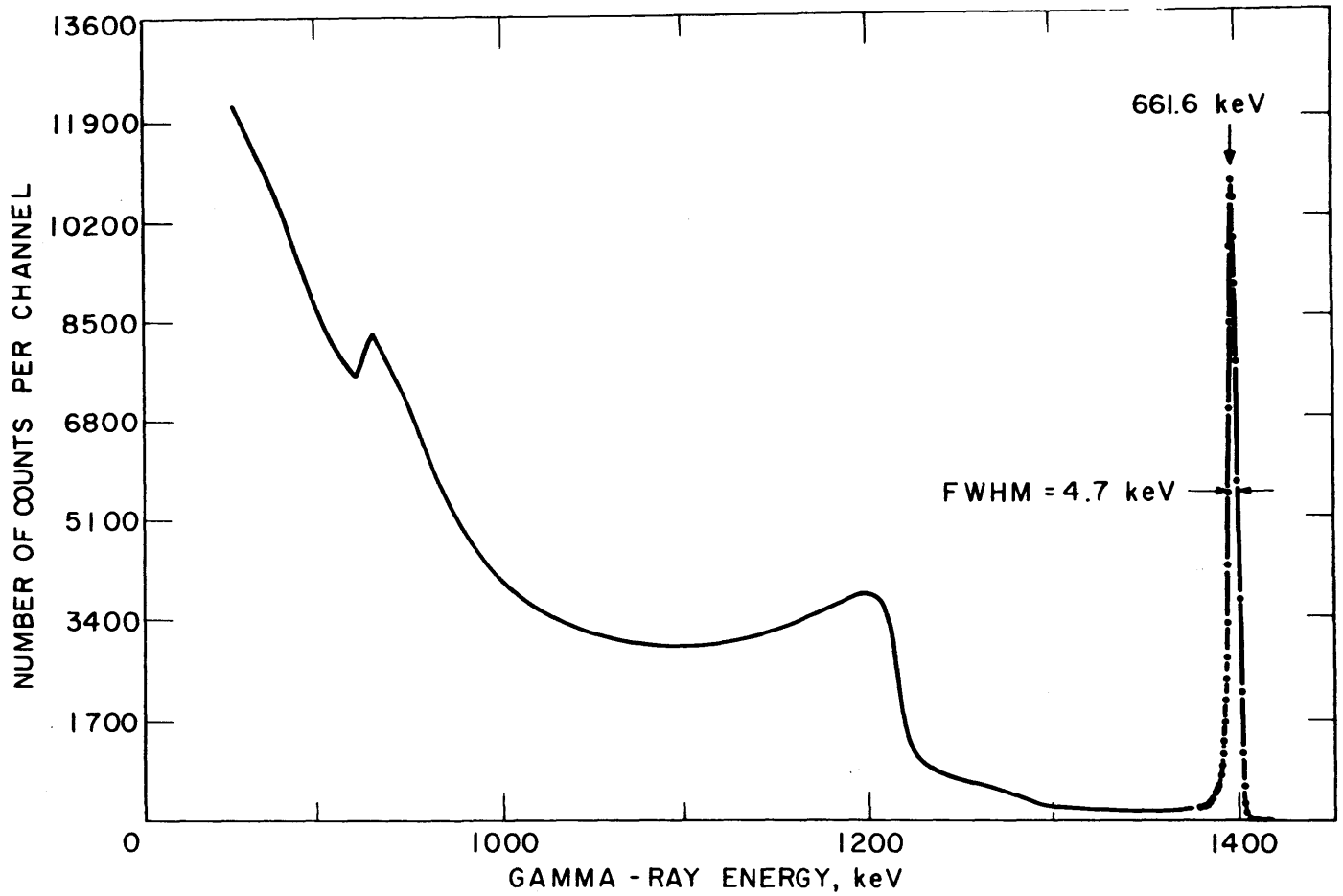

FIGURE 13 Cs^{137} GAMMA - SPECTRUM GERMANIUM LITHIUM DRIFT DETECTOR No. 9-19.1
3.5 mm DEPLETION DEPTH, 1.6 cm^2 200 VOLTS BIAS, 77°K RUN S8

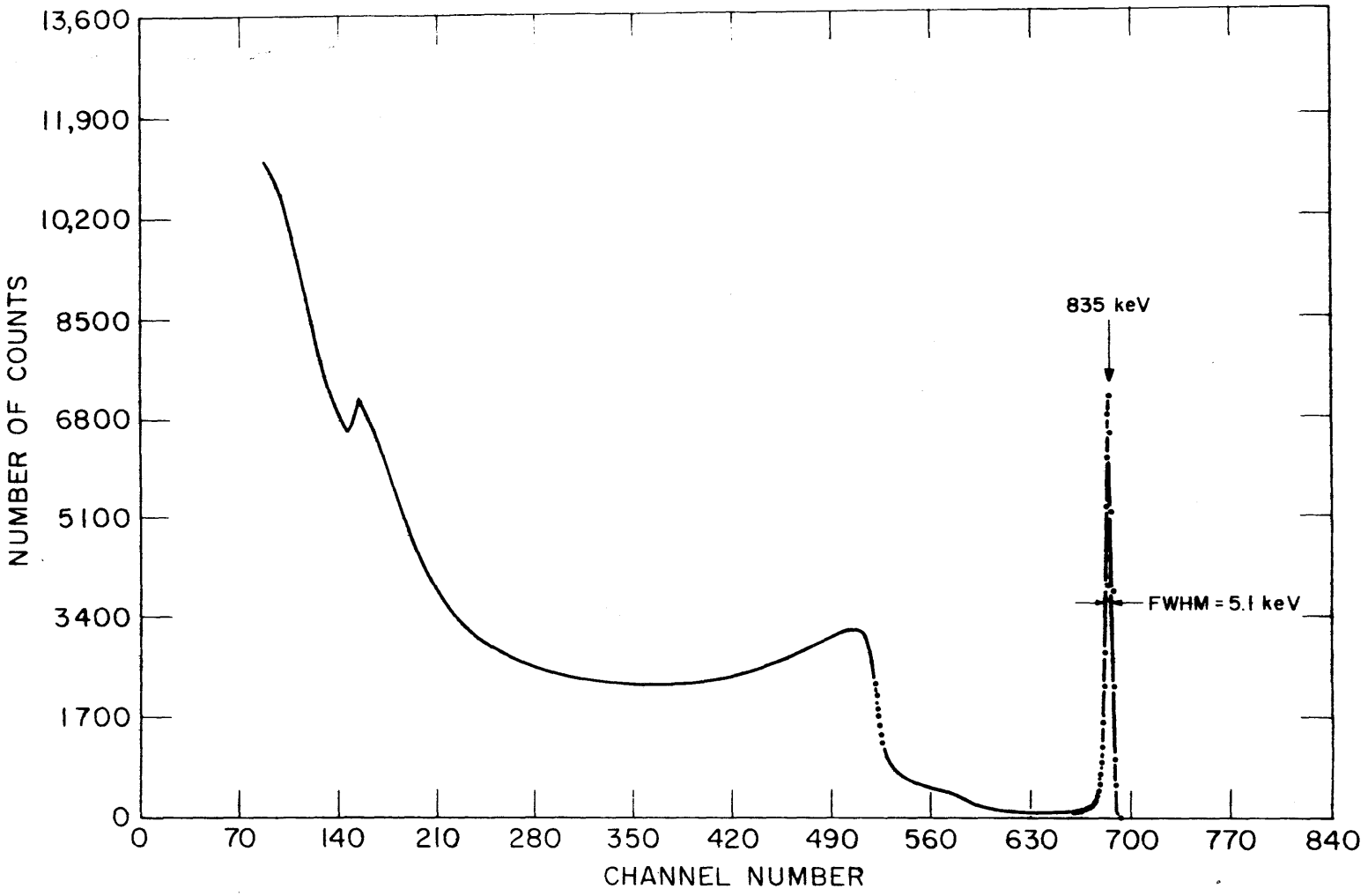

FIGURE 14 $-Mn^{54}$ GAMMA SPECTRUM

GERMANIUM LITHIUM DRIFT DETECTOR No. 9-191, 3.5 MM DEPLETION DEPTH, 1.6 CM^2 AREA, 200 VOLTS BIAS, 77°K

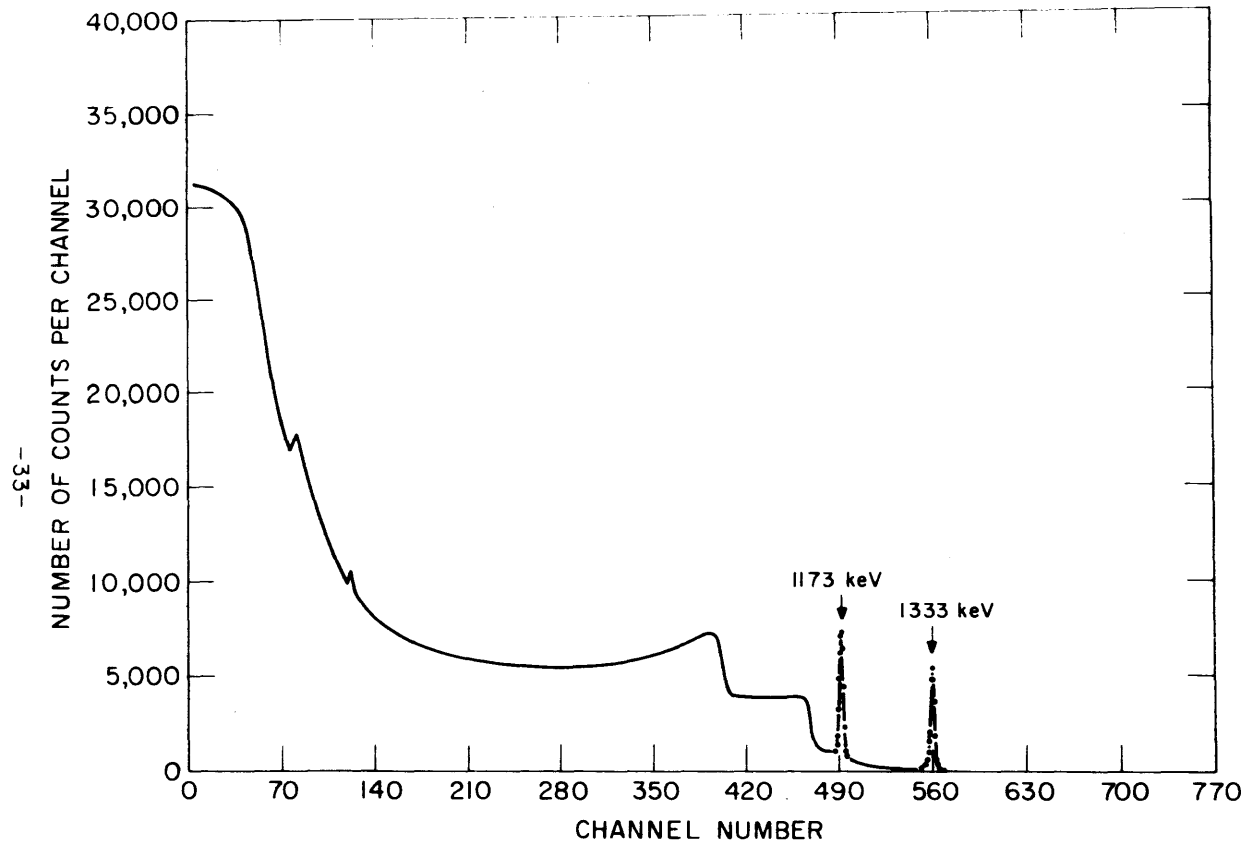

FIGURE 15 - Co^{60} GAMMA SPECTRUM, 0.1 to 1.35 MeV
GERMANIUM LITHIUM DRIFT DETECTOR No. 9-19.1, 3.5 MM DEPLETION DEPTH,
1.6 CM^2 AREA, 200 VOLTS BIAS, 77°K

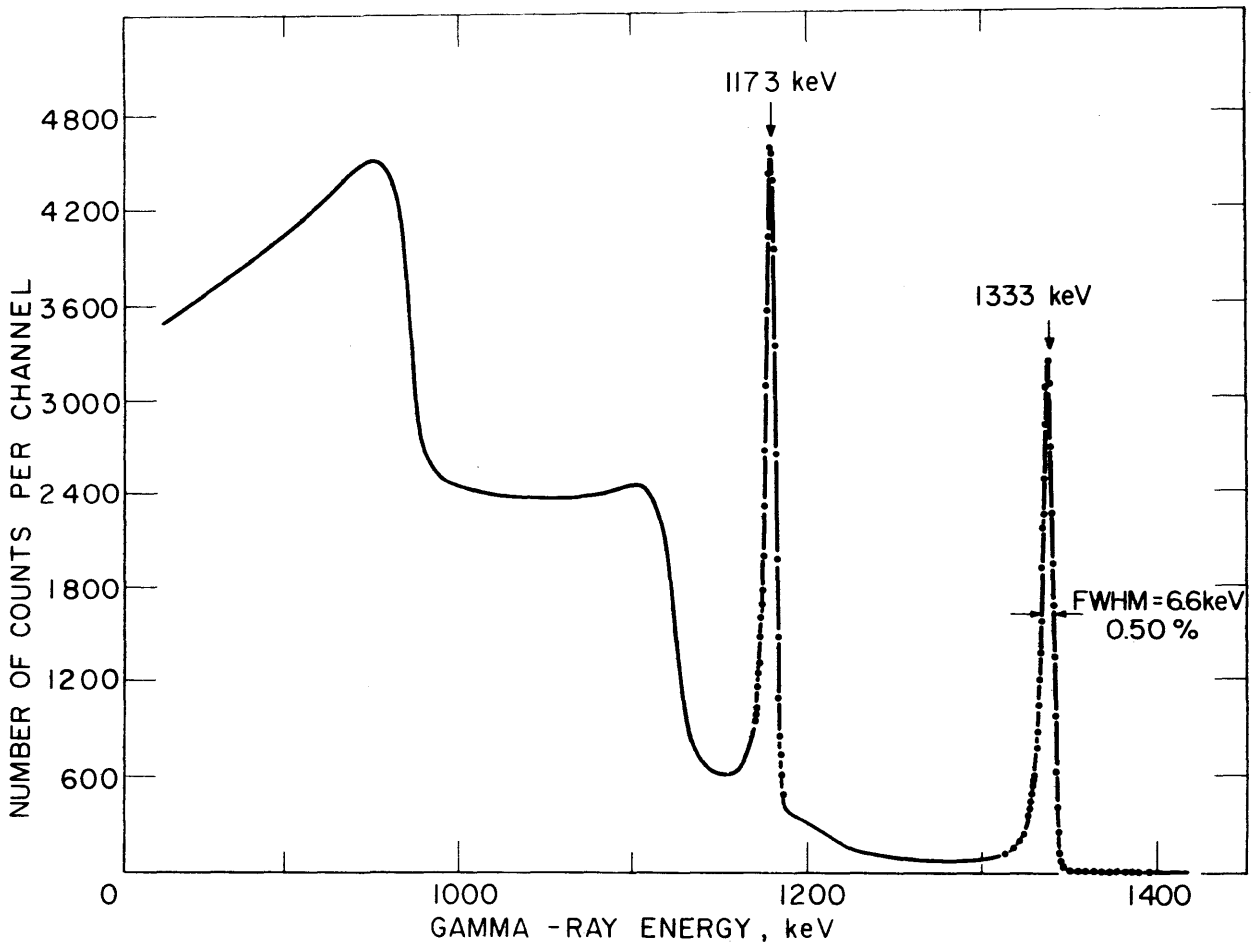

FIGURE 16 Co^{60} GAMMA-SPECTRUM GERMANIUM LITHIUM DRIFT DETECTOR No. 9-19.1
3.5 mm DEPLETION DEPTH 200 VOLTS BIAS, 77° K

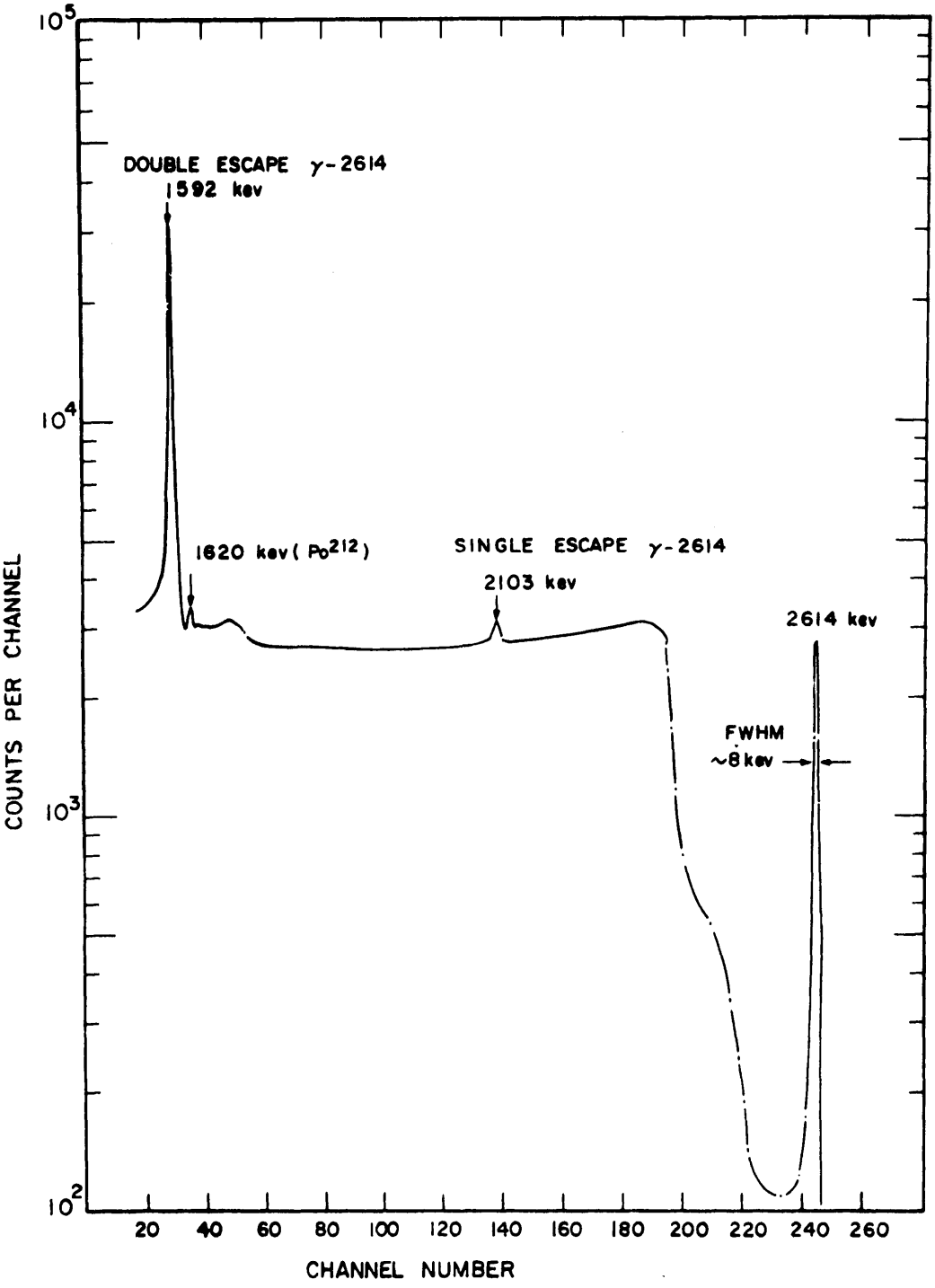

FIGURE 17 Th C" γ RAY SPECTRUM Li-Drifted Germanium Detector No. 9-191 3.5mm Depletion Depth, 1.6 cm^2 200 Volts Bias, 77°K 20th October 1964

3. Efficiency

The intrinsic photopeak efficiency of the detector used in these experiments as a function of energy is shown in Fig. 18. The points were obtained with calibrated point sources and a calculated geometry factor. The experimental efficiencies are known to be considerably higher than what would be calculated from the photoelectric cross-section due to re-absorption of some of the Compton-scattered photons (T3).

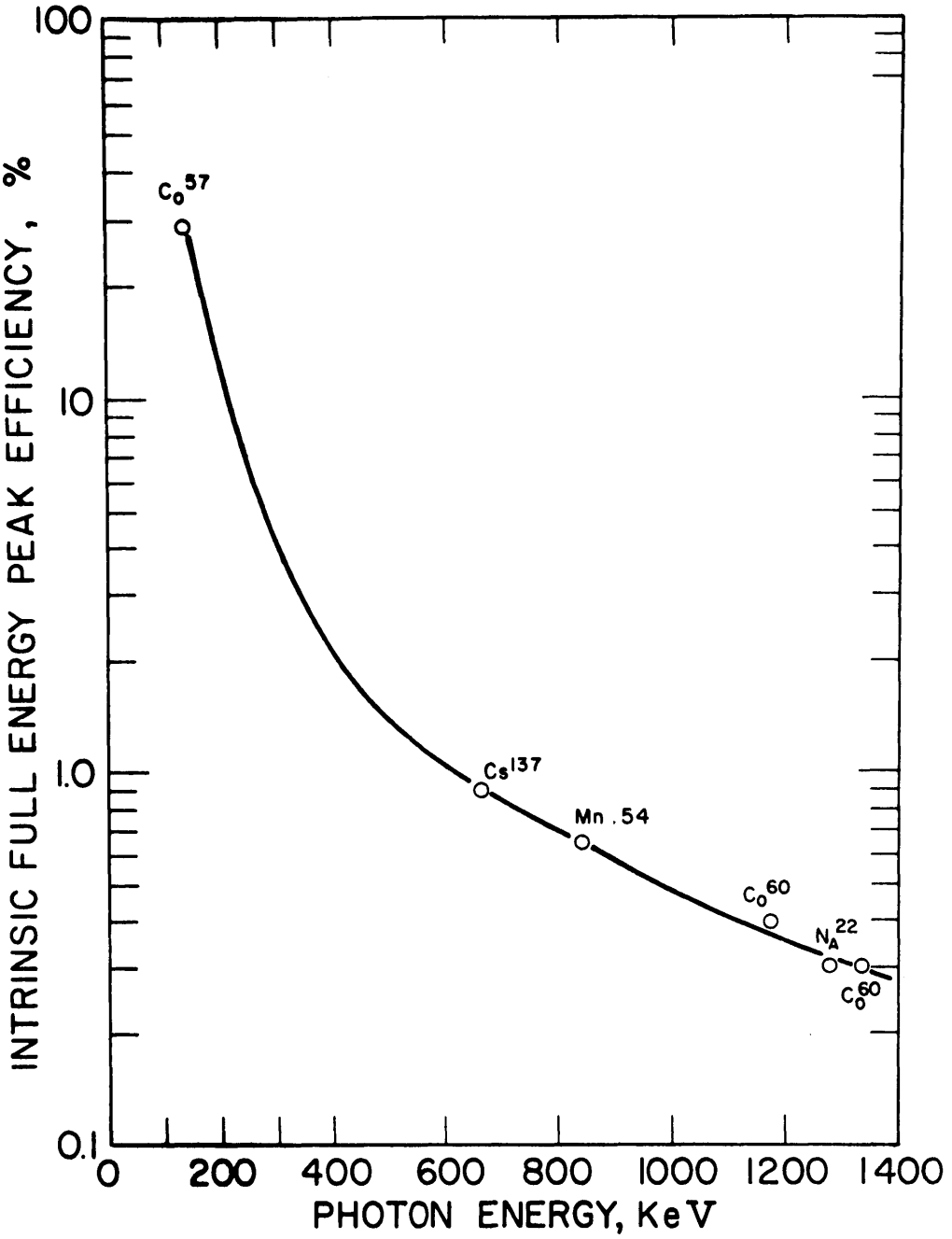

FIGURE 18 INTRINSIC FULL PEAK EFFICIENCY OF LITHIUM DRIFTED GERMANIUM DETECTOR 9-19.1 3.5 mm THICK 12 NOV., 1964 200 VOLTS BIAS 77° K

III. NONDESTRUCTIVE ANALYSES OF IRRADIATED MITR FUEL ELEMENTS USING A Ge(Li) GAMMA-RAY SPECTROMETER

A. INTRODUCTION

The determination of the irradiation history of spent reactor fuel is generally accomplished by relating physics parameters, such as total neutron exposure, neutron flux and irradiation time, to the measured fission product content in the fuel. The use of gamma-ray spectroscopy for this purpose requires that the fission product being measured emit a gamma-ray having a unique energy. This property, in combination with the knowledge of the radionuclide's half-period, is usually sufficient for its proper identification in complex gamma-ray spectra from fuel elements. A further desired characteristic is that the gamma-ray energy be high enough to keep self-absorption losses within the fuel small.

Since not all the fission products available in a freshly irradiated sample of U^{235} have the above desired characteristics, it is necessary to choose the most suitable for further investigation. Table 2 shows a list of some of the fission products, along with some nuclear properties of interest to these studies. The list contains fission products that (a) emit gamma-rays of energies greater than 500 keV so that absorption in the fuel is small, (b) have half-lives greater than a few days and up to 30 years, and (c) have reasonably high fission yields.

The objectives of the experimental studies to be described have been

TABLE 2
PROPERTIES OF FISSION PRODUCTS
USEFUL FOR GAMMA-RAY SPECTRSCOPIC
STUDIES OF IRRADIATED FUEL

FISSION PRODUCT	GAMMA RAY ENERGY, MeV	HALF PERIOD	FISSION YIELD, %				
			THERMAL FISSION		FAST FISSION (c)		
			U^{235} (a)	Pu^{239} (b)	U^{235}	Pu^{239}	U^{238}
Zr^{95}	0.724, 0.758	65 DAYS	6.27	5.06	6.8	5.3	5.7
Nb^{95}	0.766	35 DAYS					
Ru^{106}	2.66, 2.40, 2.10, 1.55	1.0 YR.	0.38	4.04	0.5	6.3	2.7
Rh^{106}	1.05, 0.624, 0.607, 0513	30 SEC					
Cs^{134}	0.605, 0.796	2.3 YR.	6.59	$Cs^{133}(n,\gamma)$ 5.59	Cs^{134} 5.9	—	—
Cs^{133}	none	stable					
Cs^{137}	0.662	30 YR.	6.00	5.40	6.2	5.8	6.2
Ba^{140}	3.00, 2.520, 1.596	13 DAYS	6.44	5.47	5.8	5.0	5.7
La^{140}	0.92, 0.82	40 HR.					
Ce^{144}	0.079, 0.133	285 DAYS	5.62	4.09	4.8	3.7	4.9
Pr^{144}	0.697, 1.488, 2.186	17 MIN					

REFERENCES: (a) TABLE 10, (b) M9, (c) D2

(1) to determine what fission products can be identified from gamma-spectra of irradiated MITR fuel elements with the use of a Ge(Li) spectrometer, and

(2) to determine the type of information that could be obtained about fuel element irradiation history from the analysis of the Ge(Li) spectrometer data.

The following sections describe the equipment and procedures used in the experimental investigations, the results obtained and the methods used in the interpretation of these results.

B. EXPERIMENTAL EQUIPMENT AND PROCEDURES

1. MITR Fuel Elements

The MITR fuel elements, shown in Fig. 19, are of the standard MTR, plate-type construction, containing 16 fuel plates and two outside dummy plates, each rigidly located in two grooved side plates. The plates, about 24 in. in length, contained an alloy of 93% enriched U^{235} and aluminum 0.020 in. in thickness, clad on both sides with 0.020 in. of aluminum. Spacing between each plate was 0.117 in. The outside dimension of the element was approximately three inches square. Gamma-ray spectroscopic studies were made on six different fuel elements, each having a different irradiation history. In Table 3 are presented some of the known and calculated information about the fuel elements studied: 2-4, 2M1, 2M14, 2M19, 2M22 and 2M31.

2. Scanning Equipment and Procedure

Preliminary investigations on the feasibility of detecting

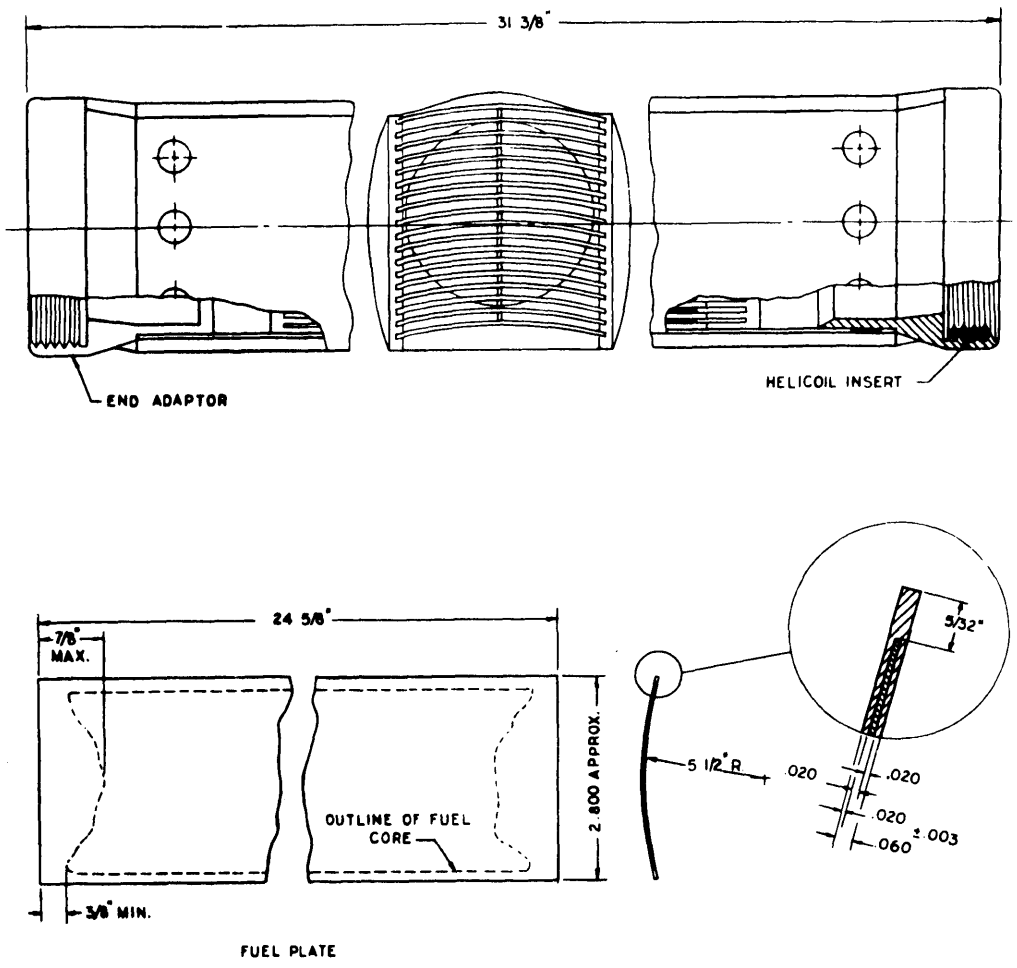

FIGURE 19 MITR FUEL ELEMENT

TABLE 3

MITR IRRADIATED FUEL ELEMENT DATA

Fuel Element	Data Charged	Data discharged	Total Res. Time, Years	Total Expos. Time, 10^8 sec.	Total[a] Energy, MWH	Orig.[a] U-235 Wt., gms.	Final[a] U-235 Wt., gms.	Final[a] U-235 Fract. N_{25}/N_{25_o},	Cooling Time
2M1	4/30/59	1/22/62	2.75		736.20	162.26	123.01	0.758	3yrs.4mos.
2-4	7/11/60	6/1/62	1.90		223.10	104.85	92.96	0.888	3yrs.
2M14	7/10/61	10/30/64	3.25		945.86	161.25	110.82	0.686	Varied
2M19	1/22/62	7/25/64	2.50	0.448	1021.82	161.25	106.78	0.661	281 d.
2M22	4/24/61	12/2/63	2.60	0.482	1216.60	161.25	96.39	0.597	1 1/2 yrs.
2M31	2/18/63	5/3/65	2.20		1123 *	161.25	104 *	0.644*	11 d.

* approx.

(a) Ref. M3.

and identifying radioactive fission products within an irradiated fuel element using a Ge(Li) gamma-ray spectrometer were made upon 2M14. A collimated gamma-ray beam was extracted from the element, which was positioned in the fuel charging flask, by means of a hole through the shielding material (see Ref. M3 for more details). The Ge(Li) detector was placed in the beam path and the gamma-ray spectra were recorded with a 256 channel analyzer (TMC). However, this arrangement did not permit satisfactory scanning of the element and modifications to the fueling flask would have been necessary. Since irradiated MITR fuel was stored in the spent fuel storage tank, a mechanism suitable for scanning the elements underwater was designed and built.

A schematic diagram, shown in Fig. 20, illustrates the main features of this apparatus. The detector dewar was positioned on a moveable carriage which allowed motion both parallel and normal to the axis of the fuel element. Lead shielding was placed around the detector to reduce background count rates. An air-filled tube 1/2 in. I.D., rigidly attached to the carriage, extended from near the bottom of the dewar, through the water to the surface of the fuel element. This tube permitted a well-collimated beam of gamma-rays to reach the detector. Additional steel and lead collimators with aperature diameters varying between 1/16 and 1/2 in. were placed at the bottom of the tube and near the detector to reduce counting rates to acceptable levels. In addition, 1/8 in. thick lead sheets were placed in the gamma-ray beam to absorb many of the

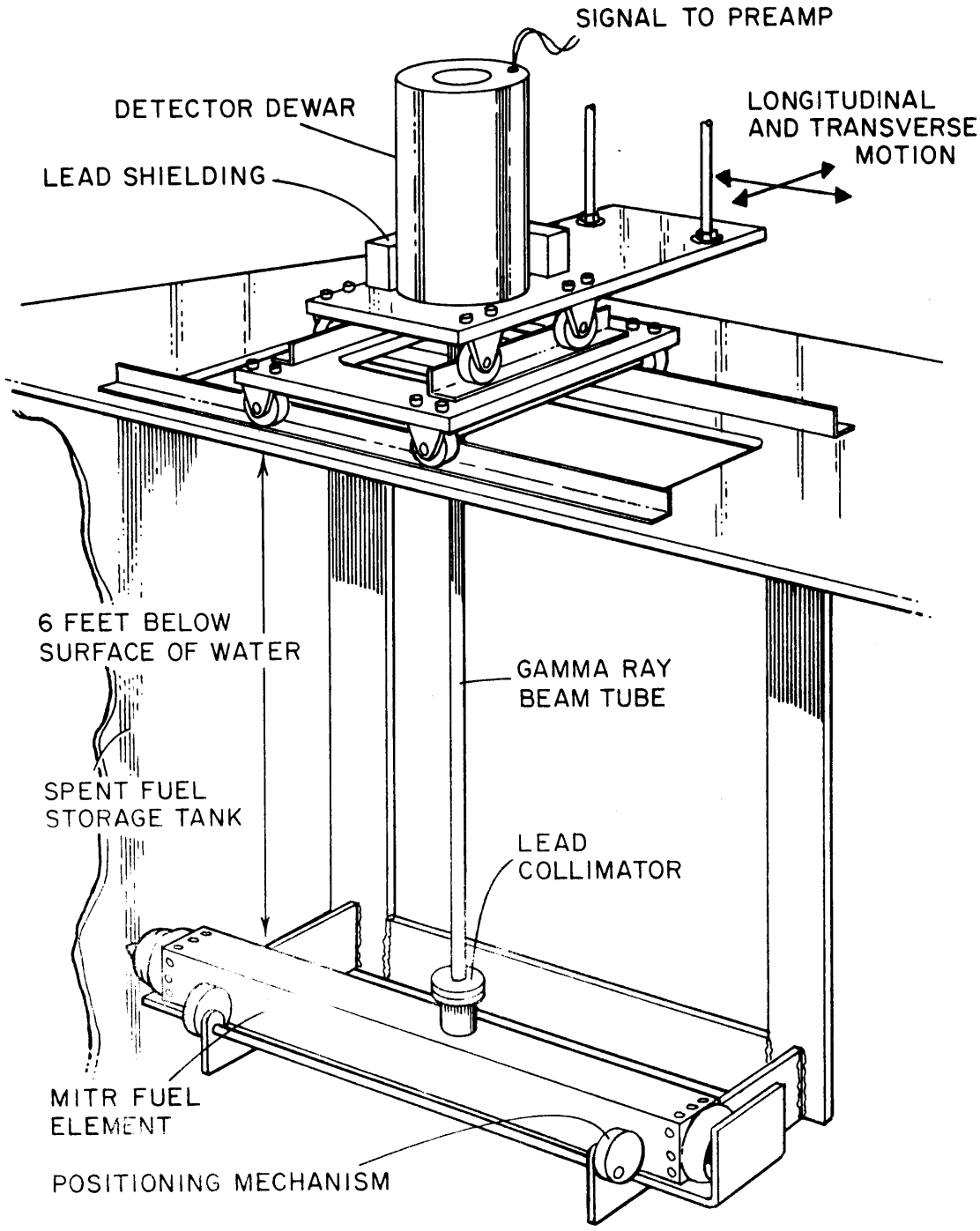

FIGURE 20 SCHEMATIC DIAGRAM OF APPARATUS FOR GAMMA-RAY SCANNING OF MITR SPENT FUEL ELEMENTS

unused lower energy photons while still allowing the higher energy photons to pass through.

The fuel element to be studied was removed from the storage racks at the bottom of the tank and was placed in a horizontal position on the holding frame about six feet below the surface of the water. A cam mechanism was used to hold the element rigidly against the frame. A photograph showing a fuel element in position for scanning is shown in Fig. 21.

Initially, measurements were made to determine the optimum collimation and shielding for that particular element. Gamma-ray spectra were then collected for 20 to 80 minutes, depending upon the count rates. Spectra were taken at two inch intervals on the central plane for longitudinal scans, while transverse scans across the element were taken at 1/2 in. intervals at several longitudinal positions. Figure 22 shows a photograph of the arrangement of the equipment in the spent fuel storage room.

C. EXPERIMENTAL RESULTS

Identification of the fission-product parents of the gamma-rays in a spectrum required relatively precise determinations of the gamma-ray energies. For energy calibrations of fuel element spectra, the gamma-ray standards previously described in Section II were used. Since the energies of the individual fission product gamma-rays were often not known accurately, it was necessary to obtain spectra of the separated fission products of interest with the Ge(Li) spectrometer. The gamma-ray spectra of Zr^{95}+Nb^{95}, Rh^{106}, Cs^{134}, Cs^{137} and Ce^{144}+Pr^{144} are presented

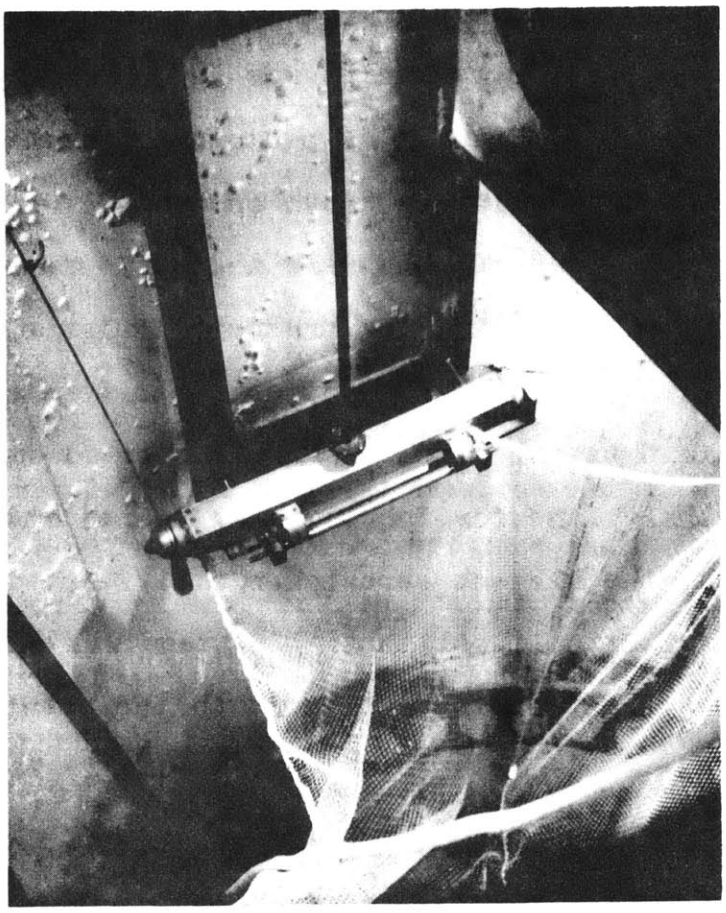

FIGURE 21 PHOTOGRAPH OF FUEL ELEMENT IN SCANNING ASSEMBLY

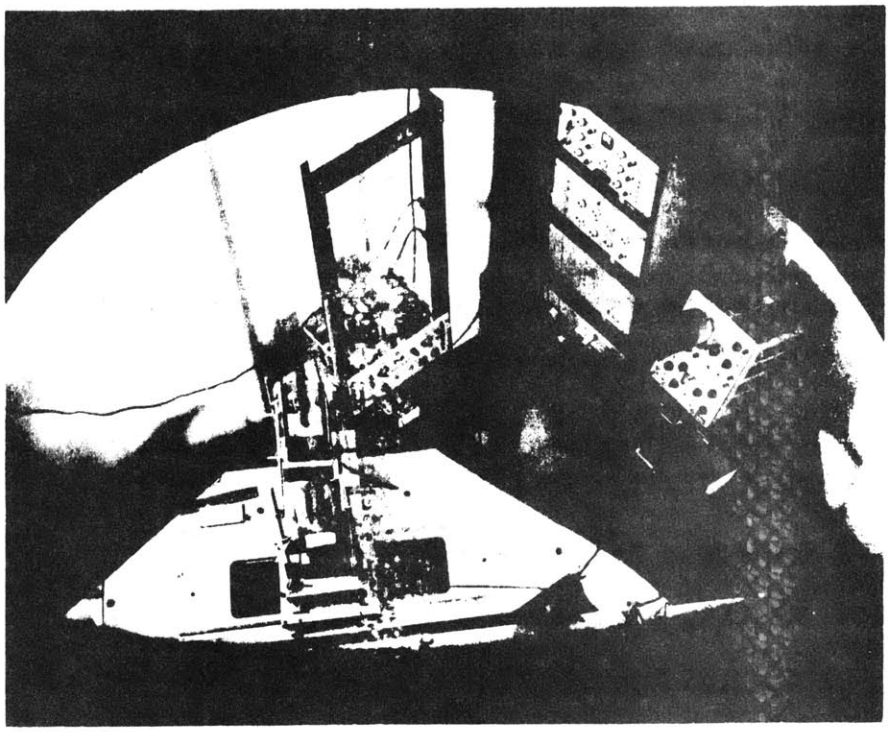

FIGURE 22 PHOTOGRAPH OF SCANNING APPARATUS AND ELECTRONIC EQUIPMENT IN THE SPENT FUEL STORAGE ROOM

in Appendix C, along with the gamma-ray energies determined in these studies.

1. Fission Product Gamma-Ray Spectra from Elements with Different Cooling Periods

(a) Fuel Element 2M14

As mentioned previously, preliminary studies were made upon 2M14 to determine how soon after removal from the core could satisfactorily resolved gamma-ray spectra be obtained. The results were recorded with a 256 channel analyzer and thus, in order to retain a sufficient number of points per gamma-ray peak, the spectrum was obtained in a series of overlapping sections with the use of the biased amplifier. Spectra were obtained after cooling periods of 18 hours, 40 hours, 5 days and 18 days.

(i) Cooling Period of 18 hours:

The low energy (< 300 keV) portion of the gamma-ray spectrum after 18 hours cooling time is shown in Fig. 23. Although a large number of gamma-rays are known to exist in this energy range, they have not been resolved because of the intense Compton electron background due to higher energy gamma-rays. The shape of this spectrum does not change appreciably with cooling time. Only after cooling periods of two or more years, when most of the shorter-lived fission products have decayed, is it possible to resolve some gamma-rays below 300 keV. Since self-absorption corrections in fuel and water are rather large below these energies, all subsequent investigations were limited to gamma-ray energies greater than about

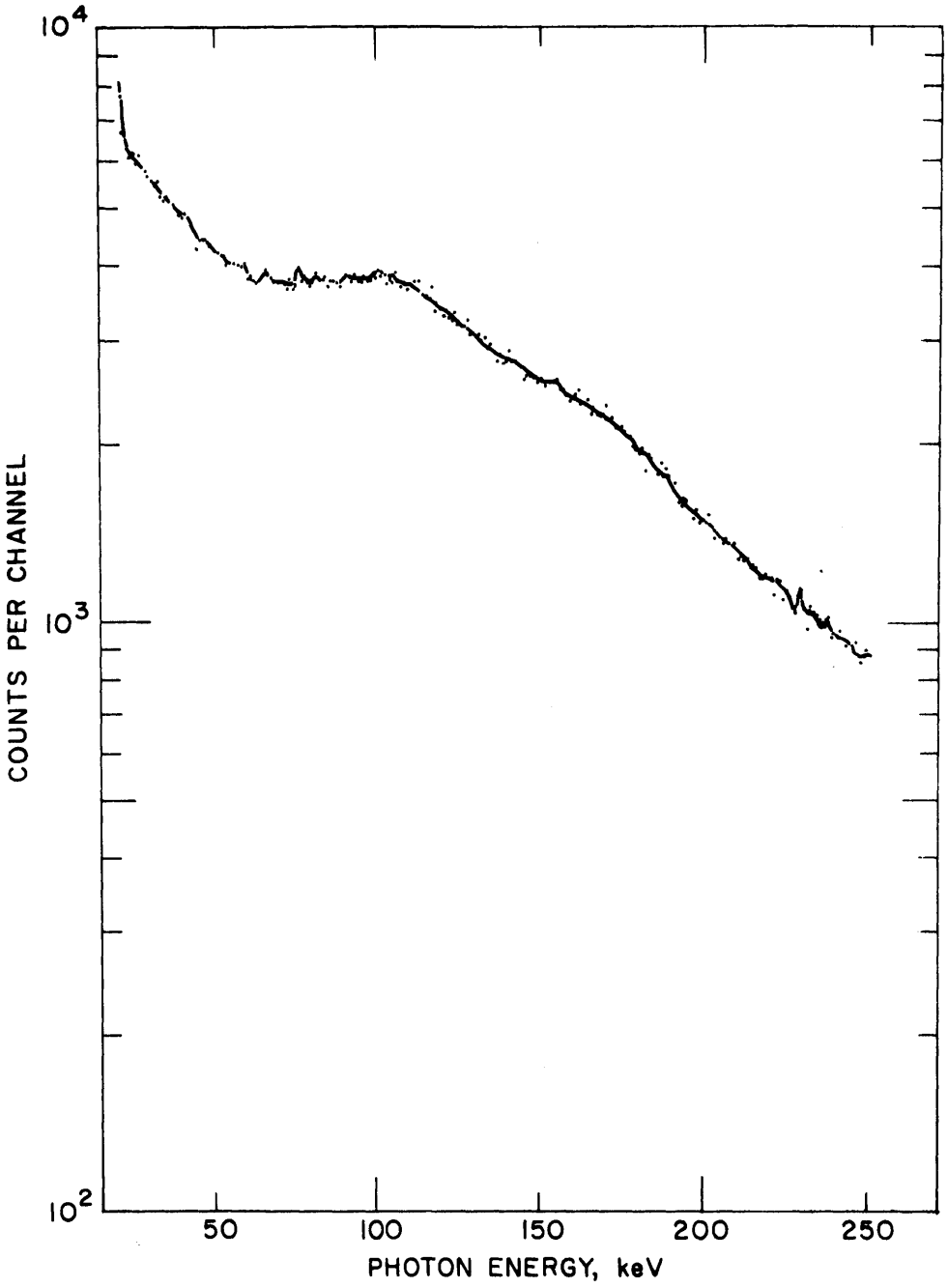

FIGURE 23 LOW ENERGY PORTION OF γ-RAY SPECTRUM OF FUEL ELEMENT 2M14 AFTER 18 HRS COOLING. Ge(Li) DETECTOR No. 9-19.1

(No page 50)

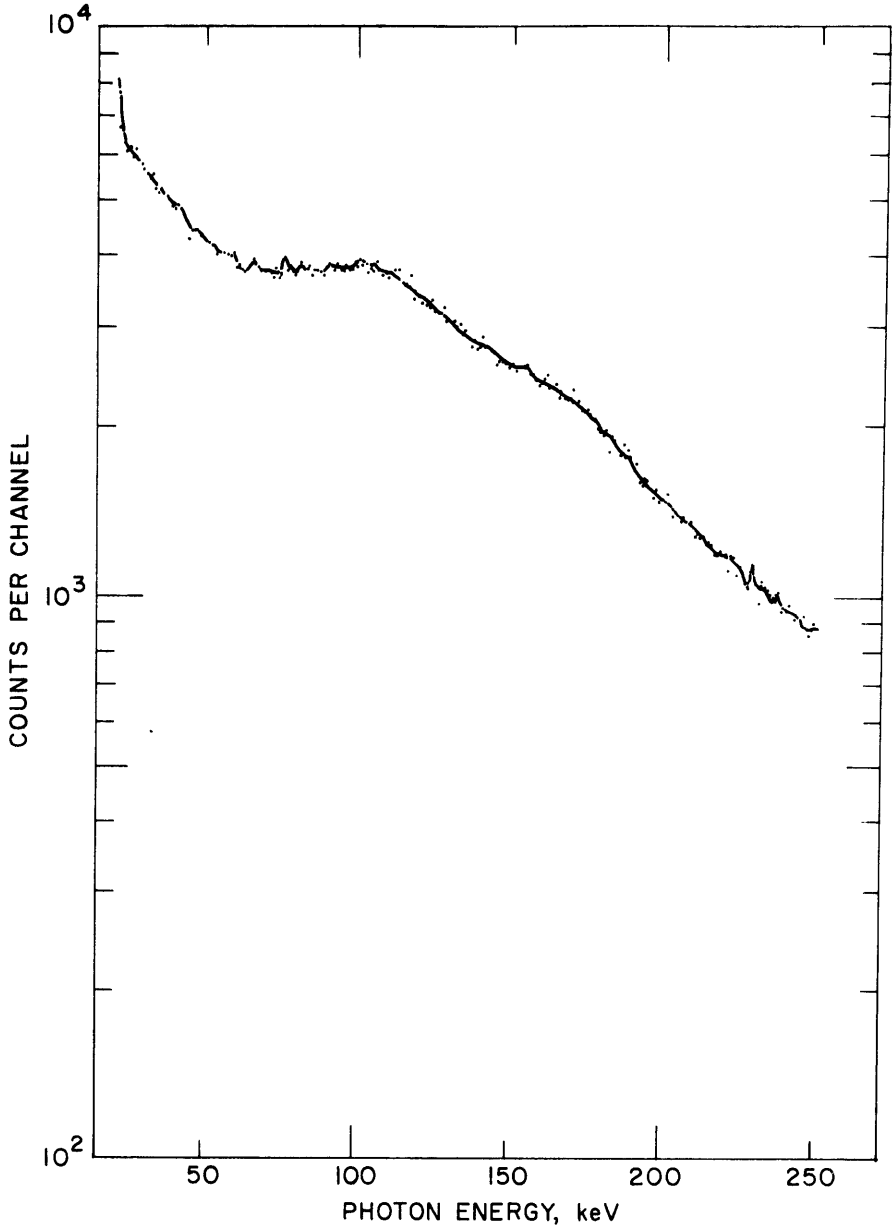

FIGURE 23 LOW ENERGY PORTION OF γ-RAY SPECTRUM OF FUEL ELEMENT 2M14 AFTER 18 HRS COOLING. Ge(Li) DETECTOR No. 9-19.1

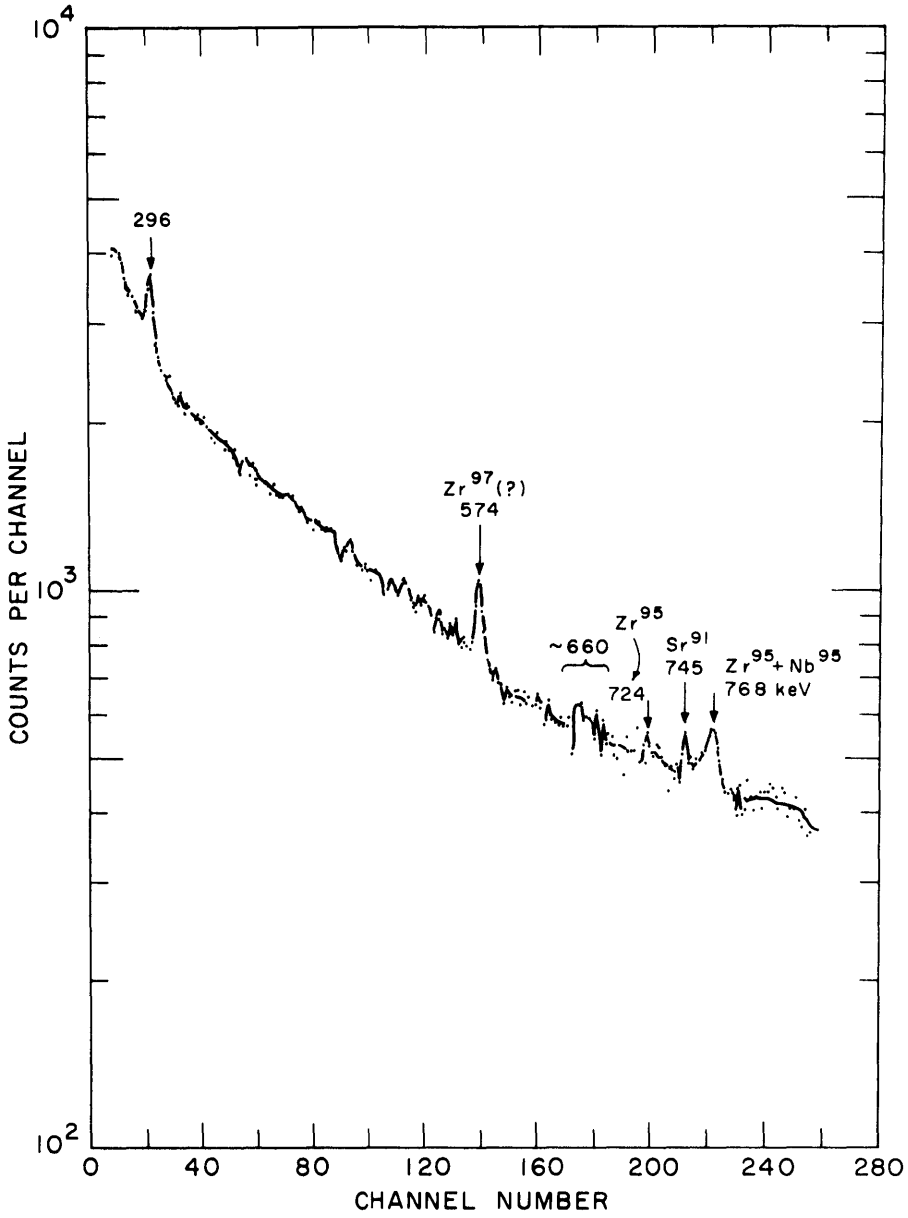

FIGURE 24 γ-RAY SPECTRUM OF FUEL ELEMENT 2M14 AFTER 18 HRS COOLING FOR ~280 TO 840 keV Ge (Li) DETECTOR No. 9-19.1

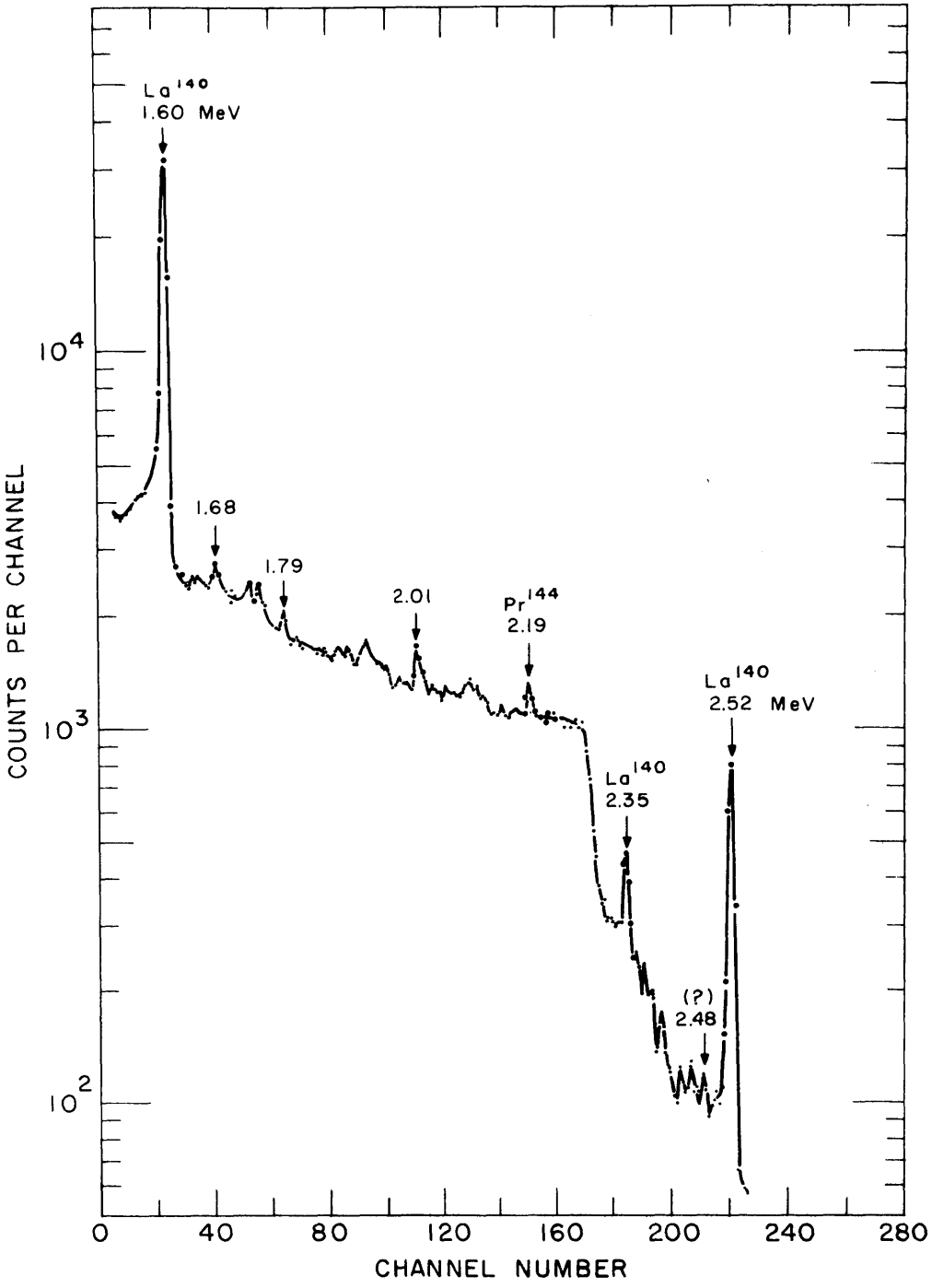

FIGURE 25 γ-RAY SPECTRUM OF FUEL ELEMENT 2M14 AFTER 18 HRS COOLING – ~1500 TO 2550 keV Ge(Li) DETECTOR No. 9-19.1

structure is apparent in the spectrum compared to that after 18 hours shown in Fig. 24. However, the large number of gamma-rays from short-lived isotopes plus the high Compton background prevents satisfactory resolution of the spectrum. The high energy portion after 40 hours cooling, shown in Fig. 27, is essentially the same as after 18 hours cooling of Fig. 25.

(iii) Cooling Period of 5 days:

The middle energy portion of the gamma-ray spectrum after five days cooling time is shown in Fig. 28. More gamma-rays are now resolved but have not been identified. Further studies are required to provide more definitive results for cooling times less than one week.

(iv) Cooling Period of 18 days:

The effect of the decay of short-lived gamma-emitters can be seen in Fig. 29 which shows the gamma-ray spectrum of 2M14 from about 570 to 835 keV after 18 days cooling. The Zr^{95}+Nb^{95} peaks are now well-defined, although they are probably still contaminated by other gamma-rays. The Cs^{137} peak at 662 keV is just discernible above the background, while the peak at 575 keV (Zr^{97}?) has decreased considerably in intensity. A group of gamma-rays with energies between 810 and 825 keV is also responsible for a broad peak in this region.

(b) Gamma-Scanning in Spent Fuel Storage Tank

The five fuel elements scanned in the spent fuel storage tank setup were 2-4, 2M1, 2M22, 2M19 and 2M31. Typical gamma-ray spectraof four elements are shown in Fig. 30. The relative

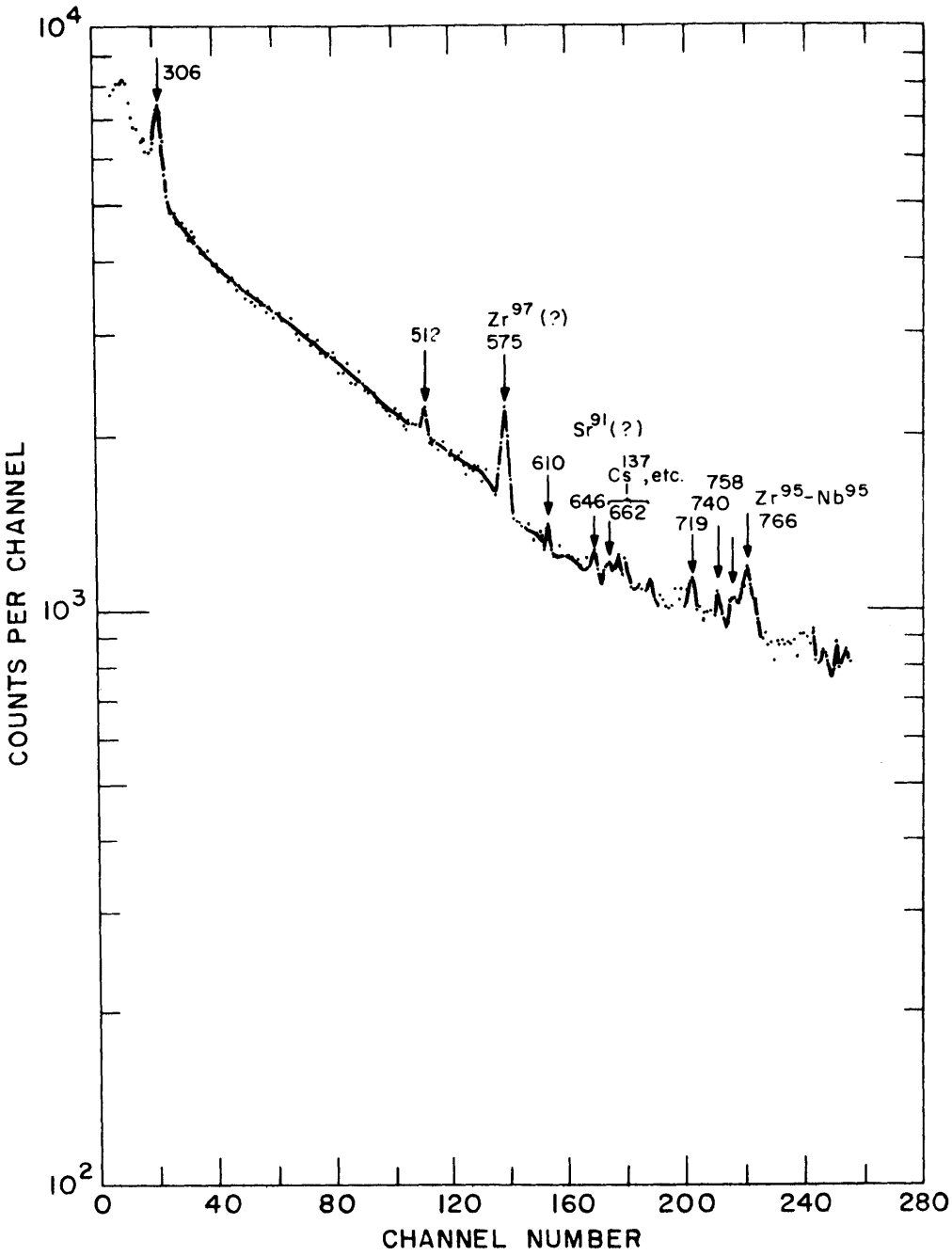

FIGURE 26 γ-RAY SPECTRUM OF FUEL ELEMENT ZM14
AFTER 40 HRS COOLING ~ 300 TO 850 keV
Ge(Li) DETECTOR No. 9-19.1

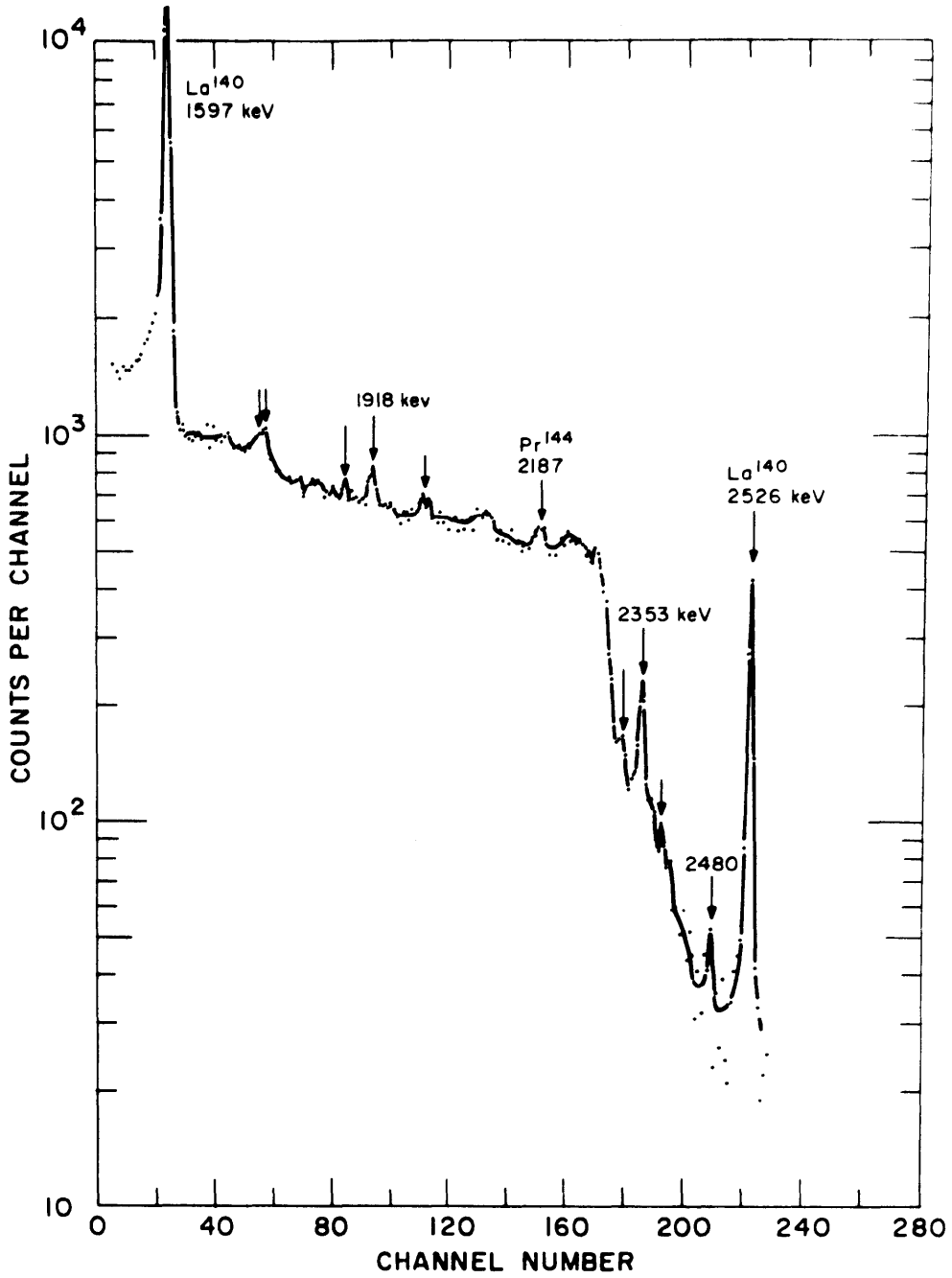

FIGURE 27 γ-RAY SPECTRUM (~1550 TO 2530 keV) OF FUEL ELEMENT 2MI4 AFTER 40 HRS COOLING TIME Ge(Li) DETECTOR No. 9-19.1 3.5 MM DEPLETION LAYER, 1.6 CM^2

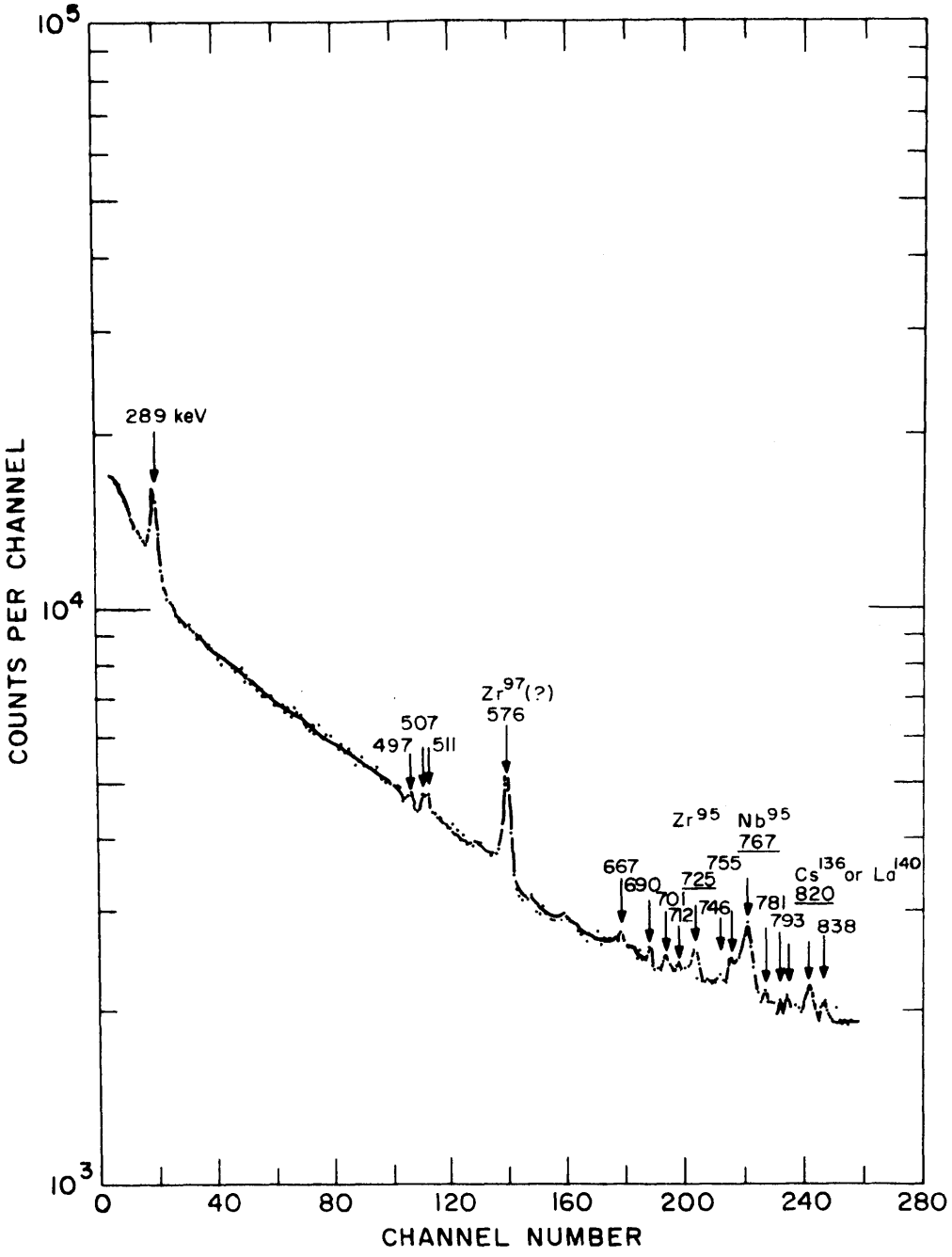

FIGURE 28 γ-RAY SPECTRUM OF FUEL ELEMENT 2M14
AFTER 5 DAYS COOLING ~ 275 TO 840 keV
Ge(Li) DETECTOR No. 9-19.1

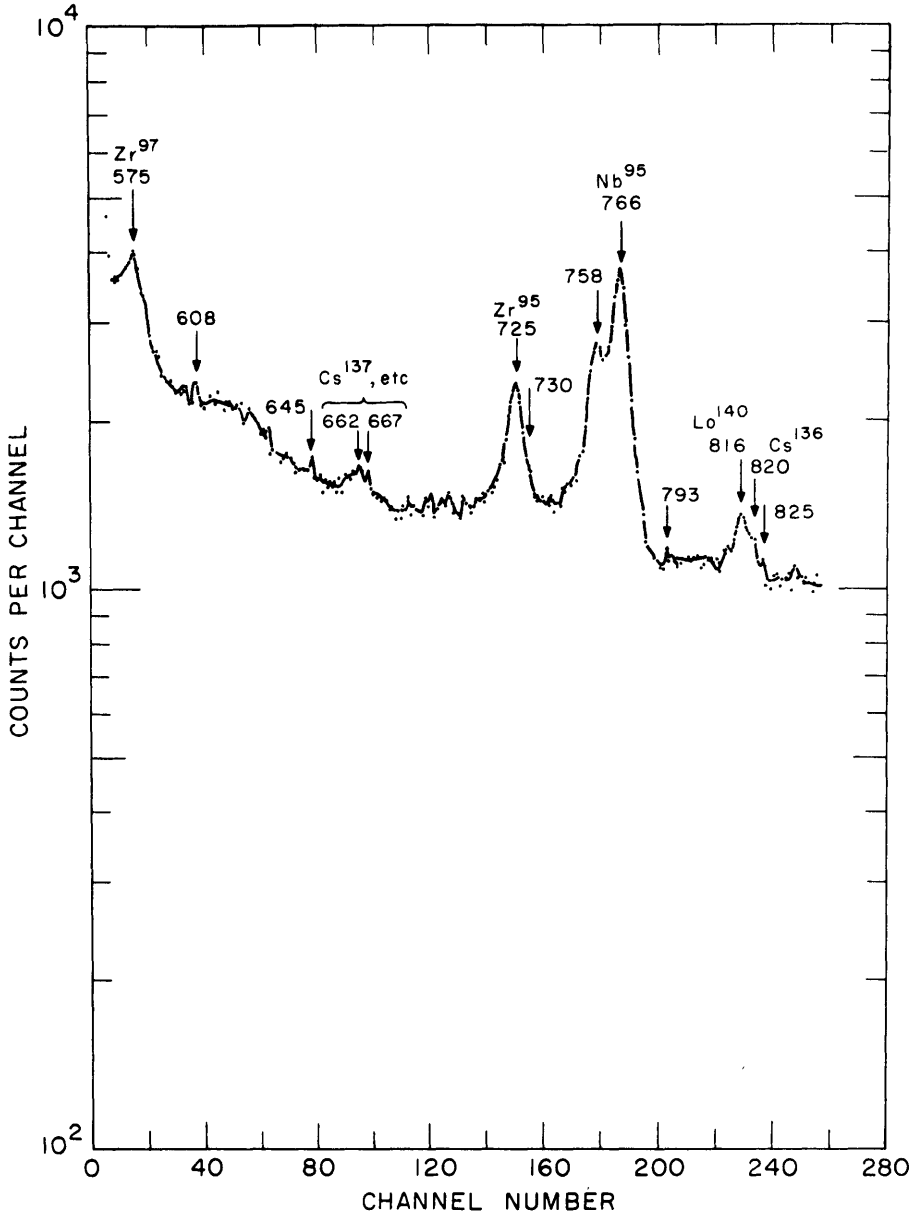

FIGURE 29 γ-RAY SPECTRUM OF FUEL ELEMENT 2M14 AFTER 18 DAYS COOLING- ~560 TO 830 keV Ge(Li) DETECTOR No. 9-19.1

heights of the curves are arbitrary as the purpose of the Figure was to show how the character of the spectra changes with cooling time.

(i) Fuel Element 2M31:

The gamma-spectrum of 2M31, Curve A in Fig. 30, after a cooling time of 11 days, shows resolved peaks for Ba^{140}+La^{140} and Zr^{95}+Nb^{95}. Background count rates during these runs were too excessive for high resolution studies because of inadequacy of the six feet of water to provide satisfactory shielding against the high level of radiation from the element. The amount of lead shielding the detector in turn was limited by space and strength of the supporting track.

(ii) Fuel Element 2M19:

Curve B of Fig. 30 gives the gamma-ray spectrum of 2M19 after nine months cooling, and shows peaks identified with gamma-rays from Zr^{95}+Nb^{95}, Rh^{106}, Cs^{134}, Cs^{137} and Pr^{144}. Most of these occur in the range 500 to 800 keV with only the Pr^{144} gamma-ray at 2186 keV contributing to the high energy portion. An enlarged view of the 500-800 keV region is presented in Fig. 31, and shows resolved peaks for Cs^{134} (2.19 yr.) at 605 and 796 keV; Rh^{106} (30 sec., daughter of Ru^{106}, $t_{1/2}$ = 1.0 yr.) at 624 keV; Cs^{137} (30 yr.) at 662 keV; Pr^{144} (12.5 min., daughter of Ce^{144}, $t_{1/2}$= 280 days) at 697 keV; Zr^{95} (65 days) at 724 keV with two partially resolved peaks for Zr^{95} at 758 keV and Nb^{95} (35 days) at 766 keV. For shorter cooling times than about one year, the Zr^{95}+Nb^{95} pair provide the major gamma-ray activity in this energy range.

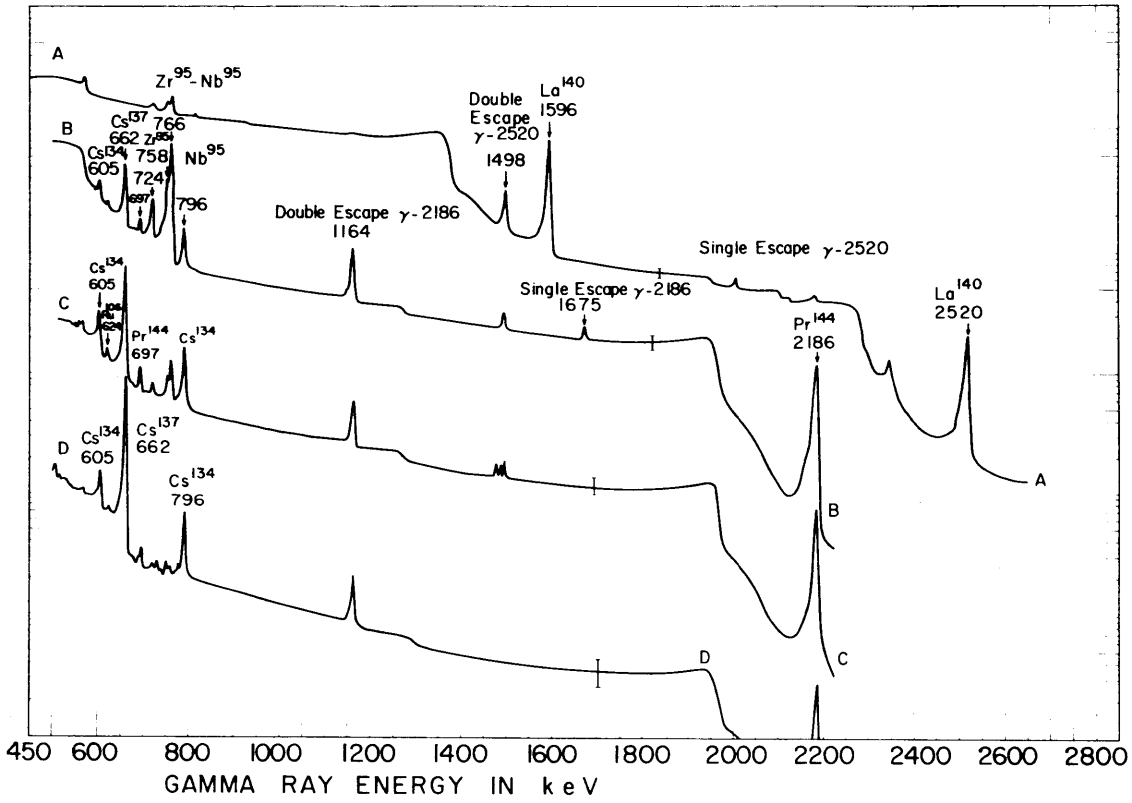

FIGURE 30 GAMMA-RAY SPECTRA OF MITR SPENT FUEL AS A FUNCTION OF COOLING TIME
GERMANIUM LITHIUM DRIFT DETECTOR No 9-19.1 3.5 mm DEPLETION DEPTH
170 VOLTS BIAS, 77°K

CURVE	FUEL ELEMENT	COOLING TIME
A	2M31	1 1/2 WEEKS
B	2M19	9 MOS.
C	2M22	1YR 6 MOS.
D	2M1	3YR 6 MOS.

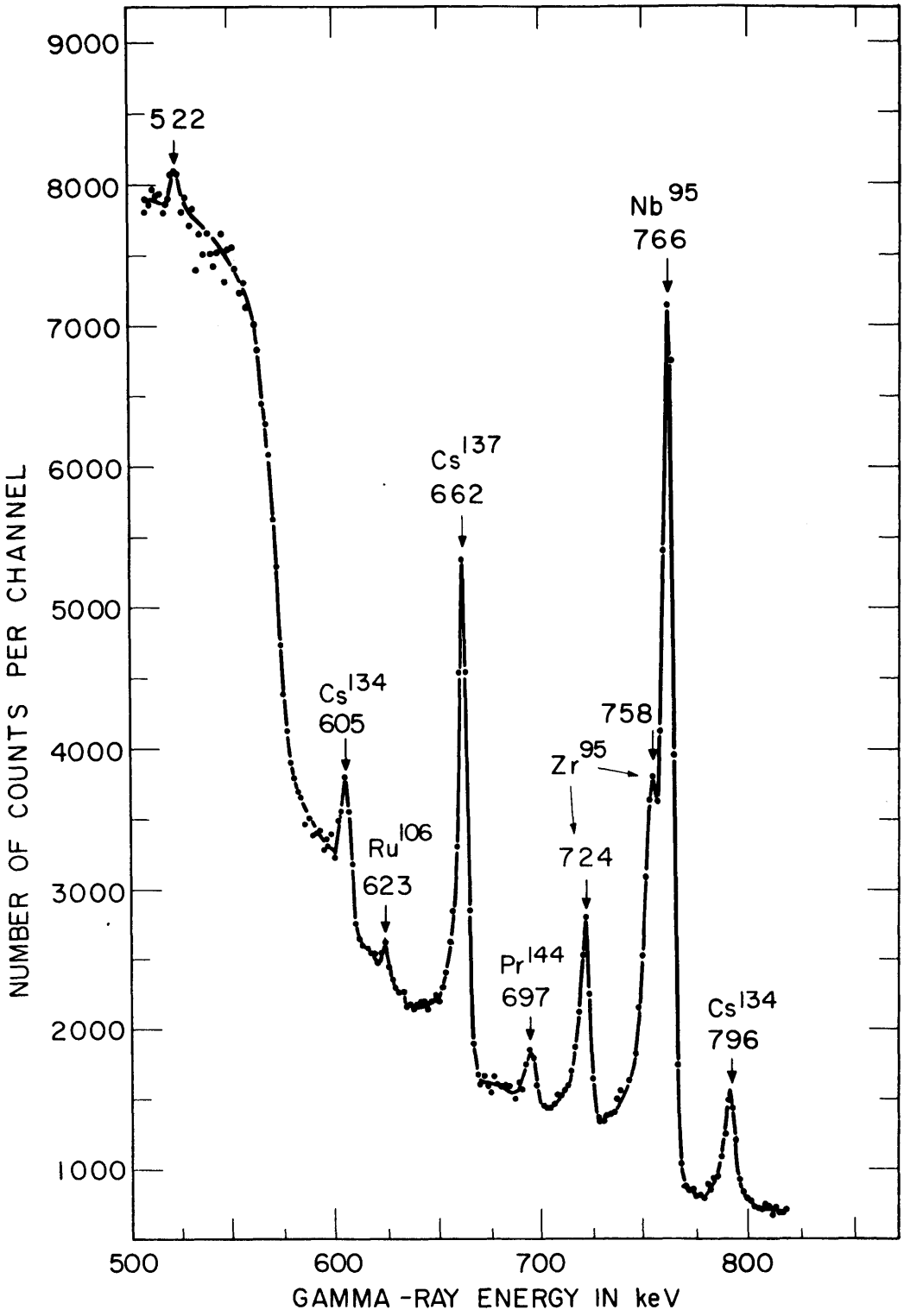

FIGURE 31 GAMMA-RAY SPECTRUM OF MITR FUEL ELEMENT 2M19 AFTER 9 MONTHS COOLING GERMANIUM LITHIUM DRIFT DETECTOR No. 9-19.2 3.5 mm DEPLETION DEPTH, 1.6 cm^2 170 VOLTS BIAS, 77°K RUN D4, 5/5/65

(iii) Fuel Element 2M22:

After 1 1/2 years cooling time, as shown in Curve C of Fig. 30 and in Fig. 32, the most prominent peaks are due to Cs^{134} and Cs^{137}, whereas the Zr^{95}+Nb^{95} activity is considerably reduced.

(iv) Fuel Element 2M1:

The element investigated having the longest cooling time, 3 1/2 years, was 2M1, for which the gamma-ray spectrum is shown in Curve D of Fig. 30 and an enlarged view is given in Fig. 33 for the medium energy range. Cesium-137 provides the major activity, with a smaller contribution from Cs^{134}. However, because of the low burnup attained in 2M1, there is a proportionally smaller amount of Cs^{134} in this element than in those previously discussed with higher burnups. This is because Cs^{134} is not a direct fission product but is an (n,γ) reaction product of Cs^{133}. Further discussion of this is made in Section IV to follow.

Close examination of some of the peaks indicates the possibility of the presence of other fission product gamma-rays. Both in Fig. 32 and Fig. 33, for elements 2M22 and 2M1, the Pr^{144} peak at 697 keV had a width greater than would be expected from the prevailing experimental energy resolution. It is felt that some other fission product was contributing a gamma-ray of low intensity at an energy slightly below 697 keV. The low energy tail of the 697 keV gamma-ray in Fig. 33 appears to be due to this other gamma-ray at about 692 keV, with a half-life greater than that of Ce^{144} (280 days). Europium-154

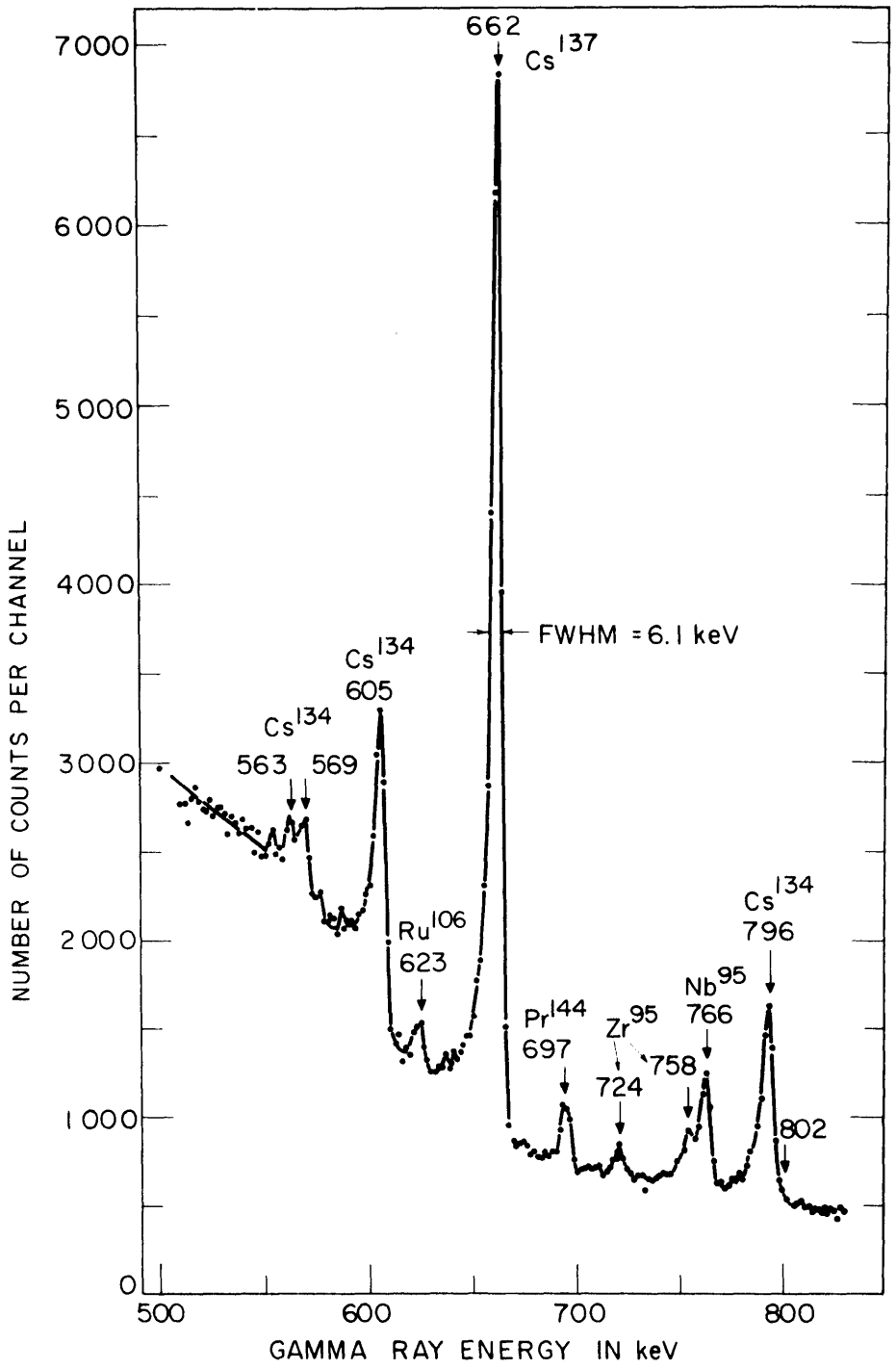

FIGURE 32 GAMMA-RAY SPECTRUM OF MITR FUEL ELEMENT 2M22 AFTER 1 1/2 YEARS COOLING GERMANIUM LITHIUM DRIFT DETECTOR No. 9-19.1 3.5 mm DEPLETION DEPTH, 1.6 cm^2 170 VOLTS BIAS, 77°K RUN H1, 5/19/65

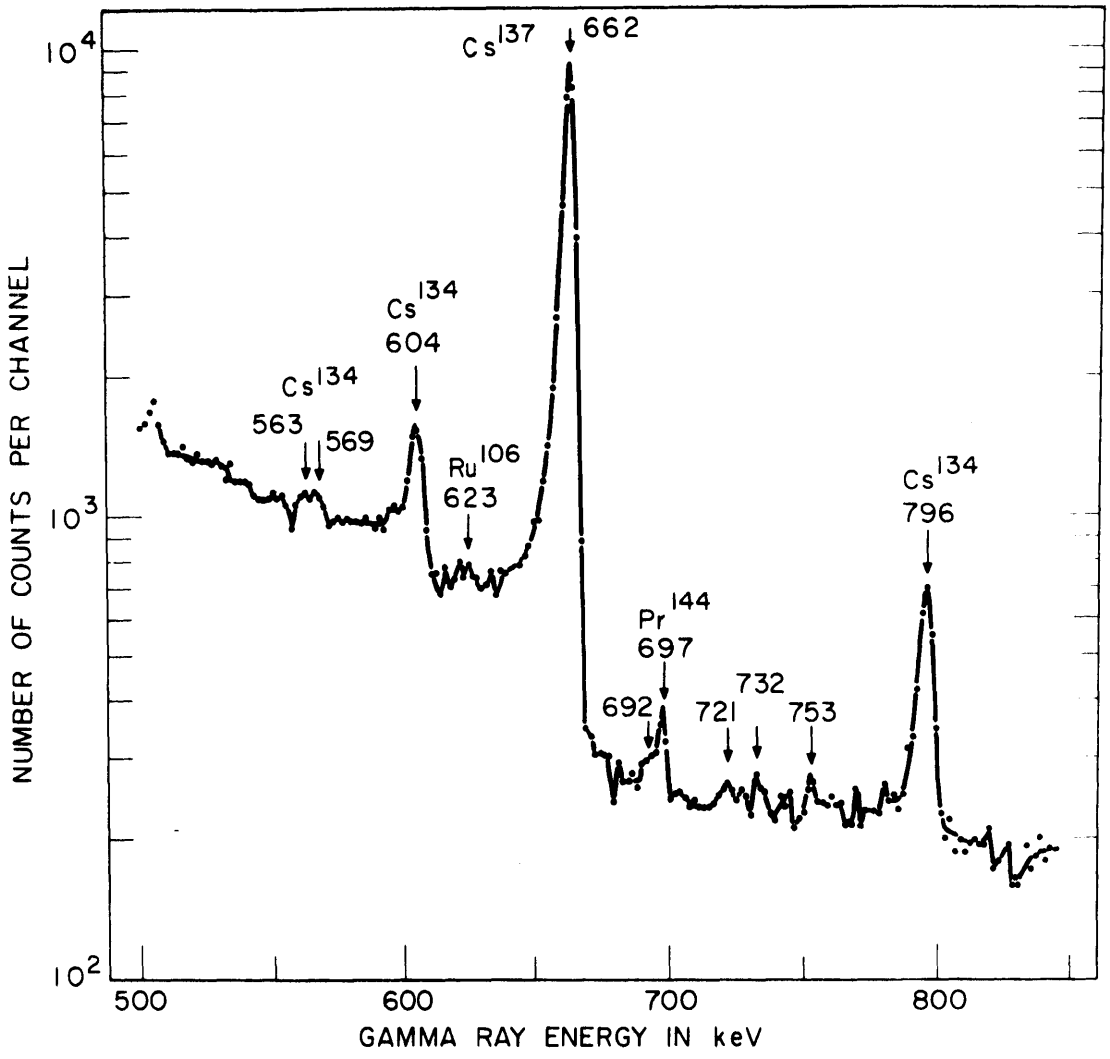

FIGURE 33 GAMMA-RAY SPECTRUM OF MITR FUEL ELEMENT 2M1 AFTER 3 1/2 YEARS COOLING GERMANIUM LITHIUM DRIFT DETECTOR No. 9-19.1 3.5 mm DEPLETION DEPTH, 1.6 cm^2 170 VOLTS BIAS, 77°K RUN G14, 5/18/65

(16 yr.) or Eu^{152} (12.7 yr.) have gamma-rays in this region, are of low yield and have the necessary long half-lives.

Similar circumstances were noticed for the Rh^{106} peak at 624 keV. Energy determinations of this gamma-ray from a Ru^{106}+Rh^{106} source indicated a value near 622 keV. However, fuel element spectra calibrations gave a value between 623 and 624 keV. It is possible that another peak of lower intensity slightly higher in energy than 622 keV is causing the peak to shift. Figure 33 indicates this possibility as a number of peaks appear to be present in the 623 keV region.

2. Calculation of Gamma-Ray Intensities

In order to determine the fission product activities in the fuel elements, it was necessary to calculate the intensities of their gamma-rays from spectra as shown above. The gamma-ray intensities were then converted to the corresponding activities using known or measured nuclear data. A number of methods have been developed for calculating gamma-ray intensities from scintillation crystal spectrometer results, e.g. spectrum stripping, least squares analysis, etc. (01). However, since gamma-ray spectra from Ge(Li) detectors are considerably different than those from NaI crystals, it was not certain that computer techniques developed for the latter would be as successful for the germanium detectors. Similarly, the spectrum stripping method requires using a known intensity of the same gamma-ray source as is present in the unknown. The fission product sources used in these investigations were not available at the time the fuel element spectra were being recorded. Con-

sequently, this method was not possible. Initial attempts to calculate the intensities with the use of a simple background subtraction method led to inconsistent results. Therefore, a series of experiments were conducted and their results analyzed to determine a satisfactory method for calculating gamma-ray intensities. These experiments and results are described in more detail in Appendix D.

The method developed essentially calculates an average integral under the gamma-ray peak using several channels on either side of the peak as end-points. First, an average background is calculated over three or five channels on the high energy side of the peak. Then, a linearly varying background under the peak is assumed using the counts in a channel on the low energy side of the peak as the low energy background value. The net counts contributed by the gamma-ray are obtained by subtracting the total background from the total integral, both being calculated between the two end points. This procedure is repeated using a number of different channels on the low energy side of the peak as one of the end-points, with each resulting in a value for the net number of counts under the photopeak. Because of statistical fluctuations, the net integral varies considerably. However, the mean of five or more such adjacent values was shown to yield results reproducible to within about twice the statistical uncertainty.

The above procedure was programmed in FORTRAN for the IBM 7094 and the resulting code, GRAPIN, was used to calculate the net counts under the gamma-ray peaks for the fuel element

spectra. A listing of GRAPIN, along with a description of input data format is given in Appendix E.

Tables of the net counts under the various fission product gamma-ray peaks as calculated by the code are presented in Appendix F. A graphical presentation and discussions of these data are made in the following section.

3. Spatial Distributions of Gamma-Ray Intensities in MITR Fuel Elements

(a) Fuel Element 2M19

Fuel Element 2M19 was studied more extensively than any of the others because it had the most constant irradiation pattern during its in-pile residence time, having remained in position 17 from the beginning of its operation to its removal. The cooling time of nine months meant that most short-lived isotopes had decayed, while the gamma-ray spectra indicated the feasibility of calculating intensities for a number of the long-lived fission products. Consequently, much of the following discussion will be devoted to the analysis and results of the experiments on 2M19.

Each spectrum was recorded for 80 minutes using an aperature diameter of 1/8 inch for the bottom lead collimator and a 0.135 in. thick lead shield across the gamma-ray beam to decrease the low energy photon count rates. The net gamma-ray peak counts for each run are given in Table F.1 in Appendix F.

The relative axial distributions of the counts for Cs^{137}, Zr^{95} (γ-724 keV) and Cs^{134} (γ-605 keV) are shown in Fig. 34. The Cs^{137} activity, having a long half-period, is proportional to the local total fission density, and thus also is a good

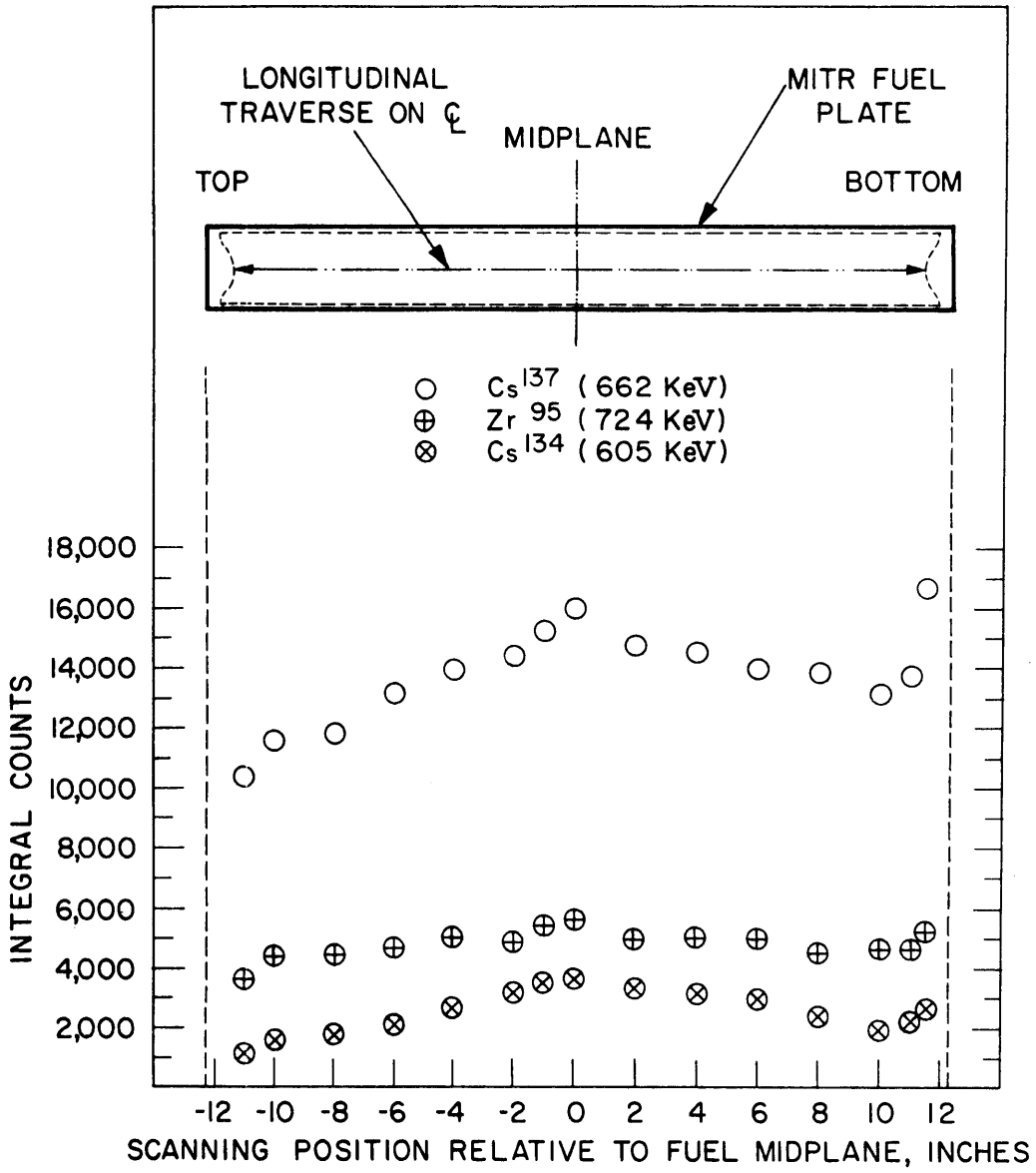

FIGURE 34 RELATIVE AXIAL DISTRIBUTIONS OF Cs^{137}, Zr^{95} (γ-724) AND Cs^{134} (γ-605) ACTIVITIES FOR MITR FUEL ELEMENT 2MI9 AFTER 9 MONTHS COOLING

neutron flux indicator. For this reason, the Cs^{137} activity is assymetric about the central midplane because of the flux depression at the top created by the presence of the control rods. Meanwhile, a pronounced peak in the Cs^{137} load is seen at the bottom of the element near the fuel-moderator interface. This corresponds to the increase in the neutron flux in this region due to the decreased neutron absorption in the moderator. Similar distributions were measured for the Cs^{134} and Zr^{95} activities.

The axial distributions of the three gamma-ray activities of Pr^{144} at 697, 1164 and 2186 keV are shown in Fig. 35, while that for the 624 keV gamma-ray peak of Rh^{106} is shown in Fig. 36. Because of the low intensity of the Rh^{106} gamma-ray and the high background, the statistical deviations in the net counts of Rh^{106} are at times larger than the integral; thus meaningful interpretations of the distribution of this fission product were not possible. However, since the yield of the mass 106 chain in Pu^{239} thermal fissions is more than 10 times greater than in U^{235} fissions (see Table 2), the Rh^{106} gamma-ray peak should be considerably greater in spectra of low enrichment irradiated fuel, in which a significant fraction of the fissions are in plutonium.

The values for the fission product net counts at the fuel midplane appear anomalously high in Figs. 34 and 35. This phenomenon is probably not real but rather is due to electronics. The data at -1 in. (Run D4) and 0 in. (Run D5) were taken soon

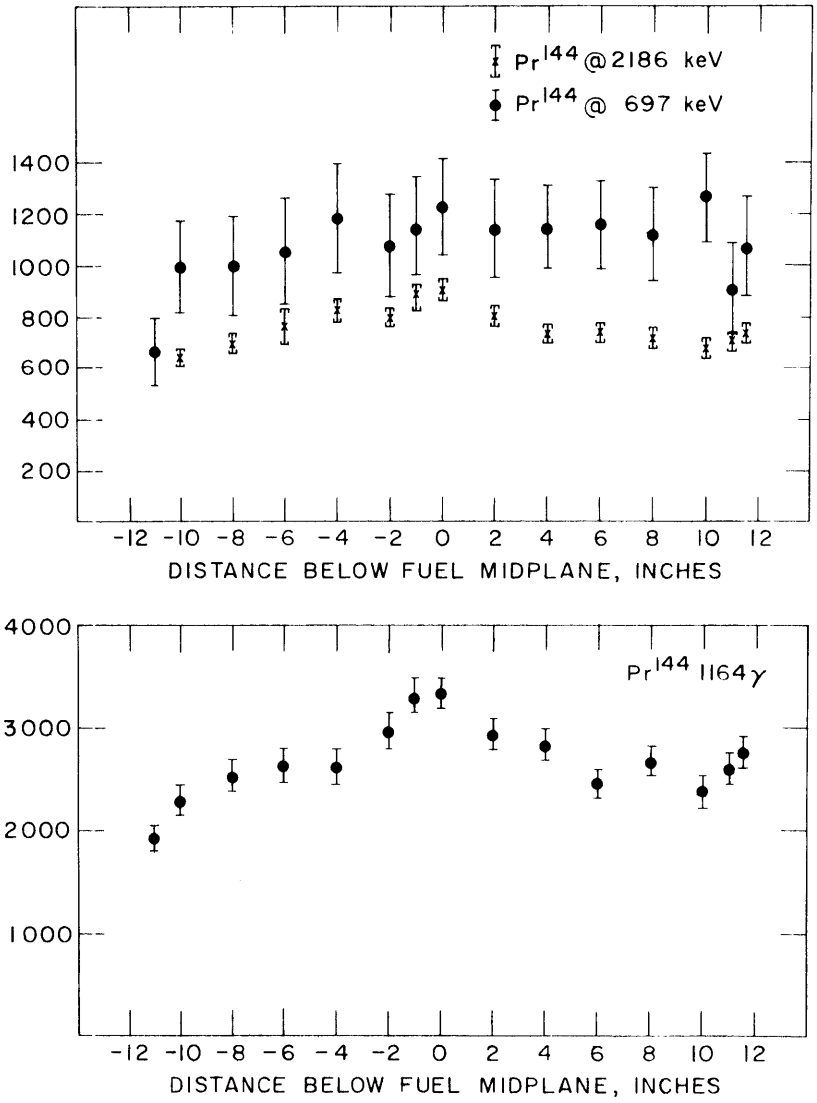

FIGURE 35 γ-RAY ACTIVITIES FOR Pr^{144} ALONG FUEL ELEMENT 2M19

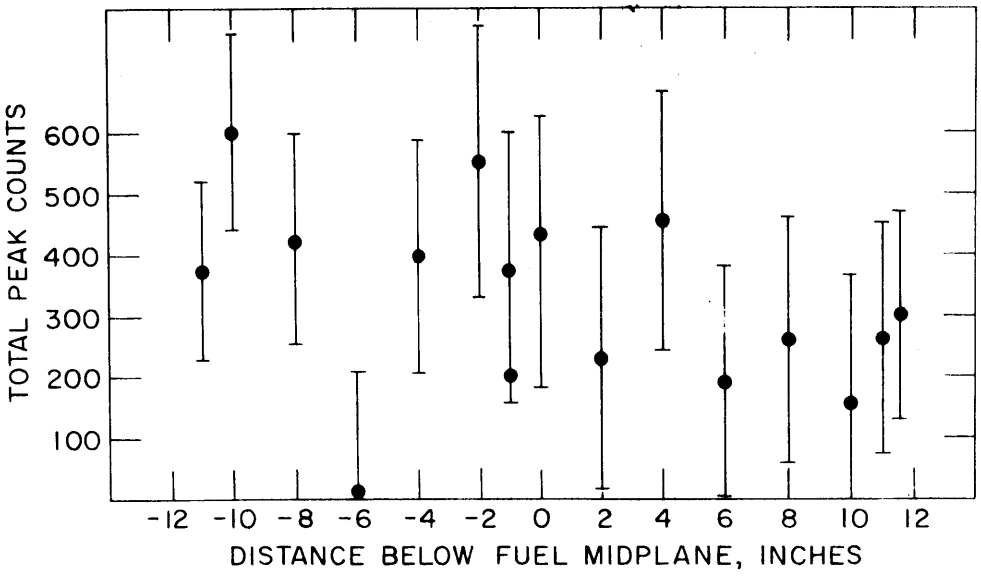

FIGURE 36 Rh^{106} ACTIVITY (624 keV γ)
ALONG FUEL ELEMENT 2M19

after some vacuum tubes in the preamplifier and amplifier had been replaced. The electronic system thus may not have completely stabilized. Consequently, the absolute values of the fission product activities may be in error. The point at -1 in. was repeated at a later time in Run D18 and gave a lower value, as shown in Table F.1. The ratios of activities should not, however, be greatly in error (see Table 6).

The results of a transverse scan are shown in Fig. 37 for Cs^{134}, Zr^{95} and Cs^{134} at an axial position 1 in. above the fuel midplane. Included is a schematic diagram showing the direction of scanning across the large-area faces of the fuel plates. The results are repeated in Fig. 38 along with those for Rh^{106}, Pr^{144} and Zr^{95}+Nb^{95}. Results of similar transverse scans made at 6 in. below and 6 in. above the element midplane are given in Table F.1, Appendix F.

Partial results for a transverse scan in which the detector viewed the edges of the fuel plates are shown in Fig. 39. A 1/8 in. diameter aperature was used in the bottom collimator with 0.135 in. Pb shielding across the gamma-ray beam. Spectra were recorded at intervals of 1/16 in., progressing from near the central plate towards the outer plate. The large variations in the Cs^{137} activity are due to the differing amounts of fuel seen by the detector through the collimating aperature. Shown by the crosses in Fig. 39 is the positional dependence of the calculated ratio of projected area of that part of a fuel plate seen through the aperature to the total projected area of one plate if viewed from the same position. The Cs^{137} and area

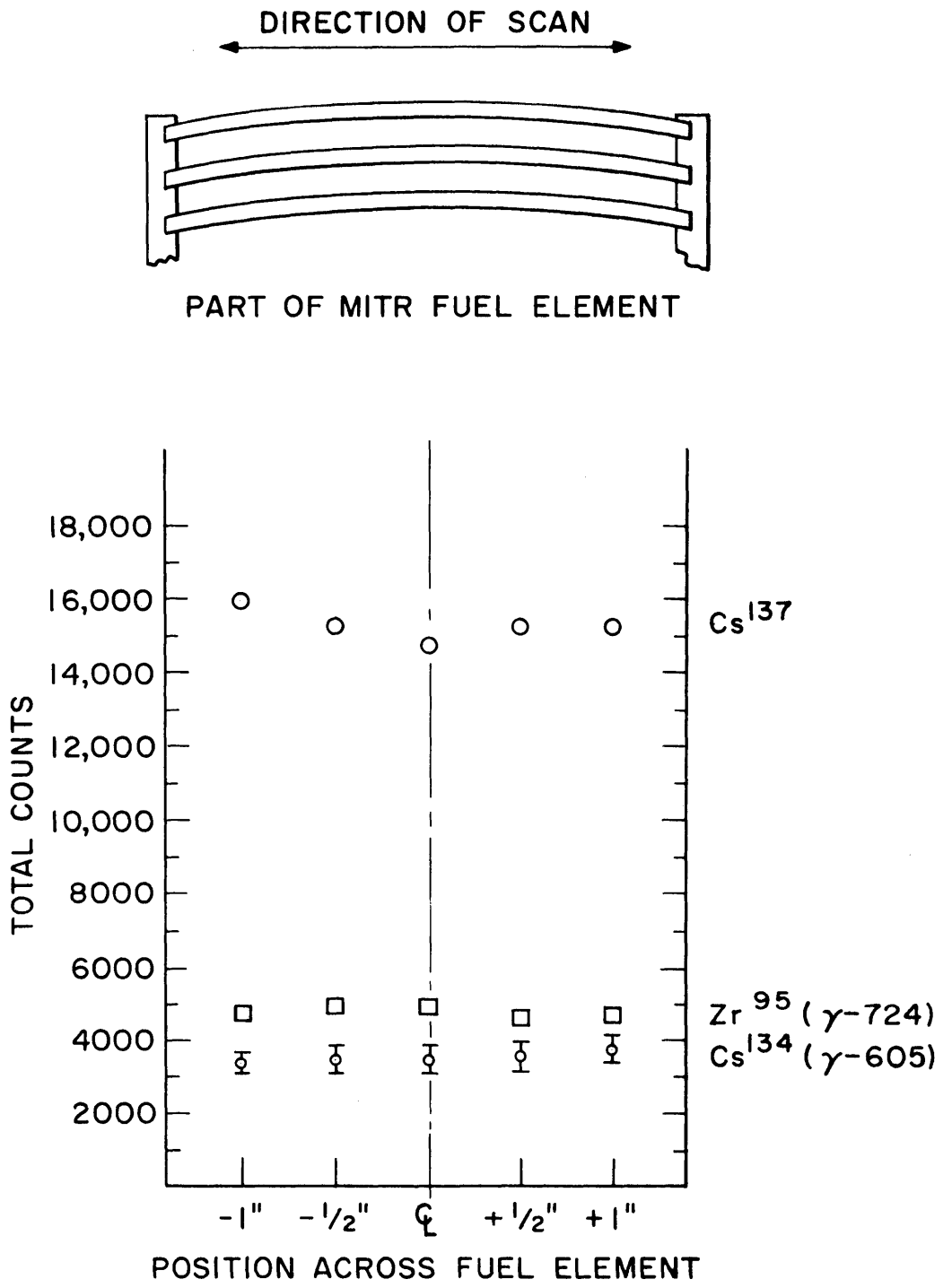

FIGURE 37 RESULTS OF TRANSVERSE SCAN SHOWING Cs^{137}, Zr^{95}(γ - 724 kev) AND Cs^{134}(γ-605 kev) ACTIVITIES AS A FUNCTION OF POSITION ACROSS FUEL ELEMENT 2M19 AFTER 9 MONTHS COOLING TIME.

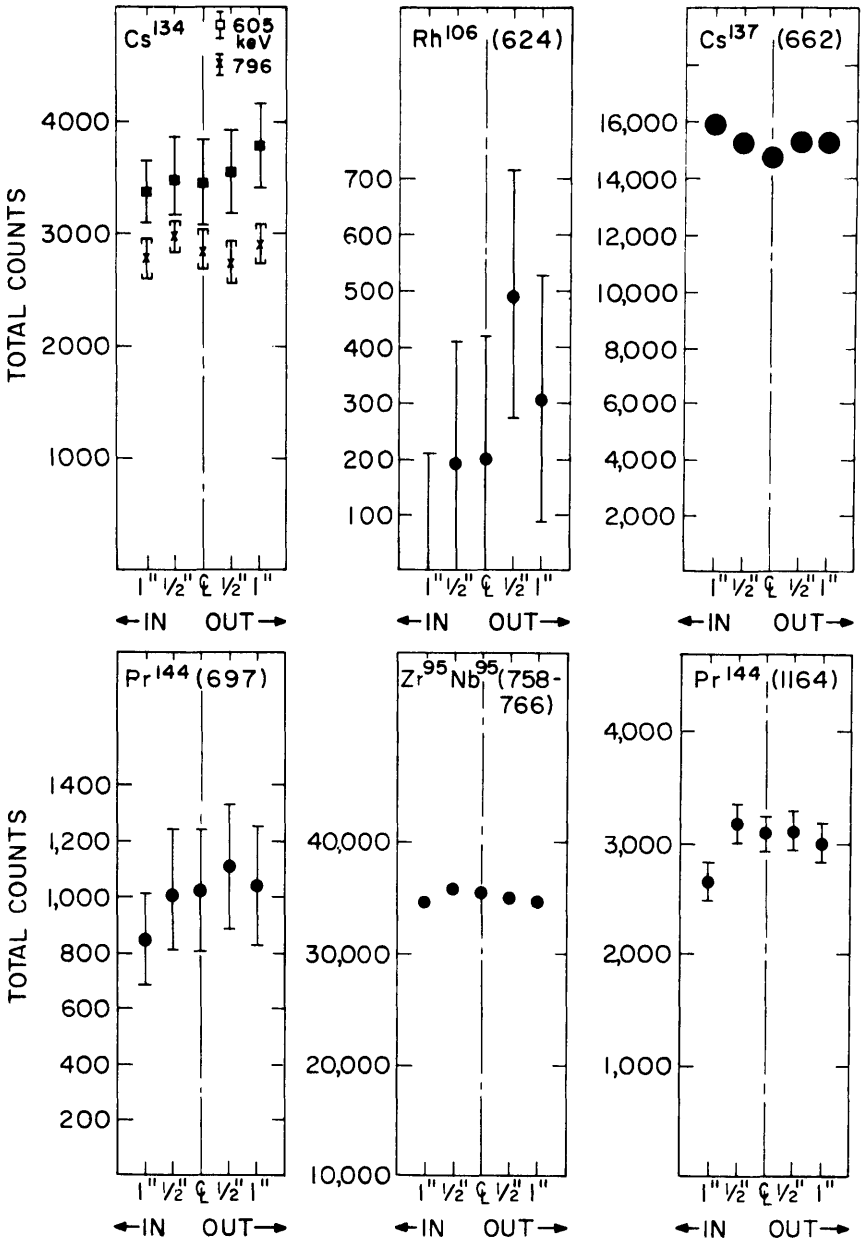

FIGURE 38 γ-RAY ACTIVITIES OF FISSION PRODUCTS Cs^{134}, Rh^{106}, Cs^{137}, Pr^{144}, Zr^{95} AND Nb^{95} AS A FUNCTION OF POSITION FOR TRANSVERSE SCAN AT 1" ABOVE MIDPLANE OF FUEL ELEMENT 2MI9

ratios were normalized in the following way: the lowest value of Cs^{137} counts was chosen to correspond to the smallest area ratio of fuel plate. This value of 8485 from Run D36 was divided by the lowest fuel plate calculated ratio of 0.55. Thus the value of the Cs^{137} ratio was set equal to the plate area ratio at a position +1/16 in. from the reference zero line. The other Cs^{137} counts were multiplied by 0.55/8485, and the resulting ratios plotted at the measured distances from the reference zero line. It is seen that the positional variations of both these quantities agree very well, therefore justifying the conclusion that the count rate fluctuations are due to variations in the amount of fuel viewed by the detector and not some other phenomenon.

These results indicate the high spatial resolution attainable with this type of experimental arrangement. Due to the curvature of the plates, it may even be possible to investigate spatial distributions of fission product activities for each individual fuel plate within the element itself using smaller aperature diameters for collimation and a more precise scanning system.

(b) Fuel Element 2M22

The results of axial scans of 2M22 are shown in Fig. 40 for Cs^{137} and Cs^{134} (γ-604 keV). This element had a predicted U^{235} burnup about 20% higher than 2M19. The low value for the fission product counts at the bottom of the element is probably due to the fact that the uranium fuel in some of the plates did not extend to within 1/2 in. of the end of the plate. Included

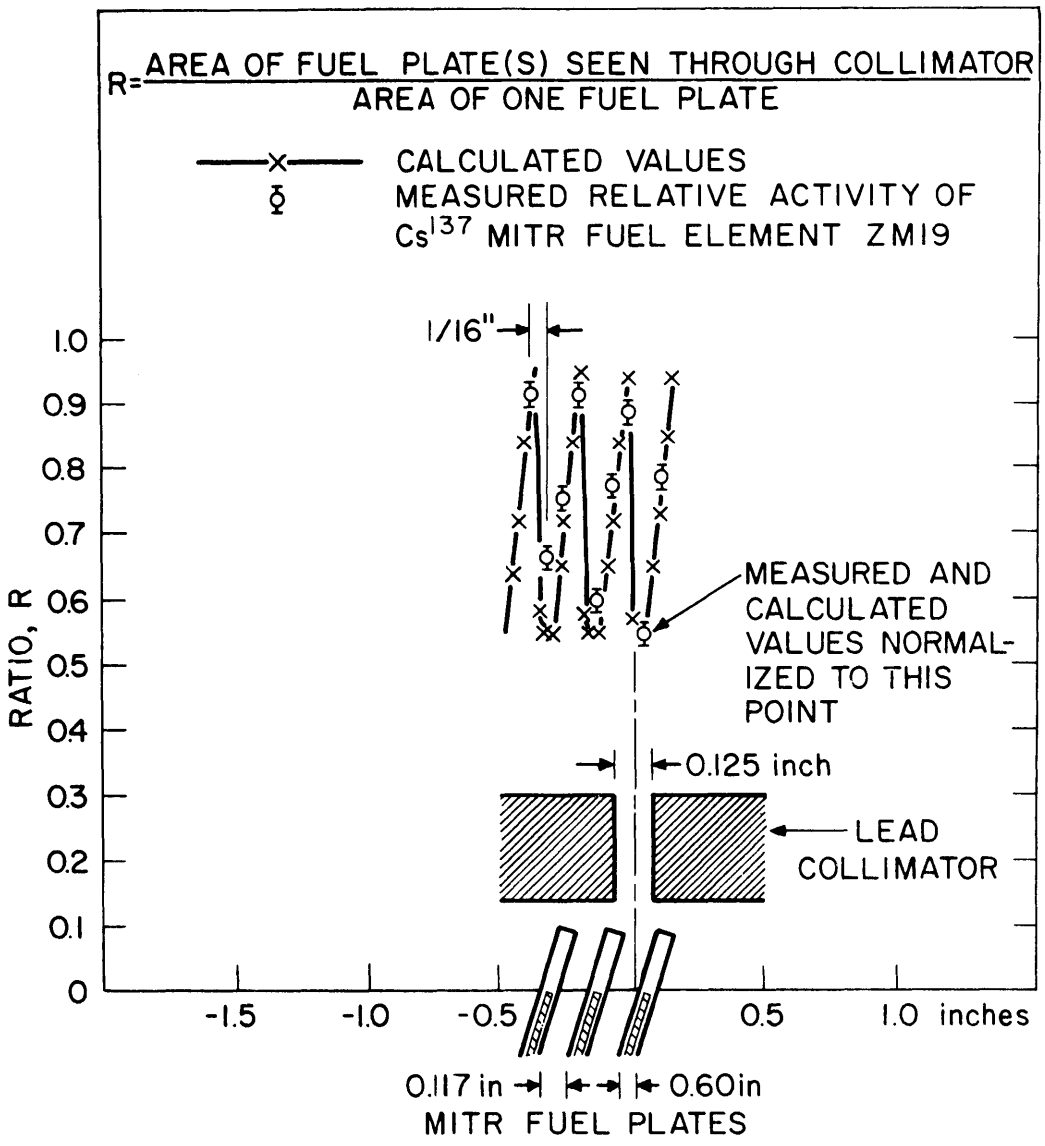

FIGURE 39 RESULTS OF TRANSVERSE SCAN USING 0.125 in. DIA. APERATURE IN Pb COLLIMATOR SHOWING COMPARISON BETWEEN MEASURED RELATIVE Cs^{137} ACTIVITY AS A FUNCTION OF POSITION WITH CALCULATED FRACTION OF FUEL PLATE AREA SEEN BY DETECTOR THROUGH APERATURE

in Fig. 40 are results of measurements made upon the same elements with the 6-meter, bent-quartz crystal spectrometer for the 133 keV gamma-ray of Ce^{144} (M3). The Ce^{144} counts have been normalized to be equal to the Cs^{137} counts at the fuel midplane. The two distributions agree reasonably well, although the Ce^{144} results are lower than the Cs^{137} results near the bottom of the element. This may not be a real phenomenon, but may be caused by the normalization itself. Some differences may be expected since the 133 keV gamma-ray of Ce^{144} will be heavily attenuated in the fuel and the results may be representative of only the first few fuel plates. The Cs^{137} gamma-ray, on the other hand, is not absorbed as greatly and therefore represents an integrated effect for the whole element.

Figure 41 shows the axial distributions of Zr^{95} (γ-724 keV), the twin peaks of Zr^{95}+Nb^{95} and the double escape peak of Pr^{144} at 1164 keV. The Zr^{95} results have a relatively large statistical error because of the small size of the photopeak above the high background (see Fig. 31). The Rh^{106} and Pr^{144} (γ-697 keV) and (γ-2186 keV) axial distributions are given in Fig. 42.

Gamma-ray spectra were not obtained between +10 in. to +11 1/2 in. below the midplane of 2M22. Consequently, no observations were made in the region where the flux peaking would have caused an increase in the fission product activity.

Results of a transverse scan at the axial midplane of 2M22 are presented in Fig. 43. Cesium-137 shows a pronounced dip

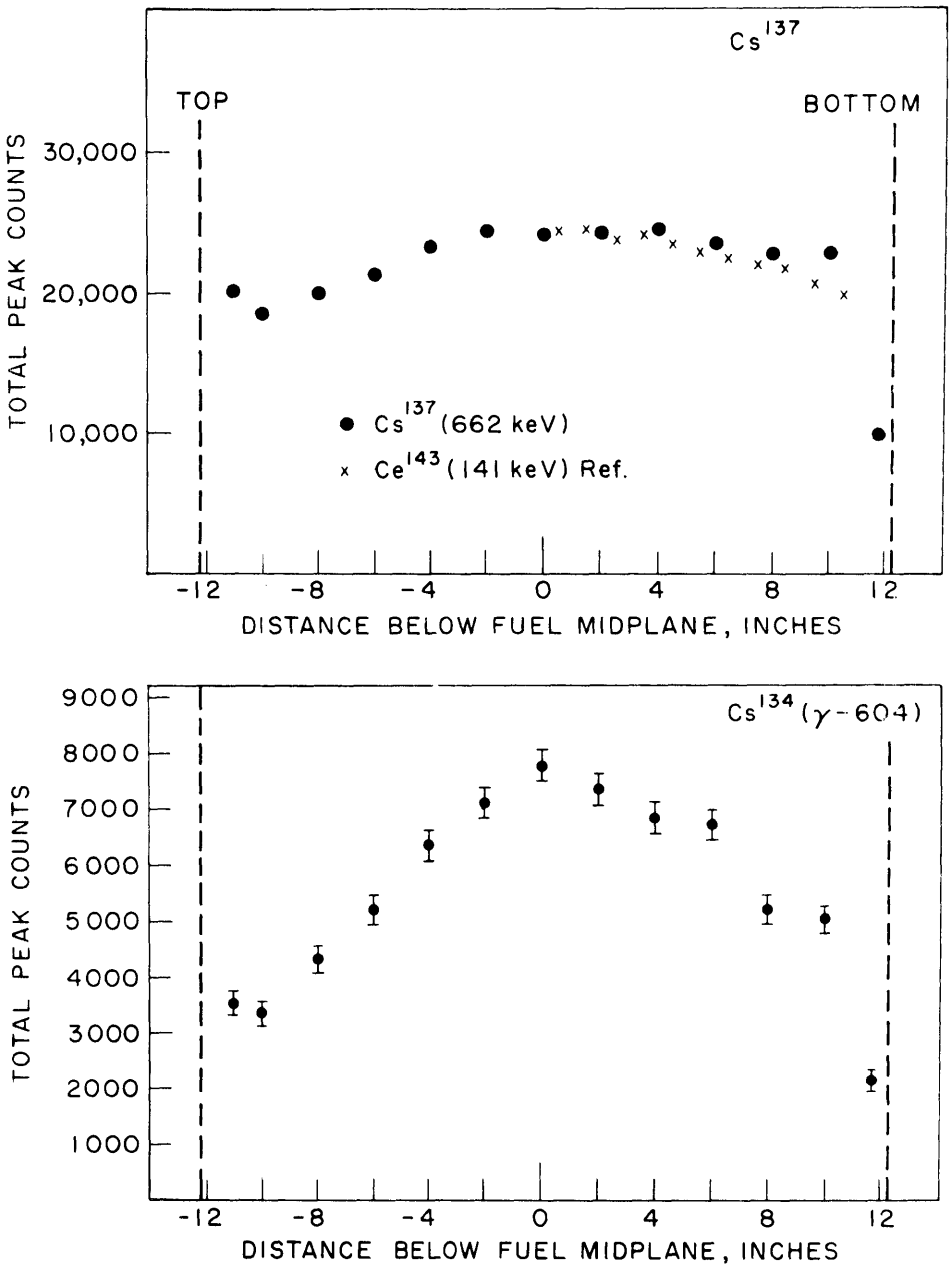

FIGURE 40 AXIAL DISTRIBUTION OF Cs^{137} AND Cs^{134} (γ-604 keV) ACTIVITIES FOR FUEL ELEMENT 2M22 AFTER 1½ YEARS COOLING TIME

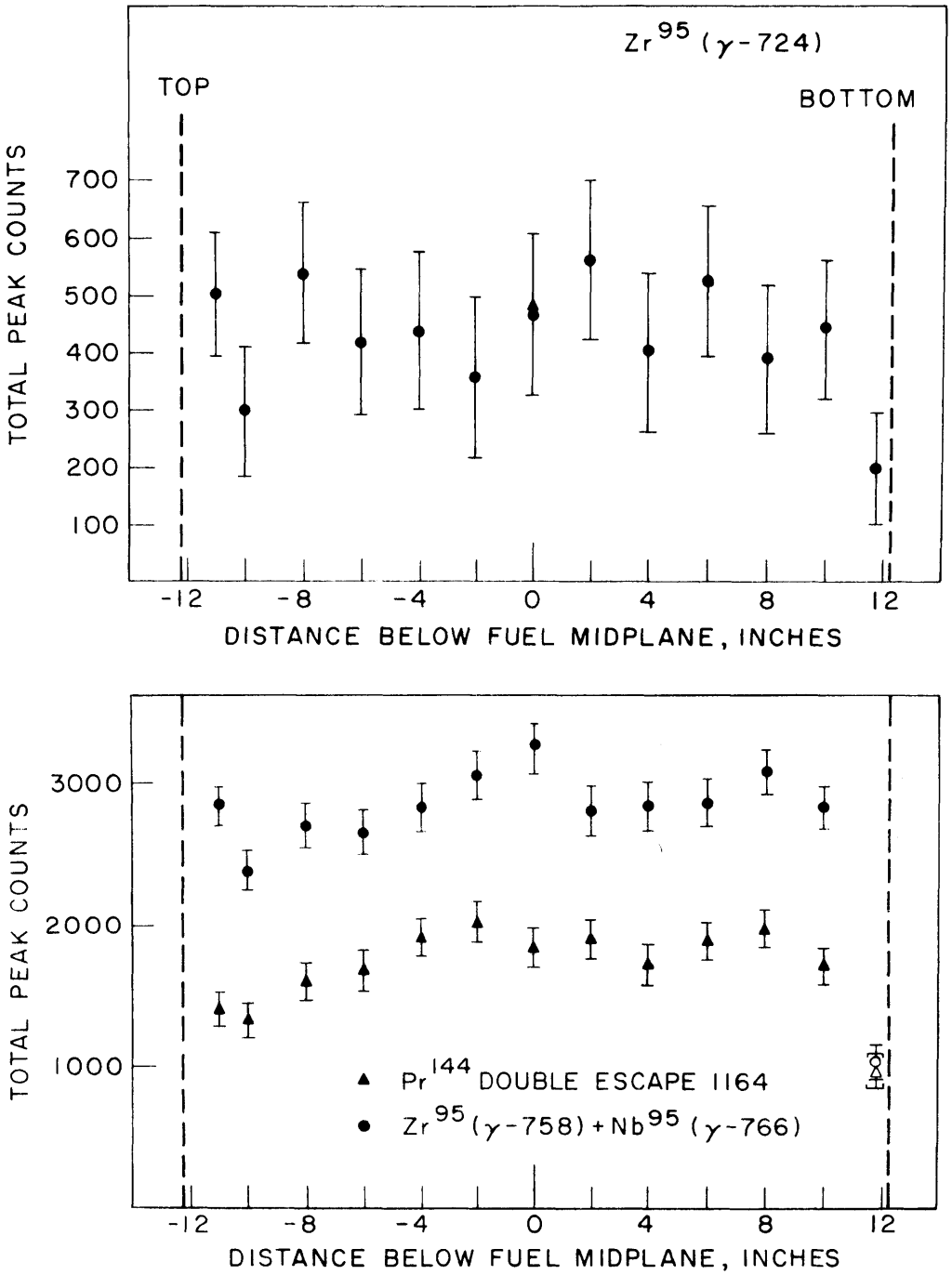

FIGURE 41 AXIAL DISTRIBUTION OF Zr^{95}, Nb^{95} AND Pr^{144} γ-RAY ACTIVITIES FOR FUEL ELEMENT 2M22 AFTER $1\frac{1}{2}$ YEARS COOLING

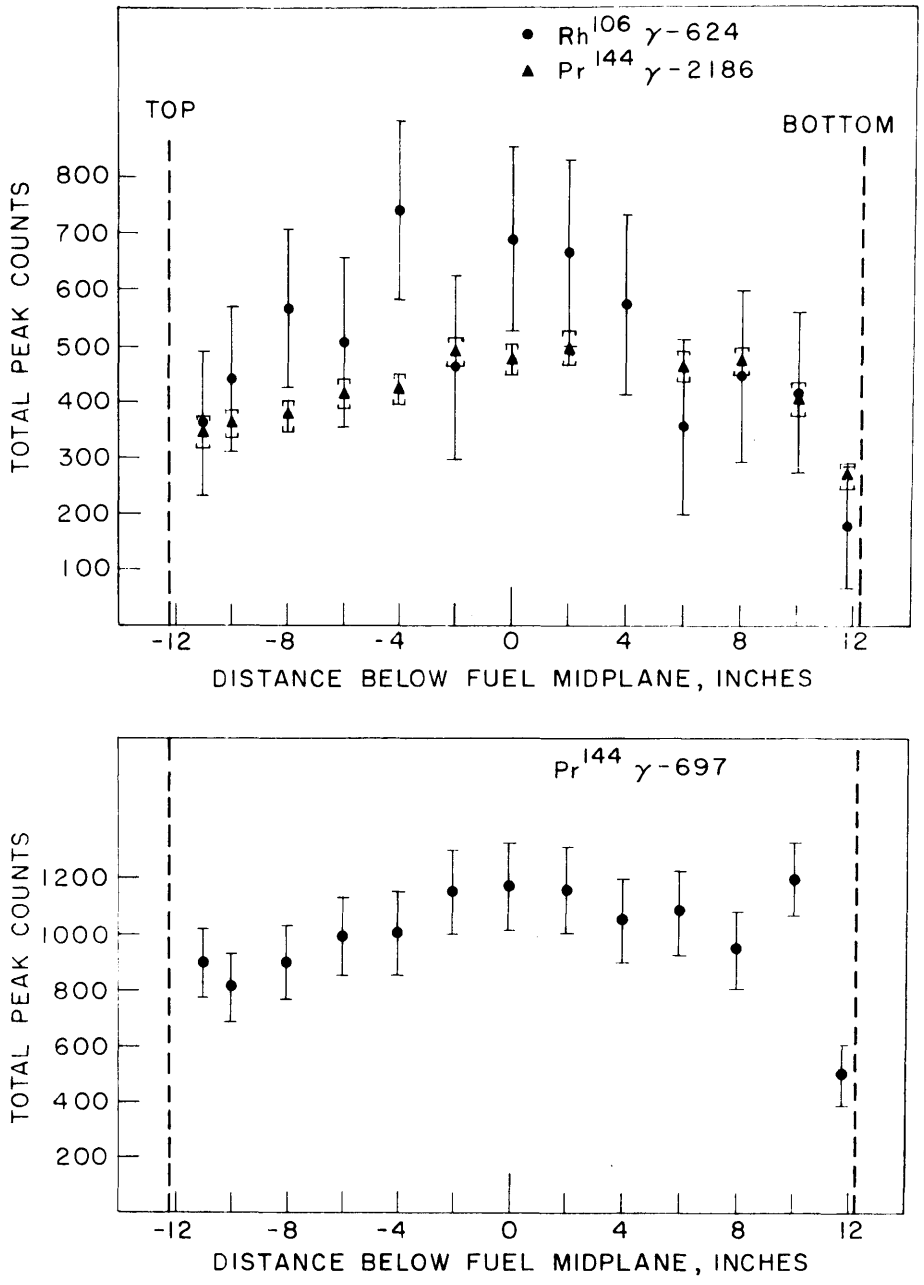

FIGURE 42 AXIAL DISTRIBUTIONS OF Pr^{144} AND Rh^{106} γ-RAY ACTIVITIES FOR FUEL ELEMENT 2M22 AFTER 1½ YEARS COOLING

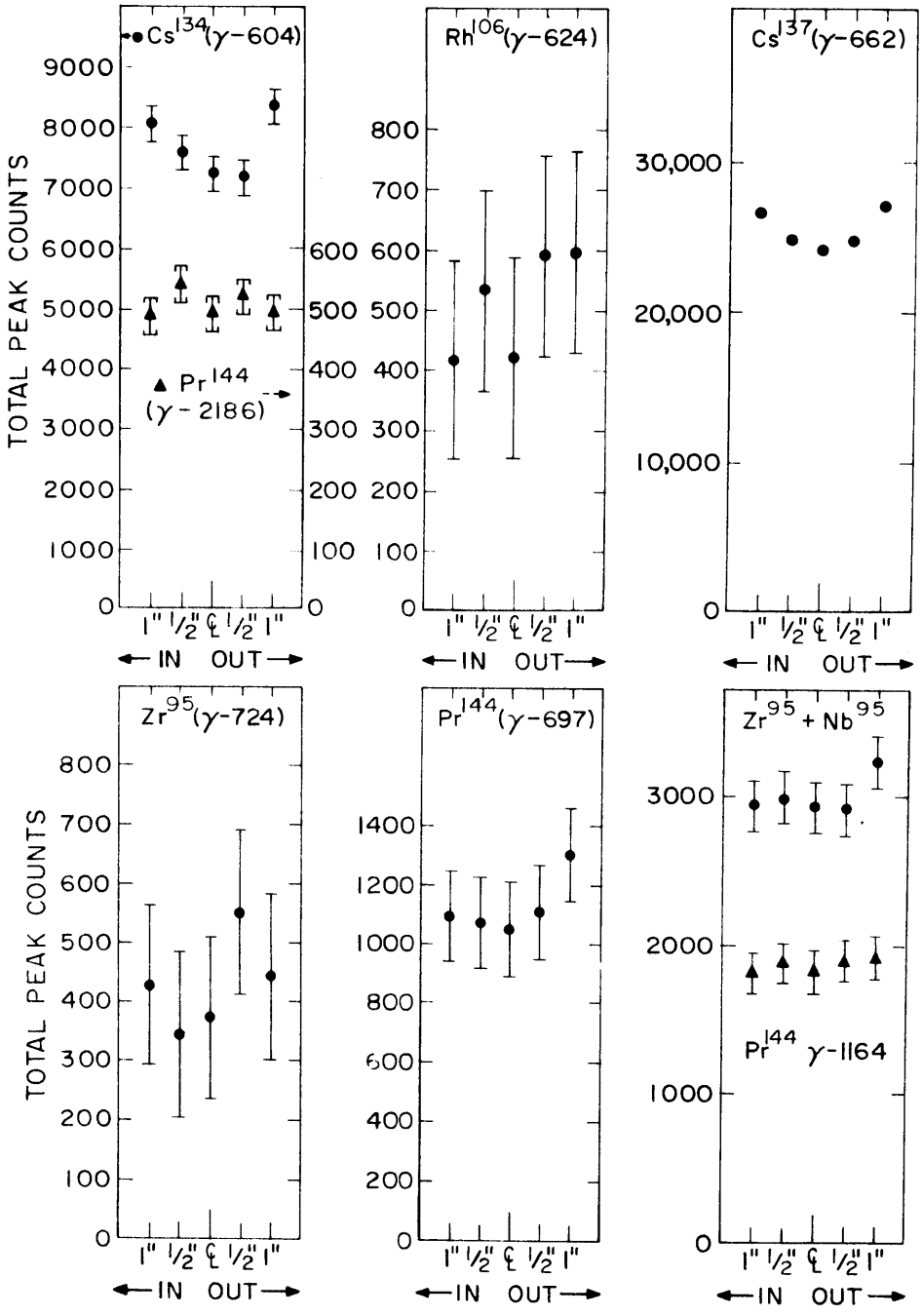

FIGURE 43 TRANSVERSE DISTRIBUTION OF γ-RAY ACTIVITIES AT AXIAL MIDPLANE OF FUEL ELEMENT 2M22 AFTER 1 1/2 YEARS COOLING

in the center as one would expect for the flux distribution. Likewise, so does Cs^{134}. The other distributions can be considered constant across the element within experimental error.

(c) Fuel Element 2-4

In element 2-4, after a cooling time of three years, only Cs^{137} and Cs^{134} gamma-rays were statistically significant. Their axial distributions are given in Fig. 44. No transverse scans were made.

(d) Fuel Element 2M1

Gamma-ray spectra were obtained for element 2M1 which had a cooling time of 3 1/2 years. The results are shown in Fig. 45. The results of a transverse scan at the axial midplane are shown in Fig. 46 for Cs^{137}, Rh^{106}, Cs^{134} (γ-604 keV) and Pr^{144} (γ-697 keV).

(e) Fuel Element 2M31

The gamma-ray spectrum for 2M31, which had a cooling time of 11 days, showed significant peaks only for La^{140}. The 1596 keV photopeak, having the highest intensity, was used in determining the axial distribution of La^{140}. This is shown in Fig. 47. There is some tendency for flattening at the axial center, with flux peaking near the bottom reflector and flux depression at the top due to control rods.

4. Correction Factors for Gamma-Ray Intensities

Corrections to gamma-ray peak integrals were made to take into account (a) self-absorption of photons in fuel plates and

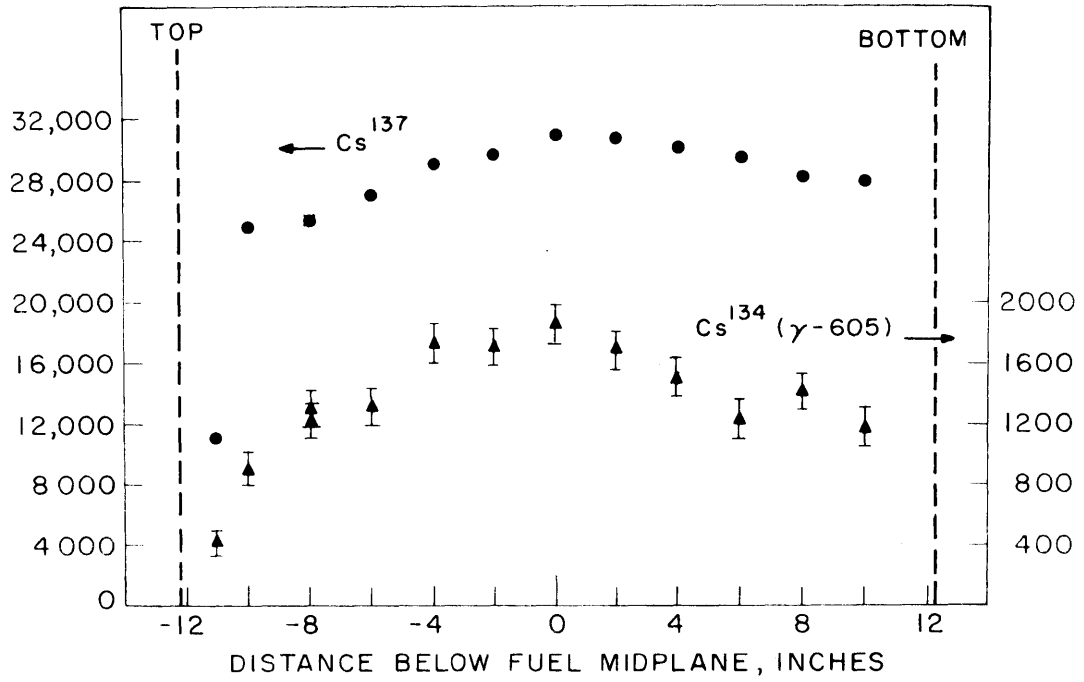

FIGURE 44 AXIAL DISTRIBUTION OF Cs^{137} AND Cs^{134} (γ-605 keV) ACTIVITIES FOR FUEL ELEMENT 2-4 AFTER 3 YEARS COOLING TIME

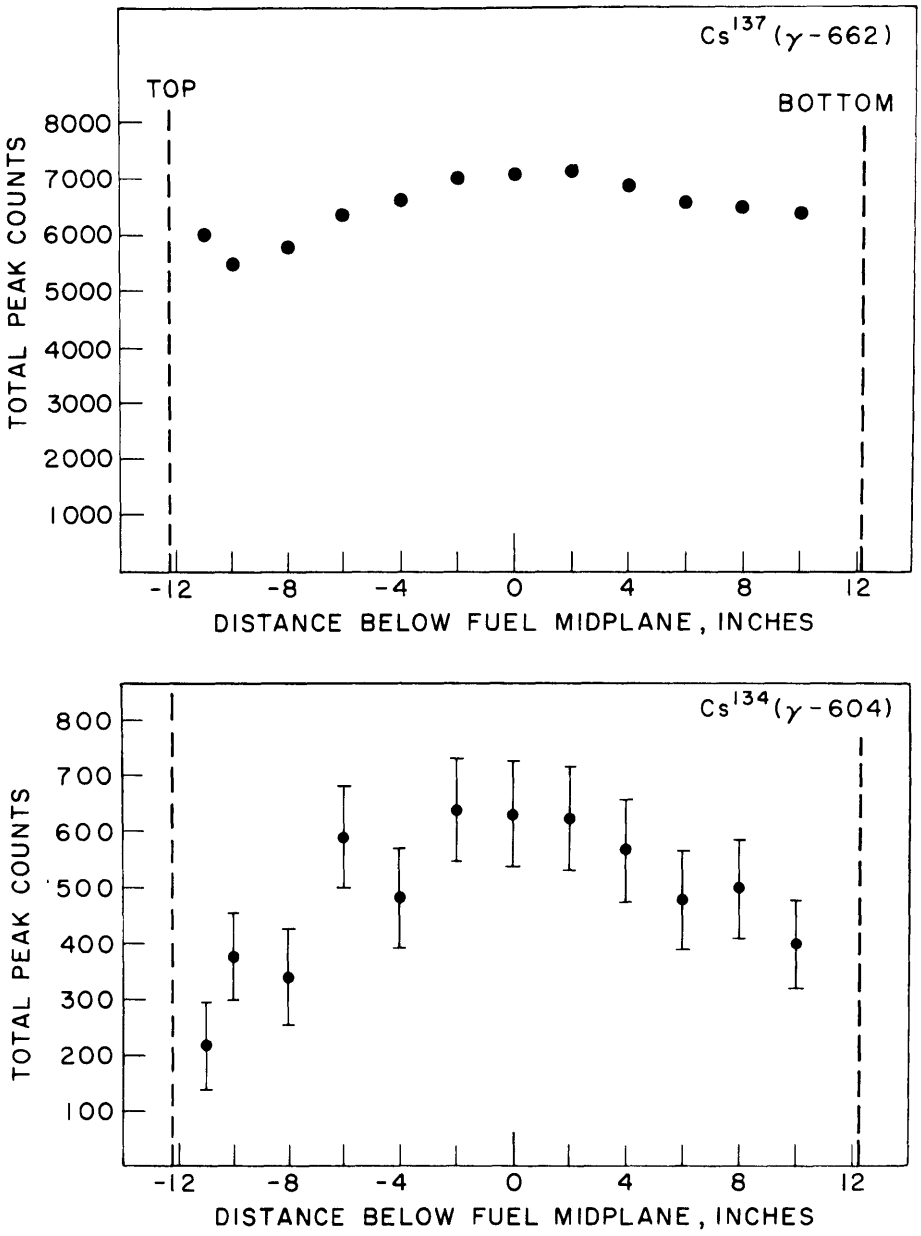

FIGURE 45 AXIAL DISTRIBUTION OF Cs^{137} AND Cs^{134} (γ-604 keV) γ-RAY ACTIVITIES FOR FUEL ELEMENT 2MI AFTER 3½ YEARS COOLING TIME

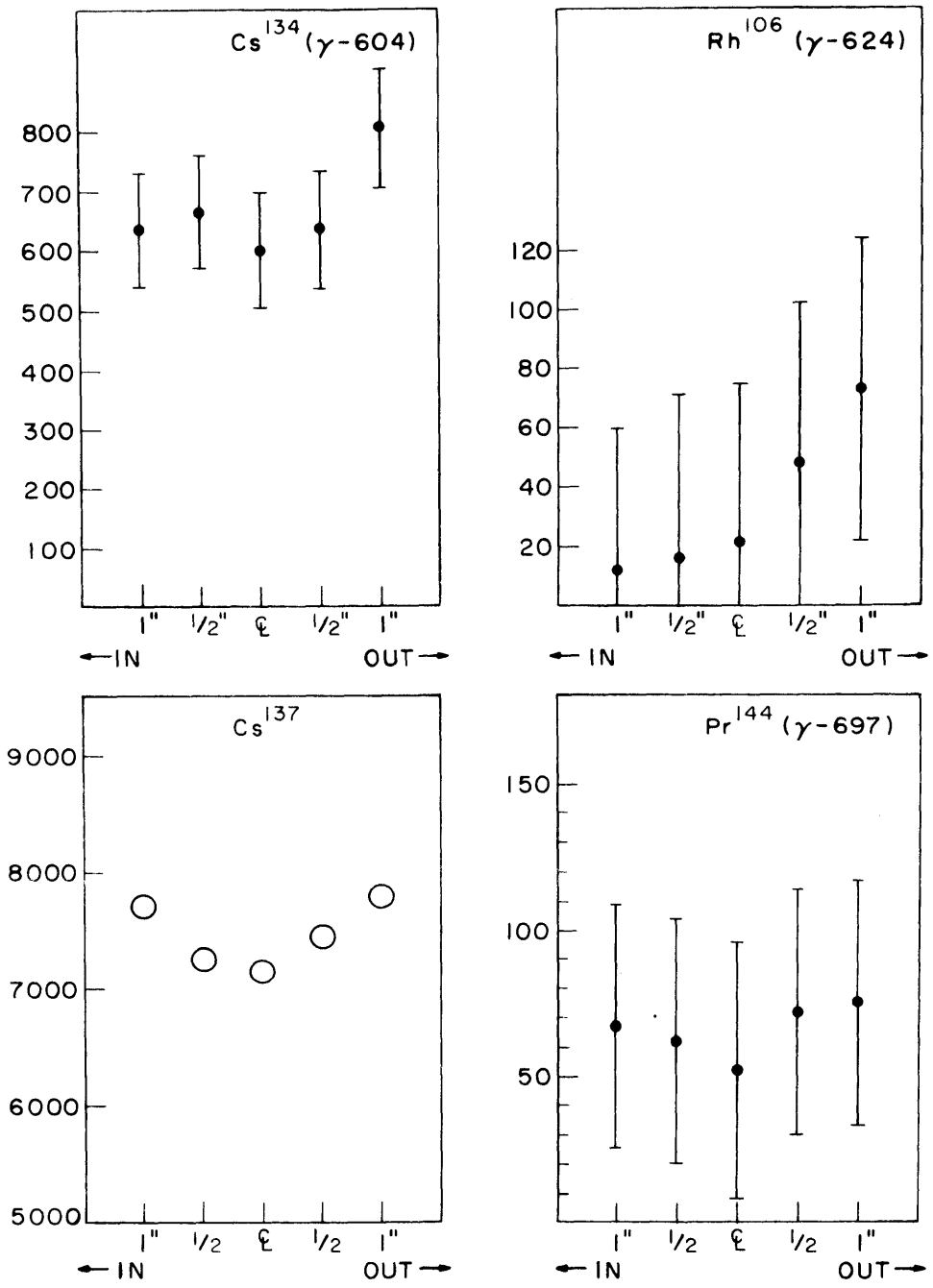

FIGURE 46 TRANSVERSE (HORIZONTAL) DISTRIBUTION OF Cs^{134} (γ-604), Rh^{106} (γ-624), Cs^{137} AND Pr^{144} (γ-697) FOR FUEL ELEMENT 2MI AFTER 3½ YEARS COOLING TIME

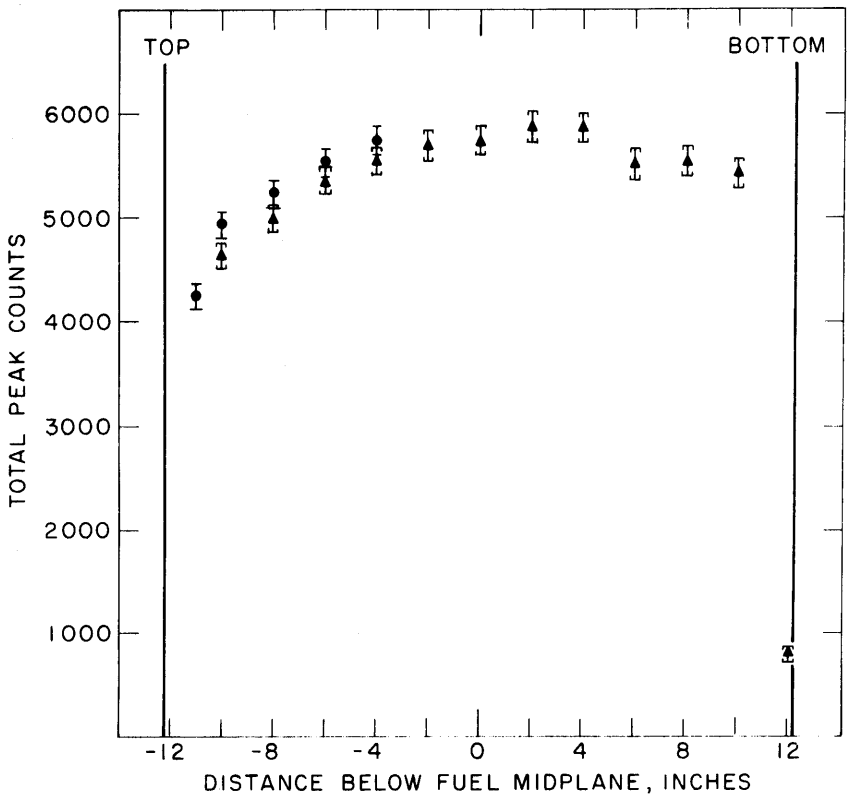

FIGURE 47 AXIAL DISTRIBUTION OF La^{140} γ-RAY ACTIVITY (1597 keV) FOR FUEL ELEMENT 2M31 AFTER 11 DAYS COOLING

water, (b) absorption in absorbers placed across the gamma-ray beam to reduce low energy counts, (c) absorption in the stainless steel bottom of the detector dewar and (d) variation of detector efficiency with photon energy. Since photon interaction cross-sections decrease with energy in the 500 to 800 keV range, a larger fraction of the higher energy photons, emitted within the fuel, reached the detector than lower energy photons. However, since the detector efficiency also decreases with photon energy, a larger fraction of the lower energy photons striking the detector resulted in a gamma-ray peak compared with higher energy photons. Thus, the overall correction factor remained relatively constant over this energy range.

The self-absorption in the fuel plates and inter-plate water was approximated by assuming that, on the average, each photon that entered the beam hole had traversed about half of the distance across the element. This was assumed to include seven fuel plates, each consisting of 0.040 in. thickness of aluminum cladding and 0.020 in. thickness of U^{235}-Al alloy, plus one dummy plate of aluminum, 0.060 in. thick, plus eight layers of water, each 0.117 in. thick. The bottom of the detector dewar was stainless steel, 0.370 in. thick. Table 4 gives the attenuation coefficients used for each of three energies for lead, water and steel. Included is the fraction of photons <u>not</u> attenuated by each of the above items, the detector efficiency and the overall correction factor. Figure 48 shows a graph of the correction factor as a function of energy.

TABLE 4

ATTENUATION AND DETECTOR EFFICIENCY CORRECTIONS

AND TOTAL CORRECTION FACTOR FOR PHOTONS BETWEEN 600 and 800 keV

	Energy, keV		
	600	662	800
Attenuation Coefficient, μ, cm^{-1}			
Aluminum[a]	0.211	0.202	0.184
Water[a]	0.090	0.087	0.080
Lead[a]	1.361	1.135	0.931
Iron[b]	0.597	0.572	0.521
$e^{-\mu x}$ for x=0.135 in. Pb	0.628	0.678	0.727
$e^{-\mu x}$ for fuel plates	0.774	0.782	0.799
$e^{-\mu x}$ for water in element	0.800	0.806	0.820
$e^{-\mu x}$ for stainless steel base plate	0.571	0.584	0.613
Total absorption correction	0.222	0.250	0.292
Efficiency of detector	0.0102	0.00872	0.00720
Total correction factor	0.00226	0.00218	0.00210

References

(a) R.D. Evans, "The Atomic Nucleus", Ch.25, p.711, McGraw-Hill Book Company, Inc. (1955).

(b) C.M. Davisson and R.D. Evans, "Gamma-Ray Absorption Coefficients", Revs. Modern Phys. 24, 79 (1952).

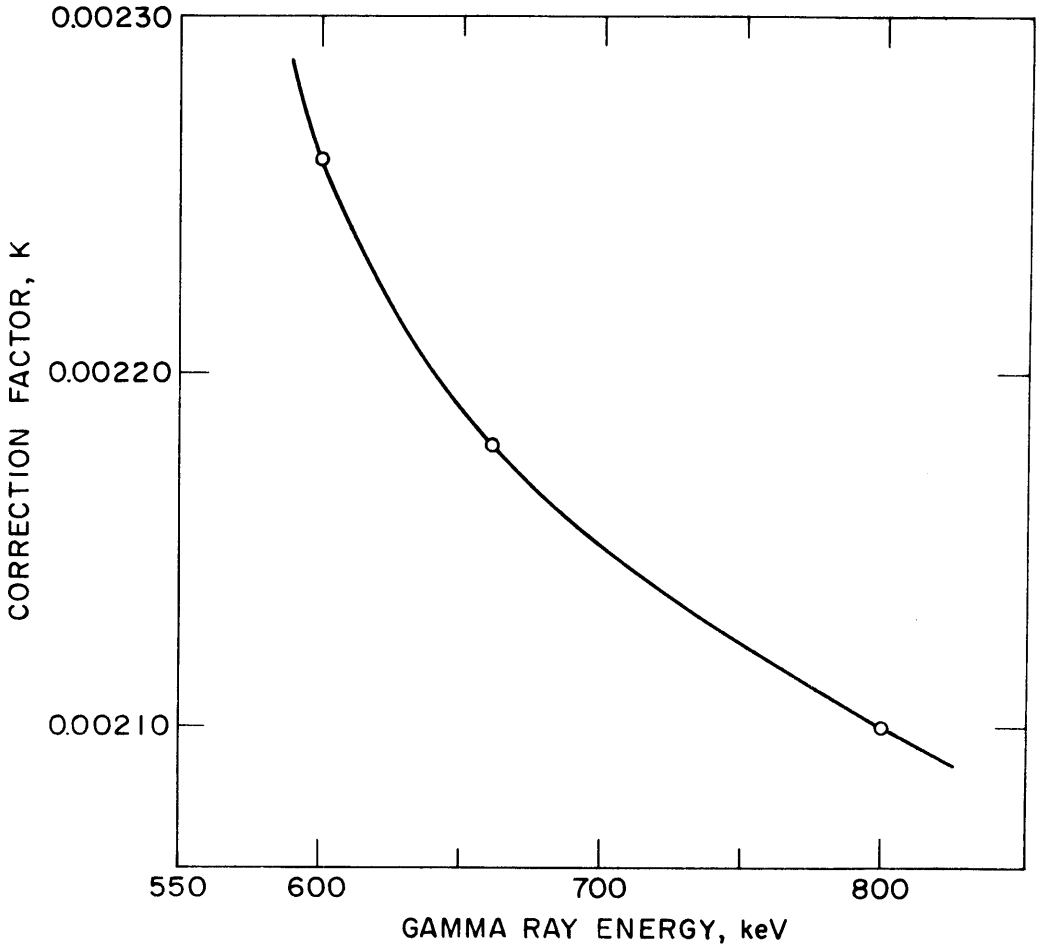

FIGURE 48 CORRECTION FACTOR AS A FUNCTION OF PHOTON ENERGY TO INCLUDE FUEL SELF-ABSORPTION, ABSORPTION IN LEAD AND STEEL AND DETECTOR EFFICIENCY

5. Corrected Ratios of Fission Product Activities

Ratios of fission product activities were calculated for use in subsequent analyses. Each of the gamma-ray peak integrals were corrected for fuel self-absorption, etc. using the corresponding correction factor from Fig. 48. Corrections were also applied, where necessary, for gamma-ray intensities, β-to-γ ratios and internal conversion coefficients. The fission product activities were then corrected for decay since the last irradiation, so that comparisons between theory and experiment were made at the time the fuel was removed from the neutron flux. The various nuclear constants used in these corrections are presented in Table 5.

The fission product activity ratios calculated were

$$R_1 = \frac{A(Cs^{137})}{A(Cs^{134})} \qquad (C.1)$$

$$R_2 = \frac{A(Cs^{137})}{A(Zr^{95})} \qquad (C.2)$$

$$R_3 = \frac{A(Cs^{137})}{A(Pr^{144})} \qquad (C.3)$$

where A = corrected activity.

The values of the corrected fission product activity ratios are given in Tables 6 and 7 for 2M19, in Table 8 for 2M22, and in Table 9 for 2M1. No ratios were calculated for elements 2M14, 2M31 or 2-4.

In calculating R_1, two values of the Cs^{134} activity were available; one obtained from the intensity of the 605 keV

TABLE 5

NUCLEAR CONSTANTS USED FOR CALCULATING CORRECTED FISSION PRODUCT RATIOS

Fission Product	$t_{1/2}$	λ, sec.$^{-1}$	Branch. Ratio $\gamma/\beta+\gamma$	Internal Convers. Coeff. $\alpha_T/(1+\alpha_T)$	Energy, keV	No. of γ-rays /disintegrtn.
Cs^{137}	30.0 yr.[a]	7.33×10^{-10}	0.92[b]	0.1066[c]	662	0.8228[c]
Zr^{95}	65 d.[d]	1.234×10^{-7}	1.0[d]	small	724	0.417[e]
					758	0.553[e]
Cs^{134}	2.19 yr.[f]	9.982×10^{-9}	1.0[g]	small	605	0.98[g]
					796	0.968[g]
					802	
Ce^{144}	280 d.[d]	2.865×10^{-10}				
Pr^{144}	17.5 m.[d]	6.60×10^{-4}	0.02[d]	-	697	0.016[h]

References

(a) K.F. Flynn, et al, J. Inorg. Nucl. Chem. 27, 21-3 (1965).

(b) R.D. Evans, "The Atomic Nucleus", Ch.6, p.232, McGraw-Hill Book Co., Inc. (1955).

(c) Calculated from $\alpha_K=0.0976$, $\alpha_K/\alpha_L=5.66$ and $\alpha_{M,N}=3.85$ from Y. Yoshizawa, Nucl. Phys. 5, 122 (1958).
No. of unconverted gamma-rays per gamma-ray decay = 0.8934, therefore no. of gamma-rays per Cs-137 disintegration = (0.92)(0.8934) = 0.8228.

(d) Nuclear Data Sheets.

(e) Present work with Ge(Li) detectors, see Section IIID.4.

(f) W.F. Merritt, et al, Can. J. Phys. 35, 16 (1957).

(g) R.A. Brown and G.T. Swan, Nucl.Phys. 68, 325-36 (1965).

(h) R.L. Graham et. al, Can. J. Phys. 36, 1084 (1958).

TABLE 6

CORRECTED RATIOS OF FISSION PRODUCT ACTIVITIES

R_1, R_2 AND R_3

FOR ELEMENT 2M19, RUNS D4 TO D27

Run	Position Below Fuel Midplane, Inches	$R_1=\frac{A(Cs^{137})}{A(Cs^{134})}$	$R_2=\frac{A(Cs^{137})}{A(Zr^{95})}$	$R_3=\frac{A(Cs^{137})}{A(Pr^{144})}$
D4	- 1 &	4.465	0.0712	0.1301
D5	0 &	4.753	.0721	.1272
D6	+ 2 &	4.537	.0751	.1263
D7	+ 4 &	4.707	.0717	.1228
D8	+ 6 &	5.252	.0709	.1175
D9	+ 8 &	5.263	.0771	.1207
D10	+ 10 &	5.810	.0713	.1016
D11	+ 11 &	7.367	.0750	.1469
D12	- 2 &	4.581	.0750	.1305
D13	- 4 &	5.172	.0691	.1145
D14	- 6 &	5.704	.0704	.1218
D15	- 8 &	5.985	.0669	.1149
D16	- 10 &	7.299	.0665	.1136
D17	- 11 &	8.306	.0716	.1516
D19	- 1:½" OUT	4.943	.0827	.1340
D18	- 1 &	4.695	.0757	.1403
D20	- 1:1" OUT	4.642	.0814	.1422
D21	- 1:½" IN	4.686	.0773	.1453
D22	- 1:1" IN	5.211	.0847	.1836
D23	- 6:1" IN	6.337	.0804	.1302
D24	- 6:½" IN	6.114	.0749	.1454
D25	- 6 &	6.164	.0751	.1132
D26	- 6:½" OUT	6.200	.0766	.1161
D27	- 6:1" OUT	5.366	.0743	.1114

TABLE 7

CORRECTED RATIOS OF FISSION PRODUCT ACTIVITIES

R_1, R_2 AND R_3

FOR ELEMENT 2M19, RUNS D28 TO D46

Run	Position Below Fuel Midplane, Inches	$R_1=\frac{A(Cs^{137})}{A(Cs^{134})}$	$R_2=\frac{A(Cs^{137})}{A(Zr^{95})}$	$R_3=\frac{A(Cs^{137})}{A(Pr^{144})}$
D28	+ 6:1" OUT	6.049	0.0806	0.1371
D29	+ 6:$\frac{1}{2}$" OUT	5.446	.0775	.1304
D30	+ 6 ℄	5.221	.0765	.1710
D31	+ 6:$\frac{1}{2}$" IN	4.938	.0788	.1248
D32	+ 6:1" IN	5.005	.0757	.1320
D33	+11$\frac{1}{2}$ ℄	7.206	.0793	.1512
D34	+ 12 ℄	5.441	.0627	.0674
	Element Turned 90°	Detector Viewing Edges of Fuel Plates		
D35	- 1 ℄	5.013	.0709	
D36	$\frac{1}{16}$" OUT	4.539	.0786	
D37	$\frac{1}{8}$" OUT	4.529	.0746	
D38	$\frac{3}{16}$" OUT	4.753	.0778	
D39	$\frac{1}{4}$" OUT	4.009	.0835	
D40	$\frac{5}{16}$" OUT	4.406	.0750	
D41	$\frac{3}{8}$" OUT	4.392	.0749	
D42	$\frac{7}{16}$" OUT	3.976	.0773	
D43	$\frac{1}{2}$" OUT	4.544	.0812	
D44	1" OUT	3.911	.0836	
D45	$\frac{1}{2}$" IN	4.035	.0816	
D46	1" IN	4.046	.0782	

gamma-ray and the other obtained from the 796 keV gamma-ray intensity. The values of R_1 given for 2M19 have been calculated by weighting the results from the 796 keV gamma-ray by two and the 605 keV gamma-ray by one and determining an average

$$R_1 = \frac{2R_1(\gamma\text{-}796) + R_1(\gamma\text{-}605)}{3} \qquad (C.4)$$

This was done because the statistical uncertainties were about twice as great for the intensity of the lower energy Cs^{134} gamma-ray than for the higher energy gamma-ray.

For 2M22, a correction factor was applied to the counts of the 605 keV gamma-ray of Cs^{134} to take into account the presence of the Compton edge of the 796 keV gamma-ray. The ratio of 796 keV gamma-ray counts to the 605 keV gamma-ray counts was calculated for each run for 2M22. Since their intensities were about equal, the ratio should have been near unity. However, because counts from the Compton distribution were included in the 605 keV gamma-ray peak, the ratio was less than unity. The average value for Runs H1-H18 was 0.685. The net counts for the Cs^{134} gamma-ray at 605 keV were then multiplied by 0.685. The corrected value was combined with the counts for the 796 keV gamma-ray and the mean of these was used in calculating R_1.

For element 2M1, only the 605 keV gamma-ray of Cs^{134} and the Cs^{137} gamma-ray were recorded.

The axial distributions along element 2M19 for the ratios

TABLE 8

CORRECTED RATIOS OF FISSION PRODUCT ACTIVITIES

R_1, R_2 AND R_3

FOR FUEL ELEMENT 2M22

Run	Position Below Fuel Midplane, Inches	R_1	R_2	R_3
H1	0 ℄	3.727	0.0945	0.1085
H2	- 2 ℄	3.861	0.1231	0.1113
H3	- 4 ℄	4.176	0.0945	0.1197
H4	- 6 ℄	4.497	0.0931	0.1138
H5	- 8 ℄	5.316	0.0673	0.1171
H6	- 10 ℄	6.589	0.1129	0.1208
H7	- 11 ℄	6.416	0.0730	0.1183
H8	+ 2 ℄	3.878	0.0788	0.1111
H9	+ 4 ℄	4.132	0.1115	0.1234
H10	+ 6 ℄	4.105	0.0822	0.1148
H11	+ 8 ℄	4.856	0.1068	0.1280
H12	+ 10 ℄	5.171	0.0943	0.1005
H13	+11 3/4 ℄	4.963	0.0907	0.1039
H14	0 ℄	3.840	-	0.1218
H15	0 ½" OUT	3.764	0.0817	0.1176
H16	0 1" OUT	3.689	0.1112	0.1096
H17	0 ½" IN	3.735	0.1315	0.1223
H18	0 1" IN	3.772	0.1132	0.1282

TABLE 9

CORRECTED RATIO OF FISSION PRODUCT ACTIVITIES

R_1

FOR FUEL ELEMENT 2M1

Run	Position Below Fuel Midplane, Inches	R_1
G1	- 6 "	5.325
G2	- 8 "	8.424
G3	- 10 "	7.206
G4	- 11 "	13.822
G5	- 4 "	6.785
G6	- 2 "	5.406
G7	0 "	5.533
G8	+ 2 "	5.615
G9	+ 4 "	6.005
G10	+ 6 "	6.746
G11	+ 8 "	6.447
G12	+ 10 "	7.877
G18	0 "	5.845
G19	0 $\frac{1}{2}$" OUT	5.759
G20	0 1" OUT	4.747
G21	0 $\frac{1}{2}$" IN	5.360
G22	0 1" IN	5.979

R_1 and R_2 are shown in Figs. 49 and 50 respectively. It is seen that R_1 varies considerably with position, being lower at the center than elsewhere, whereas R_2 remains relatively constant. The reasons for this unexpected difference will be discussed in the next section, which is devoted to the interpretation of the above results.

D. INTERPRETATION OF RESULTS

1. Introduction

The interpretation and analysis of the above experimental results required theoretical predictions of fission product activities in the MITR spent fuel, utilizing the fission yields, half-lives and genetic relations of the nuclides of interest. The concentration of a fission product in irradiated fuel is a function of a number of parameters; the operating flux level, the irradiation time, the operating pattern and the decay time since removal from the core. A large number of calculations and experimental determinations of fission product activities have been reported in the literature. These have been useful for predicting various properties of fission product mixtures such as heat evolution (B6, W2 and U1), shielding requirements (M8), thermal neutron poisoning (E3, S1, B7, W1) and individual fission product concentrations (B5, F1, H4). However, most of the calculations did not present the results in a form most convenient for the analysis of the present results. Also, recent and more accurate determinations of nuclear constants and fission yields have been reported that were not used in the above calculations. Therefore, it was decided to develop a computer code to calculate values for the solutions describing the fission product concentrations in irradiated MITR fuel.

This section presents the differential equations that describe the rate of accumulation of certain types of fission products and gives the forms of the solution for each.

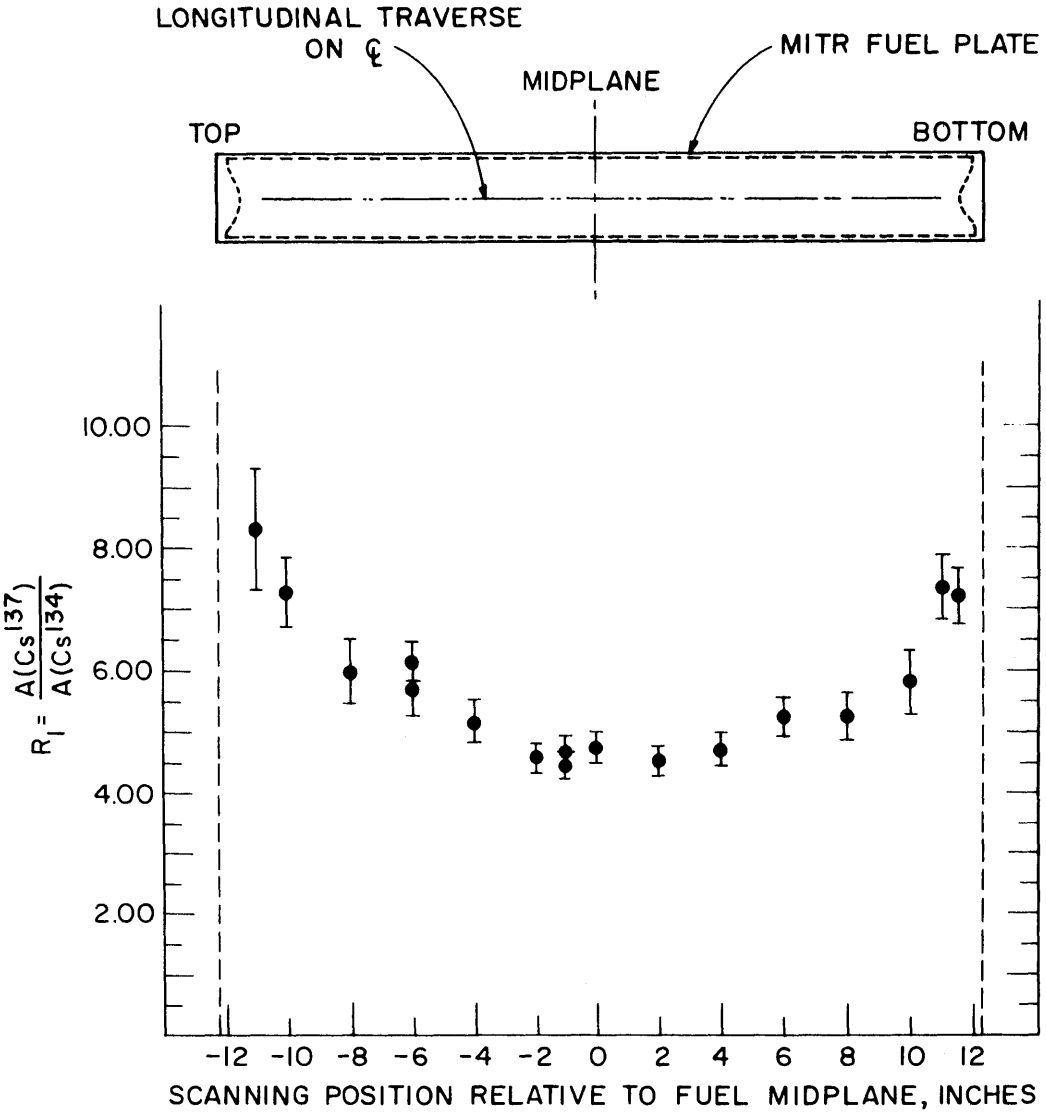

FIGURE 49 AXIAL PROFILE OF RATIO OF Cs^{137} TO Cs^{134} ACTIVITIES, AT REMOVAL FROM CORE, FOR FUEL ELEMENT 2MI9. (R_1 HAS BEEN CORRECTED FOR ABSORPTION IN FUEL, WATER, DETECTOR EFFICIENCY AND Pb ABSORBERS)

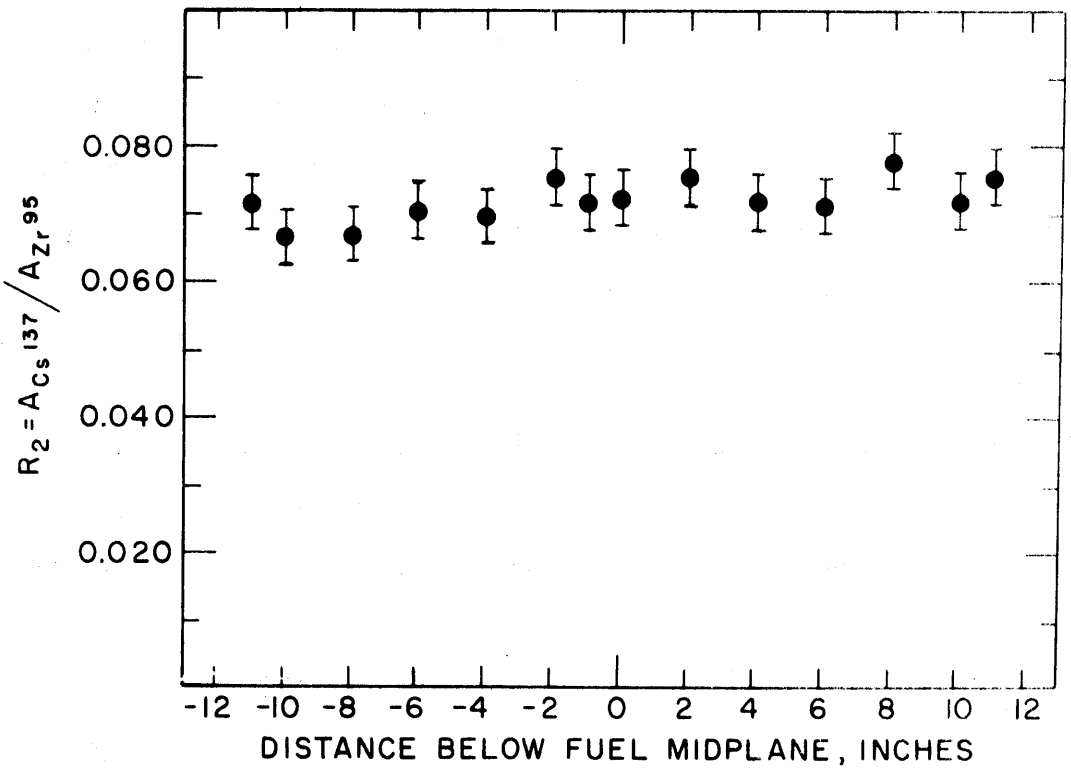

FIGURE 50 RATIO OF Cs^{137} ACTIVITY TO Zr^{95} ACTIVITY ALONG FUEL ELEMENT 2M19 - CORRECTED FOR DECAY SINCE SHUTDOWN, EFFICIENCIES AND ABSORPTION

Values of fission product concentrations and activities as a function of irradiation time are predicted for different neutron fluxes. Their use in interpreting the experimental results from fuel element gamma-ray spectra is illustrated with determinations of the spatial distributions of absolute neutron flux, irradiation time and neutron exposure. Comparisons of results obtained by this method are made with independent determinations of these quantities and agreement is shown to be very good. Included are discussions of some of the problems and disadvantages of the analysis with possible remedies and improvements.

2. Predicted Fission Product Concentrations in MITR Fuel

The gamma-ray peaks observed in spectra obtained with the Ge(Li) spectrometer were identified with one of the following fission products: Zr^{95}, Nb^{95}, Rh^{106}, Cs^{134}, Cs^{137}, Ba^{140}, La^{140}, Ce^{144} or Pr^{144}. These can be divided into three different groups, each having a different mode of production. The first group includes those products that are produced directly in the fission process or are the products of precursors having half-lives much shorter than their own. The second group includes daughters of the first group that are not in secular equilibrium with their parents and have negligible direct fission yield. The third group contains the radioisotopes that have negligible fission yield but are produced by neutron capture reactions on other fission products. More detailed treatment of each of these groups is given in the following sections:

(a) Group 1 Type Fission Products

The rate of accumulation of Group 1 type of fission products is given by

$$\frac{dN_A}{dt} = N_{25}\sigma_{25}^{f}\phi y_A - N_A\lambda_A - N_A\sigma_A^a\phi \qquad (D.1)$$

where N_A = concentration of nuclide A, atoms/cc

N_{25} = concentration of U^{235}, atoms/cc

σ_{25}^{f} = fission cross-section of U^{235}, cm^2

ϕ = absolute neutron flux, n/cm^2-sec.

y_A = fission yield of A, including short-lived precursors

λ_A = decay constant of A, sec^{-1}

σ_A^a = absorption cross-section of A, cm^2

t = irradiation time, sec.

The first term on the right-hand side of Eq. (D.1) represents production of A by U^{235} fission, while the second and third terms represent destruction of A by decay and neutron capture, respectively.

For many fission products, the capture cross-section, σ^a is negligibly small and thus, N_A follows Eq. (D.2)

$$\frac{dN_A}{dt} = N_{25}\sigma_{25}^{f}\phi y_A - N_A\lambda_A \qquad (D.2)$$

Equation (D.2) applies to the accumulation of Zr^{95}, Ru^{106}, Cs^{137}, Ba^{140} and Ce^{144}. Daughter products such as Rh^{106},

La^{140} and Pr^{144} each have half-lives short enough so that in most cases their activities are the same as that of the parent.

In order to solve Eq. (D.2) and subsequent equations, it is required to know the concentration of U^{235} as a function of time. This has been assumed to follow Eq. (D.3)

$$\frac{dN_{25}}{dt} = - N_{25}\sigma_{25}^{a}\phi \qquad (D.3)$$

where σ_{25}^{a} = absorption cross-section of U^{235}, cm^2.

The solution to (D.3) is given by Eq. (D.4)

$$N_{25} = N_{25}^{o}e^{-\sigma_{25}^{a}\phi t} \qquad (D.4)$$

where N_{25}^{o} = initial U^{235} concentration at t=0, atoms/cc. Substituting the expression for N_{25} from (D.4) into (D.2) and solving, one obtains the solution for the concentration of A per initial U^{235} atom, assuming N_A=0 at t=0,

$$\frac{N_A(t)}{N_{25}^{o}} = \frac{\sigma_{25}^{f}\phi y_A}{(\lambda_A-\sigma_{25}^{a}\phi)}\left[e^{-\sigma_{25}^{a}\phi t} - e^{-\lambda_A t}\right] \qquad (D.5)$$

However, the MITR operates at constant power for only 55 to 60% of the time and is shut down the remainder. Thus, it was necessary to formulate the solutions to include intermittent operation.

For the period of constant flux operation, the equation

governing the concentration N_A/N_{25}^o, with irratiation time t_a, is given by Eq. (D.6)

$$\frac{N_A(t_a)}{N_{25}^o} = \frac{e^{-\sigma_{25}^a \phi\tau}\,\sigma_{25}^f \phi y_A}{(\lambda_A - \sigma_{25}^a \phi)} \left[e^{-\sigma_{25}^a \phi t_a} - e^{-\lambda_A t_a} \right] + \frac{N_A^{t_a=0}}{N_{25}^o} e^{-\lambda_A t_a} \qquad (D.6)$$

where t_a = irradiation time from the beginning of a particular constant flux period, sec.

τ = total irradiation time experienced by the U-235 up to beginning of the constant flux period, sec.

$\frac{N_A^{t_a=0}}{N_{25}^o}$ = concentration of A per initial U^{235} atom at beginning of the constant flux period.

$\frac{N_A(t_a)}{N_{25}^o}$ = concentration of A per initial U^{235} atom at time t_a, during a constant flux period.

During a shutdown period, the flux is zero and concentration of A per initial U^{235} atom follows (D.7)

$$\frac{N_A(t_d)}{N_{25}^o} = \frac{N_A^{t_d=0}}{N_{25}^o} e^{-\lambda_A t_d} \qquad (D.7)$$

where $\frac{N_A^{t_d=0}}{N_{25}^o}$ = concentration of A per initial U^{235} atom at beginning of shutdown period.

t_d = time since beginning of shutdown period, sec.

For fuel operated in such an intermittent fashion, the concentration of fission product A per initial U^{235} atom at the end of the Nth cycle, each consisting of a constant flux operating period followed by a zero flux, shutdown period is given by Eq. (D.8)

$$\frac{N_A(N^{th}\ cycle)}{N_{25}^o} = K_1\left\{\sum_{n=1}^{N} \exp\left[-\sigma_{25}^a \phi (N-n)\, t_a - n\lambda_A t_d - (n-1)\lambda_A t_a \right]\right\} \qquad (D.8)$$

where $K_1 = \dfrac{\sigma_{25}^f \phi y_A}{(\lambda_A - \sigma_{25}^a \phi)}$

t_a = length of accumulation period, sec.

t_d = length of shutdown period, sec.

(b) Group 2 Type Fission Products

The concentration of fission products of this type is governed by Eq. (D.9)

$$\frac{dN_B}{dt} = N_A\lambda_A - N_B\lambda_B - N_B\sigma_B^a\phi \qquad (D.9)$$

where A = parent nuclide

B = daughter nuclide.

Of the fission products considered here, only Nb^{95} belongs to this group. Since the absorption cross-section of Nb^{95} is small, the last term in (D.9) is neglected. Thus, for constant flux operation

$$\frac{dN_B}{dt} = N_A\lambda_A - N_B\lambda_B \qquad (D.10)$$

or in terms of initial U^{235} concentration

$$\frac{d}{dt}\left[\frac{N_B}{N_{25}^o}\right] = \frac{N_A}{N_{25}^o}\lambda_A - \frac{N_B}{N_{25}^o}\lambda_B \qquad (D.11)$$

Substituting for N_A/N_{25}^o from (D.5) and solving (D.11) for conditions of $N_B/N_{25}^o=0$ at $t=0$, the concentration of B per initial U^{235} atom as a function of irradiation time is given by (D.12)

$$\frac{N_B}{N_{25}^o} = \frac{\lambda_A\sigma_{25}^f y_A\phi}{(\lambda_A - \sigma_{25}^a\phi)(\lambda_B - \sigma_{25}\phi)(\lambda_B - \lambda_A)}$$

$$\left[(\lambda_A - \sigma_{25}\phi)e^{-\lambda_B t} + (\lambda_B - \lambda_A)e^{-\sigma_{25}^a\phi t}\right.$$

$$\left. - (\lambda_B - \sigma_{25}\phi)e^{-\lambda_A t}\right] \qquad (D.12)$$

For intermittent operation, Eq. (D.11) also governs the net rate of accumulation of N_B/N_{25}^o during the constant flux period, except now N_A/N_{25}^o is obtained from (D.6). The number of atoms of B per initial U^{235} atom at time t_a after the start of that period follows (D.13)

$$\frac{N_B(t_a)}{N_{25}^o} = \frac{K_2\lambda_A}{(\lambda_B - \sigma_{25}^o\phi)}\left(e^{-\sigma_{25}^a\phi t_a} - e^{-\lambda_B t_a}\right)$$

$$+ \frac{\lambda_A\left[\frac{N_A^{t_a=0}}{N_{25}^o} - K_2\right]}{(\lambda_B - \lambda_A)}\left[e^{-\lambda_A t_a} - e^{-\lambda_B t_a}\right]$$

$$+ \frac{N_B^{t_a=0}}{N_{25}^o} e^{-\lambda_B t_a} \qquad \text{(D.13)}$$

where $K_2 = \dfrac{\sigma_{25}^f\phi y_A e^{-\sigma_{25}^a\phi\tau}}{(\lambda_A - \sigma_{25}^a\phi)}$ (D.14)

and $\dfrac{N_B^{t_a=0}}{N_{25}^o}$ = concentration of B per initial U^{235} atom at beginning of the operating period.

The net rate of accumulation of N_B/N_{25}^o during periods of shutdown with $\phi=0$ also follows Eq. (D.11), except that the parent concentration, $N_A(t_a)/N_{25}^o$, is governed by Eq. (D.7). Substituting this expression into (D.11) and solving, one obtains, for the concentration of B per initial U^{235} atom during the shutdown period, Eq. (D.15)

$$\frac{N_B(t_d)}{N_{25}^o} = \frac{\lambda_B N_A^o/N_{25}^o}{(\lambda_B - \lambda_A)}\left[e^{-\lambda_A t_d} - e^{-\lambda_B t_d}\right]$$

$$+ \frac{N_B^{t_d=0}}{N_{25}^o} e^{-\lambda_B t_d} \qquad \text{(D.15)}$$

where $\left.\frac{N_B}{N_{25}^o}\right|_{t_d=0}$ = concentration of B per initial U^{235} atom at the beginning of the shutdown period.

(c) Group 3 Type Fission Products

The third type of fission product includes those produced by (n,γ) reactions. Of the fission products identified in the experiments, only Cs^{134} is such a radionuclide. Having a small direct fission yield, it is formed only by the (n,γ) reaction on Cs^{133} which is a stable end-product of the mass 133 fission product chain. The net rate of accumulation of atoms of the third type, per initial U^{235} atom, N_D/N_{25}^o, follows Eq. (D.16)

$$\frac{d}{dt}\left[\frac{N_D}{N_{25}^o}\right] = \frac{N_C}{N_{25}^o}\sigma_C^a\phi - \frac{N_D}{N_{25}^o}\lambda_D - \frac{N_D}{N_{25}^o}\sigma_D^a\phi \qquad \text{(D.16)}$$

where $\frac{N_C}{N_{25}^o}$ = concentration of stable parent nuclide C per initial U-235 atom.

σ_C^a = absorption cross-section of C, cm^2

σ_D^a = absorption cross-section of D, cm^2

The first term in Eq. (D.13) represents the rate of production of D by the (n,γ) reaction on nuclide C, while the second term represents loss by decay and the third, destruction by neutron absorption. Meanwhile, the concentration of C, with irradiation time at constant flux, is given by

$$\frac{N_C}{N_{25}^o} = \frac{\sigma_{25}^f y_C}{(\sigma_C^a - \sigma_{25}^a)} \left[e^{-\sigma_{25}^a \phi t} - e^{-\sigma_C^a \phi t} \right] \qquad (D.17)$$

Substituting the expression for N_C from (D.17) into (D.16) and solving for conditions of constant flux and no initial concentration of D atoms, one obtains

$$\frac{N_D}{N_{25}^o} = K_3 \left[e^{-\sigma_{25}^a \phi t} - e^{-(\lambda_D + \sigma_D^a) t} \right] - K_4 \left[e^{-\sigma_C^a \phi t} - e^{-(\lambda_D + \sigma_D^a) t} \right] \qquad (D.18)$$

where $$K_3 = \frac{\sigma_{25}^f y_C \sigma_C^a \phi}{(\sigma_C^a - \sigma_{25}^a)(\lambda_D + \sigma_D^a \phi - \sigma_{25}^a \phi)} \qquad (D.19)$$

and $$K_4 = \frac{\sigma_{25}^f y_C \sigma_C^a \phi}{(\sigma_C^a - \sigma_{25}^a)(\lambda_D + \sigma_D^a \phi - \sigma_C^a \phi)} \qquad (D.20)$$

Similarly, for intermittent operation, the concentration N_D/N_{25}^o follows Eq. (D.21) during the operating period

$$\frac{N_D(t_a)}{N_{25}^o} = K_3' \left[e^{-\sigma_{25}^a \phi t_a} - e^{-(\lambda_D + \sigma_D^a \phi) t_a} \right] - K_4' \left[e^{-\sigma_C^a \phi t_a} - e^{-(\lambda_d + \sigma_D^a \phi) t_a} \right] + \frac{N_C^{t_a=0} \sigma_C^a \phi}{N_{25}^o (\lambda_D + \sigma_D^a \phi)} \left[1 - e^{-(\lambda_D + \sigma_D^a \phi) t_a} \right]$$

$$+ \frac{N_D}{N_{25}^o}^{t_a=0} e^{-(\lambda_D+\sigma_D^a\phi)t_a} \qquad (D.21)$$

where $K_3' = K_3 e^{-\sigma_{25}^a \phi\tau}$ (D.22)

and $K_4' = K_4 e^{-\sigma_{25}^a \phi\tau}$ (D.23)

During the shutdown period, D is given by

$$\frac{N_D}{N_{25}^o}(t_d) = \frac{N_D}{N_{25}^o}^{t_d=0} e^{-\lambda_D t_d} \qquad (D.24)$$

The above solutions were programmed for two computer codes. One, called NUCON, was used to obtain nuclide concentrations for constant flux operation with no shutdown periods and for Eq. (D.8) Group 1 intermittent operation. The other, called NOTSFI, was used to obtain values for solutions for intermittent operation, with alternating periods of operation and shutdown. The FORTRAN listings of these codes are given in Appendix G along with descriptions of the required input data.

The fission yields and other nuclear constants used in the codes for calculating fission product concentrations are presented in Table 10. The absorption cross-sections used were Westcott "average" cross-section, $\bar{\sigma}^a$ (W6) where

$$\bar{\sigma}^a = \sqrt{\frac{\pi T_o}{4T_n}}\,\hat{\sigma}^a = \sqrt{\frac{\pi T_o}{4T_n}}\,\sigma_{2200}^a \quad (g+rs) \qquad (D.25)$$

TABLE 10

VALUES OF NUCLEAR DATA USED IN CALCULATING PREDICTED FISSION PRODUCT ACTIVITIES IN MITR FUEL ELEMENTS

Nuclide	$t_{1/2}$ (a)	λ, sec^{-1} (a)	U-235 Thermal Fission Yield %	Cross-Section, barns
Zr^{95}	65 d.	1.234×10^{-7}	6.27 (b)	0
Nb^{95}	35 d.	2.292×10^{-7}	0	0 (c)
Ru^{106}	1.01 yr.	2.175×10^{-8}	0.38 (b)	0
Rh^{106}	30 s.	-	0	0
Cs^{133}	Stable	0	6.75 (d)	30.3 (e)
Cs^{134}	2.19 yr.	9.982×10^{-9}	0	103.89 (e)
Cs^{137}	30.0 yr.	7.33×10^{-10}	6.00 (f)	0
Ba^{140}	12.8 d.	6.268×10^{-7}	6.44 (b)	0
La^{140}	40.2 h.	4.79×10^{-6}	0	0
Ce^{144}	280 d.	2.865×10^{-8}	5.62 (b)	0 (g)
Pr^{144}	17.5 m.	6.60×10^{-4}	0	0
U^{235}	-	-	-	$\sigma_{25}^{f}=427.45$ (h) $\sigma_{25}^{a}=511.90$

References

(a) See Table 5.

(b) S. Katcoff, Nucleonics 18 (11), 201-8 (1960).

(c) ORNL-3488, Nuclear Chemistry - upper limit of ~7 barns.

(d) R.P. Larson, ANL-6900, p.335-340 (1964).

(e) See Appendix H.

(f) R.G. Hart, et al, Nuclear Sci. Eng. 18, 6-17 (1964).

(g) P.M. Lantz, Nuclear Sci. Eng. 13, 289 (1962)

(h) Ref. M3.

where T_o = 293.6°K

T_n = neutron temperature = 383.6°K for MITR (M3)

Thus,
$$\sqrt{\frac{\pi T_o}{4T_n}} = 0.7753 \qquad (D.26)$$

The use of "average" cross-sections required the use of the average neutron flux $\bar{\phi}$ to obtain correct reaction rates. The values of U^{235} absorption and fission cross-sections are the same as those used by Mayman in his two-group depletion code (M3), so that valid comparisons in burnup predictions could be made. Similarly, the value of Westcott's "r" factor used was 0.0715 calculated by Mayman from experimental data for the MITR fuel supplied by Mathews (M4). Calculation of the Cs^{133} absorption cross-section is presented in detail in Appendix H. Also included in Appendix H are graphs giving fission product activities per initial U^{235} atom for constant flux operation as a function of irradiation time for Zr^{95}, Nb^{95}, Ru^{106}+Rh^{106}, Cs^{134}, Cs^{137}, Ba^{140}+La^{140}, and Ce^{144}+Pr^{144}.

Curves are presented here for the activities per initial U^{235} atom vs. total in-pile residence time for various fluxes for MITR fuel. The intermittent operating conditions assumed for the calculations were 95 hours at constant flux, followed by a shutdown period of 73 hours. The solutions to Eq. (D.6) and Eq. (D.7) for these conditions are shown in Fig. 51 for Zr^{95}, in Fig. 54 for Cs^{137}, in Fig. 55 for Ba^{140} and in Fig. 56 for Ce^{144}. Similarly, Fig. 52 gives values for Eqs. (D.13)

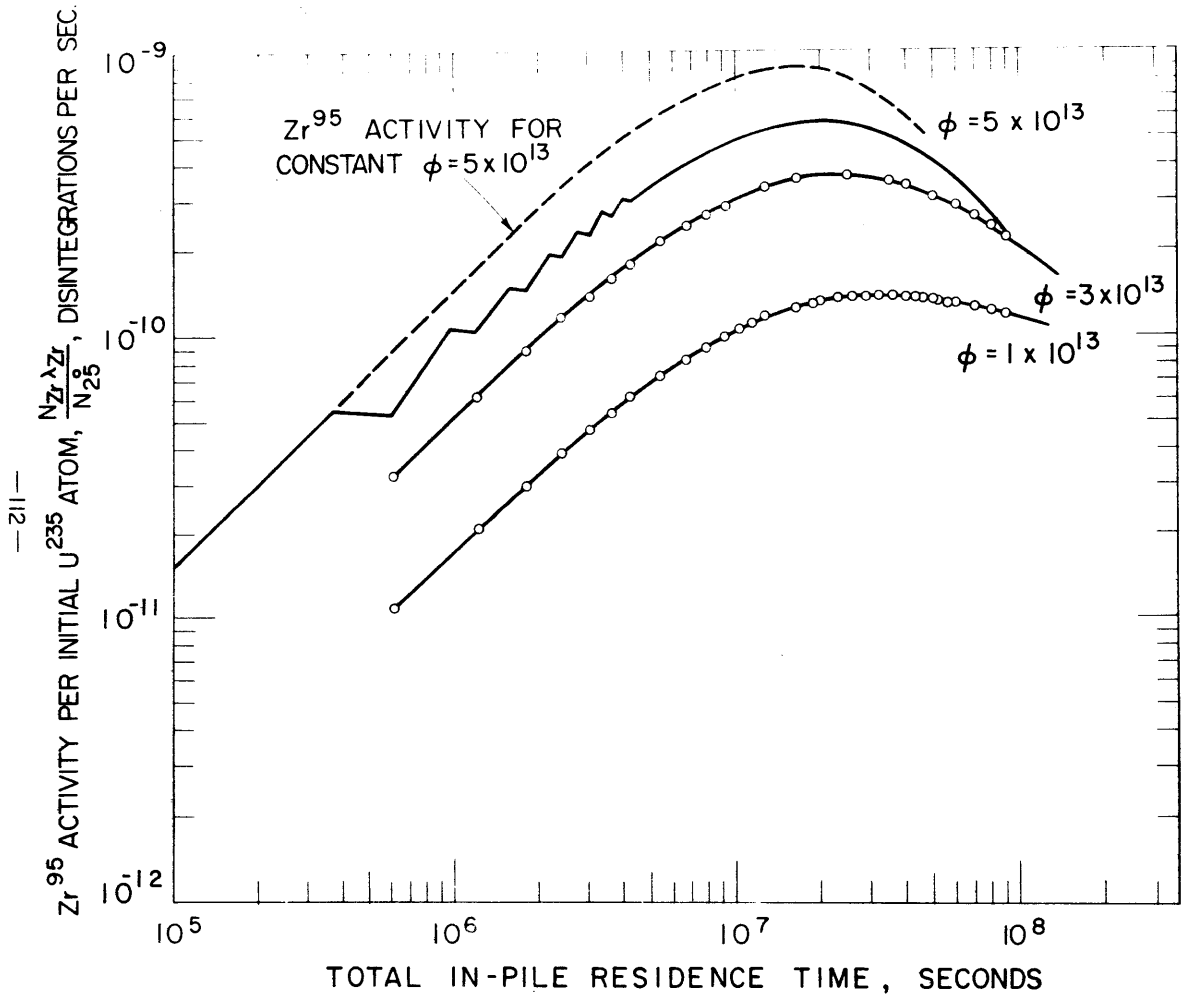

FIGURE 51 Zr^{95} ACTIVITY IN MITR FUEL FOR INTERMITTENT OPERATION (95 HRS ON, 73 HRS OFF) AS A FUNCTION OF IN-PILE RESIDENCE TIME FOR VARIOUS FLUXES

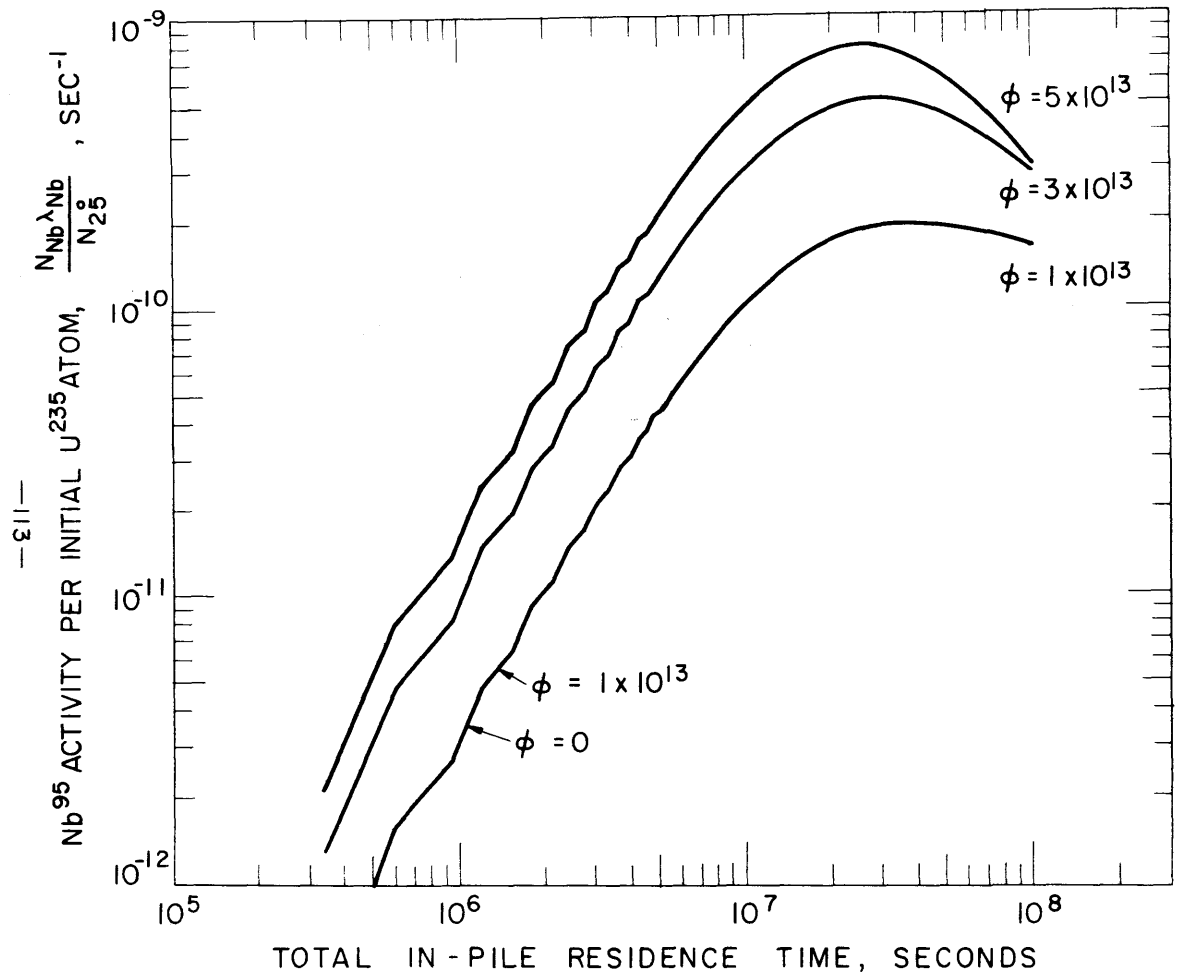

FIGURE 52 Nb^{95} ACTIVITY PER INITIAL U^{235} ATOM vs TOTAL RESIDENCE TIME FOR INTERMITTENT OPERATION (95 HRS ON : 73 HRS OFF)

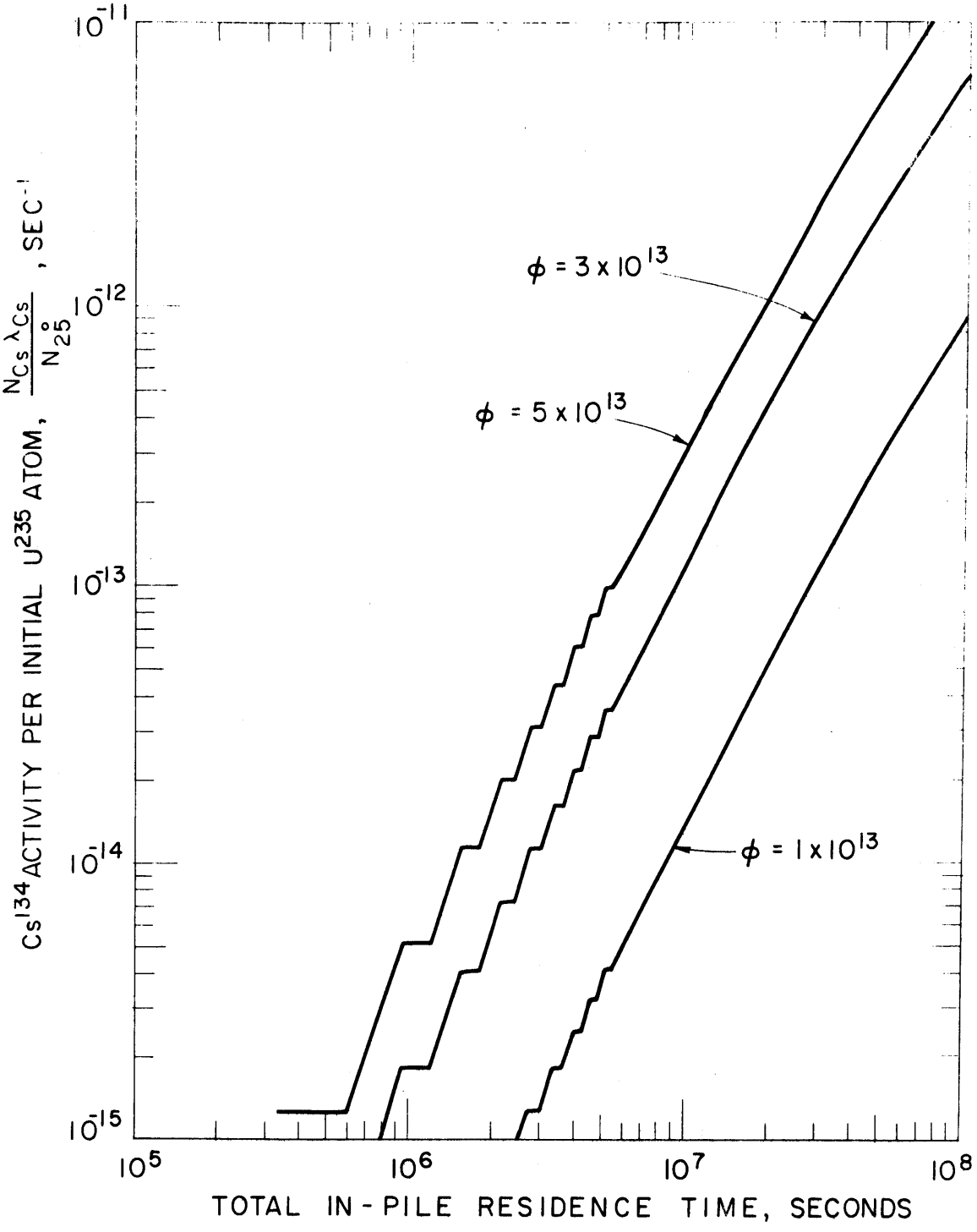

FIGURE 53 Cs^{134} ACTIVITY PER INITIAL U^{235} ATOM vs TOTAL RESIDENCE TIME FOR INTERMITTENT OPERATION (95 HRS ON : 73 HRS OFF)

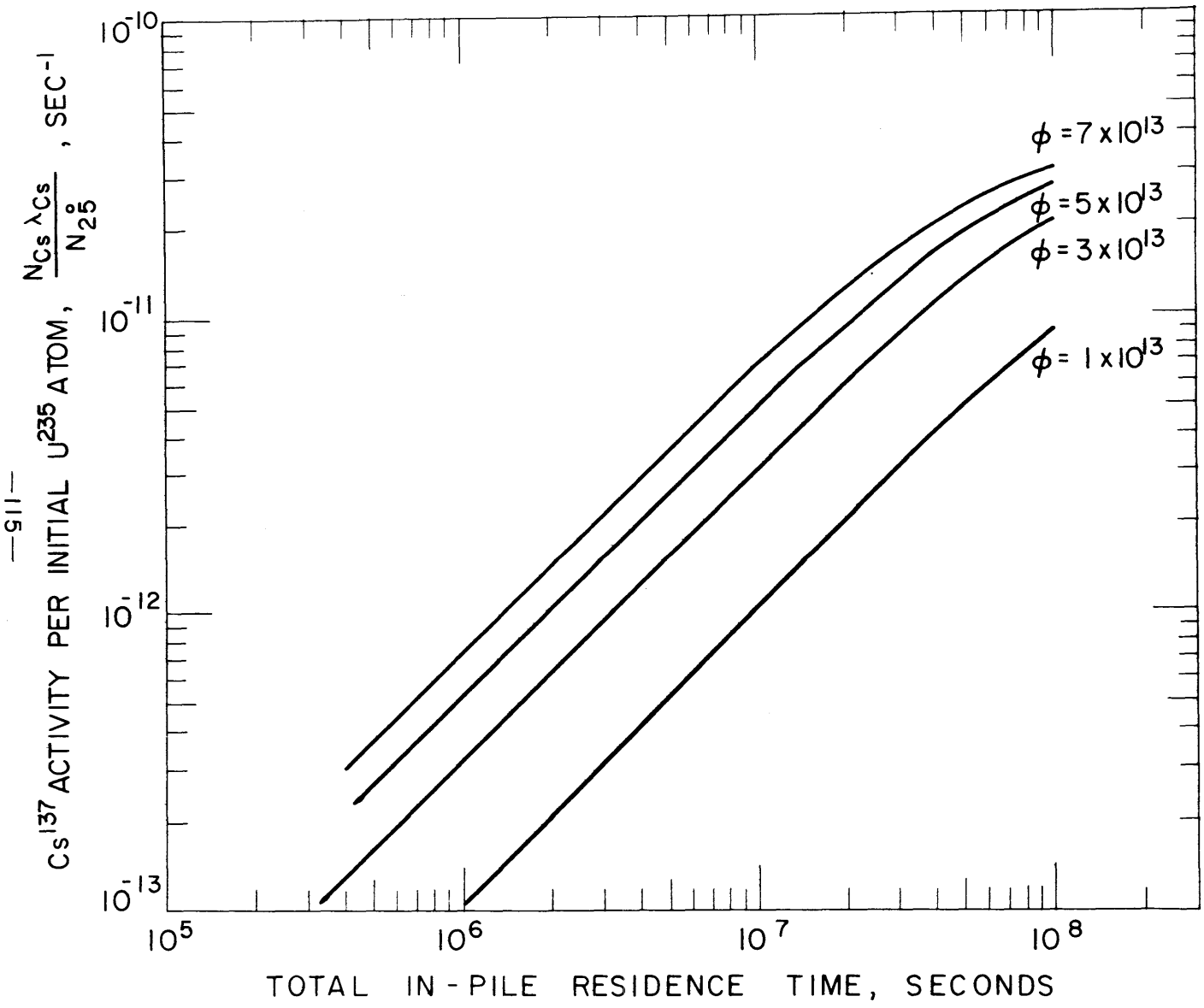

FIGURE 54 Cs^{137} ACTIVITY PER INITIAL U^{235} ATOM vs TOTAL RESIDENCE TIME FOR INTERMITTENT OPERATION (95 HRS ON: 73 HRS OFF)

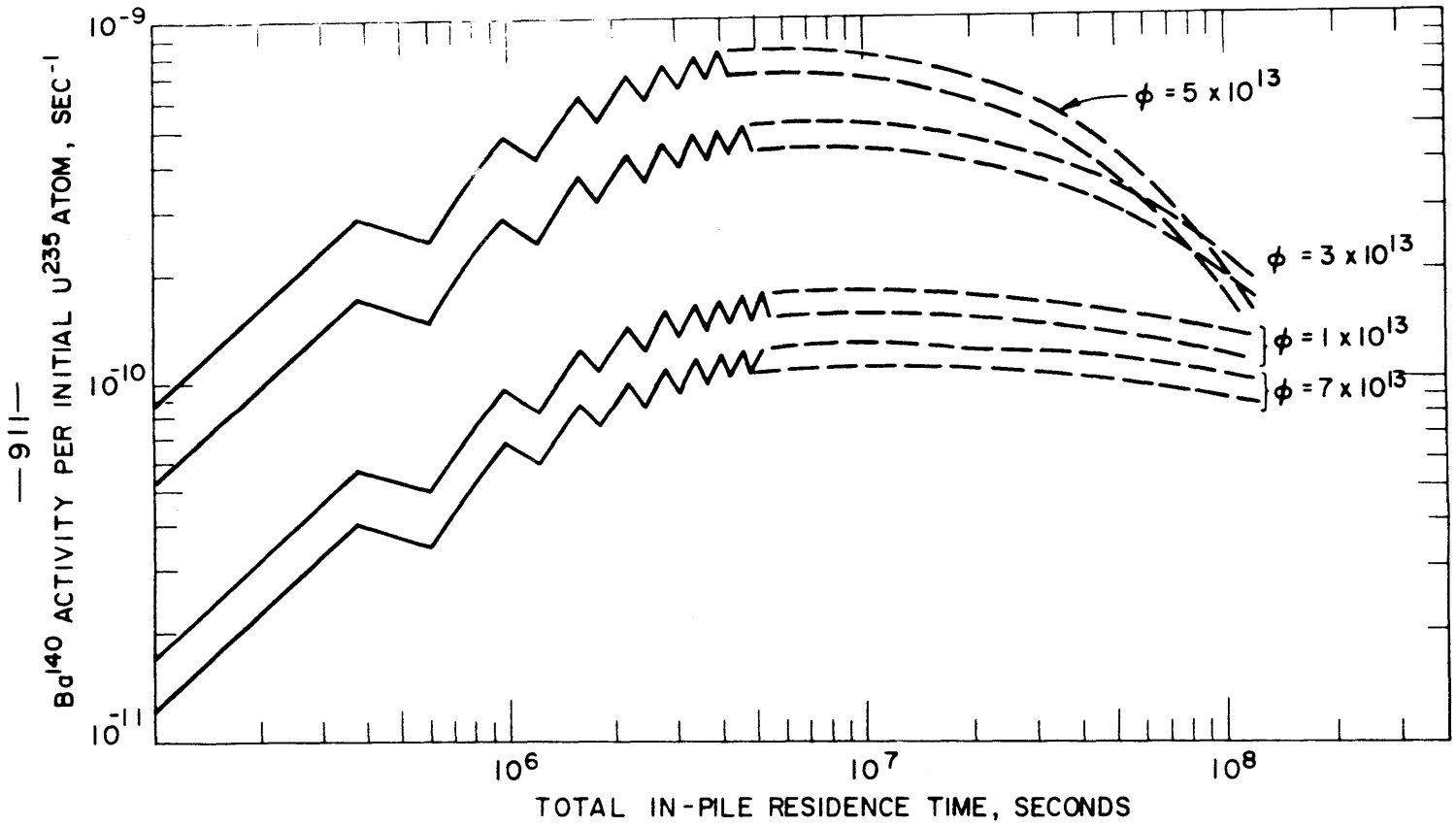

FIGURE 55 Ba^{140} ACTIVITY PER INITIAL U^{235} ATOM IN MITR FUEL FOR INTERMITTENT OPERATION (103/65) AS A FUNCTION OF IN-PILE RESIDENCE TIME FOR VARIOUS NEUTRON FLUXES

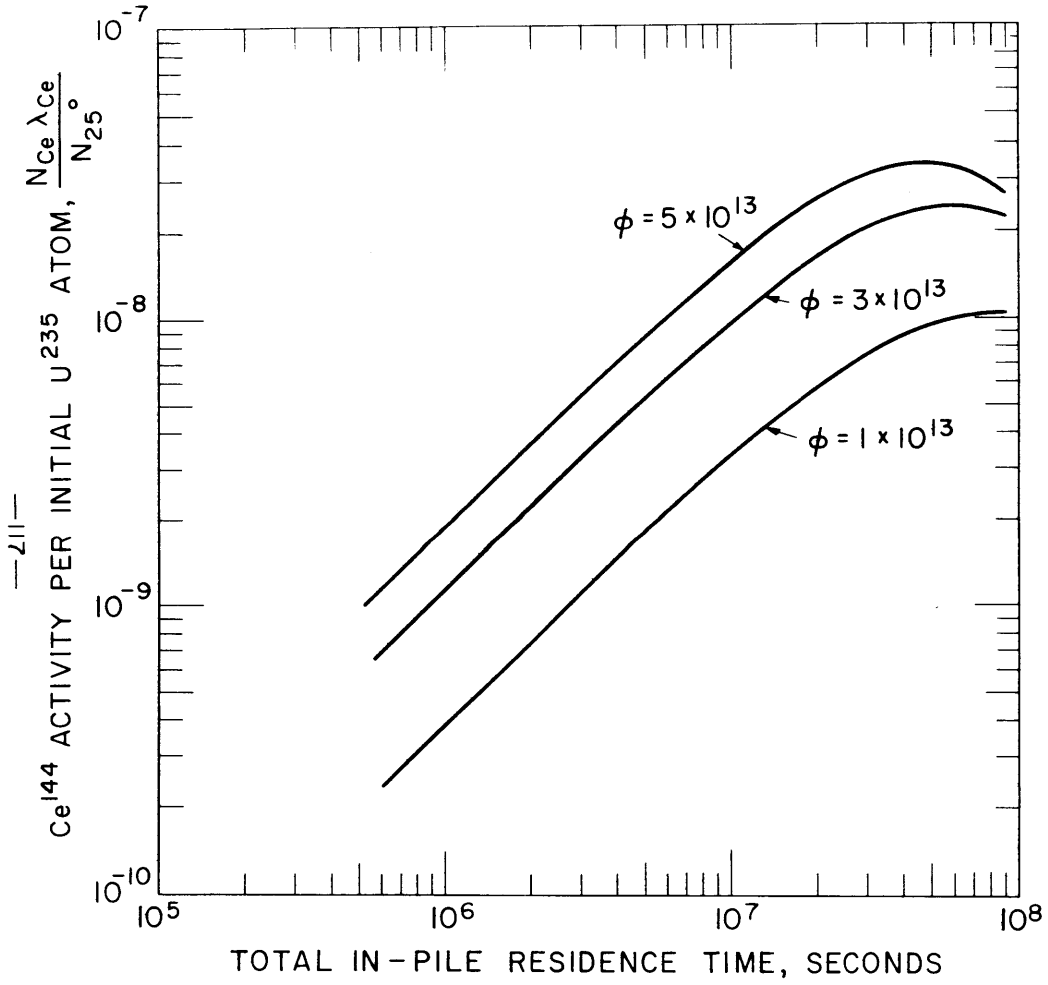

FIGURE 56 Ce^{144} ACTIVITY PER INITIAL U^{235} ATOM IN MITR FUEL FOR INTERMITTENT OPERATION (95 HRS ON : 73 HRS OFF) vs. TOTAL IN-PILE RESIDENCE TIME FOR VARIOUS FLUXES

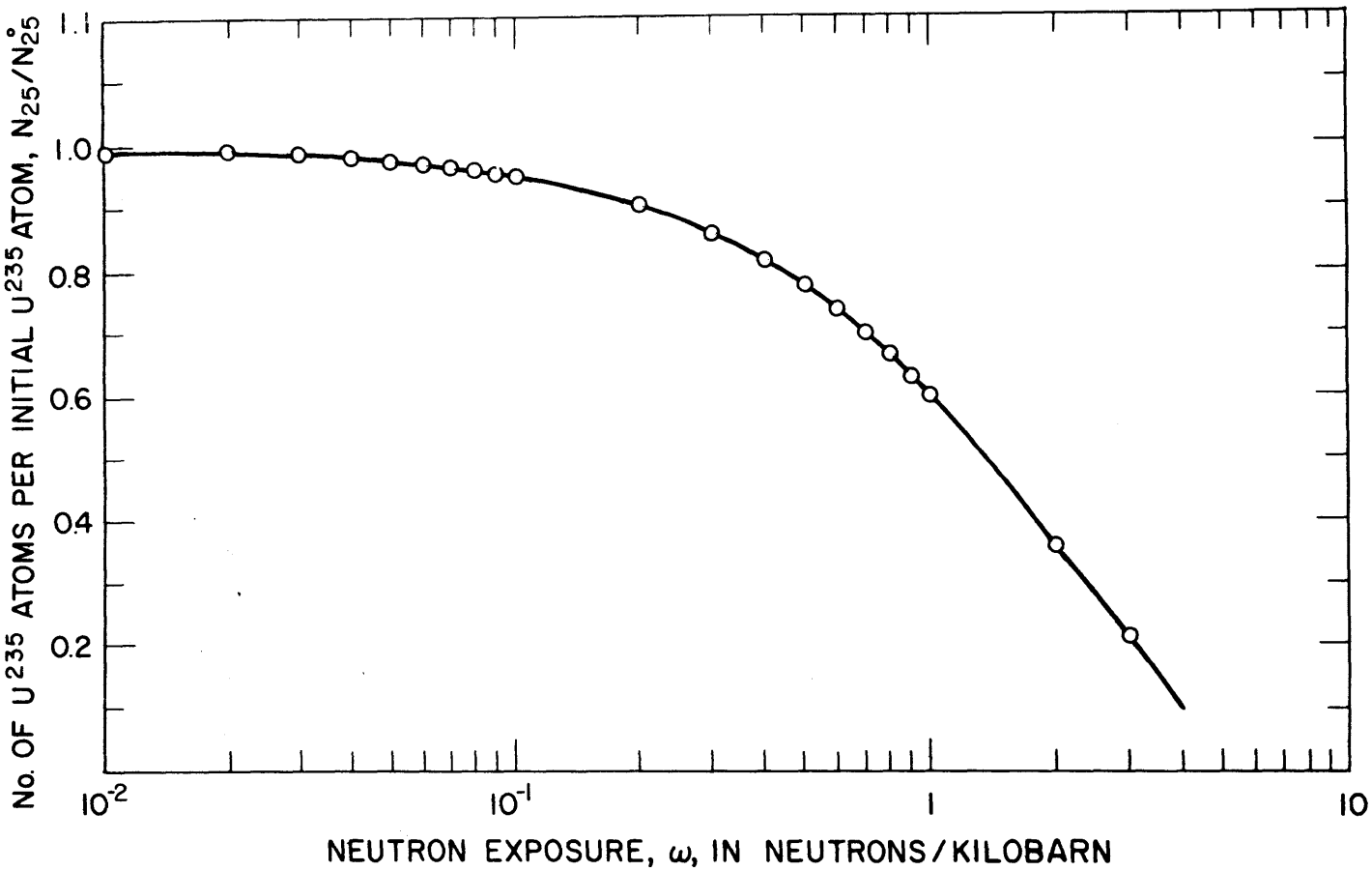

FIGURE 57 NUMBER OF U^{235} ATOMS REMAINING PER INITIAL U^{235} ATOM, N_{25}/N_{25}° AS A FUNCTION OF NEUTRON EXPOSURE, CALCULATED FOR MITR FUEL

and (D.15) for Nb^{95}, while Fig. 53 gives values for Cs^{134} using Eqs. (D.21) and (D.24). Those curves not showing the full cycle have been plotted for times corresponding to the end of each shutdown period.

The variation of the number of atoms of U^{235} per initial U^{235} atom from Eq. (D.4), as a function of neutron exposure $\phi\tau$, where τ is the total irradiation time, is shown in Fig. 57. The effect of U^{235} burnup is to cause a maximum in the value of all the fission product activities except Cs^{137}.

Activity ratios as a function of neutron exposure, $\phi\tau$, were calculated and are shown in Fig. 58 for

$$R_1 = \frac{A(Cs\text{-}137)}{A(Cs\text{-}134)} = \frac{(N\lambda)Cs\text{-}137}{(N\lambda)Cs\text{-}134}$$

in Fig. 59 for $$R_2 = \frac{A(Cs\text{-}137)}{A(Zr\text{-}95)} = \frac{(N\lambda)Cs\text{-}137}{(N\lambda)Zr\text{-}95}$$

and in Fig. 60 for $$R_3 = \frac{A(Cs\text{-}137)}{A(Pr\text{-}144)} = \frac{(N\lambda)Cs\text{-}137}{(N\lambda)Pr\text{-}144}$$

The dotted lines in the Figures correspond to the corrected experimental values of these ratios obtained in Run D4 for element 2M19.

The important fact to be noted is the marked difference in behavior with exposure and flux between R_1 and the others. The ratio R_1 decreases with exposure and is relatively unaffected by the flux level except at high exposures, whereas R_2 and R_3 increase with exposure and depend strongly on the

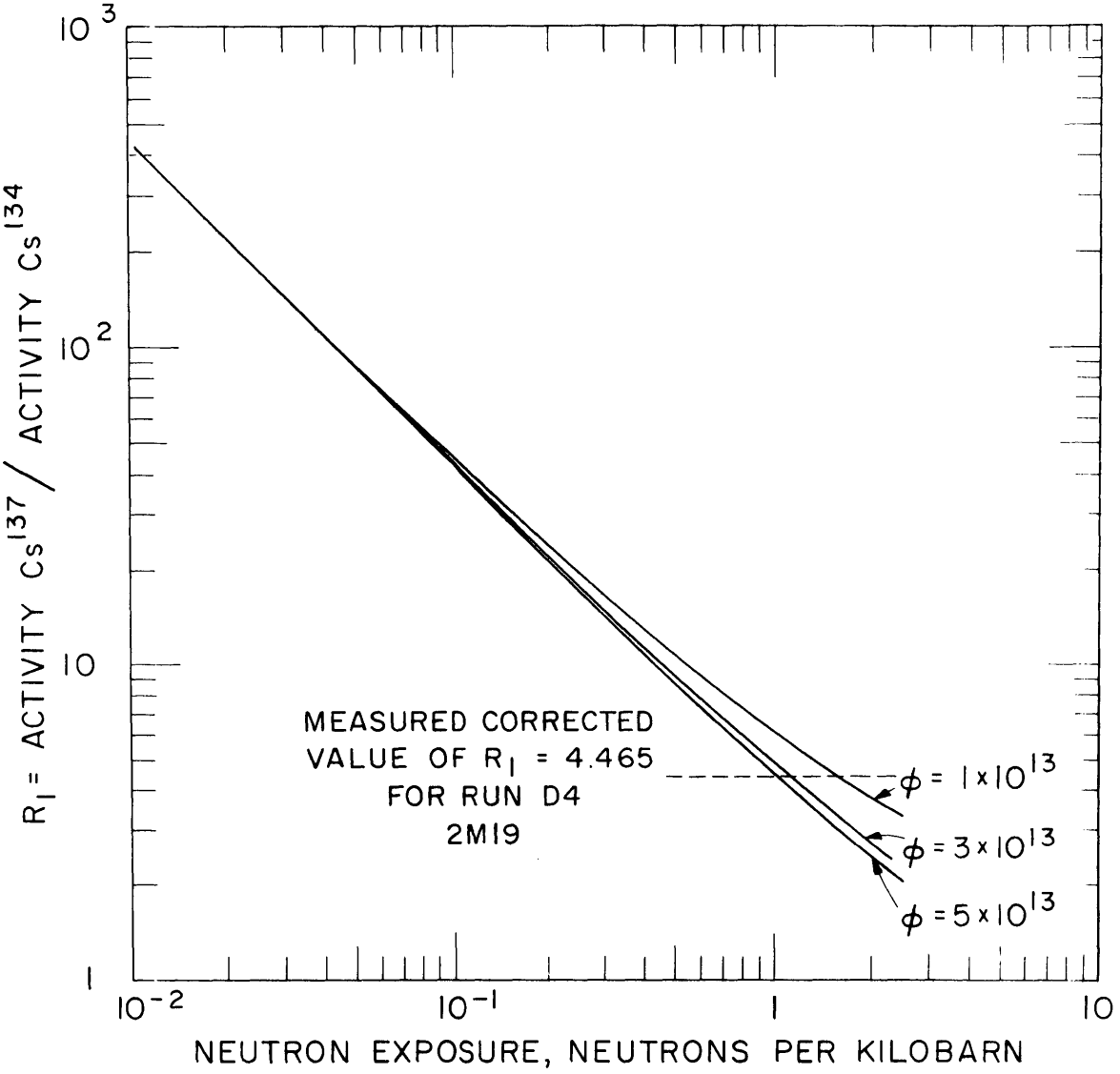

FIGURE 58 RATIO OF Cs^{137} TO Cs^{134} ACTIVITIES vs. NEUTRON EXPOSURE FOR MITR FUEL AT VARIOUS FLUXES FOR INTERMITTENT OPERATION, 95 HRS ON, 73 HRS OFF

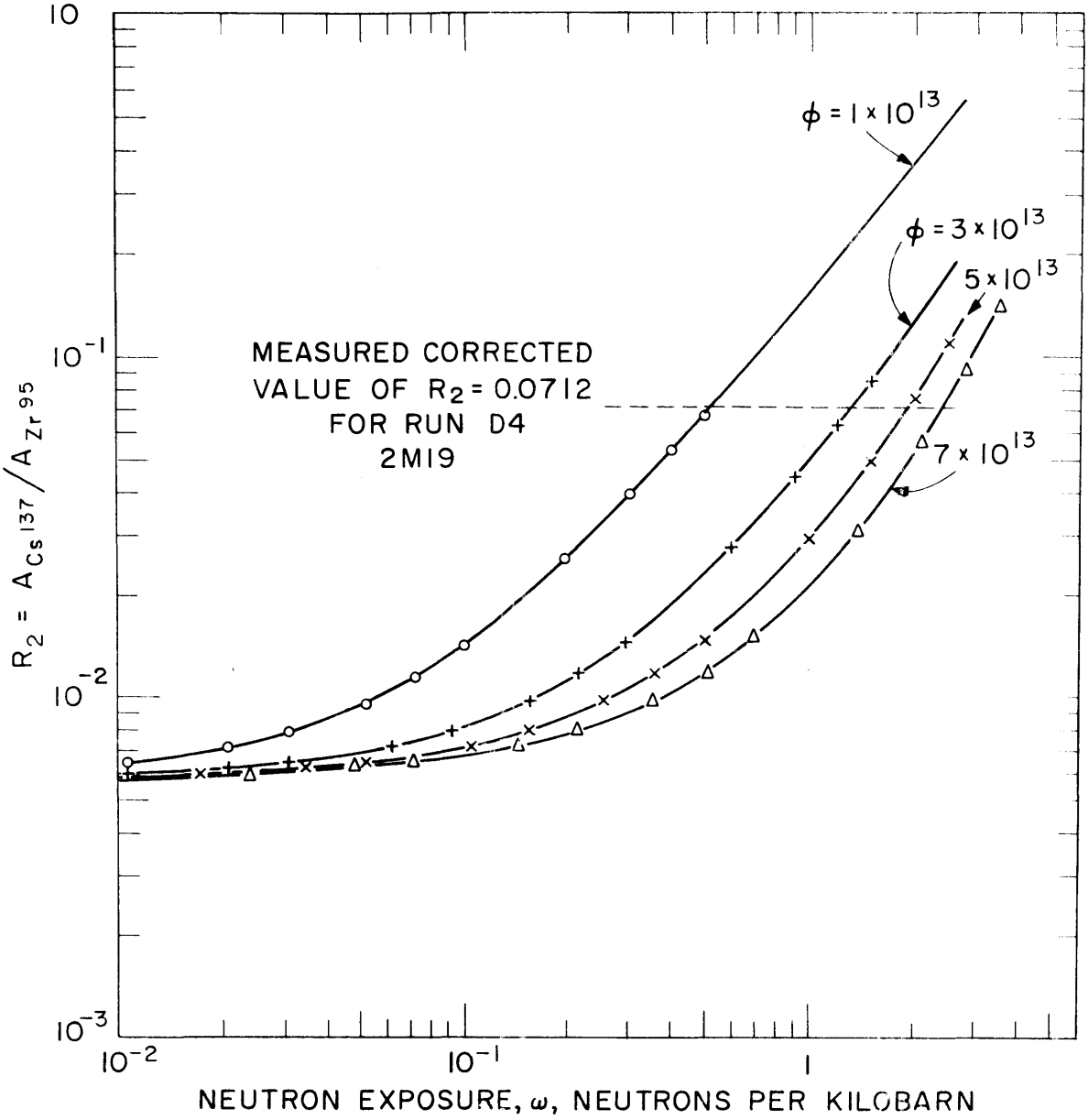

FIGURE 59 RATIO OF Cs^{137} TO Zr^{95} ACTIVITY AS A FUNCTION OF NEUTRON EXPOSURE FOR VARIOUS FLUXES. MITR INTERMITTENT. OPERATION 95 HRS ON, 73 HRS OFF.

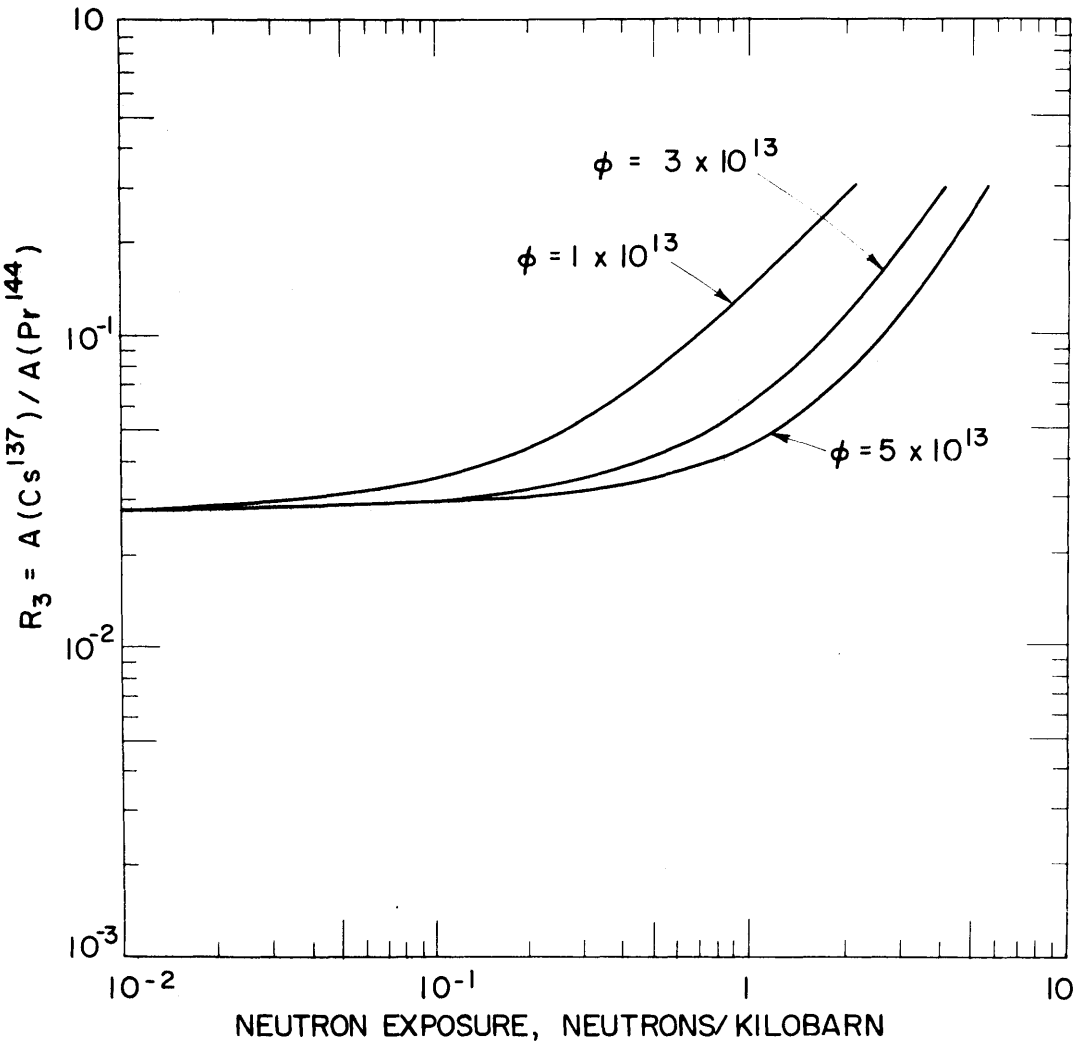

FIGURE 60 RATIO OF Cs^{137} TO Pr^{144} ACTIVITIES, R_3 AS A FUNCTION OF NEUTRON EXPOSURE FOR INTERMITTENT OPERATION (95 HRS ON: 73 HRS OFF)

flux level. It is this difference which makes the subsequent analyses possible.

3. Determination of Irradiation History of Fuel Element from Experimental Results

(a) Determination of Absolute Flux and Irradiation Time

The method developed for determining the absolute neutron flux and irradiation time experienced by a fuel element will be illustrated with results from Run D4 for element 2M19. The values of corrected measured activity ratios R_1 and R_2, as given in Table 6, are shown drawn as dotted lines in Figs. 58 and 59 respectively, where $R_1 = 4.465$ and $R_2 = 0.0712$. The intersections of the experimental dotted lines with the theoretical lines for the various fluxes gives two sets of values of neutron flux and exposure. These two sets are now plotted as flux vs. exposure, as shown in Fig. 61. The intersection of the two curves gives a unique solution for the absolute neutron flux, ϕ, and the total exposure, $\phi\tau$. Hence, the irradiation time consistent with these values follows directly.

For the example given, this method obtains

$$\phi = 2.71 \times 10^{13} \text{ n/cm}^2\text{-sec}$$

$$\text{and} \quad \sigma = 1.20 \text{ neutrons/kilobarn.}$$

$$\text{Thus} \quad \tau = 0.443 \times 10^{8} \text{ seconds.}$$

To improve the accuracy and reproducibility of the method, an enlarged version of Fig. 58 was used while an equivalent plot of R_1 vs. flux for various irradiation times was used instead of Fig. 59.

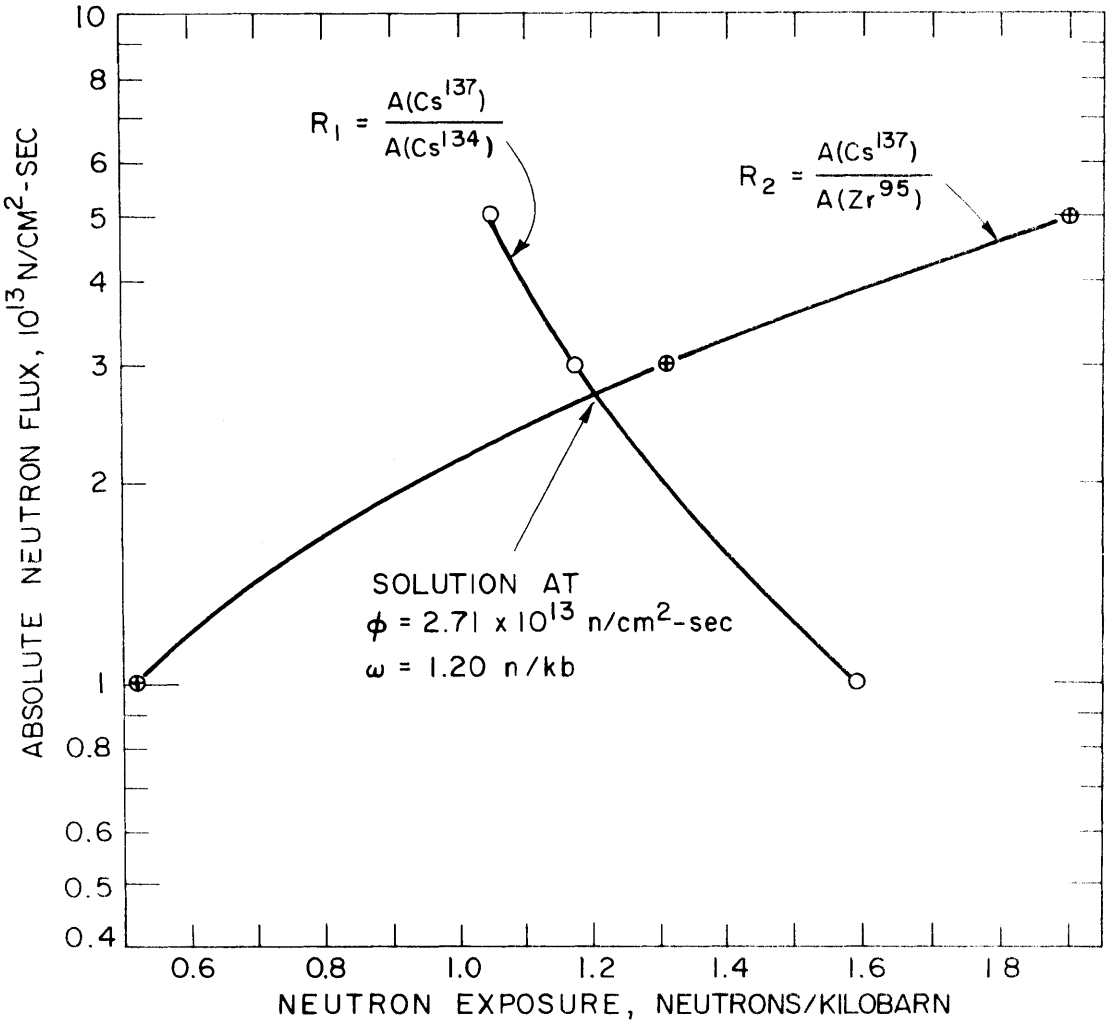

FIGURE 61 CURVES OF NEUTRON FLUX vs NEUTRON EXPOSURE FOR ACTIVITY RATIOS R_1 AND R_2 INDICATING METHOD OF SOLUTION FOR FLUX AND EXPOSURE

The same procedure was then applied to the other values of R_1 and R_2 at different positions along the element. The axial distribution of the absolute average neutron flux* within 2M19 is shown in Fig. 62. Included for comparison are values calculated from results obtained by Mathews (M4) using cobalt wire monitors for a 162-gram element in position 18. These particular results were used because the core positions for 2M19 and Mathews' data were equivalent and in both cases, the initial U^{235} weight in the element was 162 grams. In addition, sufficient axial data points were reported so that detailed comparisons of axial flux distributions could be made. The cobalt results were obtained when the core was loaded with 105-gram elements in positions 1 through 7, 8, 11, 14 and 17 and with 162-gram elements in positions 9, 10, 12, 13, 15, 16, 18 and 19. The shim-safety rods were at 22.92 inches, the regulating rod was at 20.88 inches and the D_2O temperature was 22.8°C. Relative cobalt wire activity results were taken from Table 4.18.16, p.163 for position 18.M (M4).

Some flux transverses were obtained by Mathews for a

---

* The cross-sections used in the solutions for fission product activities were "average" values. Thus, in order to obtain corrected reaction rates, an "average" neutron flux must be used. Therefore, the values obtained here represent the average neutron flux defined by

$$\bar{\phi} = n\bar{v} = nv_o\sqrt{\frac{4T}{\pi T_o}}$$

where v_o = 2200 m/sec. and n = no. of neutrons/cc.

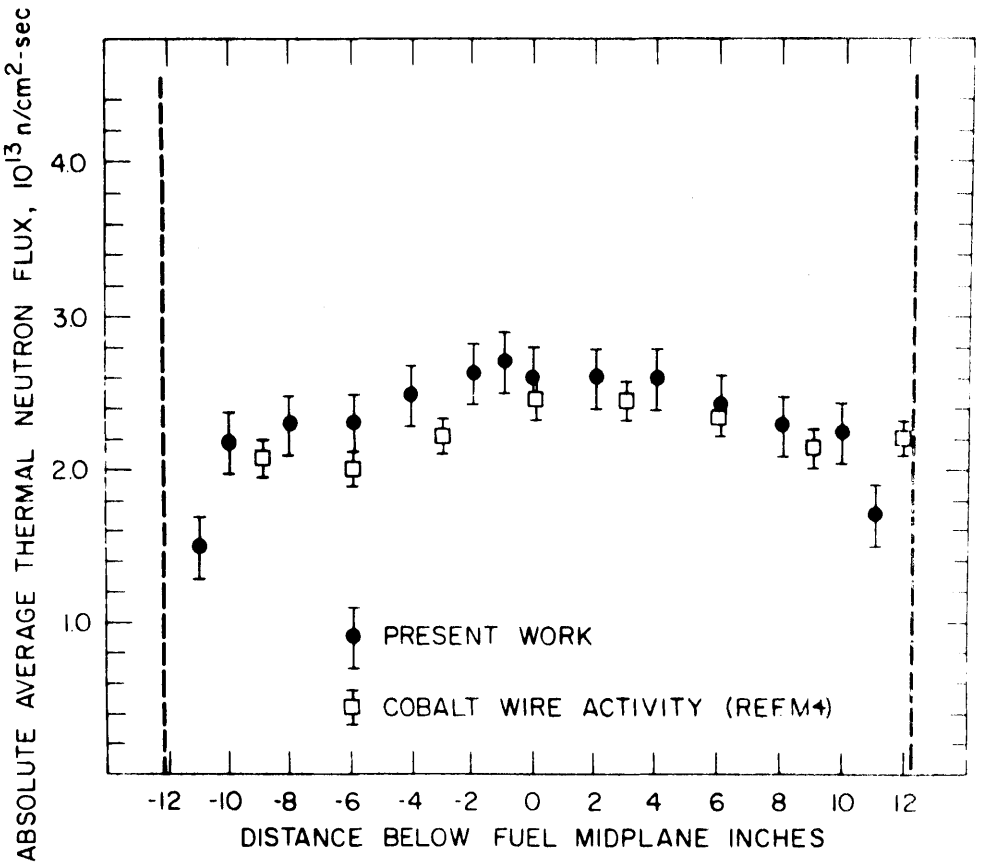

FIGURE 62 AXIAL DISTRIBUTION OF AVERAGE THERMAL NEUTRON FLUX IN ELEMENT 2MI9

core poisoned to simulate the effect of fission products. Comparisons of the fluxes would probably be more valid if these results could have been used. However, insufficient data points were available and the core positions were not equivalent to 2M19.

Since the present method obtains a flux value that is an average across the element, the cobalt wire results were corrected for the effect of flux depression within the element. The relative cobalt activity, spatially averaged across 16 fuel plates, was calculated to be 0.70, while the central value at point 18.M was 0.64. Thus the correction factor applied was 0.70/0.64 = 1.095. The maximum relative activity used was 1.558 (M4, p.194) while the maximum value of the absolute average flux used was 2.74×10^{13} n/cm^2-sec (from M4, p.196, $2.4 \times \sqrt{T/T_o} \times 10^{13}$ n/cm^2-sec for T = 383.6°K). Therefore, at 1.95 MW the maximum average flux in the core (i.e. in the moderator near the center of the core) from Mathews' results was 5.35×10^{13} n/cm^2-sec. The corrected flux in the element was then obtained by dividing 5.35×10^{13} by 1.558 and multiplying by the corrected relative cobalt activity. For example, at the central midplane,

$$\text{relative Co activity} = 0.64$$

$$\text{corrected rel. Co activity} = (0.64)(1.095) = 0.70$$

$$\therefore \text{corrected average flux at position 17} = \frac{(5.35 \times 10^{13})}{1.558} \times 0.70$$

$$= 2.41 \times 10^{13} \text{ n/cm}^2\text{-sec.}$$

The error assigned in the present calculations is ±10%, while the cobalt wire results were quoted to ±5%.

As can be seen in Fig. 62, the agreement between the two measurements is within the assigned error. The flux depression at the top of the element due to the presence of the shim control rods is evident in results obtained by the present method but not in the cobalt results.

The axial distribution of neutron exposure in neutrons/kilobarn for 2M19, as calculated by the above method, is shown in Fig. 63. The results are summarized in Table 11. The average value of exposure obtained by graphical integration was 1.08 n/kb., while the average value obtained for the irradiation time, $\bar{\tau}$ was $(0.464 \pm 0.008) \times 10^8$ seconds. The actual irradiation time as determined from operating records was $(0.448 \pm 0.013) \times 10^8$ seconds. The two values differ by 3.6%.

Using the average exposure for the element of 1.08 n/kb., the fraction of U^{235} remaining in 2M19 from Fig. 58 was $N_{25}/N_{25}^{o} = 0.57 \pm 0.06$. The value predicted for this element by MITBURN, a two-group depletion code (M3) was 0.656. The discrepancy between the two values is about 14%. A number of explanations are possible for this discrepancy. It has been found that in comparing the power production from a single element as obtained by experimentally measured thermodynamic balances, to that predicted by the MITBURN for the same element and conditions, the code underestimates the total power produced in the element by as much as 17% in some cases (B13).

TABLE 11

SUMMARY OF RESULTS OF ANALYSIS

OF FUEL ELEMENT 2M19

FOR FLUX, EXPOSURE AND IRRADIATION TIME

Run	Position Below Fuel Midplane, Inches	Neutron Flux ϕ, 10^{13} n/cm^2,sec.	Neutron Exposure ϖ, n/kb	Irradiation Time τ, 10^8 seconds
D4	- 1	2.71	1.20	0.443
D5	0	2.61	1.17	0.446
D6	+ 2	2.62	1.21	0.461
D7	+ 4	2.61	1.26	0.484
D8	+ 6	2.42	1.08	0.448
D9	+ 8	2.31	1.19	0.513
D10	+ 10	2.23	1.17	0.525
D11	+ 11	1.72	0.84	0.488
D12	- 2	2.61	1.20	0.461
D13	- 4	2.50	1.09	0.436
D14	- 6	2.30	1.03	0.448
D15	- 8	2.29	0.984	0.430
D16	- 10	1.93	0.848	0.439
D17	- 11	1.54	0.738	0.479

Average exposure, $\bar{\varpi}$ = 1.08 n/kb.

Mean Irradiation Time, $\bar{\tau}$ = $(0.464 \pm 0.008) \times 10^8$ seconds

Actual Irradiation Time = $(0.448 \pm 0.013) \times 10^8$ seconds

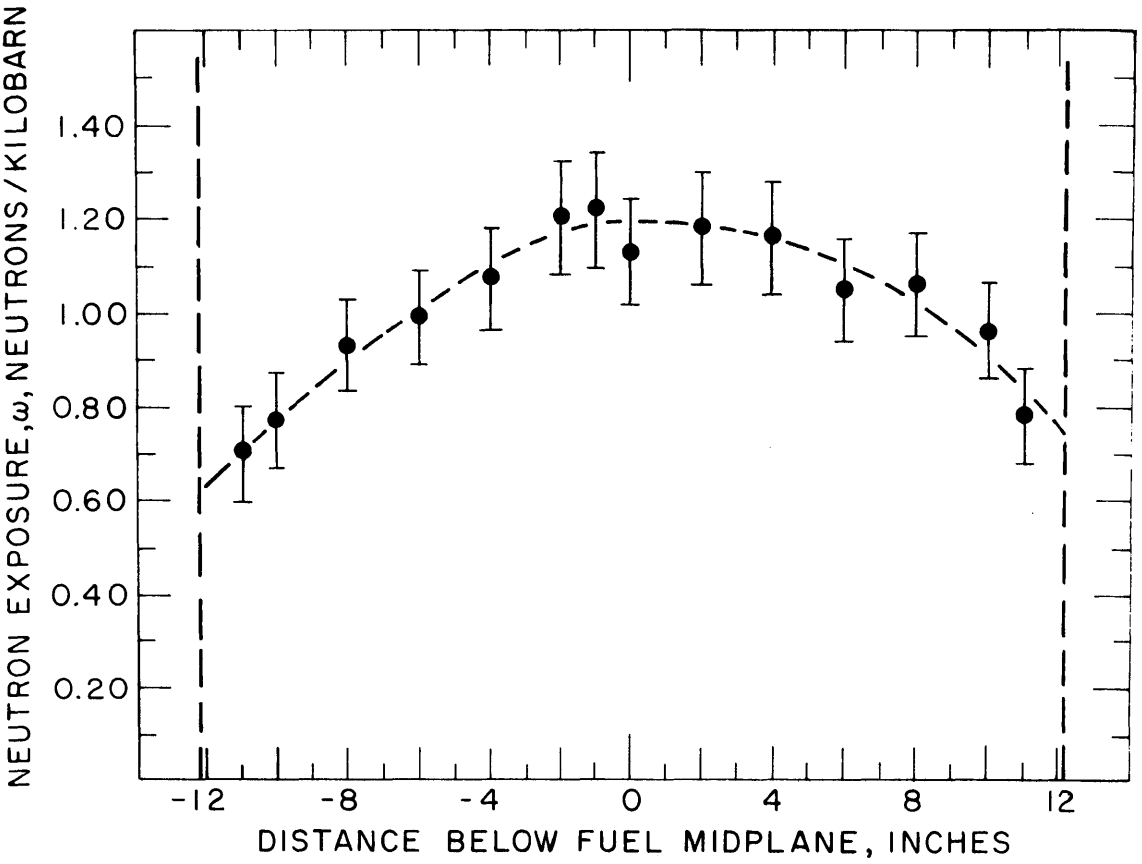

FIGURE 63 AXIAL DISTRIBUTION OF NEUTRON EXPOSURE IN NEUTRONS/KILOBARN FOR FUEL ELEMENT 2M19

Thus, in order for the code to obtain the same amount of power from the element, a corresponding larger amount of U^{235} must be burned. Allowing for this correction, the burnup of U^{235} predicted by the code is in reasonable agreement with that obtained by the present method.

Similar calculations for element 2M22 were carried out, and the results are summarized in Table 12. The irradiation time was calculated to be $(0.572 \pm 0.028) \times 10^8$ seconds, compared to the actual exposure time of 0.482×10^8 seconds; an error of less than 19%. The average exposure obtained was 1.23 n/kb., with $N_{25}/N_{25}^{o} = 0.525$. Mayman's code predicted 0.596 for N_{25}/N_{25}^{o}. The absolute thermal flux distribution along the element is given in Fig. 64, including values from Mathews' results*. The uncertainty in the flux values is about 25% because of the large statistical

---

* Since element 2M22 was located in position 7 during its final year of operation, Mathews' results for position 7 were used: Table 4.18.4, p.161, line 7.M. However, these results were obtained for a 105-gram element whereas 2M22 is a 162-gram element. Therefore, since flux depression would be greater in 2M22, and the absolute flux lower, Mathews' results were reduced by the ratio of the thermal disadvantage factors for 105- and 162-gram elements. (Table 5.2.6, p.184, copper results for position 1.)

$$\frac{\left[\bar{\phi}_m/\bar{\phi}_F\right]_{105\ gm}}{\left[\bar{\phi}_m/\bar{\phi}_F\right]_{162\ gm}} = \frac{1.374}{1.51} = 0.911$$

Other calculations were as for 2M19.

TABLE 12

SUMMARY OF RESULTS OF ANALYSIS

OF FUEL ELEMENT 2M22

FOR FLUX, EXPOSURE AND IRRADIATION TIME

Run	Position Below Fuel Midplane, Inches	Neutron Flux, ϕ, 10^{13} n/cm^2-sec.	Neutron Exposure, ϖ, n/kb	Irradiation Time, τ, 10^8 seconds
H1	0	2.65	1.41	0.532
H2	- 2	2.13	1.55	0.728
H3	- 4	2.45	1.39	0.567
H4	- 6	2.37	1.33	0.561
H5	- 8	2.48	1.05	0.423
H6	- 10	1.49	1.10	0.738
H7	- 11	2.00	0.96	0.480
H8	+ 2	2.81	1.36	0.484
H9	+ 4	2.21	1.50	0.679
H10	+ 6	2.62	1.34	0.511
H11	+ 8	2.01	1.13	0.562
H12	+ 10	1.90	1.14	0.600

Average Exposure, $\bar{\varpi}$ = 1.23 n/kb

Mean Irradiation Time, $\bar{\tau}$ = $(0.572 \pm 0.028) \times 10^8$ seconds

Actual Irradiation Time = $(0.484 \pm 0.014) \times 10^8$ seconds

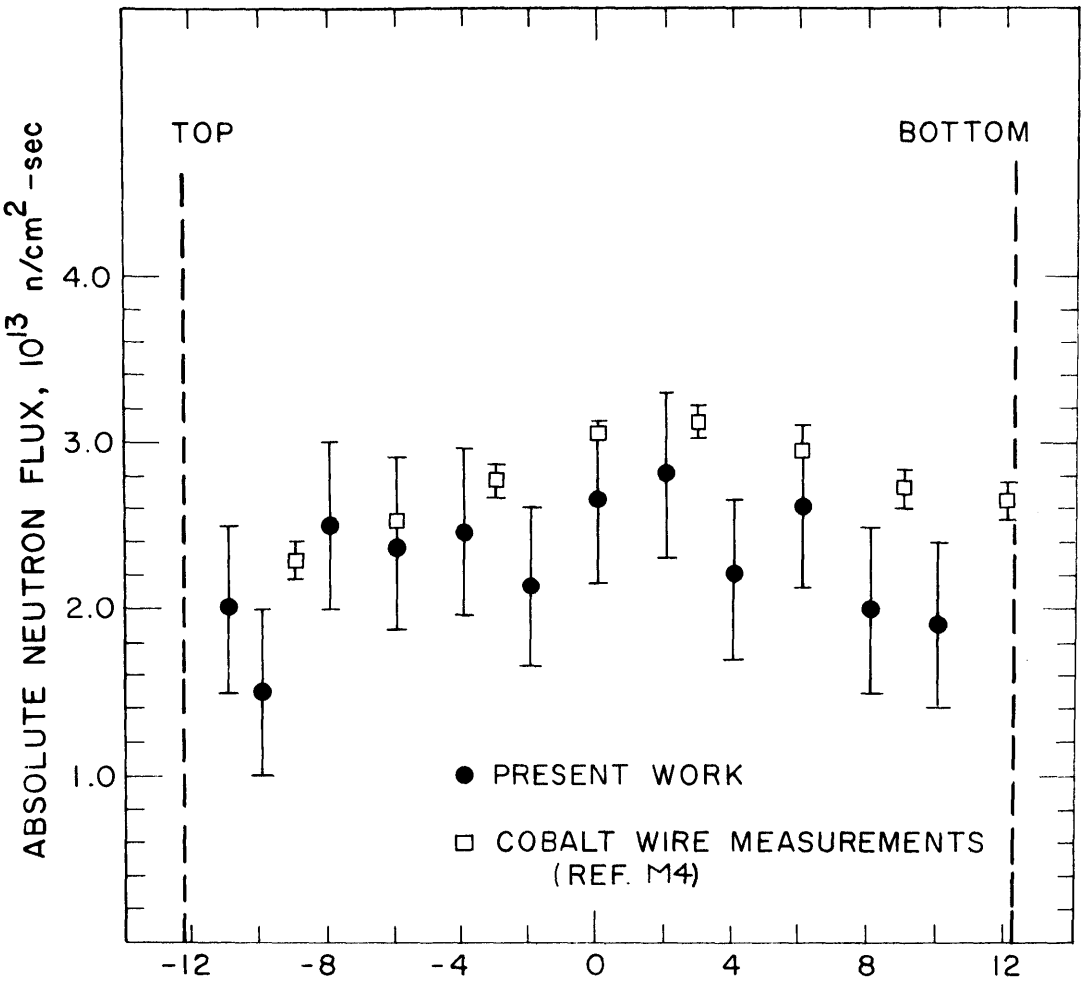

FIGURE 64 AXIAL DISTRIBUTION OF THERMAL NEUTRON FLUX IN FUEL ELEMENT 2M22

deviations in the intensity of the Zr^{95} gamma-ray at 724 keV. It is felt that the poor agreement for irradiation time is in part due to this large uncertainty in Zr^{95} activity. Also, and possibly as important, is the fact that 2M22 did not reside in the same location in the core during its in-pile residence time. It was charged into position 11 where it remained for one year, then was moved to position 7 were it remained for about 1 2/3 years when it was discharged. In addition, during its first four months of in-pile residence, the reactor was operating at 1 MW, after which it began operation at 2 MW. In view of these considerations, the agreement is as good as could be expected.

Following the same procedures as above, using R_1 and R_3 instead of R_1 and R_2, approximately the same results for flux, exposure and irradiation time should have been obtained for these elements. However, using the corrected ratios of R_3 and R_1, lower values for fluxes and high values for exposure, and thus higher values for the irradiation time were obtained. This discrepancy is probably due to errors in the calculation of the intensity of the Pr^{144} gamma-ray at 697 keV. It was noted in Section II that there appeared to be some other gamma-ray present just below 697 keV whose presence would result in a background subtraction larger than necessary. Thus, a low value of Pr^{144} activity would be calculated, resulting in a high value for R_3. This in turn results in solutions for the flux being too low, the exposure being too high, and the irradiation time being too large, as was in fact

found. To calculate the Pr^{144} activity in the fuel using the 1164 double escape peak or the 2186 keV photopeak, it would be necessary to determine the detector efficiency for these gamma-rays with calibrated sources having gamma-rays near these energies. These were not available ; therefore, no further calculations were made using R_3.

From Fig. 58 it is seen that, given an approximate value of operating flux, reasonably accurate values of neutron exposure can be determined with R_1 alone. Neutron exposure and U^{235} burnup estimates were attempted for elements 2M1 and 2-4 using ratios of R_1 alone, since there was no appreciable Zr^{95} activity left in either after over three years cooling time. Unfortunately, the values of the corrected ratio, R_1, for 2M1 as given in Table 10, fluctuated considerably even between adjacent points, and gave high values for exposure. This is attributed to the uncertainty in calculating the total counts under the Cs^{134} 605 keV peak which is located on the Compton edge of the 796 keV gamma-ray. In addition, it was pointed out in the spectrum for 2-4, Fig. 33, that a gamma-ray of about 597 keV appeared to be present. This other activity would be included in the calculation for Cs^{134} activity, causing an overestimate in the Cs^{134} content and thus in the neutron exposure. The use of the 796 keV gamma-ray would probably have avoided this difficulty. However, it was not recorded in the spectra for all runs.

(b) Determination of Cooling Time

In the above cases, the cooling time since removal from the core was obtained from records. However, it should be possible to determine this quite accurately from a comparison of a measured gamma-ray spectrum of unknown cooling time with a series of spectra taken after different cooling periods such as shown in Fig. 30.

For fuel which has been operated at constant power for an irradiation time of about one year or more, the Zr^{95} and Nb^{95} will essentially be in equilibrium (see Fig. H.1). Upon removal from the core, the ratio of the area under the combined Zr^{95}+Nb^{95} to the area under the isolated Zr^{95} peak will vary with cooling time as shown in Fig. 65. For intermittent operation, the value of this ratio at the time of removal from the core depends upon the ratio of operating time to shutdown time during in-pile residence. The values for (103 hours on)/(65 hours off) and for (95 hours on)/(73 hours off) are shown on the ordinate. For all cases though, this ratio approaches the equilibrium value of 0.153 and it would not be useful for cooling times greater than three or four months. The experimental ratio determined from 24 different spectra for 2M19 gave an average value of 0.140, or about 8.5% lower than the calculated value using the half-lives and gamma-ray intensities of Zr^{95} and Nb^{95}. This is in reasonable agreement since uncertainties in gamma-ray peak integrals could give errors of 5-10%, while

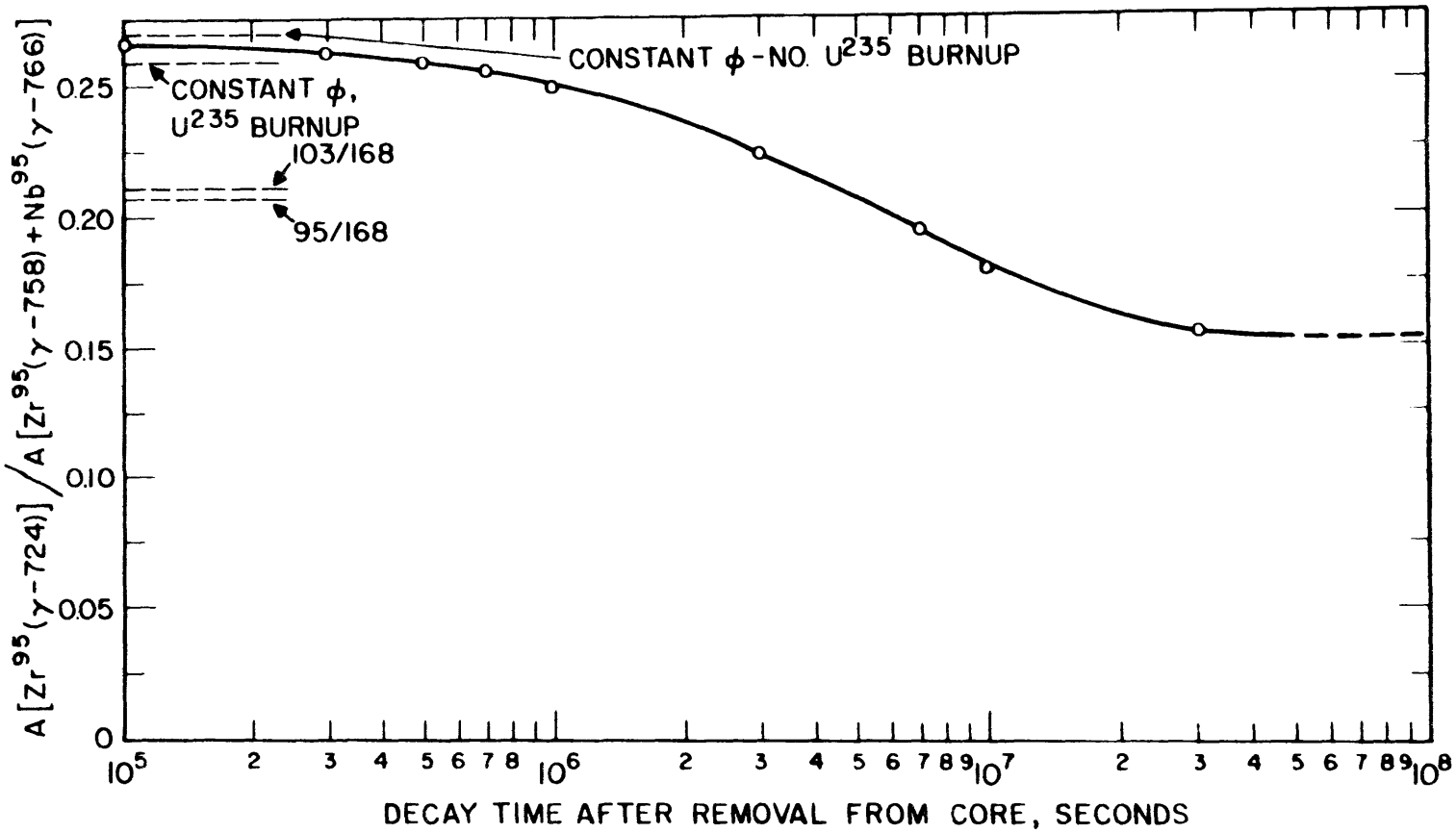

FIGURE 65 RATIO OF Zr^{95} ACTIVITY FOR 724 kev γ-RAY TO ACTIVITY OF Zr^{95} 758 kev γ-RAY PLUS Nb^{95} 766 kev γ-RAY AS A FUNCTION OF DECAY TIME AFTER REMOVAL FROM CORE OPERATED AT CONSTANT FLUX.

uncertainties in decay constants and gamma-ray intensities could also be as much as 5% in error.

(c) Determinations of Flux and Burnup Distributions Within a Fuel Element

The results of the analysis of the transverse scan of 2M19, in which the edges of the fuel plates were scanned, are summarized in Table 13. The values for the neutron flux vary between 2.78 and 2.41 x 10^{13}. Calculation of the fluxes from results of Table 4.10.12 of Ref. (M4) for the central plate yielded values of 2.19 x 10^{13} at the center and 3.02 x 10^{13} at the edge. Because of the integrating effect of the fairly large aperature diameter (1/8 in.) the difference in the fluxes obtained by the present method is not as great as that obtained from the cobalt wire results which are more localized. The present results, falling within the limits of the cobalt wire results, are nonetheless in good agreement with them. A smaller aperature should enable more accurate scans along each individual fuel plate.

4. Discussion of Results

(a) General

In the preceding sections, a method has been described for inferring a fuel element's irradiation history from analyses of gamma-ray spectra obtained with a Ge(Li) spectrometer. The results included determinations of absolute neutron flux, total neutron exposure, U^{235} burnup and ir-

TABLE 13

RESULTS OF ANALYSIS OF TRANSVERSE SCAN

VIEWING EDGES OF FUEL PLATES

OF 2M19

Run	Pos'n Below Fuel Midpl. Inches	Cs^{137}	R_1	R_2	ϕ in 10^{13} n/cm^2,sec.	ω in n/kb	τ in 10^8sec.
D35	0 &	12,184	5.013	0.0785	2.50	1.13	0.452
D36	$\frac{1}{16}$" OUT	8,485	4.539	0.0786	2.49	1.225	0.492
D37	$\frac{1}{8}$" OUT	13,746	4.529	0.0746	2.56	1.205	0.471
D38	$\frac{3}{16}$" OUT	11,987	4.753	0.0778	2.415	1.197	0.496
D39	$\frac{1}{4}$" OUT	9,311	4.009	0.0835	2.62	1.365	0.521
D40	$\frac{5}{16}$" OUT	14,172	4.406	0.0750	2.63	1.23	0.468
D41	$\frac{3}{8}$" OUT	11,692	4.392	0.0749	2.63	1.23	0.468
D42	$\frac{7}{16}$" OUT	10,229	3.976	0.0773	2.78	1.31	0.471
D43	$\frac{1}{2}$" OUT	14,151	4.544	0.0812	2.41	1.24	0.515

Mean Irradiation Time, $\bar{\tau}$ = 0.484×10^8 seconds

Actual Irradiation Time = 0.448×10^8 seconds

Error = 8%

radiation time. Comparisons with independently obtained data showed good agreement. It should be stressed that the flux obtained by the present method is actually an averaged value, representative of conditions present in the fuel during its in-pile residence. The results, of course, depend more strongly upon the immediate past history than on the distant past. If operating schedules have not been constant, the results obtained may not be the same for different combinations of fission product ratios because of the influence of the fission product half-periods upon the calculations.

One major advantage of the present method, in addition to being nondestructive, is that the results obtained are representative of the irradiation conditions existing within the fuel itself during normal operation (i.e. at operating temperatures, pressures, etc.). Other methods, such as the cobalt wire activity measurements, obtain the flux at positions adjacent to the fuel, and usually not at full operating conditions. Methods that determine the absolute Cs^{137} content in the fuel, such as described in Ref. (W5), will give the total number of fissions, but require a careful calibration of the system. Furthermore, they do not yield the additional information such as can be obtained here. Since these two methods give values for the U^{235} burnup determined in two different ways, a combination of the two would be useful. This could be done using the same experimental data from the present apparatus if a calibration of

the system were made.

It was pointed out that some systematic errors were present in the analysis. In particular, the Cs^{134} activity, calculated from the intensity of the 604 keV gamma-ray, can be considerably overestimated by including counts from the Compton edge of the 796 keV gamma-ray. Because of the importance of this fission product in this method, a more satisfactory way of calculating the net counts under a gamma-ray peak should be developed.

Also, other fission products, with long half-periods, appeared to be present in the gamma-ray spectra. The Pr^{144} activity inferred from the 697 keV gamma-ray was not consistent with theory. This was attributed to the error caused by the presence of a low intensity gamma-ray at about 692 keV from some other fission product. In addition, due to the low intensity of the 697 keV photon, (about 1.6%) accurate determinations are difficult. The use of the 1164 keV double escape peak, with its smaller statistical errors, should improve the accuracy of the Pr^{144} calculation. It would then be possible to use the present method for nondestructive analysis of fuel having much longer cooling periods, as well as providing a check on the use of Zr^{95} activity as described.

The lack of precise nuclear data for the fission products also presented a problem. Gamma-ray energies have generally not been determined to better than a few kilovolts in the

best cases and only within ±10 kilovolts for most. For this reason, gamma-ray spectra of the separated fission products considered here were obtained with the Ge(Li) spectrometer. The identification of the many gamma-rays present in a spectrum of an element with a short cooling period is thus a very difficult problem without this data. In addition, accurate values are required for the half-periods of the fission products. Errors in decay constants affect both the theoretically predicted values and the corrected experimental values of fission product activities.

The use of proper cross-sections is also important, especially for the Cs^{133} and Cs^{134} predictions. In the present calculations, no account was taken of flux spectrum hardening due to fission product build-up in the fuel. Because of the high resonance integral of Cs^{133} ($RI(\infty)=450$ barns) this may have a considerable effect for high burnup fuel. Similarly, in this work the Cs^{133} was assumed to be created directly from fission. However, its precursor, Xe^{133}, has a half-period of 5.3 days and an absorption cross-section of 190 barns. This results in about a 2% decrease in the Cs^{133} concentration due to the $Xe^{133}(n,\gamma)$ Xe^{134} reaction.

The use of accurate values for fission yields is likewise very important. It is, however, very difficult to obtain good absolute values experimentally.

The availability of independent measurements of absolute

flux, irradiation time and calculations of fuel burnup has been valuable in evaluating the accuracy of the present results. In particular, it was found that overall consistency and agreement with all the data was not possible until all the nuclear constants were consistent. One result of this inability to achieve internal consistency was the independent determination of the relative intensities of the Zr^{95} gamma-rays. Conflicting values were reported by different investigators as shown in Table 14.

TABLE 14

TRANSITION PROBABILITIES IN Zr^{95} DECAY

Reference	Transition, Percent			
	β 885 keV γ 0 keV	β 396 keV γ 724 keV	β 364 keV γ 758 keV	β 250 keV γ 635 keV
a	2 ± 0.5	55 ± 5	43 ± 5	
b	0.9	34	53	11
c	3	43	54	
Present work	3*	41.7 ± 2	55.3 ± 2	

* Assumed value taken from Ref. (c).

(a) Drabkin, et. al, Izvest. Akad. Nauk. SSSR, Ser. Fiz. 19, 324 (1955).

(b) P.P. Zarubin, Akad. Nauk. SSSR, Ser. Fiz. (Trans.) 18, 244 (1954).

(c) P.S. Mittleman, Phys. Rev. 94, 99 (1954).

The results of calculations of the intensities from a gamma-spectrum of a Zr^{95}+Nb^{95} source shown in Fig. C.1 are presented in the bottom line of the Table. These indicate intensity values of 41.7% for the 724 keV gamma-ray and 55.3% for the 758 keV gamma-ray. Agreement is good with results of Mittelman and Zarubin, but not with those of Drabkin. A more satisfactory determination of the intensities would require the radiochemical separation of the Nb^{95} from the source, leaving only the Zr^{95} gamma-rays to be measured with a Ge(Li) spectrometer. The fuel element analyses used a value of 41.7% for the 724 keV gamma-ray.

Another factor that had considerable effect on the consistency of the results was the assumed ratio of operating to shutdown times. This was most noticeable for the comparisons of predicted and measured ratios of Cs^{137} to Zr^{95} activities. The Cs^{137} level is not affected appreciably by the shutdowns because of its long half-period (30 yr.). However, the level of Zr^{95}, with a half-period of 65 days, was considerably reduced by the shutdowns. It is felt that the use of R_1 and R_2 alone for analyses of irradiation history could yield misleading results for fuel that experienced an unsteady operating schedule. Therefore, parallel analyses using the ratio R_3 and the Ce^{144}+Pr^{144} chain, with its longer half-period of 280 days, would be necessary for obtaining correct information by this method.

The effect of U^{235} burnup can be seen in Fig. 66 which

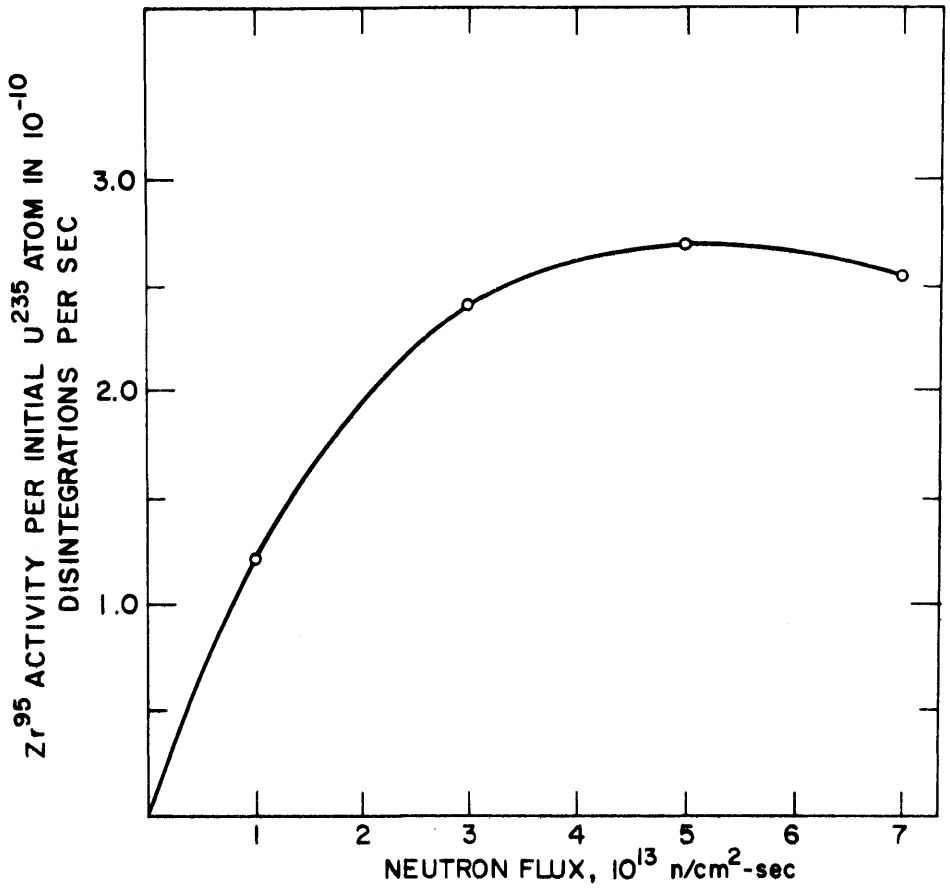

FIGURE 66 Zr^{95} ACTIVITY PER INITIAL U^{235} ATOM AT IN-PILE RESIDENCE TIME = 0.79×10^8 SEC, AS A FUNCTION OF NEUTRON FLUX FOR INTERMITTENT MITR OPERATION (95/168)

shows the Zr^{95} activity per initial U^{235} atom as a function of flux at an in-pile residence time of 0.79×10^8 seconds taken from Fig. 51. For fluxes between 3.5×10^{13} and 7×10^{13} n/cm^2-sec, the Zr^{95} activity is essentially constant. Beyond a flux of 5×10^{13}, the Zr^{95} activity decreases with increasing flux. In MITR fuel, operation at 1.95 MW results in a maximum flux of about 3×10^{13}. Thus, the Zr^{95} activity is directly related to the flux level for in-pile residence times less than about 10^8 sec. or 3 years.

Similar comments can be made for the use of Ba^{140}-La^{140} activities as indicators of relative flux distribution. Because of the shorter half-period of Ba^{140} relative to Zr^{95}, the effect of U^{235} burnup will be evidenced sooner. Thus, in Fig. 55 the Ba^{140} activity for $\phi = 5 \times 10^{13}$ crosses that for $\phi = 3 \times 10^{13}$ at a shorter irradiation time than for Zr^{95}.

Because of the anomalous behavior of shorter-lived fission products due to fuel burnup, the use of gross gamma-activity scans to infer flux distributions within fuel elements can easily lead to erroneous conclusions, especially for high burnup fuel such as from power reactors.

Meanwhile, Fig. 57, giving the variation of Cs^{137} activity per initial U^{235} atom as a function of neutron exposure, shows that for this fission product, the effect of U^{235} burnup is not great, even for large exposures. Thus, relative Cs^{137} spatial distributions are a good measure of relative flux distributions.

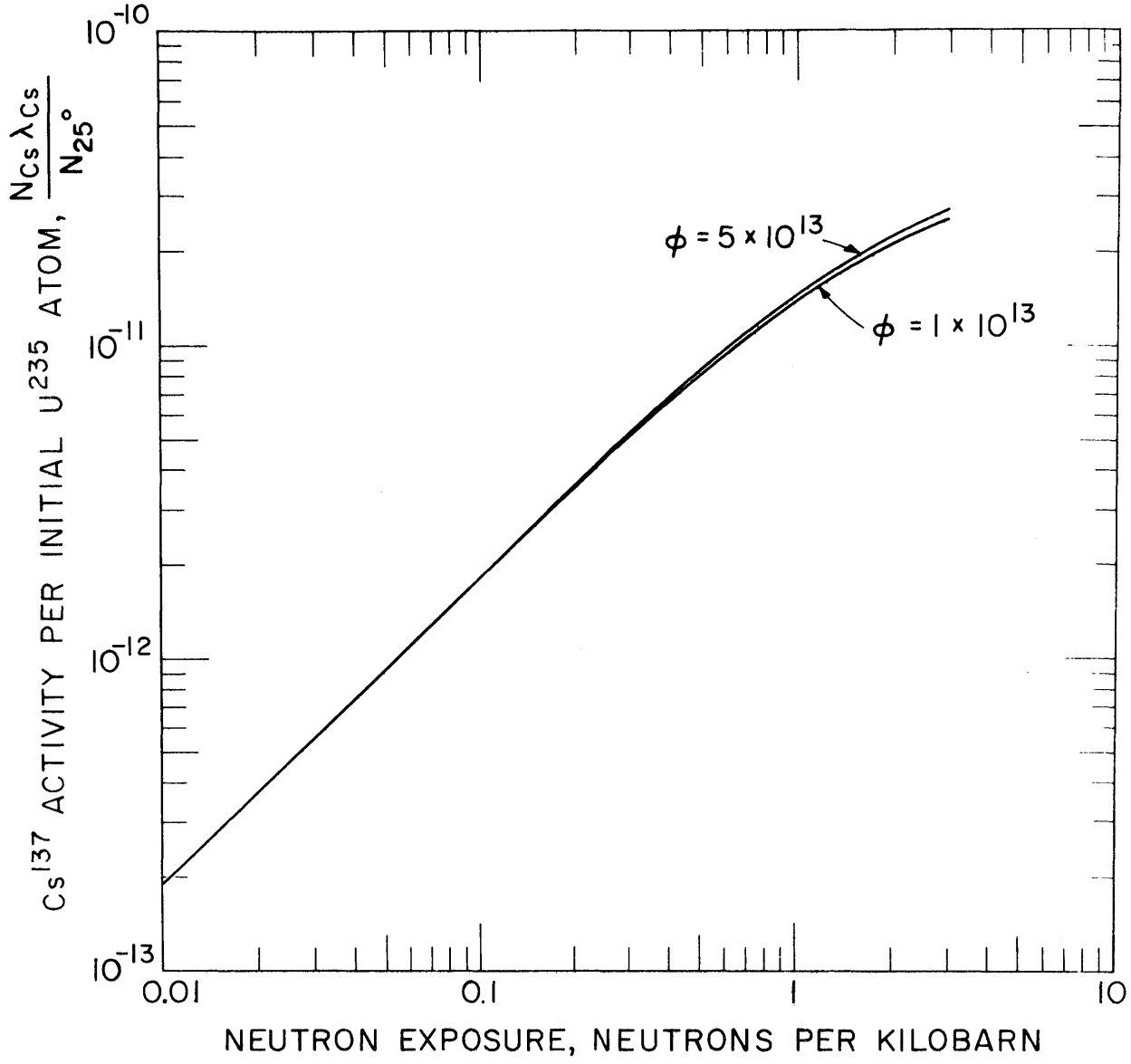

FIGURE 67 Cs^{137} ACTIVITY PER INITIAL U^{235} ATOM AS A FUNCTION OF NEUTRON EXPOSURE

(b) Errors

With the present method it is possible to obtain values for the absolute neutron flux and local burnup values accurate to about ±10%. The average burnup for the whole element and the irradiation time are probably accurate to ±5 to 7%. These accuracies are presently limited by errors in the calculation of gamma-ray counts from the spectra, in the values for nuclear constants, and in the graphical solutions for flux and burnup. Measurements made with standard sources, described in Appendix D, and those made upon 2M22, summarized in Table F.3 Appendix F, showed that results could be reproduced, with deviations from the mean being about twice the statistical uncertainty. However, some systematic errors have been pointed out and others may also be present.

The errors are also a function of cooling time of the fuel element. For cooling times of less than two months, the high background due to short-lived fission products introduces statistical uncertainties of 10% or more into calculations of gamma-ray intensities. On the other hand, for cooling times greater than about one year, the Zr^{95} activity has decayed to less than 1% of its original level, and again calculation of its gamma-ray intensity will contain more than 10% statistical uncertainty. Improvements should be possible with the use of a computer-coded spectrum stripping method for calculating gamma-ray intensities.

In addition, reduction in the scattered background

radiation by increasing the detector shielding or lowering the fuel element further into the water should improve results. Similarly, the use of better electronics, with capabilities of higher energy resolution should result in more accurate values for gamma-ray intensities. However, unless some technique is used to reduce the intense Compton background in the 500-800 keV region, such as the use of an anticoincidence arrangement, this work seems to indicate that it will be difficult to reduce the errors to less than 3%, even for the optimum cooling time.

(c) Other Applications of Present Techniques

The high resolution of Ge(Li) spectrometers has been shown to be adequate to resolve some of the fission product gamma-rays in irradiated fuel even after only 18 hours cooling time. The analyses described above, however, required that the fuel have cooled two months or more so that gamma-rays in the 500-800 keV region be satisfactorily resolved. Gamma-ray spectra taken after short cooling periods showed the presence of unidentified fission products that might be useful in similar analyses.

In the determination of reactor physics lattice parameters, measurements using NaI spectrometers are made of fission product activity shortly after irradiation (L2). It is likely that the use of Ge(Li) spectrometers could yield considerably more information. For example, determinations of fast fission effects in U^{238} may be possible with the

measurement of fission products having differences in yield between U^{235} and U^{238}. Similarly, the present techniques could be applied to irradiated fast reactor fuel in which, besides burnup and average flux determinations, the dependence of fission yields upon neutron energy could be used to study variations in the flux energy spectrum.

The excellent spatial resolution available with the present arrangement indicates that detailed studies could be made of single rods of bundle type elements such as for the CANDU reactor fuel (D3) or the YANKEE reactor fuel (S4).

The difference in fission yield of Ru^{106} between U^{235} and Pu^{239}, as shown in Table 2, might be useful for determining U^{238} to Pu^{239} conversion ratios in low enrichment fuels and thus supply information about resonance capture parameters.

From the short list given above, it is apparent that the application of Ge(Li) spectrometers, with their high energy resolution, to areas of experimental reactor physics could make possible the development of a number of new approaches to the determination of lattice physics variables.

IV. SUMMARY AND CONCLUSIONS

Nondestructive analyses have been made of irradiated MITR fuel elements with a lithium-ion drift germanium spectrometer to obtain information about the irradiation history of each element. Techniques for the preparation of Ge(Li) detectors were developed and are described in detail. Included are descriptions of the apparatus and equipment necessary for satisfactory performance of the spectrometers. The equipment used for the positional scanning of irradiated fuel elements in the MITR spent fuel storage tank is described. Gamma-ray spectra, in which peaks due to Zr^{95}, Nb^{95}, Rh^{106}, Cs^{134}, Cs^{137}, Ba^{140}, La^{140}, Ce^{144} and Pr^{144} fission products were identified, are presented for elements after different cooling periods. Fission product activities were determined from calculations of the intensities of the gamma-rays in the spectra. Spatial distributions of the fission products for a number of fuel elements are shown.

A method for interpreting the experimental results, requiring theoretical predictions of fission product activities in the fuel, is presented. The results of the application of this method include spatial variations of absolute neutron flux, neutron exposure and total U^{235} burnup and irradiation time of the fuel. The operating pattern of each element, and the time since its removal from the reactor, could also be inferred. Comparison of the results of the present investigations with independent determinations of these quantities

showed that the agreement was within the 10% error assigned. Some of the problems and limitations of the method are discussed and suggestions are made for improving the accuracy and precision of the results. Other areas of possible use in reactor physics measurements are indicated.

V. RECOMMENDATIONS FOR FUTURE WORK

A. Preparation of Ge(Li) Detectors

(1) A number of improvements are required in the techniques of etching the germanium, which in their present form are difficult to control accurately. In order to increase the success rate and also to decrease the time required to properly finish a drifted p-i-n diode, prior to testing at liquid nitrogen temperatures, apparatus should be developed to allow the controlled etching of the diode faces. The use of etchants other than CP4A or the HNO_3/HF mixture (B3) may improve stability of the detector surfaces against contamination.

(2) The use of lower resistivity germanium (about 5 ohm-cm) is recommended, so as to permit higher drift temperatures and the possibility of faster drift rates.

(3) It is recommended that efforts be made to determine if there is any way that Ge(Li) detectors can be stored at room temperature for an indefinite period of time without requiring a clean-up and etch treatment. The only requirement for the detector would then be to cool it down to liquid nitrogen temperatures. This could possibly involve some chemical process to stabilize the lithium near the surface and prevent it from diffusing out, in conjunction with some form of encapsulation.

B. Investigations of the Irradiation History of Fuel Elements

(1) A specially instrumented element has been constructed to obtain power production rates by means of a thermodynamic

heat balance (E4). Results with this element have been used to determine that the power production predicted by the MITBURN code is underestimated. It is recommended that gamma-spectra scans should be made of this element, and the results analyzed by the present method. Accurate comparisons should then be possible of fuel burnup, irradiation time and flux distributions.

(2) It is recommended that a more satisfactory method of calculating the net counts in a gamma-ray peak from complex spectra be developed. This may possibly include recording separated fission product gamma-ray spectra under the same electronic conditions as for the fuel elements. A spectrum-stripping calculation would then be made upon fuel element spectra with the use of a computer code.

(3) The computer codes for obtaining values for the solutions of fission product concentrations in irradiated fuel should be revised, condensed and made more efficient. Calculation of the various activity ratios should be made in the program, thus avoiding the hand calculations required at the present time. Computer experiments should be made to determine the magnitude of effects of changes in nuclear constants for the fission products and fuel upon the results of the present method.

(4) The solutions for the flux, neutron exposure and irradiation time are presently obtained graphically. This is time-consuming and can result in systematic errors. Therefore, a computer program should be written which will obtain these quantities and permit a more thorough analysis of each

fuel element.

(5) The results of calculations with R_1 and R_2 which make use of the ratios of Cs^{137} to Cs^{134} and Cs^{137} to Zr^{95} activities in the fuel respectively, should agree with those using R_3, the Cs^{137} to Pr^{144} activities and R_1. However, these two approaches did not agree, as discussed in Section III.5. Therefore, it is recommended that the reasons for this disagreement be determined and the use of the Pr^{144} activity in these calculations be developed. This may require the calibration of the detector for the 2186 keV double escape peak at 1164 keV.

(6) Experiments are recommended to determine the lower limit of spatial resolution of the scanning mechanism and thereby investigate the possibility of obtaining absolute flux distributions within the element by making use of the curvature of the fuel plates.

APPENDIX A

PREPARATION OF LITHIUM-ION DRIFT GERMANIUM GAMMA-RAY DETECTORS

The procedures and techniques developed will be described under the following headings: (1) Preparation of crystal for lithium diffusion, (2) Lithium diffusion, (3) Application of nickel contacts, (4) Lithium drifting, (5) Final processing and testing, and (6) Recipes.

1. Preparation of Crystal for Lithium Diffusion

The germanium crystals used for the preparation of detectors were supplied by Sylvania Electric Products in the form of p-type, gallium-doped, zone-levelled ingots, trapezoidal in cross-section, weighing 60 or 120 gms/in. Crystal orientation was with the (1,1,1) plane perpendicular to the ingot axis. Two resistivity ranges have been used with comparable success: 8-10 ohm-cm and 30-45 ohm-cm. Dislocation densities were less than 2000/cm^2 and minority carrier lifetimes were greater than 100 μsec.

(a) A thin blade, high speed, diamond saw was used to cut the ingot into slices 5 to 15 mm in thickness. Initial development was carried out on parallelopiped samples, each 5 mm thick and about 1 cm^2. Therefore, each slice required further sawing. Presently, no additional sawing is done and the slices are processed in their trapezoidal configuration.

(b) The slice was lapped on all sides with water slurries of

600 and 1000 mesh silicon carbide powders*, taking care to wash the crystal with water after each step. The crystal was then ultrasonically cleaned in a hydrocarbon solvent and washed in methanol and deionized water.†

(c) The crystal was etched in CP4A (see Section D.6) for three minutes. The reaction was quenched by diluting the acid solution with deionized water, decanting and repeating. Care was required to prevent exposure of the crystal to the air until all the etchant had been washed away. Failure to do so resulted in the formation of a dull, white film on the surface of the germanium which was found to be deleterious to the proper performance of the crystals.

(d) If smooth, mirror-like surfaces had not resulted, another etching step was performed. One of the large area faces was then lapped with 1000 mesh slurry, washed, ultrasonically cleaned, and rinsed in methanol and water.

2. Lithium Diffusion

(a) A thin uniform layer of a lithium-in-oil suspension** was applied to the lapped face with a tapered glass rod.

(b) The crystal was then placed on a quartz plate located

---

* Supplied by A.B. Beuhler Ltd., Evanstown, Ill.

† Deionized water was obtained by passing water from the main supply through two resin cartridges supplied by Barnstead Still and Sterilizer Co., Boston 31, Mass., a mixed resin to remove anions and cations and a resin to remove organic matter.

** Supplied by Lithium Corp. of America. 30% Li - 2% oleic acid, remainder mineral oil.

inside the 2 in. I.D. Vycor glass tube that passed through a muffle furnace, shown in Fig. A.1. The furnace was pre-heated to about 450°C before the diffusion was to take place. Argon gas was kept flowing through the tube during this and all subsequent steps in the diffusion process. The temperature inside the tube and on the quartz plate near the crystal was monitored with Chrome-alumel thermocouple junctions.

(c) The quartz plate was positioned within the furnace so that the temperature of the crystal was near 200°C, thus evaporating the mineral oil and leaving behind the lithium powder. This occurred within a few minutes.

(d) The crystal was then located in the furnace at a temperature of about 425°C for 10 minutes, allowing the lithium to diffuse into the crystal.

(e) The quartz plate was positioned outside the furnace (but still within the tube) and the crystal was allowed to cool for about 1/2 to 1 hour, with the argon gas flow continuing.

3. Application of Nickel Contacts

(a) After cooling, the loose lithium was scraped off and the crystal was placed into methanol then water. The remaining excess lithium reacted with the water which usually resulted in a pitted surface that appeared not to harm the subsequent performance of the diodes.

(b) The lithium-rich surface and the opposing large area surface were lapped with 800 mesh powder, the crystal was washed, cleaned and rinsed with methanol and water.

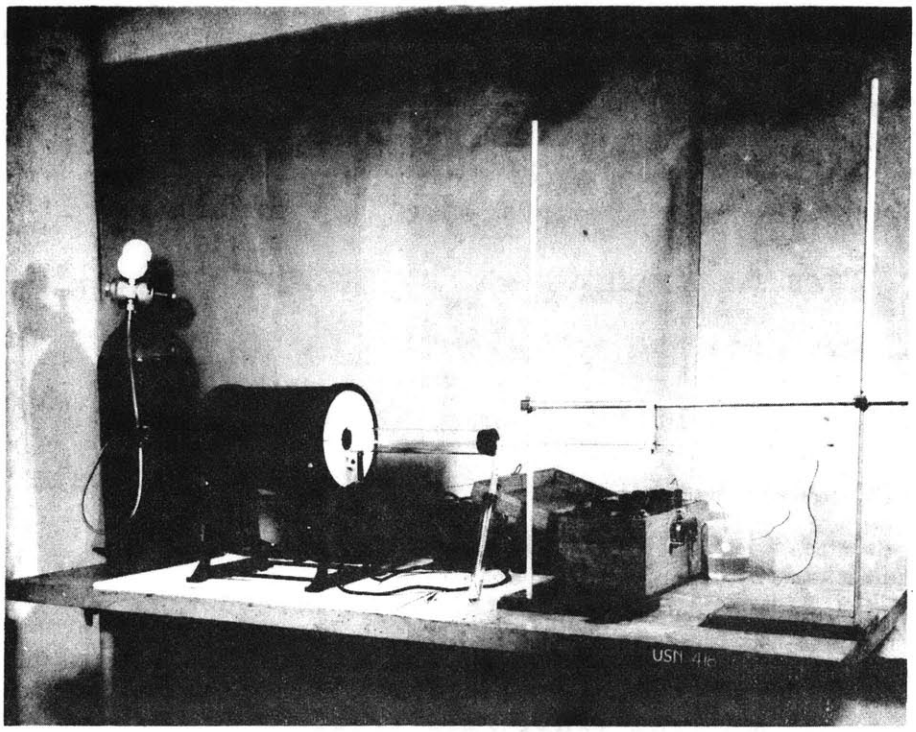

FIGURE A.I PHOTOGRAPH OF FURNACE USED FOR LITHIUM DIFFUSION

(c) The crystal was dipped in concentrated HF acid for one minute and the acid was diluted and decanted in the usual manner.

(d) It was then placed into an electroless nickel plating solution (see Section A.6) that had been preheated to 95°C. Additional ammonium hydroxide was added as required to keep the solution bright blue in color (pH > 8). Satisfactory plating was accompanied by rapid evolution of bubbles (of H_2 gas) from the lapped surfaces of the crystal. It was removed after three to five minutes and the surface resistance of the nickel contacts was measured with an ohm-meter. If the resistance was greater than 2 ohms, the crystal was placed back into the plating bath for two more minutes. The crystal was then washed thoroughly and dried.

(e) The four sides of the crystal were lapped with 1000 mesh powder, washed, cleaned, and rinsed, leaving nickel contacts only on the two opposing large area faces.

(f) Apiezon wax, dissolved in trichloro-ethylene, was applied to the nickel contacts and allowed to dry.

(g) The crystal was given two three-minute etches in CP4A, and two or more two-minute etches in a 2:1 mixture of HNO_3:HF acids. At this stage, it was usually possible to observe the n^+-p junction between the lithium-rich n^+ region and the original p-type region. The latter was etched by the 2:1 mixture at a faster rate than the n^+ region. Approximately 1/2 to 1 mm diffusion depths were usually observed.

(h) The protective wax was dissolved from the nickel contacts with trichloroethylene and the crystal washed with methanol and water. The resulting p-n^+ diode was tested for resistance with an ohm-meter. Reverse and forward resistances were dependent upon the size of the diode and the resistivity of the p-type germanium. Typical values for satisfactory diodes made from 40 ohm-cm material, 5 mm thick, 4 cm^2 in area, were 500Ω and 4 Ω for reverse and forward resistances respectively. A diode having a low reverse resistance was rediffused with lithium and the subsequent steps repeated. Satisfactory diodes were now ready for the drifting process.

4. Lithium Drift Process

(a) The lithium-ion drifting was carried out in the apparatus shown previously in Fig. 5. A photograph of this equipment is presented in Fig. A.2 showing a 15 mm thick, 4 cm^2 crystal being drifted. A reverse bias voltage was applied from a D.C. power supply capable of an output of 500 volts and 1.5 amperes. The joule heating generated by the reverse current flowing through the diode was dissipated by boiling of the fluorocarbon liquid FX-78* at 52°C. Some diodes have been drifted at power rates up to 150 watts for a short period of time. Normal rates were between 50 and 100 watts, with voltages between 50 and 200 volts.

(b) As the drift progressed, the diode reverse resistance decreased. Consequently, the bias voltage was reduced to keep

---

* Supplied by the 3-M Company.

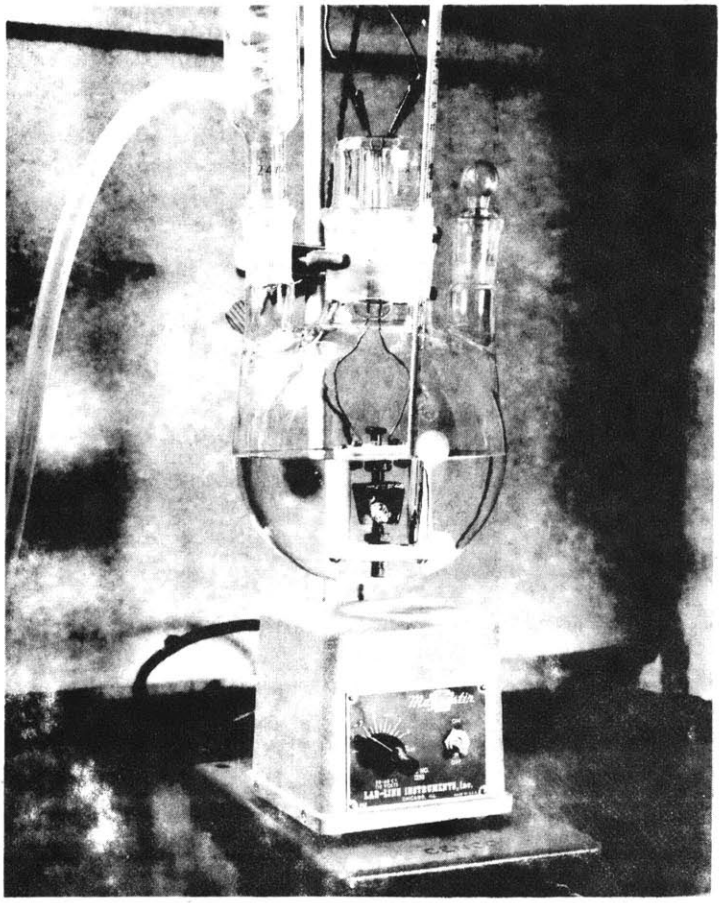

FIGURE A.2 PHOTOGRAPH OF APPARATUS FOR DRIFTING GERMANIUM DIODES

the power dissipation constant.

(c) Depletion depths were measured by removing the diode from the drift unit and placing it into a 0.5N solution of copper sulfate with a reverse bias of 1 to 10 volts, depending on the size. The copper plated only on to the p-type material, thus indicating the depth of the lithium compensation. Drift rates varied considerably with the type of germanium, the size of the diode and initial reverse resistance. However, a typical depletion layer thickness of 3 mm was attained in 2-4 days of drifting for a 4 cm^2 diode. Several detectors of 1 cm depletion layer thickness have been prepared with drift times of about one month.

(d) When a suitable depletion layer thickness had been reached, the diode was transferred from the high temperature drift unit to a lower temperature drift unit (10-20°C) for about 24 hours. Reverse bias voltages were adjusted so that the reverse current was kept below 50 ma.

5. Final Processing and Testing of Germanium p-i-n Diodes

(a) Following the low temperature drift, the sides of the diode were lapped with 1000 mesh powder, washed etc., and the nickel contacts covered with Apiezon wax.

(b) The diode was etched in the usual way, twice in CP4A (3 min. each) then three to five times in 2:1 HNO_3/HF mixture (1 1/2 to 2 min. each). Usually, both the p-i junction and the i-n^+ junction were made visible at this stage because of the preferential etching of the different regions.

(c) The wax was removed with trichloroethylene and the crystal was washed thoroughly in methanol and water and dried.

(d) It was then placed into position inside a dewar as described in Section II. The dewar was evacuated with the portable vacuum system and the inner vessel was cooled with liquid nitrogen. A reverse bias voltage (current < 20 ma) was generally kept applied to the diode during the cooling period to ensure complete compensation of the impurities in the depleted layer.

(e) Reverse current readings for successful detectors were between 10^{-8} and 10^{-10} amperes for 100 to 300 volts bias. Currents higher than this led to excessive noise during operation and thus poor energy resolution. In these cases, the diode was brought to room temperature, re-etched and tested again at liquid nitrogen temperature until the current characteristics were satisfactory.

6. Recipes

High purity, transistor grade reagents were used wherever possible.

(a) CP4A Etchant

2 parts conc. HNO_3

1 part HF (30%)

1 part Acetic Acid

1 ml/l Bromine

(b) 2:1 HNO_3:HF

2 parts conc. HNO_3

1 part HF (30%)

(c) Electroless Nickel Plating Solution (B8, S3)

Nickel Chloride	$NiCl_2 \cdot 6H_2O$	30 gm/l
Sodium Hypophosphite	$NaH_2PO_2 \cdot H_2O$	55 gm/l
Ammonium Citrate	$(NH_4)_2H \cdot C_6H_5O_7$	65 gm/l
Ammonium Chloride	NH_4Cl	50 gm/l

NH_4OH was added until the solution turned from green to blue (pH 8 to 10). It is recommended that NH_4OH be added during the plating process in sufficient quantity to maintain the blue color. The optimum plating time is three to six minutes at 95°C.

APPENDIX B

ENERGIES OF CALIBRATION GAMMA-RAYS

TABLE B.1

Source	Energy (keV)	Reference
Co^{57}	122.05 ± 0.05	(a)
Co^{57}	136.40 ± 0.06	(a)
Hg^{203}	279.16 ± 0.02	(b)
Na^{22}	511.006 ± 0.005	(c)
ThC"	583.139 ± 0.023	(d)
Cs^{137}	661.595 ± 0.076	(e)
Mn^{54}	834.9 ± 1.1	(f)
Co^{60}	1173.226 ± 0.040	(d)
Na^{22}	1275.0 ± 0.8	(g)
Co^{60}	1332.48 ± 0.05	(d)
ThC"	2614.47 ± 0.10	(d)

References

(a) E.L. Chupp, Phys. Rev. 109, 2036 (1958).
(b) C.J. Herrlander and R.L. Graham, Nuclear Phys. 58, 544 (1964).
(c) Electron rest mass from 1963 atomic constants.
(d) G. Murray, et al, Nuclear Phys. 63, 353 (1965).
(e) R.L. Graham, et.al, Nuclear Instr. Methods 9, 245 (1960).
(f) R.R. Wilson, et al, Phys. Rev. 125, 1655 (1962).
(g) Present work; measured with Ge(Li) detector.

APPENDIX C

GAMMA-RAY SPECTRA OF FISSION PRODUCTS

1. Zr^{95}+Nb^{95}

The gamma-ray spectrum of a Zr^{95}+Nb^{95} source is shown in Fig. C.1. The energies obtained for each of the primary photons is indicated on the curve. Results of the calculations of the relative intensities of the two Zr^{95} gamma-rays were shown in Table 14, which also includes values obtained by previous investigators.

2. Ru^{106}+Rh^{106}

Ruthenium-106 (1.0 yr.) decays by β^- with no gammas to Rh^{106} (30 sec.) which is a gamma-emitter. The gamma-spectrum of Rh^{106} is shown in Fig. C.2. A large number of high energy gamma-rays appear to be present. However, they are of such low intensity that no peaks are clearly identifiable above 1.5 MeV. Because of low source strength, statistics were poor and resolution was decreased by gain shifts in the amplifier.

3. Cs^{134}

Figure C.3 shows the gamma-ray spectrum of Cs^{134} (2.19 yr.). Similar results using a Ge(Li) spectrometer have been published in Ref. (g) of Table 5 where the intensities and gamma-ray energies presented in Table 5 were given. The present results taken with Detector 9-19.1 have a FWHM of about 5 keV at 800 keV, compared with less than 3 keV in the above reference.

For this reason, the weak gamma-ray at 802 keV is not properly separated from the 796 keV gamma-ray.

4. Ce^{144}+Pr^{144}

The low energy region of the gamma-ray spectrum of Ce^{144} decay (280 d.) results in four low-energy gamma-rays at 53.0, 79.4, 100.0 and 133.5 keV. The decay of Pr^{144} (17 m.) gives gamma-rays at 697 keV, 1488 keV and 2186 keV with a double escape peak at 1164 keV as shown in Fig. C.5.

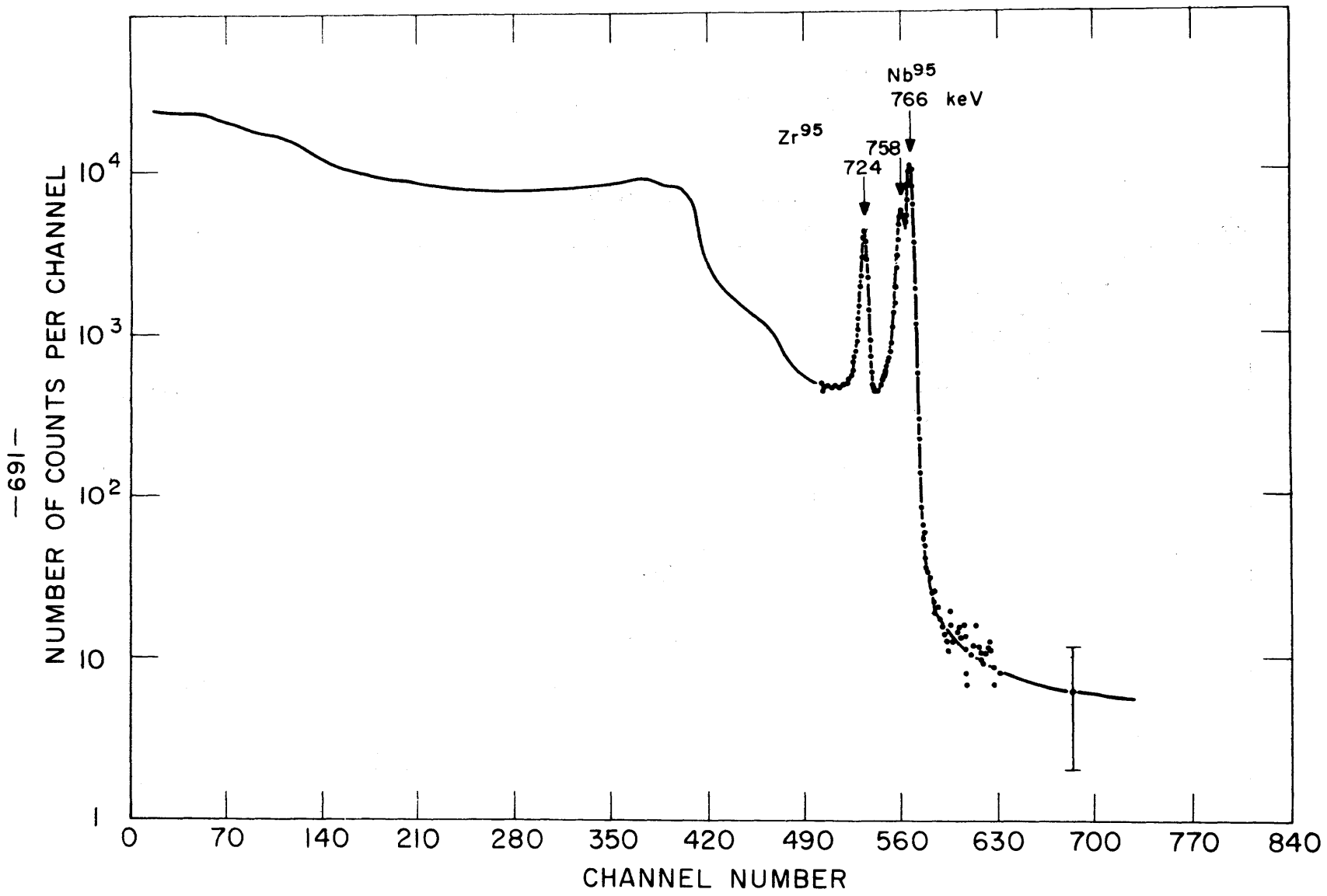

FIGURE C 1 $-Zr^{95}$ $-Nb^{95}$ GAMMA RAY SPECTRUM

GERMANIUM LITHIUM DRIFT DETECTOR No. 9-19.1, 3.5 MM DEPLETION DEPTH, 1.6 CM^2 AREA, 170 VOLTS BIAS, 77°K

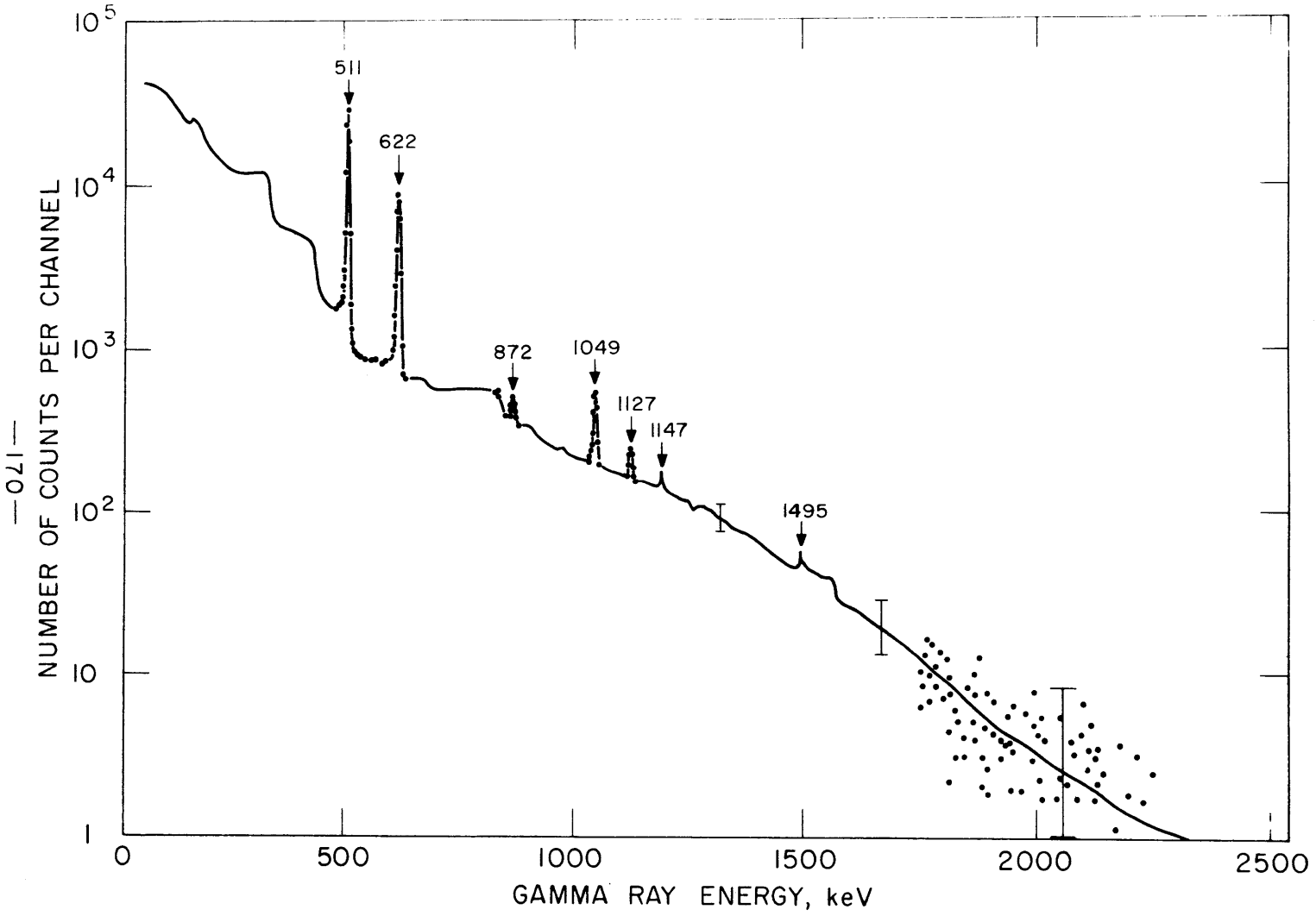

FIGURE C.2 - Rh^{106} GAMMA-RAY SPECTRUM
GERMANIUM LITHIUM DRIFT DETECTOR No. 9-19.1, 3.5 MM DEPLETION DEPTH,
1.6 CM^2 AREA, 170 VOLTS BIAS, 77°K

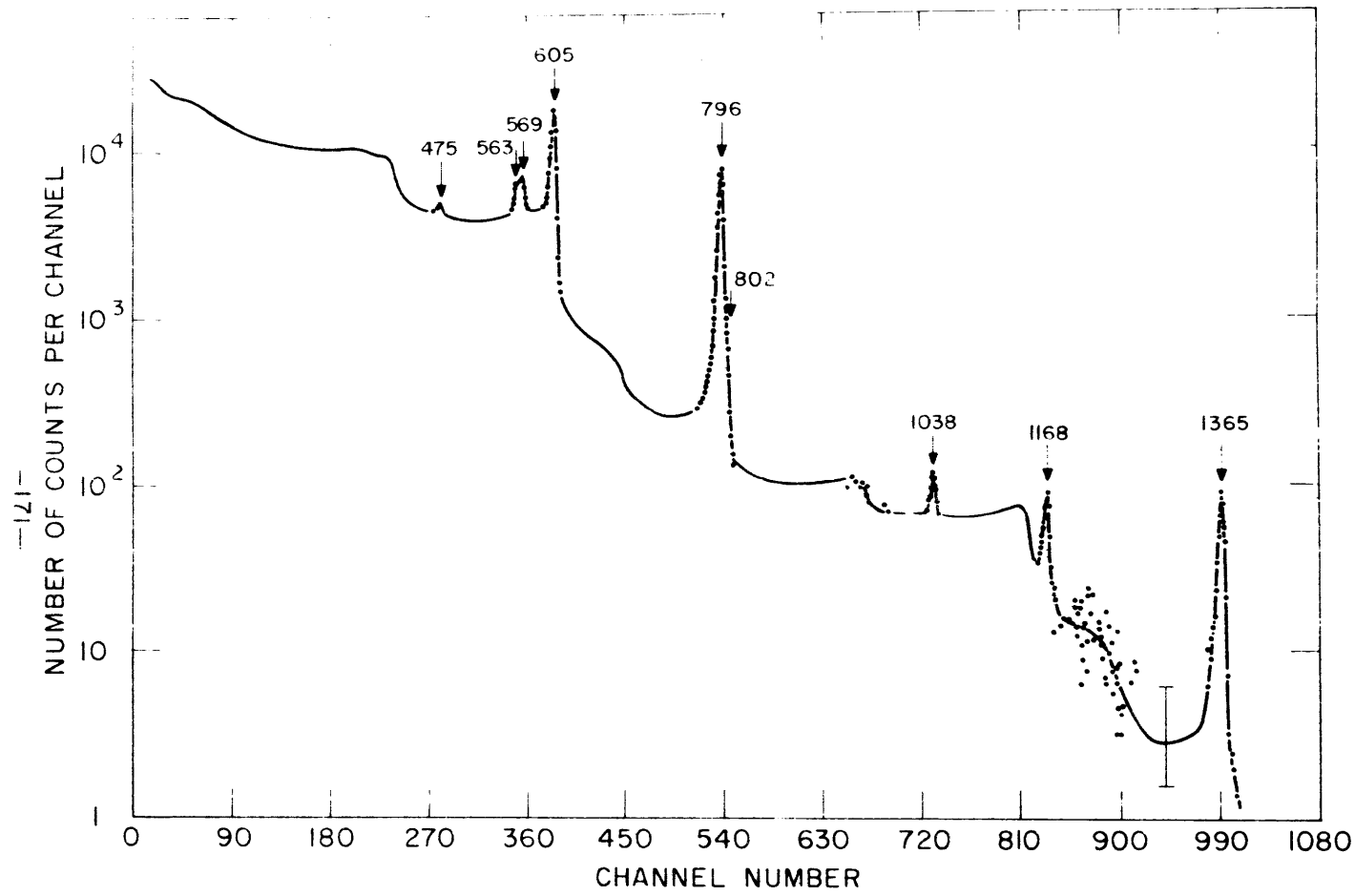

FIGURE C.3 - Cs^{134} GAMMA-RAY SPECTRUM

GERMANIUM LITHIUM DRIFT DETECTOR No. 9 19.1, 3.5 MM DEPLETION DEPTH, 1.6 CM^2 AREA, 170 VOLTS BIAS, 77°K

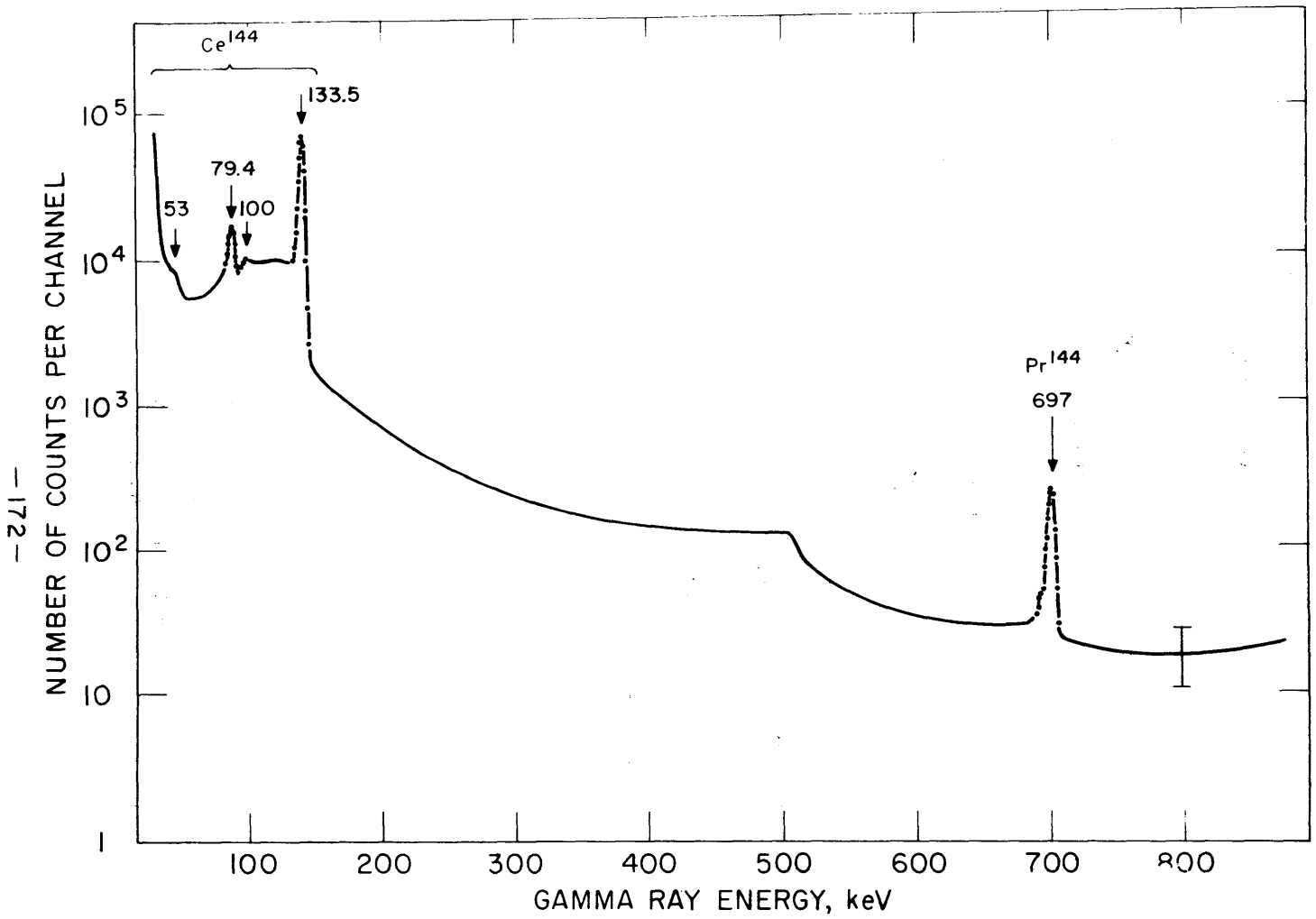

FIGURE C.4 $-Ce^{144}-Pr^{144}$ GAMMA RAY SPECTRUM, 40–850 keV
GERMANIUM LITHIUM DRIFT DETECTOR No. 9–19.1, 3.5 MM DEPLETION DEPTH,
1.6 CM^2 AREA, 170 VOLTS BIAS, 77°K

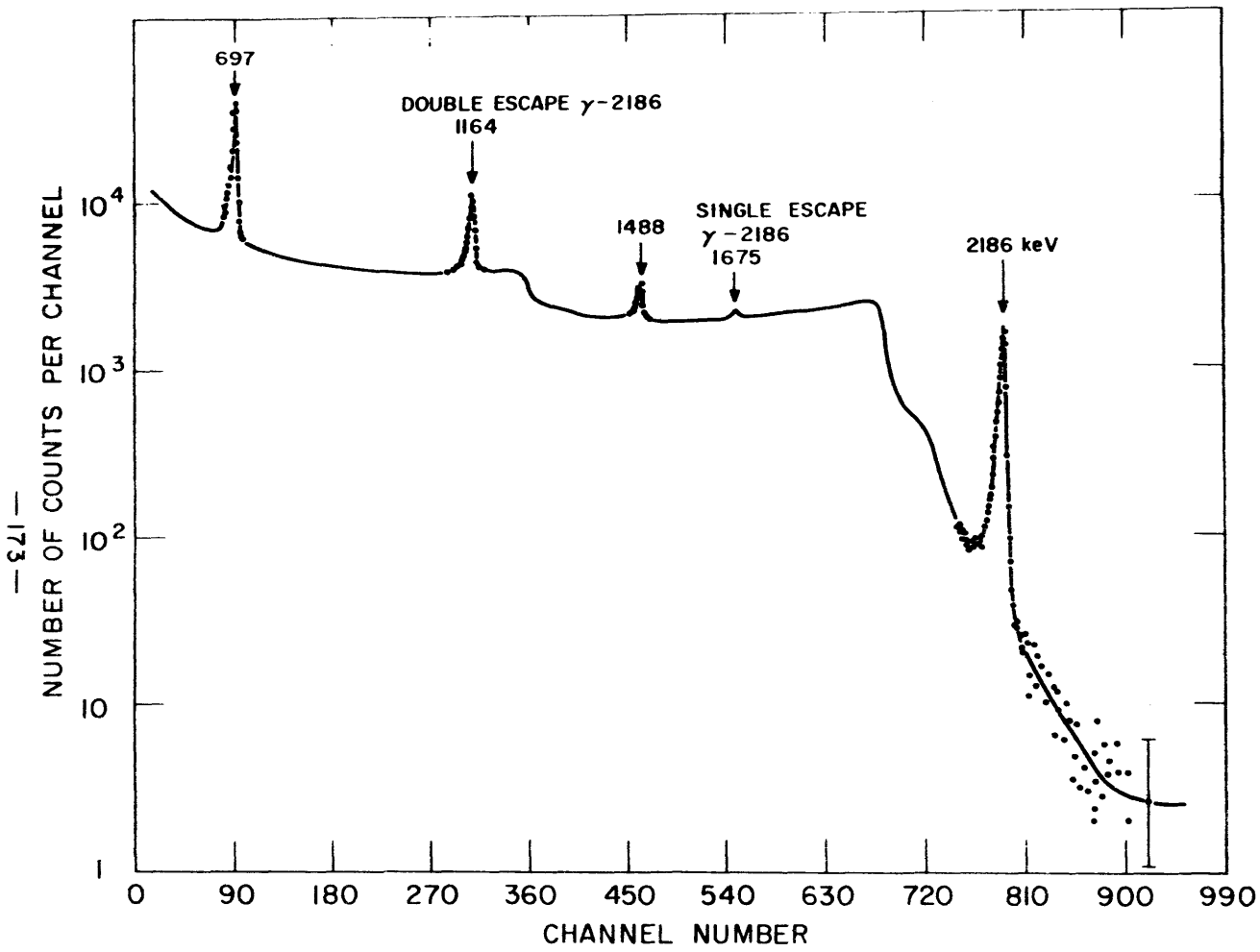

FIGURE C.5 $Ce^{144} - Pr^{144}$ GAMMA RAY SPECTRUM, > 600 KeV
GERMANIUM LITHIUM DRIFT DETECTOR No. 9-19.1, 3.5 MM DEPLETION DEPTH,
1.6 CM^2 AREA, 170 VOLTS BIAS, 77°K

APPENDIX D

DESCRIPTION OF EXPERIMENTS TO DETERMINE THE BEST METHOD OF SUBTRACTING BACKGROUND FROM UNDER A GAMMA-RAY PEAK IN SPECTRA OBTAINED WITH Ge(Li) DETECTORS

The "J" series of experiments were conducted and analyzed to determine the most satisfactory method of subtracting the background from beneath a gamma-ray peak to yield the net counts due to the gamma-ray. The procedure was as follows: The gamma-ray spectrum from a Cs^{137} source was recorded for a period of time. With the Cs^{137} source in the same position, another source was brought near the detector and new spectra of the two sources were again recorded for the same length of time. The additional source provided a Compton background beneath the photopeak of Cs^{137}. The spectral shape of this background was different for each of the secondary sources, while its intensity could be varied by changing the source-to-detector distance. Figure D.1 shows typical results obtained for (a) Cs^{137} at 2", (b) Cs^{137} at 2" plus Mn^{54} at 0" (where 0" was a convenient reference point approximately 4" from the Ge(Li) detector), (c) Cs^{137} at 2" plus Mn^{54} at 2" and (d) Cs^{137} at 2" and Na^{22} at 2".

The analysis of the gamma-ray spectra consisted of the following:

(1) The background at the high energy side of the photopeak was calculated by an arithmetic average of the

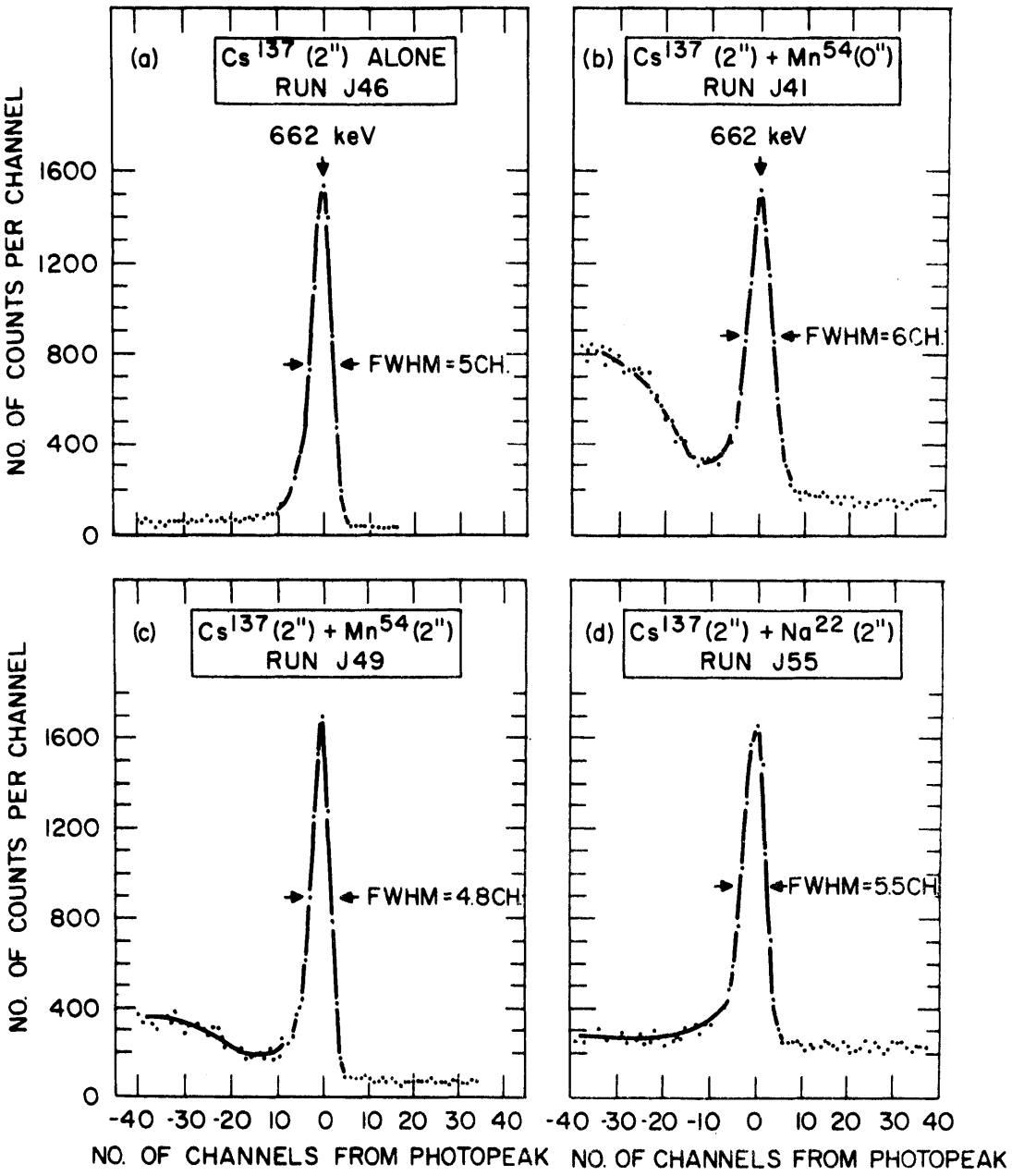

FIGURE D.I γ-RAY SPECTRA OF Cs^{137} PLUS OTHER SOURCES; USED IN DETERMINING BACKGROUND SUBTRACTION METHOD.

counts in three or five adjacent channels and assigning the average values to the middle channel of this set.

(2) The counts in a channel on the low energy side of the peak were taken as the background at this point. A straight line relationship was assumed between the low energy side channel and the high energy side channel chosen in (1) above, and the arithmetic average of the background counts per channel was calculated.

(3) The total counts under the peak including background was calculated using the two background channels on either side of the peak as end points.

(4) The net counts in the peak were obtained by subtracting the total background (average background per channel from (2) times the number of channels) from the total counts from (3).

(5) A number of other low energy background channels were chosen and the same procedure repeated. Each resulted in a value for the net counts in the gamma-ray peak.

(6) The average of all these values of net counts was calculated from the channel about 20 keV below the maximum in the gamma-ray peak to the channel about 8 to 10 keV below the maximum.

Although individual gamma-ray peak counts varied by as much as $\pm$ 10% because of statistical variations, the averaged quantity was reasonably constant. Tables D.1, D.2, D.3, D.4

and D.5 show the results of this procedure for different source combinations. In general, the deviations of the experimental results from the mean were about twice that expected from statistical uncertainties.

As can be seen from a summary of the results shown in Table D.6, the maximum deviation from the mean value of Cs^{137} activity was - 9.0% and occurred for the Cs^{137}(2") and Mn^{54}(0") group of experiments.

It appears from the results that the method of subtracting background is dependent upon the slope of the background beneath the peak being integrated. Some improvement in the accuracy of obtaining absolute photopeak count rates could probably be made by assuming a higher order type equation for the background, rather than linear as done here. This was not tried.

Instead, the assumption was made that the method described above underestimates the net counts under the gamma-ray peak by 3%. The corrected values were thus obtained by multiplying by 1.03. The maximum deviation was then -6.3% for the Cs^{137}(2") + Mn^{54}(0") runs. Since the statistical uncertainties were $\pm$ 2.1%, the experimental procedure and method of analysis gave results that had deviations of about three times the statistical uncertainties. If Run J40 is neglected, this factor reduces to about 2 rather than 3.

This error is probably smaller if ratios of gamma-ray peak counts are calculated, especially if the gamma-rays are near one another and have approximately the same background level and

spectral shape. It was thus concluded that the above method gave satisfactory results for the calculation of net counts under a gamma-ray peak. Based on this method, a computer code, to be described in Appendix E, was written for the analysis of the fuel element spectra.

TABLE D.1

TOTAL COUNTS UNDER Cs^{137} GAMMA-RAY PEAK

Source = Cs^{137}(2")

Lower Energy Channel Limits For Calculating Average No. of Counts in Peak	Run J42	Run J43	Run J44	Run J45	Run J46	Run J53	Average
- 19 to - 5			8455	8223			8339
- 19 to - 7			8694	8479			8587
- 19 to - 9			8850	8660			8755
- 18 to - 8					8408	8519	8464
- 18 to - 9	8600	8453					8527
- 18 to -10	8678	8506			8571	8636	8598
- 17 to - 5			8351	8114			8233
- 17 to - 7	8397	8257	8616	8397			8417
- 17 to - 9	8668	8402	8789	8600			8615
- 16 to - 7	8355	8204			8295	8465	8330
- 16 to - 8	8443	8271					8357
- 16 to - 9					8472	8600	8536
- 15 to - 7	8298	8160	8481	8279			8305
- 15 to - 9			8664	8506			8585
- 14 to - 9					8170	8370	8270
- 14 to -11					8368	8522	8445
- 13 to - 9			8580	8366			8473
Average	8491	8322	8669	8403	8381	8519	
						Mean =	8461

Statistical Uncertainty = $\pm$ 1.4%

Max. Deviation from Mean = + 4.6%

TABLE D.2

TOTAL COUNTS UNDER Cs^{137} GAMMA-RAY PEAK

Source = Cs^{137}(2") + Mn^{54}(0")

Lower Energy Channel Limits For Calculating Average No. of Counts in Peak	Run J39	Run J40	Run J41	Average for J39 J40 and J41	Average for J39 and J41
- 18 to - 9	7917	7235	7781	7644	7849
-10	7941	7215	7753	7636	7847
- 17 to - 7	7861	7354	7724	7646	7793
- 9	7988	7358	7819	7722	7904
- 16 to - 7	7919	7453	7769	7714	7844
- 8	7999	7473	7834	7769	7917
- 15 to - 7	7926	7508	7830	7755	7878
			Mean =	7698	7862

Statistical Uncertainty = $\pm$ 2.1%

Max. Deviation from Mean = - 6.0%

Max. Deviation from Mean if J40 Excluded = - 3.0%

TABLE D.3

TOTAL COUNTS UNDER Cs^{137} GAMMA-RAY PEAK

Lower Energy Channel Limits For Calculating Average No. of Counts in Peak	Sources= Cs-137(2") +Mn-54(2")			Average	Sources= Cs-137(2") +Mn-54(4")			Average
	J47	J48	J49		J50	J51	J52	
- 19 to - 7					8358	8262	8103	8240
- 9					8505	8395	8217	8371
-11					8591	8470	8292	8450
- 18 to - 8	8127	8142	8131	8133				
-10	8300	8311	8298	8303				
-12	8381	8430	8322	8377				
- 17 to - 7					8301	8207	8089	8198
- 9					8469	8357	8226	8350
-11					8569	8443	8325	8445
- 16 to - 8	8013	8042	8083	8069				
-10	8293	8230	8284	8269				
-12	8402	8364	8311	8358				
- 15 to - 7					9253	8146	8039	8145
- 9					8454	8323	8201	8325
-11					8589	8429	8329	8448
- 14 to - 8	7966	7935	7968	7956				
-10	8213	8157	8203	8191				
				Mean = 8207				Mean = 8330
Statistical Uncertainty = ± 1.6%					Stat. Unc'y = ± 1.5%			
Max. Deviation from Mean = + 3.3%					Max. Dev. = - 3.5%			

TABLE D.4

TOTAL COUNTS UNDER Cs^{137} GAMMA-RAY PEAK

Sources = $Cs^{137}(2")$ + $Na^{22}(2")$

Lower Energy Channel Limits For Calculating Average No. of Counts in Peak	Run J54	Run J55	Average
- 19 to - 7	8410	8425	8418
- 9	8614	8599	8607
- 17 to - 7	8309	8313	8311
- 9	8535	8501	8518
- 15 to - 7	8184	8136	8160
- 9	8440	8327	8384
			Mean = 8400

Statistical Uncertainty = 1.8%

Max. Deviation from Mean = -3.1%

TABLE D.5

TOTAL COUNTS UNDER Cs^{137} GAMMA-RAY PEAK

Lower Energy Channel Limits For Calculating Average No. of Counts in Peak	Sources= Cs-137(2") +Na-22(4")		Average	Sources= Cs-137(2") +Na-22(6")		Average
	J56	J57		J58	J59	
- 19 to - 7	8369	8153	8261	8452	8407	8445
- 19 to - 9	8533	8310	8422	8614	8529	8572
- 17 to - 7	8286	8075	8181	8392	8329	8361
- 17 to - 9	8469	8249	8359	8532	8461	8497
- 15 to - 7	8182	7980	8081	8305	8227	8266
- 15 to - 9	8387	8177	8282	8461	8368	8415
			Mean = 8264			Mean = 8426

Statistical Uncertainty = $\pm$ 1.7°/o St. Unc'y = $\pm$1.6°/o

Max. Deviation from Mean = - 3.4°/o Max. Dev'n = -2.4°/o

TABLE D.6

SUMMARY OF RESULTS OF "J" SERIES OF EXPERIMENTS

TO DETERMINE METHOD OF SUBTRACTING BACKGROUND

FROM UNDER GAMMA-RAY PEAK

Sources	Mean Average	Statistical Uncertainty o/o	Maximum Deviation From Mean o/o	Deviation From Mean Cs-137(2") o/o	Corrected Mean	Deviation of Corrected Mean from Mean Cs-137(2") o/o
$Cs^{137}(2")$	8461	± 1.4	+ 4.6	0		
$Cs^{137}(2")+Mn^{54}(0")$	7698	± 2.1	- 6.0	- 9.0	7929	- 6.3
*$Cs^{137}(2")+Mn^{54}(0")$	7862	± 2.1	- 3.0	- 7.1	8098	- 4.3
$Cs^{137}(2")+Mn^{54}(2")$	8207	± 1.6	- 3.3	- 3.0	8453	0.1
$Cs^{137}(2")+Mn^{54}(4")$	8330	± 1.5	- 3.5	- 1.5	8580	+ 1.4
$Cs^{137}(2")+Na^{22}(2")$	8400	± 1.8	- 3.1	- 0.7	8652	+ 4.6
$Cs^{137}(2")+Na^{22}(4")$	8264	± 1.7	- 3.4	- 2.3	8512	0.6
$Cs^{137}(2")+Na^{22}(6")$	8426	± 1.6	- 2.4	+ 0.2	8679	+ 2.6

* Neglecting Run J40

APPENDIX E

"GRAPIN", COMPUTER CODE TO CALCULATE THE NET COUNTS IN A GAMMA-RAY PEAK

A computer code, called "GRAPIN" was written to calculate the net counts in a gamma-ray peak by the method described in Appendix D. The input data includes the counts per channel for a gamma-ray spectrum obtained with a multichannel pulse height analyzer. Up to 1025 channel values can be read in, although only those near the gamma-ray peak are required. A number of control parameters must also be given, specifying the gamma-ray source, the channels to be used for background subtraction, etc. as is described in Table E.1. As an example of the input data required, the results from Run J41, described in Appendix D, were used. Figure E.1 shows a plot of the spectrum, and includes identification of the control parameters that are referred to in Table E.1.

The input data for Run J41 are shown in Table E.2, while the GRAPIN code output is given in Table E.3. To show an example of the input parameters used for analysis of fuel element gamma-ray spectra, the data for Run D4 from element 2M19 is given in Table E.4 and the output is presented in Table E.5. A FORTRAN listing of the code is given in Table E.6.

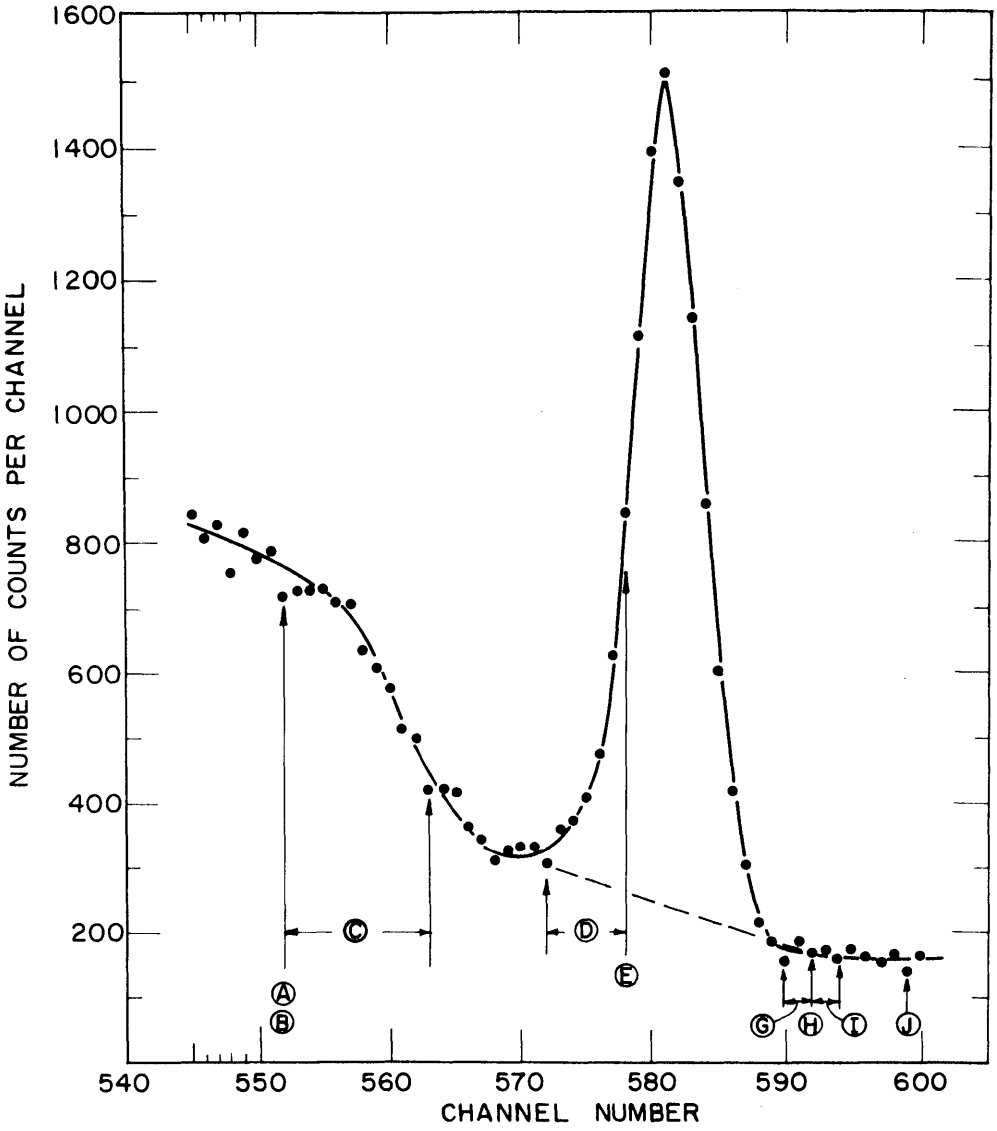

FIGURE E.1 GAMMA-RAY SPECTRUM FOR RUN J40 $[Cs^{137}(2") + Mn^{54}(0")]$ SHOWING EXAMPLE OF INPUT DATA FOR THE "GRAPIN" CODE.

TABLE E.1

INPUT DATA FOR "GRAPIN"

Card	Column	Name	Format	Description	Fig. E.1 Symbol
1	1-72	-	A	Identification	-
2	1-6	NCH1	I	Channel no. of first value of counts per channel.	A
	7-12	NCHL	I	Channel no. of last value of counts per channel. NCHL must be 1025.	J
	13-18	NRUN	I	Control number: if more runs to follow, NRUN=1 if this is last or only run of series, NRUN=0.	
	19-24	NPAN	I	Number of gamma-ray peaks to be analyzed.	
3 to 2+M	1-72	CPC(I)	I	Values of counts per channel from channel NCH1 to NCH. Each card contains 8 values of CPC(I) in Format 8(F6.0,1X). Total no. of cards = $\frac{NCHL-NCH1}{8} = M$	
3+M	1-6	NPEAK	I	Control number of gamma-ray peak to be analyzed.	

Gamma-ray	NPEAK
(a) Cs^{134}(605keV)	1
(b) Rh^{106}(624keV)	2
(c) Cs^{137}(662keV)	3
(d) Pr^{144}(697keV)	4
(e) Zr^{95}(724keV)	5
(f) Zr^{95}(758keV) + Nb^{95}(766keV)	6
(g) Cs^{134}(796keV)	7
(h) Pr^{144}(1164keV)	8
(i) Pr^{144}(2186keV)	9
(j) La^{140}(1498keV)	10

TABLE E.1 (cont'd.)

Card	Column	Name	Format	Description	Fig.E.1 Symbol
				Gamma-ray — NPEAK (k) La^{140}(1597keV) — 11 (l) La^{140}(2520keV) — 12	
3+M	7-12	NLLO	I	Channel no. at which low energy background subtraction is to begin	B
	13-18	NLUP	I	Channel no. at which low energy background is to end.	E
	19-24	NBGHE	I	Channel no. to be used for high energy background.	H
	25-30	KLOB	I	Number of channels below NBGHE to be used for calculating average high energy background.	G
	31-36	KHIB	I	No. of channels above NBGHE to be used for calculating average high energy background.	I
	37-42	JAY	I	No. of channels above NLLO at which averaging for net peak counts is to begin.	C
	43-48	KAY	I	No. of channels below NLUP at which averaging for net peak counts is to begin.	D

TABLE E.2

RUN J41 INPUT DATA FOR GRAPIN

```
1 RUN J41, 3 SERIES,  CS 137, 2 INCHES - MN 54, 0 INCHES
    552   599      1      1
000715 000727 000728 000729 000730 000704 000692 000667 000654
000577 000512 000500 000418 000421 000416 000361 000341 000367
000331 000329 000332 000332 000333 000356 000375 000409 000375
000479 000524 000546 001115 001595 001569 001545 001141 000983
000826 000601 000416 000301 000217 000139 000197 000163 000091
000175 000172 000162 000176 000163 000133 000166 000139 000099
       2   552   578   592   590   594    11     5
```

TABLE E.3 GRAPIN OUTPUT FOR RUN J41

RUN J41, S SERIES, CS 137, 2 INCHES - MN 54, 0 INCHES

NO. OF FIRST CHANNEL	NO. OF LAST CHANNEL	NRUN	NPAN
552	599	1	1

CH. NO.	VALUES OF RAW COUNTS PER CHANNEL, CPC(I)															
552	715	727	728	729	708	704	632	607	577	512	500	418	421	416	361	341
568	310	329	332	332	303	358	373	409	475	624	846	1113	1395	1509	1345	1141
584	858	601	418	301	217	189	157	183	170	172	162	176	163	153	168	139

NPEAK	NLLO	NLUP	NBGHE	KLOB	KHIB	JAY	KAY
3	552	578	592	590	594	11	5

CESIUM-137 GAMMA RAY AT 661.6 KEV

NO. OF COUNTS OF ABOVE FISSION PRODUCT ACTIVITY AS A FUNCTION OF LOWER CHANNEL LIMIT

LO CH LIM	TOT COUNTS	BKGD COUNTS	NET FP COUNTS	FP+ERROR	FP-ERROR
552	23384	18118	5266	5470	5062
553	22669	17916	4753	4954	4552
554	21942	17488	4454	4653	4256
555	21214	17058	4156	4351	3960
556	20485	16221	4264	4456	4073
557	19777	15710	4067	4255	3878
558	19073	14014	5059	5241	4877
559	18441	13189	5252	5430	5075
560	17834	12306	5528	5702	5355
561	17257	10893	6364	6532	6196
562	16745	10366	6379	6543	6214
563	16245	8802	7443	7601	7285
564	15827	8552	7275	7431	7119
565	15406	8187	7219	7372	7065
566	14990	7152	7838	7987	7689
567	14629	6627	8002	8147	7856
568	14288	5985	8303	8445	8161
569	13978	5974	8004	8146	7863
570	13649	5759	7890	8029	7750
571	13317	5509	7808	7945	7671
572	12985	4954	8031	8165	7897
573	12682	5268	7414	7548	7280
574	12324	5147	7177	7309	7045
575	11951	5200	6751	6882	6620
576	11542	5472	6070	6200	5939
577	11067	6342	4725	4857	4593
578	10443	7611	2832	2966	2698

NO. OF COUNTS OF ABOVE FISSION PRODUCT ACTIVITY, AVERAGED OVER LOWER LIMIT CHANNELS 563 TO 572 = 7781

BACKGROUND COUNTS PER CHANNEL ON HIGH ENERGY SIDE OF PEAK, BGHE = 169

TABLE E.4

RUN D4 INPUT DATA FOR GRAPIN

```
1 RUN D4, FE 2M19, 25 INCHES, CENTER-LINE, CHS 56-199
    56   199     1     7
005310 004734 004400 004137 003907 003809 003702 003663 000063
003468 003518 003395 003416 003422 003289 003369 003395 000071
003228 003492 003558 003809 003566 003185 002763 002665 000079
002595 002578 002538 002541 002476 002543 002628 002421 000087
002355 002293 002263 002264 002167 002186 002178 002186 000095
002191 002201 002139 002210 002238 002211 002309 002408 000103
002627 002853 003308 004544 005354 004541 002866 001897 000111
001670 001613 001668 001588 001545 001668 001618 001587 000119
001608 001598 001580 001496 001622 001572 001746 001857 000127
001796 001602 001457 001442 001439 001442 001468 001532 000135
001532 001578 001601 001702 001872 002117 002529 002804 000143
002261 001654 001379 001345 001341 001393 001391 001410 000151
001510 001565 001563 001632 001713 001827 002169 002525 000159
003087 003645 003813 003627 004149 005412 007146 006749 000167
003966 001741 001042 000872 000848 000868 000813 000824 000175
000790 000886 000865 000939 000960 001093 001265 001498 000183
001442 001214 000930 000847 000786 000777 000734 000725 000191
000732 000752 000748 000671 000731 000688 000684 000718 000199
     1    59    73    80    79    81     2     3
     2    80    85    90    89    91     0     1
     3    86   101   113   112   114     2     5
     4   116   125   131   130   132     2     2
     5   131   139   148   146   150     0     3
     6   147   156   173   171   175     0     5
     7   173   180   191   190   192     0     2
1RUN D4, FE 2M19, 25 INCHES, CENTER-LINE, CHS 376-415
   376   415     1     1
000465 000473 000453 000420 000463 000441 000433 000449 000383
000463 000449 000441 000427 000505 000468 000494 000497 000391
000500 000521 000569 000686 000786 000923 001006 000945 000399
000749 000541 000464 000440 000417 000381 000390 000388 000407
000391 000375 000358 000406 000384 000376 000365 000430 000415
     8   376   395   407   404   415     0     4
1RUN D4, FE 2M19, 25 INCHES, CENTER-LINE, CHS 960-1007
   960  1007     0     1
000010 000011 000008 000011 000013 000013 000015 000016 000967
000008 000011 000005 000008 000005 000015 000019 000014 000975
000011 000022 000011 000016 000014 000016 000024 000028 000983
000025 000030 000042 000050 000051 000076 000093 000101 000991
000108 000118 000102 000051 000021 000005 000004 000004 000999
000001 000002 000005 000004 000001 000003 000001 000004 001007
     9   960   983   999   998  1007     3    10
```

TABLE E.5 GRAPIN OUTPUT FOR RUN D4

RUN D4, FE 2719, .5 INCHES, CENTER-LINE, CHS 56-199

NO. OF FIRST CHANNEL	NO. OF LAST CHANNEL	NRUN	NPAN
56	199	1	7

CH. NO. VALUES OF RAW COUNTS PER CHANNEL, CPC(I)

56	5310	4734	4400	4137	3907	3309	3702	3663	3468	3518	3395	3416	3422	3289	3369	3395
72	3228	3492	3550	3[illegible]9	3566	3185	2763	2665	2595	2578	2538	2541	2476	2543	2628	2421
88	2353	2293	2263	2264	2167	2186	2178	2106	2191	2201	2139	2210	2238	2211	2309	2438
104	2627	2853	3308	4544	5354	4541	2866	1897	1670	1613	1668	1588	1545	1668	1618	1587
120	1638	1593	1589	1496	1622	1572	1746	1857	1796	1602	1457	1442	1439	1442	1468	1532
136	1532	1578	1621	17[illegible]2	1872	2117	2529	2804	2261	1654	1379	1345	1341	1393	1391	1410
152	151[illegible]	1565	1563	1632	1713	1827	2169	2525	3087	3645	3813	3627	4149	5412	7146	6749
168	3966	1741	1242	972	848	868	813	824	790	886	865	939	960	1093	1265	1498
184	1442	1214	930	847	786	777	734	725	732	752	748	671	731	688	684	718

NPEAK	NLLO	NLUP	NBGHE	KLOB	KHIB	JAY	KAY
1	59	73	8[illegible]	79	81	2	3

CESIUM-134 GAMMA RAY AT 604 KEV

NO. OF COUNTS OF ABOVE FISSION PRODUCT ACTIVITY AS A FUNCTION OF LOWER CHANNEL LIMIT

LC CH LIM	TOT COUNTS	BKGD COUNTS	NET FP COUNTS	FP+ERROR	FP-ERROR
59	75351	74246	1105	1491	718
60	71214	68456	2758	3131	2384
61	67[illegible]7	64217	3[illegible]9[illegible]	3453	2728
62	63498	59939	3509	3860	3157
63	59796	56481	3315	3656	2974
64	56133	51686	4447	4776	4119
65	52665	49[illegible]45	3620	3939	3301
66	49147	45757	4390	4396	3783
67	45752	42201	3551	3848	3255
68	42336	39225	3111	3396	2825
69	38914	3541[illegible]	3504	3777	3231
70	35625	32899	2726	2988	2464
71	32256	30038	2218	2467	1968
72	28861	26283	2579	2313	2343
73	25633	24419	1214	1438	991

NO. OF COUNTS OF ABOVE FISSION PRODUCT ACTIVITY, AVERAGED OVER LOWER LIMIT CHANNELS 61 TO 70 = 3496

BACKGROUND COUNTS PER CHANNEL ON HIGH ENERGY SIDE OF PEAK, BGHE = 2613

NPEAK	NLLO	NLUP	NBGHE	KLOB	KHIB	JAY	KAY
2	8[illegible]	95	9	89	91	[illegible]	1

RUTHENIUM-106 GAMMA RAY AT 624 KEV

NO. OF COUNTS OF ABOVE FISSION PRODUCT ACTIVITY AS A FUNCTION OF LOWER CHANNEL LIMIT

LC CH LIM	TOT COUNTS	BKGD COUNTS	NET FP COUNTS	FP+ERROR	FP-ERROR
83	27231	26776	455	688	223

81	24636	24257	379	6[illegible]	158
82	22253	21651	4[illegible]7	616	198
83	19521	19257	263	46[illegible]	66
84	16979	16623	356	54[illegible]	173
85	14513	14449	54	224	-116

NO. OF COUNTS OF ABOVE FISSION PRODUCT ACTIVITY, AVERAGED OVER LOWER LIMIT CHANNELS 80 TO 84 = 372

BACKGROUND COUNTS PER CHANNEL ON HIGH ENERGY SIDE OF PEAK, BGHE = 2273

NPEAK	NLLO	NLUP	NBGHE	KLOW	KHIB	JAY	KAY
3	86	1[illegible]1	113	112	114	2	5

CESIUM-137 GAMMA RAY AT 661.6 KEV

NO. OF COUNTS OF ABOVE FISSION PRODUCT ACTIVITY AS A FUNCTION OF LOWER CHANNEL LIMIT

LO CH LIM	TOT COUNTS	BKGD COUNTS	NET FP COUNTS	FP+ERROR	FP-ERROR
86	72121	59897	12224	12588	11861
87	69493	54963	14530	14883	14177
88	67372	52069	15303	15348	14657
89	64717	49292	15425	15763	15088
90	62424	46960	15464	15795	15133
91	60161	45015	15146	15470	14822
92	57897	41991	15906	16222	15590
93	55730	40281	15449	15758	15139
94	53544	38283	15261	15564	14958
95	51366	36445	14921	15217	14625
96	49185	34572	14608	14897	14319
97	46989	32736	14253	14535	13970
98	44788	30315	14473	14747	14199
99	42649	28952	13697	13964	13429
100	40439	27219	13221	13481	12961
101	38251	25099	13152	13354	12851

NO. OF COUNTS OF ABOVE FISSION PRODUCT ACTIVITY, AVERAGED OVER LOWER LIMIT CHANNELS 88 TO 96 = 15243

BACKGROUND COUNTS PER CHANNEL ON HIGH ENERGY SIDE OF PEAK, BGHE = 1652

NPEAK	NLLO	NLUP	NBGHE	KLOW	KHIB	JAY	KAY
4	116	125	131	13[illegible]	132	2	2

PRASEODYMIUM-144 GAMMA RAY AT 697 KEV

NO. OF COUNTS OF ABOVE FISSION PRODUCT ACTIVITY AS A FUNCTION OF LOWER CHANNEL LIMIT

LO CH LIM	TOT COUNTS	BKGD COUNTS	NET FP COUNTS	FP+ERROR	FP-ERROR
116	25794	23928	1866	2089	1643
117	24249	23355	[illegible]94	1112	676
118	22551	21448	1[illegible]33	1343	923
119	2[illegible]263	18715	1[illegible]49	145[illegible]	1[illegible]47
120	1[illegible]476	1[illegible]234	1[illegible]87	1244	9[illegible]29
121	1[illegible]263	1[illegible]474	[illegible]88	[illegible]513	[illegible]46[illegible]
122	1[illegible]1	[illegible]0[illegible]5	[illegible]4	[illegible]1[illegible]2	[illegible]63
123	[illegible]9[illegible]7	[illegible]7[illegible]3	[illegible]24	[illegible]1[illegible]2	1[illegible]94

124	13394	12272	122	981	663
125	11472	10563	109	1057	761

NO. OF COUNTS OF ABOVE FISSION PRODUCT ACTIVITY, AVERAGED OVER LOWER LIMIT CHANNELS 118 TO 123 = 1142

BACKGROUND COUNTS PER CHANNEL ON HIGH ENERGY SIDE OF PEAK, BGHE = 1446

NPEAK	NLLO	NLUP	NBGHE	KLOW	KHIG	JAY	KAY
5	131	139	148	146	157	7	3

ZIRCONIUM-95 GAMMA RAY AT 724 KEV

NO. OF COUNTS OF ABOVE FISSION PRODUCT ACTIVITY AS A FUNCTION OF LOWER CHANNEL LIMIT

LO CH LIM	TOT COUNTS	BKGD COUNTS	NET FP COUNTS	FP+ERROR	FP-ERROR
131	31038	25306	5732	5969	5494
132	29596	23875	5721	5952	5490
133	28157	22494	5663	5888	5438
134	26715	21283	5432	5651	5212
135	25247	20313	4934	5148	4721
136	23715	18862	4853	5060	4647
137	22183	17687	4496	4696	4297
138	20635	16339	4296	4458	4073
139	19004	15359	3645	3830	3460

NO. OF COUNTS OF ABOVE FISSION PRODUCT ACTIVITY, AVERAGED OVER LOWER LIMIT CHANNELS 131 TO 136 = 5389

BACKGROUND COUNTS PER CHANNEL ON HIGH ENERGY SIDE OF PEAK, BGHE = 1370

NPEAK	NLLO	NLUP	NBGHE	KLOW	KHIG	JAY	KAY
6	147	156	173	171	175	5	5

ZIRCONIUM-95 GAMMA AT 757 KEV PLUS NIOBIUM-95 GAMMA AT 766 KEV

NO. OF COUNTS OF ABOVE FISSION PRODUCT ACTIVITY AS A FUNCTION OF LOWER CHANNEL LIMIT

LO CH LIM	TOT COUNTS	BKGD COUNTS	NET FP COUNTS	FP+ERROR	FP-ERROR
147	68349	29565	38784	39297	38471
148	67504	28414	39086	38895	38277
149	65663	27975	37688	37994	37382
150	64272	26932	37439	37742	37136
151	62879	25933	36947	37245	36648
152	61469	25905	35564	35863	35268
153	59959	25305	34654	34946	34362
154	58394	24080	34314	34631	34027
155	56831	23532	33300	33583	33016
156	55199	23022	32177	32457	31897

NO. OF COUNTS OF ABOVE FISSION PRODUCT ACTIVITY, AVERAGED OVER LOWER LIMIT CHANNELS 147 TO 151 = 37889

BACKGROUND COUNTS PER CHANNEL ON HIGH ENERGY SIDE OF PEAK, BGHE = 845

NPEAK	NLLO	NLUP	NBGHE	KLOW	KHIG	JAY	KAY
7	173	182	191	190	192	9	2

CESIUM-134 GAMMA RAY 796 KEV //
NO. OF COUNTS OF ABOVE FISSION PRODUCT ACTIVITY AS A FUNCTION OF LOWER CHANNEL LIMIT

LO CH LIM	TOT COUNTS	BKGD COUNTS	NET FP COUNTS	FP+ERROR	FP-ERROR
173	18256	15184	3072	3255	2889
174	17388	13890	3498	3675	3321
175	16575	13212	3363	3536	3191
176	15751	12163	3589	3755	3421
177	14961	12122	2839	3003	2674
178	14075	11167	2908	3067	2749
179	13210	10851	2359	2514	2204
180	12271	10142	2129	2279	1979

NO. OF COUNTS OF ABOVE FISSION PRODUCT ACTIVITY, AVERAGED OVER LOWER LIMIT CHANNELS 173 TO 178 = 3211

BACKGROUND COUNTS PER CHANNEL ON HIGH ENERGY SIDE OF PEAK, BGHE = 730

RUN 04, FF 2419, 25 INCHES, CENTER-LINE, CHS 376-415

NO. OF FIRST CHANNEL	NO. OF LAST CHANNEL	NRUN	NPAN
376	415	1	1

CH. NO.	VALUES OF RAW COUNTS PER CHANNEL, CPC(I)														
376	465	473	453	42[illegible]	463	441	433	449	463	449	441	427	505	468	494	497
392	5[illegible]	521	569	686	786	923	1026	945	749	541	464	440	417	381	399	388
408	391	375	358	436	384	376	365	430	00	00	00	00	00	00	00	00

NPEAK	NLLO	NLUP	NHGHE	KLOB	KHIB	JAY	KAY
8	376	395	407	404	415	4	4

PRASEODYMIUM-144 DOUBLE ESCAPE PEAK AT 1164 KEV (FOR 2186 KEV GAMMA)

NO. OF COUNTS OF ABOVE FISSION PRODUCT ACTIVITY AS A FUNCTION OF LOWER CHANNEL LIMIT

LO CH LIM	TOT COUNTS	BKGD COUNTS	NET FP COUNTS	FP+ERROR	FP-ERROR
376	17047	13655	3392	3568	3217
377	16582	13352	3230	3403	3057
378	16109	12621	3488	3657	3318
379	15656	11722	3934	4099	3768
380	15236	11920	3316	3481	3151
381	14773	11197	3576	3737	3415
382	14332	10678	3654	3912	3495
383	13899	10468	3431	3587	3275
384	13450	10217	3233	3387	3079
385	12987	9630	3357	3507	3206
386	12538	9124	3414	3562	3267
387	12097	8562	3535	3679	3391
388	11670	8934	2736	2879	2592
389	11165	8136	3029	3168	2890
390	10697	7942	2755	2892	2619
391	10203	7526	2677	2810	2544
392	9706	7107	2599	2728	2469
393	9206	6821	2385	2512	2259
394	8605	6702	1983	2107	1859
395	8116	6984	1132	1255	1009

NO. OF COUNTS OF ABOVE FISSION PRODUCT ACTIVITY, AVERAGED OVER LOWER LIMIT CHANNELS 376 TO 391 = 3297

BACKGROUND COUNTS PER CHANNEL ON HIGH ENERGY SIDE OF PEAK, BGHE = 388

RUN D4, FE 2M19, 25 INCHES, CENTER-LINE, CHS 960-1007

NO. OF FIRST CHANNEL	NO. OF LAST CHANNEL	NRUN	NPAN
960	1007	3	1

CH. NO.	VALUES OF RAW COUNTS PER CHANNEL, CPC(I)															
960	10	11	8	11	13	13	15	16	8	11	5	8	5	15	19	14
976	11	22	11	16	14	16	24	28	25	30	42	50	51	76	93	101
992	108	118	102	51	21	5	4	4	1	2	5	4	1	3	1	4

NPEAK	NLLO	NLUP	NBGHE	KLOB	KHIB	JAY	KAY
9	960	983	999	998	1007	3	10

PRASEODYMIUM-144 GAMMA RAY AT 2186 KEV

NO. OF COUNTS OF ABOVE FISSION PRODUCT ACTIVITY AS A FUNCTION OF LOWER CHANNEL LIMIT

LO CH LIM	TOT COUNTS	BKGD COUNTS	NET FP COUNTS	FP+ERROR	FP-ERROR
960	1205	258	947	985	909
961	1195	271	924	962	886
962	1184	207	977	1014	940
963	1176	257	919	957	881
964	1165	286	879	917	841
965	1152	278	874	912	836
966	1139	304	835	873	797
967	1124	312	812	850	774
968	1108	174	934	969	898
969	1100	215	885	921	848
970	1089	118	971	1005	936
971	1084	158	926	961	891
972	1076	111	965	1000	931
973	1071	242	829	866	793
974	1056	285	771	808	735
975	1037	211	825	861	790
976	1023	167	856	891	822
977	1012	286	726	762	690
978	990	153	837	871	803
979	979	198	781	815	746
980	963	169	794	828	760
981	949	180	769	803	736
982	933	242	691	725	657
983	909	263	646	681	612

NO. OF COUNTS OF ABOVE FISSION PRODUCT ACTIVITY, AVERAGED OVER LOWER LIMIT CHANNELS 963 TO 973 = 893

BACKGROUND COUNTS PER CHANNEL ON HIGH ENERGY SIDE OF PEAK, NGHE = 3

TABLE E.6

FORTRAN LISTING OF "GRAPIN"

```
C      GRAPIN, CODE TO CALC THE NET INTEGRAL UNDER A GAMMA RAY PEAK DUE
C      TO A KNOWN RADIONUCLIDE, INCLUDING BACKGROUND SUBTRACTION, FOR
C      SPECTRA OBTAINED WITH LITHIUM DRIFT GERMANIUM DETECTORS
       DIMENSION CPC(1025),TCH(1025), BKCH(1025), FPTOT(1025),
      1ERSQ(1025),ERR(1025), FPTOP(1025),FPTOM(1025)
     5 READ 2
     2 FORMAT(72H
      1                                                    )
       READ 8, NCH1,NCHL,NRUN,NPAN
8      FORMAT(4I6)
       READ 9, (CPC(I), I=NCH1,NCHL)
 9     FORMAT(8(F6.0,1X))
       PRINT 2
       PRINT 50, NCH1,NCHL,NRUN,NPAN
50     FORMAT(61HONO. OF FIRST CHANNEL   NO. OF LAST CHANNEL   NRUN
      1NPAN  //(7X,I4,19X,I4,12X,I3,7X,I3))
       PRINT 55
55     FORMAT(52HOCH. NO.     VALUES OF RAW COUNTS PER CHANNEL, CPC(I))
       JCHAN=NCH1
       JBEG=NCH1
       JEND=NCH1+15
59     PRINT 60, JCHAN,(CPC(I),I=JBEG,JEND)
60     FORMAT(I6,2X,16F7.0)
       IF (NCHL-JEND) 10,10,61
61     JCHAN=JCHAN+16
       JBEG=JBEG+16
       JEND=JEND+16
       GO TO 59
10     READ 12,NPEAK,NLLO,NLUP,NBGHE,KLOB,KHIB,JAY,KAY
12     FORMAT(8I6)
C      CALCN OF HIGH ENERGY PART OF BACKGROUND BELOW GAMMA PEAK,BGHE
       SUM1=0.
       DO 15 I=KLOB,KHIB
15     SUM1=SUM1+CPC(I)
       FKLO=FLOATF(KLOB)
       FKHI=FLOATF(KHIB)
       BGHE=SUM1/(FKHI-FKLO+1.)
C      SUMMATION OF TOTAL COUNTS UNDER PEAK
       TOTSUM=0.
       DO 20 I=NLLO,NBGHE
20     TOTSUM=TOTSUM+CPC(I)
C      NO. OF COUNTS UNDER THE PEAK AS A FUNCTION OF LOWER
C      CHANNEL LIMIT
       TCH(NLLO)=TOTSUM
       NPL1=NLLO+1
       DO 25 J=NPL1,NLUP
25     TCH(J)=TCH(J-1)-CPC(J-1)
C      NO. OF BACKGROUND COUNTS AS A FUNCTION OF LOWER CHANNEL LIMIT
       DO 30 J=NLLO,NLUP
       NDIF=NBGHE-J+1
       DELCH=FLOATF(NDIF)
30     BKCH(J)=(CPC(J)+BGHE)*0.5*DELCH
C      NO. OF COUNTS OF FISSION PRODUCT ACTIVITY AS A FUNCTION
C      OF LOWER CHANNEL LIMIT
       SUM4=0.
```

```
      DO 36 J=NLLO,NLUP
      FPTOT(J)= TCH(J)-BKCH(J)
      ERSQ(J)=TCH(J)+BKCH(J)
35    ERR(J)=SQRTF(ERSQ(J))
      FPTOP(J)=FPTOT(J)+ERR(J)
36    FPTOM(J)=FPTOT(J)-ERR(J)
      NAVLO=NLLO+JAY
      NAVHI=NLUP-KAY
      NDEL=NAVHI-NAVLO+1
      DELAV=FLOATF(NDEL)
      DO 40 J=NAVLO,NAVHI
40    SUM4=SUM4+FPTOT(J)
      FPAV=SUM4/DELAV
65    PRINT 70,NPEAK,NLLO,NLUP,NBGHE,KLOB,KHIB,JAY,KAY
70    FORMAT(57H0 NPEAK   NLLO   NLUP  NBGHE   KLOB   KHIB    JAY    KAY
     1    /(4X,I2,4X,I3,6I7) //)
      GO TO (80,81,82,83,84,85,86,87,88,89,90,91),NPEAK
80    PRINT 801
801   FORMAT(33H  CESIUM-134 GAMMA RAY AT 604 KEV//)
      GO TO 700
81    PRINT 811
811   FORMAT(38H  RUTHENIUM-106 GAMMA RAY AT 624 KEV  //)
      GO TO 700
82    PRINT 821
821   FORMAT(35H CESIUM-137 GAMMA RAY AT 661.6 KEV //)
      GO TO 700
83    PRINT 831
831   FORMAT(40H  PRASEODYMIUM-144 GAMMA RAY AT 697 KEV //)
      GO TO 700
84    PRINT 841
841   FORMAT(35H  ZIRCONIUM-95 GAMMA RAY AT 724 KEV //)
      GO TO 700
85    PRINT 851
851   FORMAT(64H ZIRCONIUM-95 GAMMA AT 757 KEV PLUS NIOBIUM-95 GAMMA AT
     1766 KEV //)
      GO TO 700
   86 PRINT 861
  861 FORMAT(33H0 CESIUM-134 GAMMA RAY 796 KEV //)
      GO TO 700
87    PRINT 871
  871 FORMAT(72H  PRASEODYMIUM-144 DOUBLE ESCAPE PEAK AT 1164 KEV (FOR
     12186 KEV GAMMA)  //)
      GO TO 700
88    PRINT 881
  881 FORMAT(40H  PRASEODYMIUM-144 GAMMA RAY AT 2186 KEV //)
      GO TO 700
89    PRINT 891
  891 FORMAT(68H  LANTHANUM-140 DOUBLE ESCAPE PEAK AT 1498 KEV (FOR 2520
     1KEV GAMMA)  //)
      GO TO 700
90    PRINT 901
  901 FORMAT(37H  LANTHANUM-140 GAMMA RAY AT 1597 KEV //)
      GO TO 700
   91 PRINT 911
  911 FORMAT (37H  LANTHANUM-140 GAMMA RAY AT 2520 KEV  //)
```

```
700    PRINT 71
71     FORMAT(86H  NO. OF COUNTS OF ABOVE FISSION PRODUCT ACTIVITY AS A F
      1UNCTION OF LOWER CHANNEL LIMIT )
       PRINT 711
  711 FORMAT(79HOLO CH LIM    TOT COUNTS    BKGD COUNTS    NET FP COUNTS
      1FP+ERROR       FP-ERROR  //)
       DO 72 J=NLLO,NLUP
   72    PRINT 75, J, TCH(J), BKCH(J),FPTOT(J),FPTOP(J),FPTOM(J)
   75   FORMAT(I7,5(6X,F8.0))
       PRINT 77,NAVLO,NAVHI,FPAV
77     FORMAT(85H NO. OF COUNTS OF ABOVE FISSION PRODUCT ACTIVITY, AVERAG
      1ED OVER LOWER LIMIT CHANNELS  ,I4,4H TO ,I4,3H = ,F8.0)
       PRINT 78, BGHE
    78 FORMAT(68H0 BACKGROUND COUNTS PER CHANNEL ON HIGH ENERGY SIDE OF P
      1EAK, BGHE = ,   F8.0)
       NPAN=NPAN-1
       IF(NPAN) 781,781,780
780    GO TO 10
781    IF(NRUN) 785,785,784
784    GO TO 5
785    CALL EXIT
       END
```

APPENDIX F

DATA ON FUEL ELEMENT EXPERIMENTS AND RESULTS OF CALCULATIONS OF NET COUNTS OF FISSION PRODUCT GAMMA-RAYS

1. Fuel Element 2M19

Gamma-ray spectra from 2M19 were obtained in the "D" series of experiments (May 5 to 11, 1965). An 1/8 in. dia. aperature collimator was used in the bottom position of the gamma-ray beam tube and a lead absorber, 0.135 in. thick, was placed in the beam. The 1.6 cm^2 area n^+ contact of the detector was orientated normal to the photon beam. Each spectrum was recorded for 80 minutes. Analyzer dead time was a maximum of 4 to 6% at the fuel midplane position.

The results of the GRAPIN code used for calculating the net counts of fission product gamma-rays are presented in Table F.1 in the chronological order of the experiments. The following gamma-ray peaks were analyzed: Cs^{134} at 605 keV and 796 keV, Rh^{106} at 624 keV, Cs^{137} at 662 keV, Pr^{144} at 697 keV, Zr^{95} at 724 keV, the partially resolved peaks of Zr^{95} at 758 keV and Nb^{95} at 766 keV, and the double escape peak at 1164 keV and photopeak at 2186 keV of Pr^{144}.

TABLE F.1
NET COUNTS OF FISSION PRODUCT GAMMA-RAYS
AT VARIOUS POSITIONS FOR FUEL ELEMENT 2M19
AFTER NINE MONTHS COOLING TIME

Run	Position Below Fuel Midplane, Inches	Cs^{134} at 605 keV	Cs^{134} at 796 keV	Rh^{106} at 624 keV	Cs^{137} at 662 keV
D4	- 1 &	3496±312	3211±183	319±232	15,243±346
D5	0 &	3665±362	3079±183	434±232	16,012±345
D6	+ 2 &	3364±351	3048±158	231±216	14,771±340
D7	+ 4 &	3094±349	2934±162	455±210	14,528±332
D8	+ 6 &	2964±339	2410±155	195±219	13,987±326
D9	+ 8 &	2413±330	2629±163	231±213	13,861±318
D10	+ 10 &	1913±314	2384±155	128±201	13,179±303
D11	+ 11 &	2223±307	1885±154	262±190	13,743±296
D12	- 2 &	3205±345	2964±170	553±221	14,404±331
D13	- 4 &	2638±337	2588±170	398±218	13,921±325
D14	- 6 &	2066±325	2334±162	11±202	13,158±312
D15	- 8 &	1824±311	1947±157	427±202	11,762±300
D16	- 10 &	1648±300	1479±150	603±238	11,566±282
D17	- 11 &	1117±262	1261±134	374±170	10,355±255
D18	- 1 &	3454±370	2866±176	206±215	14,778±350
D19	- 1:½" OUT	3556±370	2753±178	493±222	15,259±336
D20	- 1:1" OUT	3785±367	2919±170	308±220	15,212±330
D21	- 1:½" IN	3485±370	2998±177	192±220	15,256±334
D22	- 1:1" IN	3371±369	2788±178	-48±223	15,972±330
D23	- 6:1" IN	2598±345	1951±163	105±208	13,987±325
D24	- 6:½" IN	2233±323	2096±165	-107±211	13,527±314
D25	- 6 &	2110±324	1904±165	-79±210	12,551±313
D26	- 6:½" OUT	1967±300	2108±168	47±212	13,173±314
D27	- 6:1" OUT	2289±345	2505±160	+0±209	13,444±322

TABLE F.1 (cont'd.)

Run	Pos'n Below Fuel Midpl. Inches	Pr^{144} at 697 keV	Zr^{95} at 724 keV	Zr^{95}-Nb^{95} at 760 keV	Pr^{144} Doub.Escape at 1164 keV	Pr^{144} at 2186 keV
D4	- 1 &	1142±210	5389±238	37,501±313	3297±175	893±38
D5	0 &	1227±185	5591±240	38,298±315	3315±175	904±46
D6	+ 2 &	1140±191	4956±235	36,320±308	2927±171	805±36
D7	+ 4 &	1153±202	5099±230	36,191±305	2837±162	736±36
D8	+ 6 &	1161±198	4965±226	35,278±298	2457±164	741±34
D9	+ 8. &	1120±191	4528±220	33,809±290	2674±159	719±35
D10	+ 10 &	1265±184	4656±212	33,265±281	2128±156	679±36
D11	+ 11 &	912±175	4616±207	33,182±278	2610±152	711±33
D12	- 2 &	1076±202	4834±231	35,990±304	2674±170	796±35
D13	- 4 &	1185±212	5071±225	34,066±297	2617±168	831±37
D14	- 6 &	1053±205	4702±220	32,298±289	2638±160	765±36
D15	- 8 &	998±197	4429±212	30,679±277	2537±157	696±33
D16	- 10 &	993±182	4379±198	29,451±265	2295±150	643±32
D17	- 11 &	666±159	3641±176	23,404±240	1924±132	506±30
D18	- 1 &	1027±216	4912±233	35,508±303	3106±170	820±37
D19	- 1:½" OUT	1110±220	4645±233	35,024±307	3110±170	862±36
D20	- 1:1" OUT	1043±210	4705±211	34,871±300	3007±165	849±37
D21	- 1:½" IN	1024±218	4967±232	35,881±306	3174±170	828±35
D22	- 1:1" IN	848±215	4748±229	34,577±303	2657±167	807±36
D23	- 6:1" IN	1047±200	4378±215	32,782±286	2534±157	658±33
D24	- 6:½" IN	907±205	4546±220	32,134±287	2638±159	648±35
D25	- 6 &	1081±200	4186±219	31,188±287	2562±158	752±33
D26	- 6:½" OUT	1106±191	4329±217	31,369±287	2665±161	740±36
D27	- 6:1" OUT	1177±200	4549±214	31,809±282	2633±157	700±34

TABLE F.1 (cont'd.)

Run	Position Below Fuel Midplane, Inches	Cs^{134} at 605 keV	Cs^{134} at 796 keV	Rh^{106} at 624 keV	Cs^{137} at 662 keV
D28	+ 6:1" OUT	2871±356	2236±169	166±215	15,075±320
D29	+ 6:½" OUT	2727±347	2588±170	437±217	14,288±324
D30	+ 6 ℄	2916±357	2518±170	337±218	13,960±323
D31	+ 6 ½" IN	3086±358	2989±168	377±215	14,808±323
D32	+ 6 1" IN	3383±354	2744±165	212±213	15,023±319
D33	+11½ ℄	2662±316	2155±153	301±200	16,605±301
D34	+12 ℄	361±192	405±115	- -	2,046±194
	TRANSVERSE SCAN VIEWING EDGES OF FUEL PLATES AT - 1 INCH BELOW FUEL MIDPLANE				
D35	℄	2076±328	2475±164	172±213	12,184±330
D36	1/16" OUT	1994±299	1506±161	120±196	8,485±306
D37	2/16" OUT	2697±340	2986±170	630±218	13,746±344
D38	3/16" OUT	2536±328	2186±170	395±211	11,987±320
D39	4/16" OUT	2265±310	2084±164	436±202	9,311±314
D40	5/16" OUT	3172±390	2851±170	321±219	14,172±340
D41	6/16" OUT	2430±325	2554±169	439±209	11,692±330
D42	7/16" OUT	2585±313	2232±164	207±204	10,229±320
D43	½" OUT	3073±339	2758±171	366±217	14,151±325
D44	1" OUT	3743±349	3335±175	615±220	14,784±347
D45	½" IN	1841±304	1997±162	99±196	8,270±295
D46	1" IN	3194±333	2671±165	577±211	12,675±318

TABLE F.1 (cont'd)

Run	Pos'n Below Fuel Midpl. Inches	Pr^{144} at 697 keV	Zr^{95} at 724 keV	$Zr^{95}+Nb^{95}$ at 760 keV	Pr^{144} at 1164 keV	Pr^{144} at 2186 keV
D28	+ 6:1" OUT	1072±208	4707±220	33,104±294	2830±160	732±36
D29	+ 6:½" OUT	1068±208	4640±222	33,498±295	2707±160	743±35
D30	+ 6 ℄	796±212	4595±227	34,196±296	2702±160	751±35
D31	+ 6:½" IN	1157±210	4733±223	34,359±295	2626±163	746±34
D32	+ 6:1" IN	1110±200	4995±217	34,489±290	2123±155	744±33
D33	+11½ ℄	1071±190	5269±206	37,297±283	2762±155	738±38
D34	+ 12 ℄	296±127	821±140	5,666±169	1218±112	319±22
	TRANSVERSE SCAN VIEWING EDGES OF FUEL PLATES AT -1 INCH BELOW FUEL MIDPLANE					
D35	0	909±191	4330±219	28,952±283	2659±161	732±34
D36	1/16" OUT	764±184	2719±197	19,533±258	2491±151	727±33
D37	⅛" OUT	806±196	4639±225	33,124±296	2889±163	686±33
D38	3/16" OUT	892±193	3880±217	28,664±283	2541±164	698±35
D39	¼" OUT	628±187	2807±210	22,402±278	2794±160	668±34
D40	5/16" OUT	933±197	4756±222	32,769±290	2677±164	776±35
D41	⅜" OUT	895±192	3931±216	26,950±280	2536±162	714±33
D42	7/16" OUT	904±188	3331±209	23,547±268	2653±161	682±35
D43	½" OUT	951±196	4388±221	31,925±292	2674±162	713±33
D44	1" OUT	1011±196	4454±224	33,525±299	2998±167	825±38
D45	½" IN	764±181	2552±206	20,493±261	2385±158	650±35
D46	1" IN	844±190	4083±217	30,507±284	2594±160	678±36

2. Fuel Element 2M22

Spectra from 2M22 were obtained in the "H" series of experiments (May 19 to 21, 1965). The bottom collimator had a 1/8 in. aperature diameter and 0.135 in. Pb absorber was placed in beam. Eighty (80) min. runs were made. Other experimental conditions were as given in F.1 above.

The net fission product gamma-ray counts calculated by GRAPIN are presented in Table F.2 for Cs^{134}, Rh^{106}, Cs^{137}, Zr^{95}, Nb^{95} and Pr^{144}.

The results of four experiments to determine the reproducibility of techniques are shown in Table F.3. Before each of these runs, the scanning mechanism was moved in lateral and transverse directions then repositioned at the fuel midplane centerline (0 in. Δ). Spectra were recorded for 40 min.

The mean values for each gamma-ray are given along with maximum and mean deviations of the individual values from the mean. In all cases, the mean deviation was less than 1.5 times the statistical uncertainty of the calculation for the net counts. The maximum deviation for one case was 2.8 times the statistical error (Run H23, Cs^{137}), but for the others was less than this. It was concluded that the experimental techniques and the method of calculating gamma-ray intensities enabled results to be reproduced with uncertainties on the average being about twice the statistical uncertainties.

TABLE F.2

NET COUNTS OF FISSION PRODUCT GAMMA-RAYS AT VARIOUS POSITIONS FOR FUEL ELEMENT 2M22 AFTER $1\frac{1}{2}$ YEARS COOLING

Run	Position Below Fuel Midplane, Inches	Cs^{134} at 605 keV	Rh^{106} at 624 keV	Cs^{137} at 662 keV	Pr^{144} at 697 keV
H1	0 &	7788±288	689±163	25,055±280	1172±155
H2	- 2 &	7103±285	462±164	24,172±277	1148±151
H3	- 4 &	6350±272	740±159	22,646±270	1001±148
H4	- 6 &	5198±259	505±152	21,351±257	992±142
H5	- 8 &	4298±238	565±142	19,898±245	898±133
H6	- 10 &	3326±220	439±131	18,448±227	807±125
H7	- 11 &	3536±216	360±129	20,067±225	897±121
H8	+ 2 &	7351±287	665±166	24,248±280	1154±152
H9	+ 4 &	6857±281	571±161	24,475±277	1048±151
H10	+ 6 &	6728±271	356±156	23,547±268	1084±149
H11	+ 8 &	5214±259	448±151	22,909±260	946±142
H12	+ 10 &	5041±245	418±143	22,802±251	1199±133
H13	$+11\frac{3}{4}$ &	2167±181	178±109	9,852±183	501±108
H14	0 &	7238±288	421±166	24,148±278	1049±160
H15	0:$\frac{1}{2}$" OUT	7181±290	591±166	24,651±281	1108±155
H16	0:1" OUT	8365±292	596±166	26,955±283	1300±158
H17	0:$\frac{1}{2}$" IN	7584±289	532±167	24,747±282	1070±154
H18	0:1" IN	8047±289	416±165	26,511±282	1093±151

TABLE F.2 (cont'd.)

Run	Pos'n Below Fuel Midpl. Inches	Zr^{95} at 724 keV	Zr^{95}+Nb^{95}	Cs^{134} at 796 keV	Pr^{144} at 1164 keV	Pr^{144} at 2186 keV
H1	0 b	464±140	3232±174	4774±173	1836±142	476±28
H2	- 2 b	358±140	3050±171	4944±168	2015±140	488±29
H3	- 4 b	437±136	2814±167	4184±164	1902±137	422±28
H4	- 6 b	418±128	2651±160	3879±155	1675±131	414±36
H5	- 8 b	539±122	2695±151	2920±146	1588±127	374±28
H6	- 10 b	298±114	2381±140	2109±136	1320±118	362±25
H7	- 11 b	501±108	2841±136	2478±130	1404±119	342±25
H8	+ 2 b	561±139	2793±177	4760±172	1893±142	498±31
H9	+ 4 b	400±139	2837±170	4584±171	1714±142	-
H10	+ 6 b	522±131	2855±169	4378±163	1875±138	464±28
H11	+ 8 b	391±129	3070±160	3819±156	1965±131	471±28
H12	+ 10 b	441±123	2823±152	3457±147	1701±127	407±30
H13	+11$\frac{3}{4}$" b	198±97	1024±117	1626±116	953±102	269±23
H14	0 b	-	-	4896±171	1817±146	491±30
H15	0:$\frac{1}{2}$" OUT	550±139	2915±172	5345±172	1896±141	520±29
H16	0:1" OUT	442±140	3232±172	5718±172	1916±142	496±30
H17	0:$\frac{1}{2}$" IN	343±140	2992±173	5188±172	1882±140	541±31
H18	0:1" IN	427±135	2942±170	5449±168	1810±140	488±30

TABLE F.3

RESULTS OF EXPERIMENTS TO DETERMINE

REPRODUCIBILITY OF TECHNIQUES

ON FUEL ELEMENT 2M22 AT 0 IN. AND CENTERLINE

Run	Cs^{134} at 605 keV	Cs^{137}	Pr^{144} at 697 keV	Zr^{95}+Nb^{95}	Cs^{134} at 796 keV
H22	2418±178	7906±154	472±84	950±94	1730±94
H23	2188±178	8434±158	484±84	941±94	1720±94
H24	2148±179	7854±154	249±84	683±100	1888±94
H25	2613±179	7785±158	518±84	663±98	1733±94
Mean	2342	7995	431	809	1768
Max. Deviation	+ 271	+ 439	- 182	- 146	+ 120
Mean Deviation	174	220	91	136	60

3. Fuel Element 2M31

Gamma-ray spectra were obtained for 2M31 about 11 days after its removal from the reactor flux (May 14-15, 1965). Background radiation levels near the detector were high (> 300 mr/hr) because the six feet of water was insufficient to provide adequate shielding against the high levels of fission product activities in the element. The amount of lead shielding placed around the detector dewar was limited by the strength of the scanning carriage. The energy resolution of the detector was consequently rather poor due to the high count rates. Collimators at the bottom and the top of the beam tube had aperature diameters of 1/16 in. and 1/4 in. respectively. A total of 0.52 in. of lead shielding was placed in the beam to reduce low energy count rates. Twenty minute runs were made.

Only the La^{140} gamma-ray peak at 1597 keV was recorded. The results of the intensity calculations are given in Table F.4.

TABLE F.4

NET COUNTS OF La^{140} GAMMA-RAYS

AT 1597 keV FOR FUEL ELEMENT 2M31

AFTER 11 DAYS COOLING

Run	Position Below Fuel Midplane, Inches	La^{140} at 1597 keV
E12	- 8	5230±138
E13	- 10	4934±130
E14	- 11	4247±120
E15	- 6	5519±138
E16	- 4	5743±142
E18	- 11	4148±120
E19	- 10	4646±127
E20	- 8	4986±134
E21	- 6	5369±135
E22	- 4	5553±140
E23	- 2	5696±149
E24	0	5745±142
E25	+ 2	5873±153
E26	+ 4	5866±142
E27	+ 6	5517±147
E28	+ 8	5541±139
E29	+ 10	5428±143
E30	+ 12	783±81

4. Fuel Element 2-4

Spectra from 2-4 were obtained in the "F" series of experiments (May 16-17, 1965). Because of the long cooling time of this element (3 years), most of the fission product activities had decayed. To obtain acceptable count rates for the Cs^{137} gamma-ray, no collimators were installed in the beam. Thus, the only collimation was provided by the internal diameter of the beam tube which was 1/2 in. A lead absorber, 0.135 in. thick, was placed in the beam to reduce low energy gamma-ray counts. Each run was 20 min. long.

Table F.5 gives the net counts at various positions for fission product gamma-rays due to Cs^{134}, Rh^{106}, Cs^{137} and Pr^{144}.

5. Fuel Element 2M1

Element 2M1 was analyzed in the "G" series of experiments (May 17-18, 1965). The bottom collimator had a 1/8 in. dia. aperature. No lead absorbers were used in the beam. Forty min. runs were made.

Table F.6 presents the results of calculations of gamma-ray peak counts for Cs^{134}, Rh^{106}, Cs^{137} and Pr^{144}.

TABLE F.5

NET COUNTS FOR FISSION PRODUCT GAMMA-RAYS AT VARIOUS POSITIONS FOR FUEL ELEMENT 2-4 AFTER THREE YEARS COOLING TIME

Run	Position Below Fuel Midplane, Inches	Cs^{134} at 604 keV	Rh^{106} at 624 keV	Cs^{137} at 662 keV	Pr^{144} at 697 keV
F8	0	1853±135	520±87	30,851±207	529±59
F9	- 2	1711±131	482±85	29,644±205	570±55
F10	- 4	1729±126	480±83	28,741±202	571±53
F11	- 6	1304±121	343±80	26,919±191	540±53
F12	- 8	1215±115	403±77	25,391±189	495±51
F13	- 8	1290±116	360±78	25,446±188	494±50
F14	- 10	903±113	322±77	24,838±186	337±50
F15	- 11	406±78	123±58	11,318±126	
F16	+ 2	1675±134	438±87	30,610±208	528±60
F17	+ 4	1504±133	296±87	30,087±205	570±55
F18	+ 6	1229±130	325±86	29,454±203	487±56
F19	+ 8	1418±127	331±82	28,180±199	510±55
F20	+ 10	1180±124	366±82	27,937±198	487±53
F21	+ 12	4	10	913±46	17
F22	0	1850±133	369±86	30,089±207	568±57
F23	0 No Pb	2886±163	629±106	45,270±254	738±70

TABLE F.6

NET COUNTS FOR FISSION PRODUCT GAMMA-RAYS AT VARIOUS POSITIONS FOR FUEL ELEMENT 2M1

Run	Position Below Fuel Midplane, Inches	Cs^{134} at 605 keV	Rh^{106} at 624 keV	Cs^{137} at 662 keV	Pr^{144} at 697 keV
G1	- 6 ℄	586±92	84±52	6336±111	96±43
G2	- 8 ℄	336±86	42±45	5747±104	68±41
G3	-10 ℄	374±80	2±42	5472±100	59±37
G4	-11 ℄	213±79	15±44	5978±101	65±35
G5	- 4 ℄	479±90	-11±53	6599±114	54±40
G6	- 2 ℄	636±94	15±49	6981±116	94±45
G7	0 ℄	628±96	9±55	7056±117	100±43
G8	+ 2 ℄	621±94	44±50	7080±117	47±45
G9	+ 4 ℄	563±93	27±52	6865±116	101±42
G10	+ 6 ℄	477±90	21±47	6534±112	91±41
G11	+ 8 ℄	494±90	59±50	6467±109	80±40
G12	+10 ℄	397±80	43±47	6350±107	98±37
G18	0 ℄	601±97	21±54	7133±115	52±44
G19	0 ½" OUT	636±100	48±54	7437±118	72±42
G20	0 1" OUT	807±100	73±51	7779±122	75±42
G21	0 ½" IN	666±95	16±55	7248±120	62±42
G22	0 1" IN	635±95	12±48	7709±120	67±42

APPENDIX G

DESCRIPTION OF COMPUTER CODES "NOTSFI" AND "NUCON"

1. Introduction

Two computer codes were written to obtain numerical solutions for the equations describing fission product concentrations in irradiated fuel as given in Section IIID. The first code, called NUCON, was intended to be more general and was to have included fission products from both plutonium and uranium. However, only the solutions for constant flux operation and U^{235} fission were programmed. Satisfactory agreement and consistency could not be obtained for the experiment results using the constant flux solutions. It was then necessary to take into account the intermittent operation of the MITR fuel.

The NUCON code was modified to calculate solutions only to Eq. (D.8) for the concentrations of Group 1 type fission products during intermittent operation. Since the code was becoming too large and unwieldy for the Computation Center Time-sharing System, it was decided to write a second code, called NOTSFI, for the intermittent operation solutions. The fuel was assumed to undergo a number of equal cycles, each consisting of an irradiation period during which the neutron flux was constant, and a shutdown period during which the flux was zero. The input data required for the NUCON code is described in Section 2 following, while that for the NOTSFI code is described in Section 3.

2. Input Data for NUCON

Fertile and fissile isotope concentrations are calculated

in the first part of the code; therefore cross-sections for U^{235}, U^{238} and the plutonium isotopes are required. The equations governing the concentrations of the fuel isotopes were taken from Ref. (B12). The yields and cross-sections for the fission products are included in a separate subroutine called CONST, and were given in Table 11. Complete FORTRAN listings are given after the description of input data given in Table G.1. An example of input data for the Cs^{137} concentrations and activities per initial U^{235} atom is given in Table G.2.

3. Input Data for NOTSFI

The format specifications for the input data are given in Table G.3. An example of the form of input for Cs^{134} solutions is presented in Table G.4. The FORTRAN listing of the NOTSFI code is also included.

TABLE G.1

INPUT DATA FOR "NUCON"

Card	Column	Name	Format	Description
1	1-72	-	A	Identification.
2	1-3	NFFI	I	If NFFI=1 solutions obtained for nuclide concentrations for U-235, Pu-239, Pu-240 and Pu-241 if NFFI=0 no solutions obtained for fertile and fissile isotopes.
	4-6	NFPI	I	If NFPI=1 solutions obtained for fission product concentrations if NFPI=0 no solutions obtained.
	7-9	NGP	I	No. of group of fission product for which solution is desired. NGP=1 for Ru-106, Cs-137, Zr-95, Ba-140 and Ce-144. NGP=2 for Cs-134. NGP=3 for Nb-95, La-140 and Pr-144.
	10-12	NRUN	I	NRUN=0 data for only one run NRUN=1 data for another run to follow.
	13-15	NFP	I	No. of fission product. NFP — Fission Product 1 — Zr-95 2 — Nb-95 3 — Ru-106 4 — Cs-133 5 — Cs-134 6 — Cs-137 7 — Ba-140 8 — La-140 9 — Ce-144 10 — Pr-144
2	16-18	NONSS	I	NONSS=1 intermittent operation. Solutions for NGP=1 only. NONSS=0 Constant flux solution.

TABLE G.1 (cont'd.)

Card	Column	Name	Format	Description
	IF NONSS = 0			
3	1-12	TIN	E	Initial time at which solutions are made, in seconds.
	13-24	TAU	E	Total irradiation time, seconds.
	25-36	TDEL	E	Time increment to be used in calculations, seconds. (Use 1.0E+05)
	37-48	PHI	E	Absolute thermal neutron flux, n/cm^2-sec.
	49-60	ENRICH	E	N_{25}^o/N_{28}^o (B12)
	61-72	P1	E	Fast non-leakage probability (B12)
4	1-12	P	E	Resonance escape probability.
	13-24	EPSI	E	Fast fission factor, .
	IF NONSS = 1			
3	1-12	TACC	E	Length of accumulation period, seconds.
	13-24	TDEC	E	Length of shutdown period, seconds.
	25-36	CYCLES	E	Total number of cycles, each having 1 TACC and 1 TDEC.
	37-48	PHI	E	Absolute thermal neutron flux, n/cm^2-sec.
	49-60	ENRICH	E	N_{25}^o/N_{28}^o
	61-72	P1	E	Fast non-leakage probability.
4	1-12	P	E	Resonance escape probability.
	13-24	EPSI	E	Fast fission factor, .
5	1-12	SIG25	E	σ_{25}^a, cm^2
	13-24	SIGF25	E	σ_{25}^f, cm^2

TABLE G.1 (concl'd)

Card	Column	Name	Format	Description
	25-36	SIG28	E	σ_{28}^{a} , cm^2
	37-48	SIG40	E	σ_{40}^{a} , cm^2 (Pu^{240})
	49-60	SIG41	E	σ_{41}^{a} , cm^2 (Pu^{241})
	61-72	SIGF41	E	σ_{41}^{f} , cm^2
6	1-12	SIG49	E	σ_{49}^{a} , cm^2 (Pu^{239})
	13-24	SIGF49	E	σ_{49}^{f} , cm^2
	25-36	ETA25	E	η_{25}
	37-48	ETA49	E	η_{49}
	49-60	ETA41	E	η_{41}
	61-72	ALFA25	E	$\alpha_{25} = \alpha_{25}^{c}/\sigma_{25}^{f}$
7	1-12	ALFA49	E	$\alpha_{49} = \alpha_{49}^{c}/\sigma_{49}^{c}$

TABLE G.2

"NUCON" SAMPLE INPUT DATA FOR Cs^{137}

```
1 SAMPLE INPUT DATA FOR NUCON, FOR CS-137
  0  1  1  1  6  1
  3.4200E 05  2.6280E 03  1.5000E 02  1.0000E 13  7.9270E-02  1.0000E 00
  0.9000E 00  1.0500E 00
5.11900E-22 4.27450E-22 2.21000E-23 1.01470E-21 1.17040E-21 1.61100E-21
1.59260E-21 9.40600E-22 2.04780E 00 1.94860E 00 2.15590E 00 0.19797E 00
0.48054E 00
```

TABLE G.3

INPUT DATA FOR "NOTSFI"

Card	Column	Name	Format	Description
1	1-72	-	A	Identification.
2	1-3	NGP	I	No. of fission product group for which solution is desired. NGP=1 for Ru-106, Cs-137, Zr-95, Ba-140 and Ce-144. NGP=2 for Cs-134. NGP=3 for Nb-95
	4-6	NFP	I	No. of fission product; see Table G.1.
	7-9	NRUN	I	NRUN=0 data for one run only. NRUN=1 data for another run to follow.
3	1-12	SIG25	E	σ_{25}^{a}, cm^2
	13-24	SIGF25	E	σ_{25}^{f}, cm^2
	25-36	PHI	E	Neutron flux, ϕ, n/cm^2-sec.
	37-48	SIGFP (4)	E	σ^a for Cs^{133}, cm^2
	49-60	SIGFP (5)	E	σ^a for Cs^{134}, cm^2
4	1-12	CYCLES	E	No. of cycles for which solutions are desired.
	13-24	TACC	E	Length of accumulation cycle at constant flux, seconds.
	25-36	TDEC	E	Length of shutdown cycle at ϕ=0, seconds.
	37-48	DELTA	E	Solutions are printed out during constant flux period after each time increment DELTA, in seconds. The quotient TACC/DELTA must equal an integer.

TABLE G.3 (concl'd.)

Card	Column	Name	Format	Description
4	49-60	DELTD	E	Solutions are printed out during shutdown period after each time increment DELTD, in seconds. The quotient TDEC/DELTD must equal an integer.
	61-72	TIN	E	Time after t=0 when fission product concentrations and activities are first calculated, in seconds.

FORTRAN LISTINGS OF "NUCON" AND "CONST"

```
C      NUCON, CODE TO CALCULATE FISSION PRODUCT CONCENTRATIONS IN NUCLEAR
C      REACTOR FUEL, RELATIVE TO U-235 AT TIME ZERO, AS A FUNCTION OF
C      TIME,FLUX, AND OTHER PARAMETERS
       DIMENSION SIGFP(20),DLAM(20),Y25(20),Y49(20)
       COMMON SIG25,SIGF25,SIG40,SIG41,SIGF41,SIG42,SIG49,SIGF49,ALFA25,
      1ALFA49,ETA25,ETA49,ETA41,SIGFP,DLAM,Y25,Y49,NGP,NFP
       CALL CONST
    5  READ 10
   10  FORMAT(72H
      1                                    )
       READ 15, NFFI,NFPI,NGP,NRUN,NFP,NONSS
   15  FORMAT(6I3)
       PRINT 10
       PRINT 20,NFFI,NFPI,NGP,NRUN,NFP,NONSS
   20  FORMAT(51H0   NFFI     NFPI     NGP      NRUN      NFP      NONSS  //
      1(I7,2X,I6,4I7))
       IF (NONSS) 21,21,23
   21  READ 22, TIN,TAU,TDEL,PHI,ENRICH,P1,P,EPSI
   22  FORMAT (6E12.4)
       PRINT 25,TIN,TAU,TDEL,PHI,ENRICH,P1,P,EPSI
   25  FORMAT(98H0     TIN          TAU          TDEL           PHI        ENRI
      1CH         P1           P           EPSI       //(8E12.4))
       GO TO 31
   23  READ 24,TACC,TDEC,CYCLES,PHI,ENRICH,P1,P,EPSI
   24  FORMAT (6E12.4)
       PRINT 241, TACC,TDEC,CYCLES,PHI,ENRICH,P1,P,EPSI
  241  FORMAT(32H0 INTERMITTENT REACTOR OPERATION  //93H      TACC
      1 TDEC        CYCLES          PHI        ENRICH         P1            P
      2        EPSI     //(8E12.4))
   31  READ 35, SIG25,SIGF25,SIG28,SIG40,SIG41,SIGF41,SIG49,SIGF49,ETA25,
      1ETA49,ETA41,ALFA25,ALFA49
   35  FORMAT(6E12.5)
       PRINT 36
   36  FORMAT(56H0 CROSS SECTIONS USED FOR FISSILE AND FERTILE ISOTOPES
      1  //)
       PRINT 37,SIG25,SIGF25,SIG40,SIG41,SIGF41,SIG49,SIGF49,ETA25,ETA49,
      1ETA41,ALFA25,ALFA49,SIG28
   37  FORMAT(120H0   SIGA25       SIGF25       SIGA40       SIGA41       SIG
      1F41       SIGA49       SIGF49       ETA25        ETA49        ETA41
      2//(10E12.5)// 36H0   ALFA25       ALFA49        SIG28    //(3E12.5))
       GAM=1.- ETA49*FPSI*P1*(1.-P)
       C1= (ENRICH*SIG28)/(SIG49*GAM)
       C2= (SIG25*ETA25*EPSI*P1*(1.-P))/(SIG49*GAM-SIG25)
       C3= (ENRICH*SIG28*ALFA49)/(SIG40*GAM*(1.+ALFA49))
       C4= (ETA25*EPSI*P1*(1.-P)*SIG25*SIG49*ALFA49)/((1.+ALFA49)*(SIG25
      1-SIG49*GAM)*(SIG25-SIG40))
       C5=(C3*SIG40)/(SIG 49*GAM-SIG40)
       C6= (C3*SIG40)/SIG41
       C7= -(C4*SIG40)/(SIG25-SIG41)
       C8=-(C5*SIG40)/(SIG49*GAM-SIG41)
       C9= ((C3+C4+C5)*SIG40)/(SIG40-SIG41)
       IF (NFFI) 70,70,40
   40  IF (NONSS) 41,42,41
   41  PRINT 411
  411  FORMAT(45H1 NFFI AND NONSS BOTH NONZERO, NO EXECUTION     )
```

```
      GO TO 900
   42 PRINT 45
   45 FORMAT(97HOCONCENTRATIONS OF FERTILE AND FISSILE ISOTOPES IN FUEL
     1AFTER BURNUP IN FLUX PHI, FOR TIME, TAU      //76H TAU, IN SECONDS
     1    U-235            PU-239           PU-240           PU-241    //)
      T=TIN
      TFIN=TAU
      TIN2=10.*TIN
      TDEL2=TDEL
   46 CN25=EXPF(-SIG25*PHI*T)
      CN49= C1+C2*CN25-(C1+C2)*EXPF(-SIG49*GAM*PHI*T)
      CN40=C3+C4*CN25+C5*EXPF(-SIG49*GAM*PHI*T)-(C3+C4+C5)*EXPF(-SIG40*
     1PHI*T)
      CN41=C6+C7*CN25+C8*EXPF(-SIG49*GAM*PHI*T)+C9*EXPF(-SIG40*PHI*T)
     1-(C6+C7+ C8+C9)*EXPF(-SIG41*PHI*T)
      PRINT 50,T,CN25,CN49,CN40,CN41
   50 FORMAT(E12.4,4E13.5)
      IF (TFIN-T) 70,70,60
   60 IF (TIN2-T) 62,62,64
   62 TDEL2= 10.*TDEL2
      TIN2= 10.*TIN2
   64 T=T+TDEL2
      GO TO 46
   70 IF(NFPI) 900,900,75
   75 GO TO (80,300,500),NGP
C     GROUP 1 TYPE FISSION PRODUCTS(ZR-95,RU-106,CS-133,CS-137,BA-140
C     ,CE-144)
   80 GO TO (81,525,82,83,525,84,85,525,86,525),NFP
   81 PRINT 811
  811 FORMAT(57H0 ZR-95 CONCENTRATION IN FUEL AFTER BURNUP FOR TIME TAU
     1     //)
      GO TO 100
   82 PRINT 821
  821 FORMAT(57H0 RU-106 CONCENTRATION IN FUEL AFTER BURNUP FOR TIME TAU
     1       //)
      GO TO 100
   83 PRINT 831
  831 FORMAT(58H0 CS-133 CONCENTRATION IN FUEL AFTER BURNUP FOR TIME TAU
     1     //)
      GO TO 100
   84 PRINT 841
  841 FORMAT(58H0 CS-137 CONCENTRATION IN FUEL AFTER BURNUP FOR TIME TAU
     1       /)
      GO TO 100
   85 PRINT 851
  851 FORMAT(58H0 BA-140 CONCENTRATION IN FUEL AFTER BURNUP FOR TIME TAU
     1       //)
      GO TO 100
   86 PRINT 861
  861 FORMAT(58H0 CE-144 CONCENTRATION IN FUEL AFTER BURNUP FOR TIME TAU
     1         //)
  100 IF (NONSS) 101,101,150
  101 PRINT 103
  103 FORMAT(118H0  TAU, SEC.     FP125        FP149        FP141
     1 FP1TOT        AFP125        AFP149        AFP141        AF1TOT
```

```
     2     //)
  199 FP1TOT=0.
      T=TIN
      TDEL2=TDEL
      TIN2=10.*TIN
      FP125=0.
      FP149=0.
      AFP141=0.
      FP141=0.
      C15=(SIGF25*Y25(NFP)*PHI)/(DLAM(NFP)-SIG25*PHI)
  105 FP125=C15*(  EXPF(-SIG25*PHI*T)-EXPF(-DLAM(NFP)*T))
      AFP125=FP125*DLAM(NFP)
      AFP149=FP149*DLAM(NFP)
      FP1TOT=FP125+FP149+FP141
      AF1TOT=FP1TOT*DLAM(NFP)
      PRINT 110,T,FP125,FP149,FP141,FP1TOT,AFP125,AFP149,AFP141,AF1TOT
  110 FORMAT(E12.4,8E13.5)
      IF (TFIN-T) 115,115,112
  112 IF(TIN2-T) 113,113,114
  113 TDEL2=10.*TDEL2
      TIN2=10.*TIN2
  114 T= T+TDEL2
      GO TO 105
  115 IF (NRUN) 900,900,120
  120 GO TO 5
  150 PRINT 151
  151 FORMAT(103H0 REACTOR OPERATION NOT CONTINUOUS, TRES = TOTAL IN-PIL
     1E RESIDENCE TIME, BURNUP TIME, TAU = TACC*CYCLES  //61H CYCLE NO.
     3 TRES, SEC.    TAU, SEC.      FP125         AFP125    //)
       X1= (SIGF25*Y25(NFP)*PHI)/(DLAM(NFP)-SIG25*PHI)
       X2 = EXPF(DLAM(NFP)*TACC)
       X4= 1.0/X2
       X3 = X1*X2*(EXPF(-SIG25*PHI*TACC) -X4)
       D = SIG25*PHI*TACC -DLAM(NFP)*(TACC+TDEC)
       CNUM=1.
       SUM1= EXPF(D)
       TRES =TACC+TDEC
       TAU=TACC
  155 FP125=X3*EXPF(-SIG25*PHI*TACC*CNUM)*SUM1
       AFP125= FP125*DLAM(NFP)
       PRINT 160, CNUM,TRES,TAU,FP125,AFP125
  160 FORMAT(F7.0,3X,2E12.4,2E13.5)
       CNUM=CNUM+1.
       SUM1 = SUM1+EXPF(CNUM*D)
       IF (CYCLES-CNUM) 170,165,165
  165 TRES= CNUM*(TACC+TDEC )
       TAU =CNUM*TACC
       GO TO 155
  170 IF (NRUN) 900,900,175
  175 GO TO 5
C     GROUP 2 TYPE FISSION PRODUCTS (CS-134)
  300 T=TIN
      TDEL2=TDEL
      TIN2=10.*TIN
      AFP249=0.
```

```
      FP249=0.
      PRINT 304
  304 FORMAT(57H0 CS-134 CONCENTRATION IN FUEL AFTER BURNUP FOR TIME TAU
     1      // 92H0  TAU, SEC.      FP225         FP249         FP2TOT
     1  AFP225         AFP249         AF2TOT      // )
      C20=SIGF25*Y25(4)*SIGFP(4)*PHI
      C21= SIGFP(4) -SIG25
      C134 = DLAM(5) + SIGFP(5)*PHI
      C22= C134- SIGFP(4)*PHI
      C23= C134-SIG25*PHI
      C24= C20/(C21*C22*C23)
  310 FP225= C24*(C21*PHI*EXPF(-C134    *T)+C22*EXPF(-SIG25*PHI*T) -C23*
     1EXPF(-SIGFP(4)*PHI*T))
      FP2TOT = FP225+ FP249
      AFP225= FP225*DLAM(5)
      AF2TOT= FP2TOT*DLAM(5)
      PRINT 315,T,FP225,FP249,FP2TOT,AFP225,AFP249,AF2TOT
  315 FORMAT( E12.4,6E13.5)
      IF (TFIN-T) 325,325,320
  320 IF (TIN2-T) 321,321,323
  321 TDEL2= 10.*TDEL2
      TIN2= 10.*TIN2
  323 T= T+TDEL2
      GO TO 310
  325 IF (NRUN) 900,900,330
  330 GO TO 5
C     GROUP3 TYPE FISSION PRODUCTS (NB-95,LA-140,PR-144)
  500 T=TIN
      TIN2=10.*TIN
      TDEL2=TDEL
      FP349=0.
      PRINT 505
  505 FORMAT(75H0 GROUP 3 FISSION PRODUCT CONCENTRATION IN FUEL AFTER BU
     1RNUP FOR TIME TAU  // 92H0  TAU, SEC.      FP325         FP349
     2  FP3TOT         AFP325         AFP349         AF3TOT     //)
      C30= DLAM(NFP-1)*SIGF25*Y25(NFP-1)*PHI
      C31= DLAM(NFP-1) -SIG25*PHI
      C32 =DLAM(NFP) -SIG25*PHI
      C33 =DLAM(NFP) -DLAM(NFP-1)
      C34= C30/(C31*C32*C33)
  510 FP325= C34*(C31*EXPF(-DLAM(NFP)*T) +C33* EXPF(-SIG25*PHI*T) -C32*
     1EXPF(-DLAM(NFP-1)*T))
      FP3TOT = FP325 +FP349
      AFP325= DLAM(NFP)*FP325
      AFP349= DLAM(NFP)*FP349
      AF3TOT=DLAM(NFP)*FP3TOT
      PRINT 515,T,FP325,FP349,FP3TOT,AFP325,AFP349,AF3TOT
  515 FORMAT( E12.4,6E13.5)
      IF (TFIN-T) 525,525,520
  520 IF (TIN2-T) 521,521,523
  521 TDEL2= 10.*TDEL2
      TIN2= 10.*TIN2
  523 T= T+TDEL2
      GO TO 510
  525 IF (NRUN) 900,900,530
```

```
530 GO TO 5
900 CALL EXIT
    END
```

```
      SUBROUTINE CONST
      DIMENSION SIGFP(20),DLAM(20),Y25(20),Y49(20)
      COMMON SIG25,SIGF25,SIG40,SIG41,SIGF41,SIG42,SIG49,SIGF49,ALFA25,
     1ALFA49,ETA25,ETA49,ETA41,SIGFP,DLAM,Y25,Y49,NGP,NFP
      SIGFP(4)= 54.66E-24
      SIGFP(5)= 103.89E-24
      DLAM(1)=  1.2340F-07
      DLAM(2)=  2.2920E-07
      DLAM(3)=  2.1750E-08
      DLAM(4)=0.
      DLAM(5)=9.983E-09
      DLAM(6) = 7.33E-10
      DLAM(7)=6.268E-07
      DLAM(8)= 4.79E-06
      DLAM(9)=2.865E-08
      DLAM(10)=6.60E-04
      Y25(1)=0.0627
      Y25(2)=0.
      Y25(3)=0.0038
      Y25(4)=0.0675
      Y25(5)=0.
      Y25(6)=0.060
      Y25(7)=0.0644
      Y25(8)=0.
      Y25(9)=0.0562
      Y25(10)=0.
      Y49(1)=0.0506
      Y49(2)=0.
      Y49(3)=0.0404
      Y49(4)=0.0553
      Y49(5)=0.
      Y49(6)=0.0540
      Y49(7)=0.0547
      Y49(8)=0.
      Y49(9)=0.0409
      Y49(10)=0.
      RETURN
      END
```

FORTRAN LISTING OF "NOTSFI"

```
C      NOTSFI, CALCULATES FISSION PRODUCT CONCENTRATIONS FOR REACTOR
C      OPERATING CONDITIONS OF CONSTANT PHI FOR A PERIOD ,TACC,
C      FOLLOWED BY A PERIOD ,TDEC, WNEN PHI=0, THEN REPEATS
         DIMENSION SIGFP(20),DLAM(20),Y25(20),Y49(20)
       COMMON SIG25,SIGF25,SIG40,SIG41,SIGF41,SIG42,SIG49,SIGF49,ALFA25,
      1ALFA49,ETA25,ETA49,ETA41,SIGFP,DLAM,Y25,Y49,NGP,NFP
C      COMMON AND DIMENSION STATEMENTS INCLUDE CONSTANTS FOR PU FISSION
       CALL CONST
1      READ 2
2      FORMAT(72H
      1                                    )
       READ 3, NGP,NFP,NRUN
3      FORMAT (3I3)
       READ 4, SIG25,SIGF25,PHI,SIGFP(4),SIGFP(5)
4      FORMAT (5E12.5)
       READ 5, CYCLES, TACC,TDEC,DELTA,DELTD,TIN
5      FORMAT(6E12.4)
       PRINT 2
       PRINT 6,NGP,NFP,NRUN
    6  FORMAT(19H0  NGP  NFP  NRUN  //(3I5))
       PRINT 14,SIG25,SIGF25,PHI,SIGFP(4),SIGFP(5)
   14  FORMAT(64H0   SIG25        SIGF25        PHI     SIGA CS-133 SIGA CS-
      1134      //(5E12.5))
       PRINT 7,CYCLES,TACC,TDEC,DELTA,DELTD,TIN
    7  FORMAT(72H0   CYCLES        TACC         TDEC        DELTA        DELT
      1D         TIN      //(6E12.4))
       CNUM =1.
       T=TIN
       TRES=TIN
       TAU=TIN
       PRINT 8
    8  FORMAT(32H0INTERMITTENT REACTOR OPERATION  // 95H TACC=ACCUM PERIO
      1D,TDEC=DECAY(PHI=0)PERIOD,TRES=TOTAL IN-PILE RESIDENCE TIME,TAU=BU
      2RNUP TIME       //)
       GO TO (9,100,200),NGP
9      FPA25Z=0.
10     PRINT 12
12     FORMAT(20H  ACCUMULATION STEP   //)
       PRINT 13
   13  FORMAT(120HC CNUM        T              TRES             TAU            T
      1AU1          FPA25Z          FA25          AFA25Z          AFA25    //
      2 )
       R1= (SIGF25*Y25(NFP)*PHI)/(DLAM(NFP)-SIG25*PHI)
C      ACCUMULATION STEP
20     TAU1=TACC*(CNUM-1.)
       W1= R1*EXPF(-SIG25*PHI*TAU1)
25     EX25=EXPF(-SIG25*PHI*T)
       EXA1= EXPF(-DLAM(NFP)*T)
       FA25=W1*(EX25-EXA1) +FPA25Z*EXA1
       AFA25=FA25*DLAM(NFP)
       PRINT 30,CNUM,T,TRES,TAU,TAU1,FPA25Z,FA25,AFA25Z,AFA25
30     FORMAT(F6.0,8E14.6)
       T=T+ DELTA
       TRES=TRES+DELTA
       TAU=TAU+DELTA
```

```
      IF (TACC-T) 40,35,35
   35 GO TO 25
C     DECAY STEP WITH PHI=0
40    T=0.
      TRES=TACC*CNUM + TDEC*(CNUM-1.)
       TAU=TACC*CNUM
      FPA25Z=FA25
      PRINT 45
45    FORMAT(21H DECAY STEP, PHI=0.     //)
44    PRINT 13
50    EXA1=EXPF(-DLAM(NFP)*T)
      FA25=FPA25Z*EXA1
      AFA25=FA25*DLAM(NFP)
      AFA25Z=FPA25Z*DLAM(NFP)
      PRINT 55, CNUM,T, TRES,TAU,TAU1,FPA25Z,FA25,AFA25Z,AFA25
55    FORMAT(F6.0,8E14.6)
      T=T+DELTD
      TRES=TRES+DELTD
      IF (TDEC-T) 65,60,60
60    GO TO 50
65    CNUM=CNUM+1.
      IF (CYCLES-CNUM) 67,68,68
67    GO TO 900
68    FPA25Z=FA25
      AFA25Z=FPA25Z*DLAM(NFP)
       TRES=(TACC+TDEC)*(CNUM-1.)
       TAU=TACC*(CNUM-1.)
      T=0.
      GO TO 10
C     GROUP 2 FISSION PRODUCT= CS-134
100   FPC25Z=0.
      FPD25Z=0.
      PRINT 8
120   TAU1=TACC*(CNUM-1.)
      R2= Y25(4)*SIGF25*EXPF(-SIG25*PHI*TAU1)/(SIGFP(4)
     1-SIG25)
      PRINT 12
      PRINT 130
130   FORMAT(60H CNUM,T,TRES,TAU,TAU1,FPC25Z,FC25,FPD25Z,FD25,AFD25Z,AFD
     125  //)
140   EX25=EXPF(-SIG25*PHI*T)
      EX33=EXPF(-SIGFP(4)*PHI*T)
      EX34= EXPF((-DLAM(5)-SIGFP(5)*PHI)*T)
      FC25=R2*(EX25-EX33) +FPC25Z
      Z2 =R2*SIGFP(4)*PHI
      W1= Z2/(DLAM(5)+(SIGFP(5)-SIGFP(4))*PHI)
      W2 = Z2/(DLAM(5)+(SIGFP(5)-SIG25)*PHI)
      W3 = FPC25Z*SIGFP(4)*PHI/(DLAM(5)+SIGFP(5)*PHI)
      FD25 =(W1-W2-W3 +FPD25Z)*EX34 +W2*EX25-W1*EX33 +W3
      AFD25Z=FPD25Z*DLAM(5)
      AFD25=FD25*DLAM(5)
      PRINT 150,CNUM,T,TRES,TAU,TAU1,FPC25Z,FC25,FPD25Z,FD25,
     1AFD25Z,AFD25
150   FORMAT(F6.0   ,8E14.6/2E14.6)
      T=T+DELTA
```

```
      TRES=TRES+DELTA
      TAU=TAU+DELTA
      IF (TACC-T) 160,155,155
155   GO TO 140
160   FPC25Z=FC25
      FPD25Z=FD25
      AFD25Z=FPD25Z*DLAM(5)
      T=0.
      TRES=TACC*CNUM+TDEC*(CNUM-1.)
      TAU=TACC*CNUM
      PRINT 45
      PRINT 175
175   FORMAT(60H CNUM,T,TRES,TAU,TAU1,FPC25Z,FC25,FPD25Z,FD25,AFD25Z
     1,AFD25    //)
180   FD25=FPD25Z*EXPF(-DLAM(5)*T)
      AFD25Z=FPD25Z*DLAM(5)
      AFD25=FD25*DLAM(5)
      PRINT 181,CNUM,T,TRES,TAU,TAU1,FPC25Z,FC25,FPD25Z,FD25,
     1AFD25Z,AFD25
181   FORMAT(F6.0,8E14.6/2E14.6)
      T=T+DELTD
      TRES=TRES+DELTD
      IF (TDEC-T) 190,185,185
185   GO TO 180
190   FPD25Z=FD25
      T=0.
      TRES=(TACC+TDEC)*CNUM
      TAU=TACC*CNUM
      CNUM=CNUM+1.
      IF (CYCLES-CNUM)191,192,192
191   GO TO 900
192   GO TO 120
C     GROUP 3 TYPE FISSION PRODUCT =NB-95
  200  FPA25Z=0.
      FPB25Z=0.
      PRINT 213
213   FORMAT(73H CNUM,T,TRES,TAU,TAU1,FPA25Z,FA25,AFA25Z,AFA25,FPB25Z
     1FB25,AFB25Z,AFB25  //)
210   PRINT 12
      TAU1=TACC*(CNUM-1.)
      R1= (SIGF25*Y25(1)*PHI)/(DLAM(1)-SIG25*PHI)
      W1= R1*EXPF(-SIG25*PHI*TAU1)
      CON1 =W1*DLAM(1)/(DLAM(2)-SIG25*PHI)
      CON2= (DLAM(1)*(FPA25Z-W1))/(DLAM(2)-DLAM(1))
220   EX25=EXPF(-SIG25*PHI*T)
      EXA1 =EXPF(-DLAM(1)*T)
      EXB2 =EXPF(-DLAM(2)*T)
      FB25=CON1*(EX25-EXB2) +CON2*(EXA1-EXB2)+FPB25Z*EXB2
      AFB25 =FB25*DLAM(2)
      AFB25Z=FPB25Z*DLAM(2)
      FA25=W1*(EX25-EXA1)+FPA25Z*EXA1
      AFA25=FA25*DLAM(1)
      AFA25Z=FPA25Z*DLAM(1)
      PRINT 230,CNUM,T,TRES,TAU,TAU1,FPA25Z,FA25,AFA25Z,AFA25,FPB25Z,
     1FB25,AFB25Z,AFB25
```

```
230   FORMAT(F6.0,8E14.6/4E14.6)
      T=T+DELTA
      TRES=TRES+DELTA
      TAU=TAU+DELTA
      IF (TACC-T)240,235,235
235   GO TO 220
240   FPB25Z=FB25
      FPA25Z=FA25
      AFB25Z=FPB25Z*DLAM(2)
      AFA25Z=FPA25Z*DLAM(1)
      TRES=TACC*CNUM+TDEC*(CNUM-1.)
      TAU=TACC*CNUM
      T=0.
      CON3=(DLAM(2)*FPA25Z)/(DLAM(2)-DLAM(1))
      PRINT 45
250   EXA1=EXPF(-DLAM(1)*T)
      EXB2=EXPF(-DLAM(2)*T)
      FA25=FPA25Z*EXA1
      FB25=CON3*(EXA1-EXB2)+FPB25Z*EXB2
      AFA25=FA25*DLAM(1)
      AFB25=FB25*DLAM(2)
      AFA25Z=FPA25Z*DLAM(1)
      AFB25Z=FPB25Z*DLAM(2)
      PRINT 230,CNUM,T,TRES,TAU,TAU1,FPA25Z,FA25,AFA25Z,AFA25,FPB25Z,
     1FB25,AFB25Z,AFB25
      T=T+DELTD
      TRES=TRES+DELTD
      IF(TDEC-T) 260,255,255
255   GO TO 250
260   CNUM=CNUM+1.
      T=0.
       TRES=(TACC+TDEC)*(CNUM-1.)
      TAU=TACC*(CNUM-1.)
      FPA25Z=FA25
      FPB25Z=FB25
      IF (CYCLES-CNUM) 900,270,270
270   GO TO 210
900     IF (NRUN) 901,905,901
901     GO TO 1
905     CALL EXIT
        END
```

TABLE G.4

SAMPLE INPUT DATA FOR "NOTSFI" (Cs^{134})

```
1 SAMPLE INPUT DATA FOR NOTSFI CODE, FOR CS-134
  2  5  0
 5.11900E-22 4.27450E-22 1.00000E 13 3.03000E-23 1.03890E-22
  1.5000E 02  3.4200E 05  2.6280E 05  3.4200E 05  2.6280E 05
```

APPENDIX H

FISSION PRODUCT ACTIVITIES AS A FUNCTION OF IRRADIATION TIME AT CONSTANT FLUX

Numerical values to the solutions of the equations expressing the variations in fission product activities with time at constant flux were obtained with the code NUCON and are presented graphically in this Appendix. The nuclear data used in these calculations, and those for intermittent reactor operation, were presented in Table 11. The calculation of the Cs^{133} and Cs^{134} absorption cross-sections will be outlined in detail because of the importance of these fission products to these investigations.

The Cs^{133} absorption cross-section used was 30.3 barns and was obtained from Eq. (H.1) (W6).

$$\bar{\sigma}^a = \sqrt{\frac{\pi T_o}{4T_n}}\,\hat{\sigma}^a \qquad \text{(H.1)}$$

$$= \sqrt{\frac{\pi T_o}{4T_n}}\,\sigma^a_{2200}(g+rs) \qquad \text{(H.2)}$$

where $\sqrt{\frac{\pi T_o}{4T_n}} = 0.7753$ (see Eq. D.26)

σ^a_{2200} = 29 barns (H3)

g = 1.00

r = 0.0715 (M3)

s = 4.887

Thus, $\bar{\sigma}^a = (0.7753)(29)[1.00 + (0.0715)(4.887)] = 30.3$ barns.

The value of the factor "s" was calculated from Eq. (H.3) (W6)

$$s = \sqrt{\frac{4T_n}{\pi T_o}}\ \frac{I_{eff}}{\sigma_{2200}} - bg \qquad (H.3)$$

where I_{eff} = effective resonance integral, barns

= 230.4 barns

b = 1.176 (W6)

σ_{2200} = total cross-section for 2200 m/sec neutrons, barns

$= \sigma^a + \sigma^s$

where σ^s = scattering cross-section, barns

= 20 barns (E5)

Thus, σ_{2200} = 49 barns.

The effective resonance integral for Cs^{133} in MITR fuel of 230.4 barns was estimated from a measured value for the infinite dilution resonance integral in the following way: The effective resonance integral of U^{238}, if it were present in the MITR fuel, was calculated from Eq. (H.4) (W4)

$$I_{eff} = \left[2.8 + 25\left(\frac{S}{M}\right)^{1/2}\right] \text{barns} \qquad (H.4)$$

where S = effective surface area of fuel plate, cm^2

M = mass of fuel per plate, gm.

Since the fuel elements are closely spaced, it was assumed that on the average, the effective surface area was equal to one-half of the total fuel plate area. Thus

$$S = 367.1 \text{ cm}^2$$

and $$I_{eff}(U^{238}) = 143.3 \text{ barns}$$

The infinite dilution resonance integral of U^{238} is

$$RI(\infty)(U^{238}) = 280 \text{ barns (W4)}$$

Then

$$\frac{I_{eff}(U^{238})}{RI(\infty)(U^{238})} = 0.512 \qquad \text{(H.5)}$$

It was then assumed that I_{eff} for Cs^{133} would be the same fraction of its $RI(\infty)$ as that obtained for U^{238} in Eq. (H.5). That is

$$I_{eff}(Cs^{133}) = 0.512\ RI(\infty)(Cs^{133})$$

where $RI(\infty)(Cs^{133}) = 450$ barns (V1).

Thus, $I_{eff}(Cs^{133}) = 230.4$ barns.

The value of the Cs^{134} absorption cross-section used was 103.89 barns and was calculated from (H.1) where

$$\hat{\sigma}^{a}(Cs^{134}) = 134 \text{ barns (B9)}$$

The solutions to Eq. (D.5) were obtained for Zr^{95}, shown in Fig. H.1, Ru^{106}, shown in Fig. H.2 and Cs^{137}, shown in Fig. H.4. The solutions to Eq. (D.12) were obtained for Nb^{95}, shown also in Fig. H.1 and for Pr^{144}, shown in Fig. H.6. The Cs^{134} solutions for Eq. (D.18) are shown in Fig. H.3.

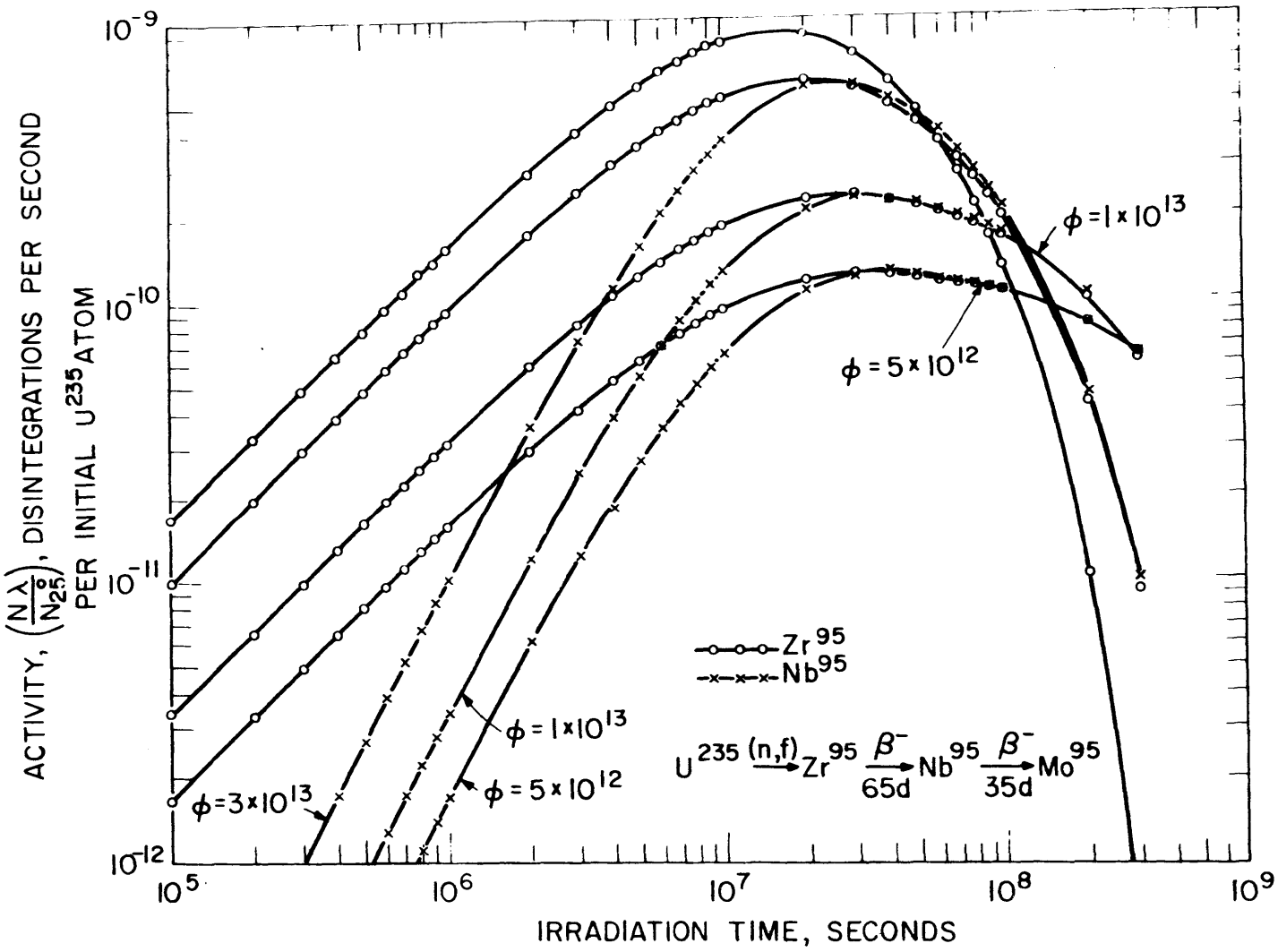

FIGURE H.1 Zr^{95} AND Nb^{95} ACTIVITIES PER INITIAL U^{235} ATOM AT CONSTANT FLUX vs. EXPOSURE TIME

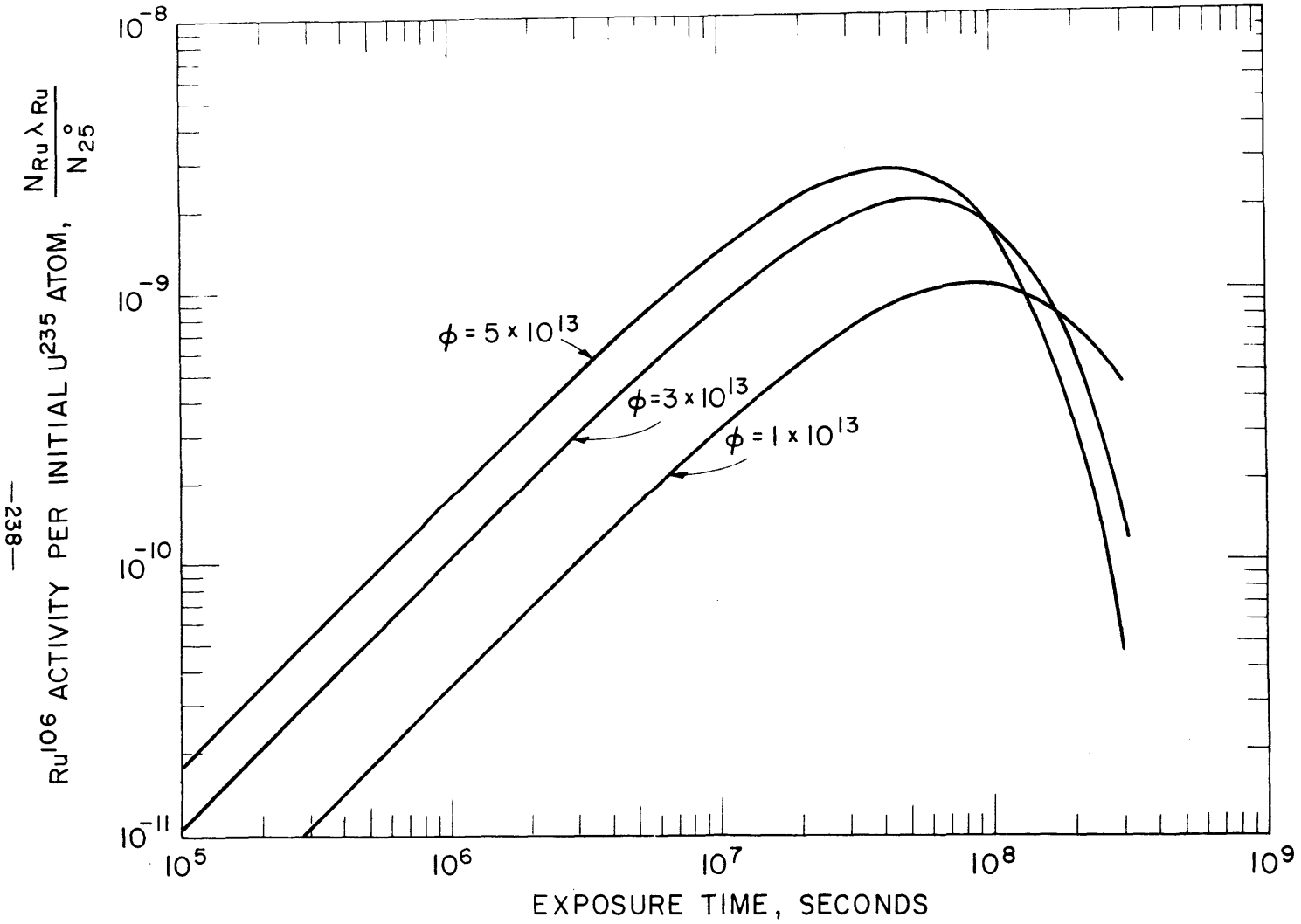

FIGURE H.2 Ru^{106} ACTIVITY PER INITIAL U^{235} ATOM AT CONSTANT FLUX vs. EXPOSURE TIME

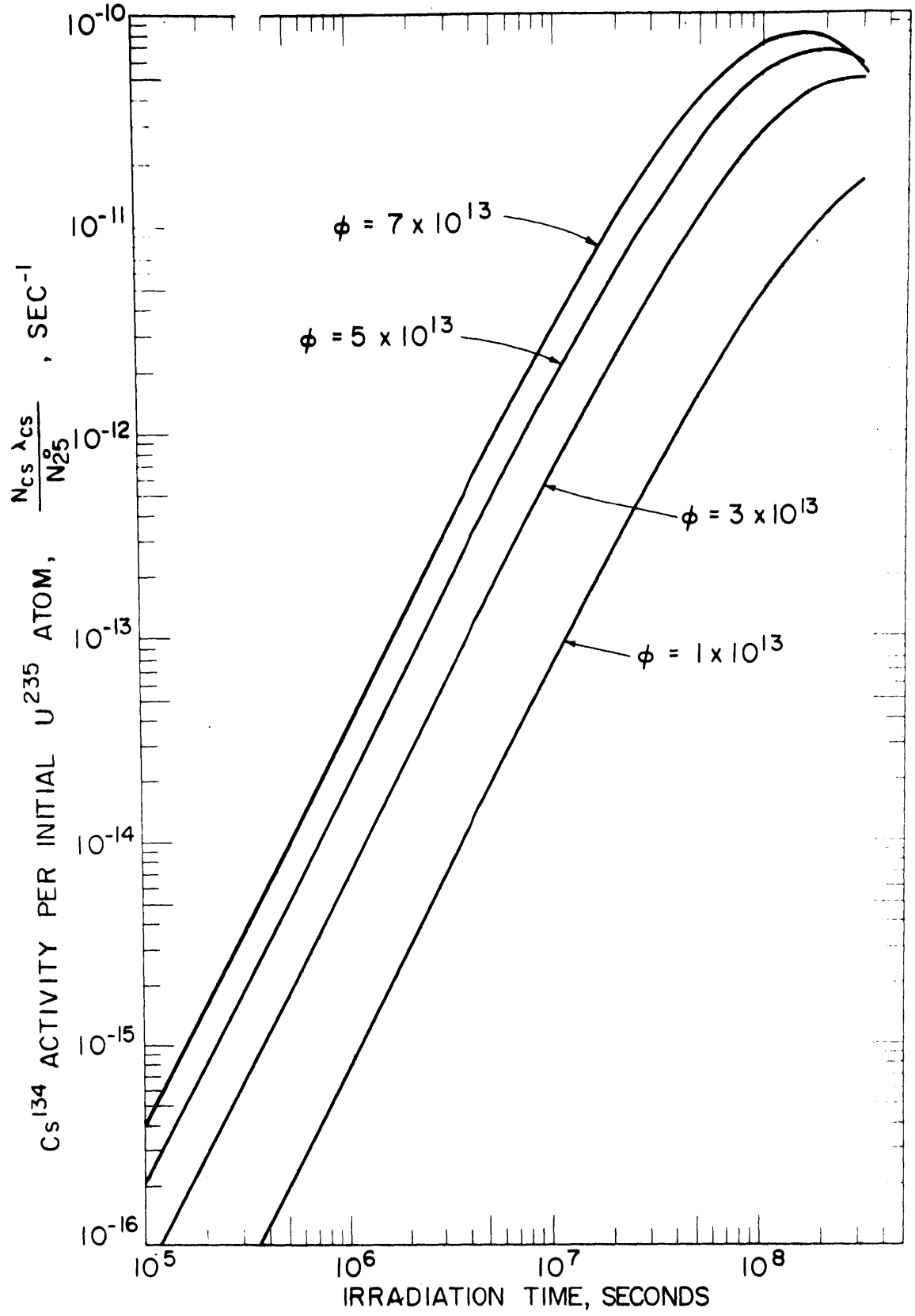

FIGURE H.3 Cs^{134} ACTIVITY PER INITIAL U^{235} ATOM VS. IRRADIATION TIME

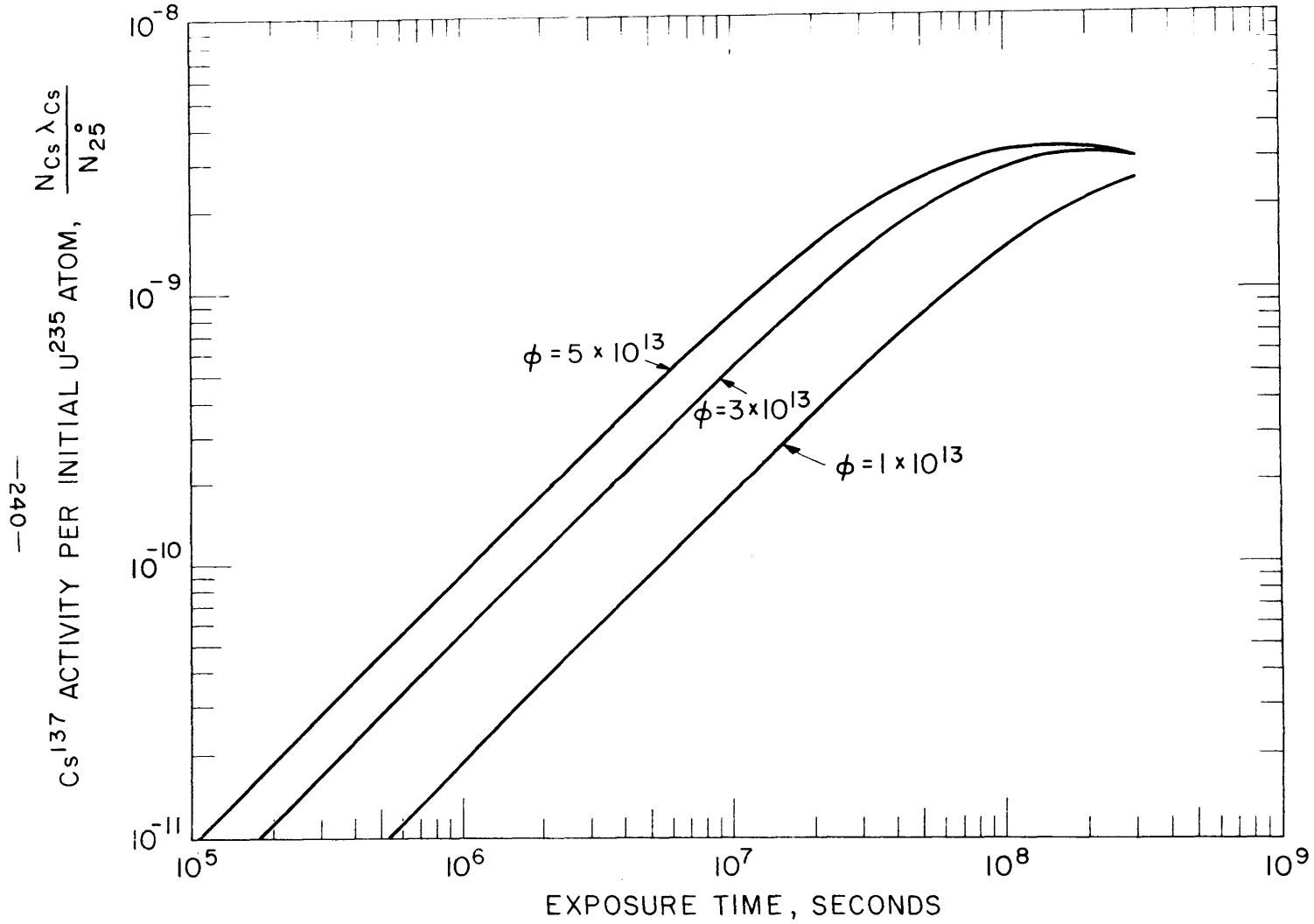

FIGURE H.4 Cs^{137} ACTIVITY PER INITIAL U^{235} ATOM vs. EXPOSURE TIME FOR VARIOUS FLUXES AT CONSTANT FLUX LEVEL

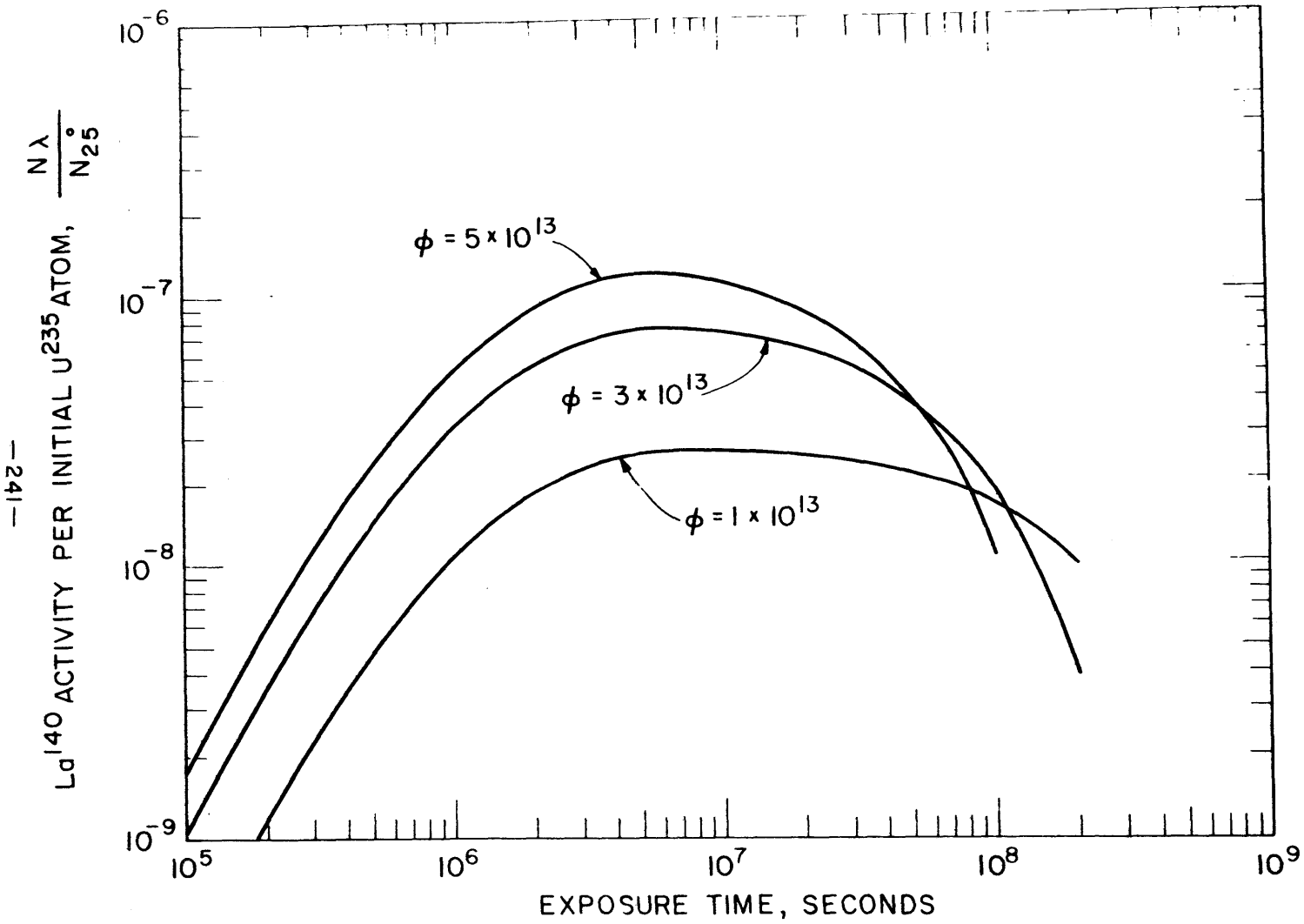

FIGURE H.5 La^{140} ACTIVITY PER INITIAL U^{235} ATOM AT CONSTANT FLUX FOR VARIOUS FLUXES vs. EXPOSURE TIME

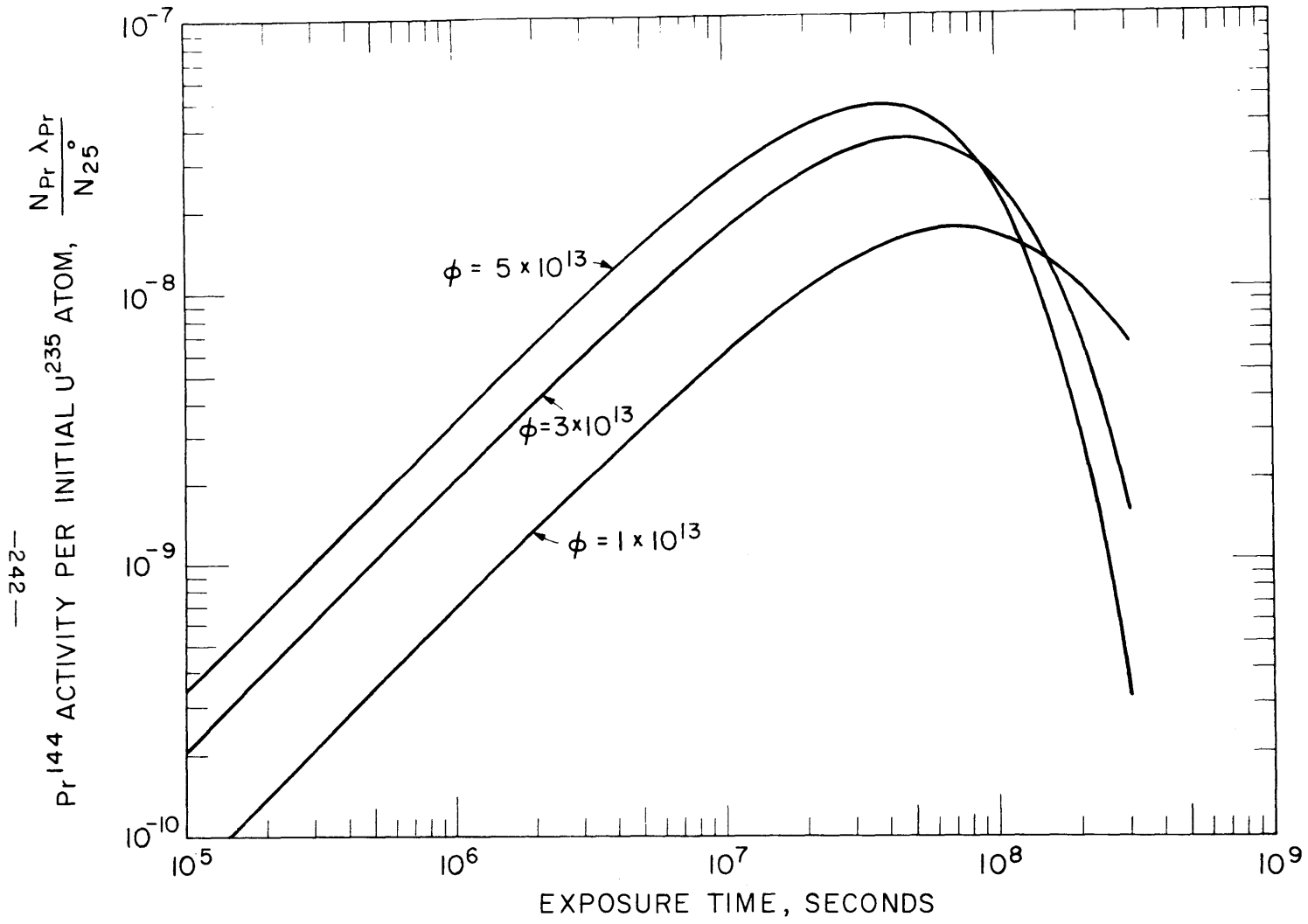

FIGURE H.6 Pr^{144} ACTIVITY PER INITIAL U^{235} ATOM AT CONSTANT FLUX FOR VARIOUS FLUXES vs. EXPOSURE TIME

APPENDIX I

REFERENCES

B1. N.A. Baily, R.J. Grainger and J.W. Mayer, "Capabilities of Lithium Drifted p-i-n Junction Detectors when used for Gamma-Ray Spectroscopy", Rev. Sci. Instr., 32, 865 (1961).

B2. M.L. Batch, R.M. Ball, R.H. Lewis and R.H. Freyberg, Jr. (Cons. Ed.), "Mid-Life Power Distribution in the Indian Point Reactor", Trans. Am. Nuclear Soc., 7, 494 (Nov., 1964).

B3. F.J. Biode, Ed., "Transistor Technology", D. Van Nostrand Co. Inc., Princeton, J.J., Vols. 2 and 3 (1958).

B4. J.L. Blankenship and C.J. Borkowski, IRE Trans. Nuclear Sci., NS-9, 181 (1962).

B5. J.O. Blomeke and M.F. Todd, "Uranium-235 Fission Product Production as a Function of Thermal Neutron Flux, Irradiation Time and Decay Time, 1, Atomic Concentrations and Gross Totals", ORNL-2127 (Nov.,1958).

B6. L.B. Borst, "Estimates of Amount of Radiation and of Accompanying Energy Liberation from Fission Products", Paper 34 in Radiochemical Studies: The Fission Products, NNES, vol IV-9, Book 1, p.344, McGraw-Hill, New York (1951).

B7. J.L. Buckner, "Effective Fission Product Absorption Cross Sections", M.Sc. Thesis, MIT Dept. of Nuclear Eng. (Sept., 1960).

B8. A. Brenner, "Electroplating Comes of Age", Metal Finishing, 52 (11), 68 (1954).

B9. J.G. Bayly, F. Brown, G.R. Hall, and A.J. Walter, J. Inorg. and Nuc. Chem., 5, 259 (1958).

B10. R.M Ball, et. al., "Indian Point Reactor Core "A" Gamma-Scan Results", BAW-1295 (July, 1964).

B11. R.A. Brown and G.T. Ewan, "Study of the Decay of Cs^{134} with a High Resolution Ge(Li) Gamma-Ray Spectrometer", Nucl. Phys., 68, 325-36 (June, 1965).

B12. M. Benedict and T.H. Pigford, "Nuclear Chemical Engineering", McGraw-Hill Book Co., Inc., New York (1957).

B13. S.T. Brewer, MIT Dept. of Nuclear Eng., Course 22.42 Project. Private Communication.

C1. F.H. Clark, "Decay of Fission Product Gammas", NDA-27-39, (Dec., 1954).

D1. G. Dearnaley and D.C. Northrop, "Semiconductor Counters for Nuclear Radiations", J. Wiley, Inc., (1963).

D2. W.R. Diggle and W.H. Blackadder, "Gamma Scanning for Burnup", Nucleonics 23, 71 (March, 1965).

D3. "Douglas Point Nuclear Generating Station", Atomic Energy of Canada Ltd., AECL 1596 (1962).

E1. M.C. Edlund, et. al., "Determination of Power Distribution in the CETR by Measurement of La-140 Activity", BAW-164, Lynchburg, Va., (Sept., 1961).

E2. J.H. Elliot, Nuclear Instr. Meth. 12, 60 (1961).

E3. T.R. England, "Time-dependent Fission Product Thermal and Resonance Absorption Cross-Sections", WAPD-TM-333 (Jan., 1965).

E4. L.R. Enstice, Jr., "Heat Transfer Study of an MIT Reactor Partial Plate Fuel Element", MIT Dept. of Nuclear Eng., S.M. Thesis (June 1965).

E5. H. Etherington, Ed., "Nuclear Engineering Handbook", McGraw Hill, New York (1958).

F1. I.L. Faller, T.S. Chapman, and J.M. West, "Calculations on U-235 Fission Product Decay Chains", ANL-4807 (May, 1952).

F2. H.J. Fiedler, L.B. Hughes, T.J. Kennet, W.V. Prestwich, and B.J. Hall, "Large Volume Lithium Drifted Germanium Gamma-Ray Detectors", Report, McMaster University, Hamilton, Ontario (June, 1965).

F3. D.V. Freck and J. Wakefield, Nature 193, 669 (1962).

G1. F.S. Goulding and W.L. Hansen, "Automatic Lithium Drifting Apparatus for Silicon and Germanium Detectors", Univ. of California,Lawrence Radiation Lab. Report UCRL-11261 (Feb., 1964).

G2. L.V. Groshev and A.M. Demidov, "Determination of Fuel Element Burn-up using a Magnetic Gamma-Spectrometer", IAEA Translation 63-0051 (1962).

H1. N.B. Hannay, Ed., "Semiconductors", Reinhold, New York (1959).

H2. W.L. Hansen and B.V. Jarrett, "Techniques for the Fabrication of Lithium Drifted Germanium Detectors", UCRL-11589 (Aug.,1964).

H3. D.J. Hughes and J.A. Harvey, "Neutron Cross-Sections", BNL-325.

H4. H.F. Hunter and N.E. Ballow, Nucleonics 9 (5), C2-7 (1951).

I1. IRE Transactions on Nuclear Science, Proceedings of the Seventh Annual National Meeting "Solid State Radiation Detectors", Oct. 3-5, 1960, NS-8, (Jan. 1961).

K1. A.H. Kazi, N.C. Rasmussen, and H. Mark, "Six-Meter Radius Bent-Crystal Spectrograph for Nuclear Gamma-Rays", Rev. Sci. Instr. 31, 983-87 (Sept., 1960).

K2. C. Kittel, "Introduction to Solid State Physics", J. Wiley and Sons, Inc., New York (1956).

K3. L. Koch, J. Messier, and J. Valin, "N-I-P Silicon Junction Detectors", IRE Trans. Nuclear Sci. NS-8, 43 (Jan., 1961).

K4. H.W. Kraner, J.A. Sovka and R.W. Breckenridge, Jr., "An Efficient Dewar for Lithium-Drifted Germanium Detectors". To be published in Nuclear Instr. Methods.

K5. P. Kristiansen and T. Rø̸geberg, "Non-Destructive Analysis of Irradiated Fuel Elements", Final Report, Research Contract No. 47 between IAEA and IFA, Kjeller, Norway, (1962).

L1. C.J.L. Lock, "Fission Product Formation in a Homogeneous Power Reactor", AERE-C/R-1715 (June, 1955).

L2. D.D. Lanning, I. Kaplan, and F.M. Klikeman (Ed.), "Heavy Water Lattice Project Annual Report", MITNE-60 (Sept., 1964).

M1. H.M. Mann, J.W. Haslett, and F.J. Janarek, IRE Trans. Nuclear Sci. NS-9, 43 (1962).

M2. J.W. Mayer, N.A. Baily, and H.L. Dunlap, IAEA Conference on Nuclear Electronics, Belgrade, Jugoslavia (May, 1961).

M3. S.A. Mayman, "Fuel Burnup in the MITR", M.Sc. Thesis, MIT Dept. of Nuclear Eng. (June, 1964).

M4. R.L. Mathews, "Flux Distributions in the MIT Reactor", Ph.D. Thesis, MIT Dept. of Nuclear Eng. (Aug. 1964).

M5. K.G. McKay, (a) "A Germanium Counter", Phys. Rev. 76, 1537 (Nov., 1949).
(b) "Electron-hole Production in Germanium by Alpha Particles", Phys. Rev. 84, 829 (Nov. 1951).

M6. G.L. Miller, W.M. Gibson, and P.F. Donovan, "Semiconductor Particle Detectors", Ann. Rev. Nuclear Sci. 12, 189 (1962).

M7. G.L. Miller, B.D. Pate, and S. Wagner, "Production of Thick Semiconductor Radiation Detectors by Lithium Drifting", IEEE Trans. Nuclear Sci., NS-10, 220 (Jan., 1963).

M8. J. Moteff, "Fission Product Decay Gamma Energy Spectrum", APEX-134 (1953).

M9. D.A. Marsden and L. Yaffe, "Mass Distribution in Thermal Neutron Fission of Pu-239", Can. J. Chem. 43, 249-67 (Jan. 1965).

M10. G.L. Miller, W.L. Brown, P.F. Donovan, and I.M. Mackintosh, "Silicon p-n Junction Radiation Detectors", IRE Trans. Nuclear Sci. NS-7, 185 (1960).

N1. R.J. Nodvik, "Evaluation of Gamma Scanning as a Tool for Determining Fuel-Burnup Distributions in Large Power-Reactor Cores", Trans. Am. Nuclear Soc. 8, 103 (June, 1965).

O1. G.D. O'Kelley, Ed., "Applications of Computers to Nuclear and Radiochemistry", Proc. of Symposium, Gatlinburg, Tenn. Oct. 17-19, 1962, NAS-NS 3107.

P1. E.M. Pell, (a) "Ion Drift in an n-p Junction", J. Appl. Phys. 31, 291 (1960).
(b) "Effect of Li-B Ion Pairing on Li^+ Ion Drift in Si", J. Appl. Phys. 31, 1675 (1960).
(c) "Semiconductor Nuclear Particle Detectors", National Academy of Sciences Report NAS-NSS 32, Publication 871, p.136 (1961).

R1. N.C. Rasmussen and M.D. Cohan, "Analysis of Radiations from Spent Fuel Elements using a Bent-Crystal Spectrograph", Trans. Am. Nuclear Soc. 5, 24 (June, 1962).

R2. N.C. Rasmussen, J.A. Sovka, and S.A. Mayman, "The Non-destructive Measurement of Burnup by Gamma-Ray Spectroscopy", Paper SM-67/45, presented at IAEA Conference on Management of Nuclear Materials, Vienna, Austria, Aug. 30-Sept. 3, 1965.

S1. J.B. Sampson, et. al., "Poisoning in Thermal Reactors due to Stable Fission Products", KAPL-1226 (Oct., 1954).

S2. R.A. Smith, (a) "Semiconductors", Cambridge University Press (1961)
(b) "Wave Mechanics of Crystalline Solids", Chapman and Hall (1961).

S3. M.V. Sullivan and J.H. Eigler, "Electroless Nickel Plating for Making Ohmic Contacts to Silicon", J. Electrochem. Soc. 104, 226 (1957).

S4. W.E. Shoupp, R.D. Coe, and W.C. Woodman, "The Yankee Atomic Electric Plant", PUAE UN Conference, P-1038, 8, 492 (1958).

T1. A.J. Tavendale, Electronique Nucleaire (O.E.C.D., Paris), 235 (1963).

T2. A.J. Tavendale and G.T. Ewan, Nuclear Instr. Methods 26, 183 (1963).

T3. G.T. Ewan and A.J. Tavendale, "High Resolution Studies of Gamma-Ray Spectra using Lithium-Drift Germanium Gamma-Ray Spectrometers", Can. J. Phys. 42, 2286 (Nov., 1964).

T4. J.M. Taylor, "Semiconductor Particle Detectors", Butterworths, Inc., (1963).

U1. S. Untermeyer and J.T. Weills, "Heat Generation in Irradiated Uranium", AECD-3454 (Feb., 1952).

V1. R. Vidal, "Mesure des Integrales de Resonance d'Absorption", CEA-R-2486 (July, 1964).

W1. W.H. Walker, "Fission Product Poisoning", CRPP-626 (Jan., 1956); "Yields and Effective Cross-Sections of Fission Products and Pseudo-Fission Products", CRRP-913 (AECL 1054), (March, 1960); "Fission Product Poisoning from the Fast Fission of U-238", CRRP-1090 (AECL-1537), (June, 1962); "The Effect of New Data on Reactor Poisoning by Non-Saturating Fission Products", AECL 2111, (Nov., 1964).

W2. K. Way and E.P. Wigner, "Rate of Decay of Fission Products", Paper 43 in "Radiochemical Studies: The Fission Products", NNES, Vol. LV-9, Book 1, p.436, McGraw-Hill, New York (1951); Phys. Rev. 70, 115 (1946); Phys. Rev. 73, 1318 (1948).

W3. P.P. Webb and R.L. Williams, Nuclear Instr. Methods 22, 361 (1963).

W4. A.M. Weinberg and E.P. Wigner, "The Physical Theory of Neutron Chain Reactors", Eq. (19.3) p.661, University of Chicago Press (1958).

W.5 P. Weinzierl, et al, "Burn-up Determination of Nuclear Fuel by High Resolution Gamma-Spectroscopy", UN Conference Paper A/CONF.28/P/399 (May, 1964).

W6. C.H. Westcott, "Effective Cross-section Values for Well Moderated Thermal Reactor Spectra", 3rd Edition, AECL 1101 (July, 1962).

Security Classification

DOCUMENT CONTROL DATA - R&D

(Security classification of title, body of abstract and indexing annotation must be entered when the overall report is classified)

1. ORIGINATING ACTIVITY *(Corporate author)* Massachusetts Institute of Technology 77 Massachusetts Avenue Cambridge, Massachusetts	2a. REPORT SECURITY CLASSIFICATION unclassifed 2b. GROUP

3. REPORT TITLE
Nondestructive Analyses of Irradiated MITR Fuel by Gamma-Ray Spectroscopy

4. DESCRIPTIVE NOTES *(Type of report and inclusive dates)*
Scientific Report Interim

5. AUTHOR(S) *(Last name, first name, initial)*
Sovka, Jerry A.
Rasmussen, Norman C.

6. REPORT DATE October 1965	7a. TOTAL NO. OF PAGES 248	7b. NO. OF REFS 70
8a. CONTRACT OR GRANT NO. AF19(604)-7492 b. PROJECT AND TASK NO. 5620-02 c. DOD ELEMENT 61445014 d. DOD SUBELEMENT 681301	9a. ORIGINATOR'S REPORT NUMBER(S) MITNE-64 9b. OTHER REPORT NO(S) *(Any other numbers that may be assigned this report)*	

10. AVAILABILITY/LIMITATION NOTICES Qualified requestors may obtain copies of this report from DDC. Other persons or organizations should apply to the Clearinghouse for Federal Scientific and Technical Information (CFSTI), Sills Building, 5285 Port Royal Road, Springfield, Virginia 22151.

11. SUPPLEMENTARY NOTES	12. SPONSORING MILITARY ACTIVITY Hq. AFCRL, OAR (CRW) United States Air Force L.G.Hanscom Field,Bedford,Mass

13. ABSTRACT

Lithium drifted Ge solid state γ ray detectors have been developed and applied to the problem of nondestructive analysis of spent reactor fuel. The energy resolution of the detector was better than 1% (FWHM) in the 600 to 800 keV range and made possible the identification of γ rays from Co-134, Cs-137, Rh-106, Nb-95, and Zr-95 in this energy region. Ratios of intensities of these γ rays were used to determine average flux and irradiation time of the fuel. The burnup was then calculated. Results of these measurements agreed with other independent measurements well within the 10% error assigned. The technique developed provides a useful method for determining the irradiation history of spent reactor fuel that has been operated at low enough temperatures so that fission product migration has not taken place.

DD FORM 1 JAN 64 1473

Security Classification

Security Classification

14. KEY WORDS	LINK A		LINK B		LINK C	
	ROLE	WT	ROLE	WT	ROLE	WT
Gamma ray spectroscopy						
Burnup						
Nondestructive Analysis						
Spent reactor fuel						

INSTRUCTIONS

1. ORIGINATING ACTIVITY: Enter the name and address of the contractor, subcontractor, grantee, Department of Defense activity or other organization *(corporate author)* issuing the report.

2*a*. REPORT SECURITY CLASSIFICATION: Enter the overall security classification of the report. Indicate whether "Restricted Data" is included. Marking is to be in accordance with appropriate security regulations.

2*b*. GROUP: Automatic downgrading is specified in DoD Directive 5200.10 and Armed Forces Industrial Manual. Enter the group number. Also, when applicable, show that optional markings have been used for Group 3 and Group 4 as authorized.

3. REPORT TITLE: Enter the complete report title in all capital letters. Titles in all cases should be unclassified. If a meaningful title cannot be selected without classification, show title classification in all capitals in parenthesis immediately following the title.

4. DESCRIPTIVE NOTES: If appropriate, enter the type of report, e.g., interim, progress, summary, annual, or final. Give the inclusive dates when a specific reporting period is covered.

5. AUTHOR(S): Enter the name(s) of author(s) as shown on or in the report. Enter last name, first name, middle initial. If military, show rank and branch of service. The name of the principal author is an absolute minimum requirement.

6. REPORT DATE: Enter the date of the report as day, month, year, or month, year. If more than one date appears on the report, use date of publication.

7*a*. TOTAL NUMBER OF PAGES: The total page count should follow normal pagination procedures, i.e., enter the number of pages containing information.

7*b*. NUMBER OF REFERENCES: Enter the total number of references cited in the report.

8*a*. CONTRACT OR GRANT NUMBER: If appropriate, enter the applicable number of the contract or grant under which the report was written.

8*b*, 8*c*, & 8*d*. PROJECT NUMBER: Enter the appropriate military department identification, such as project number, subproject number, system numbers, task number, etc.

9*a*. ORIGINATOR'S REPORT NUMBER(S): Enter the official report number by which the document will be identified and controlled by the originating activity. This number must be unique to this report.

9*b*. OTHER REPORT NUMBER(S): If the report has been assigned any other report numbers *(either by the originator or by the sponsor)*, also enter this number(s).

10. AVAILABILITY/LIMITATION NOTICES: Enter any limitations on further dissemination of the report, other than those imposed by security classification, using standard statements such as:

(1) "Qualified requesters may obtain copies of this report from DDC."

(2) "Foreign announcement and dissemination of this report by DDC is not authorized."

(3) "U. S. Government agencies may obtain copies of this report directly from DDC. Other qualified DDC users shall request through

_____."

(4) "U. S. military agencies may obtain copies of this report directly from DDC. Other qualified users shall request through

_____."

(5) "All distribution of this report is controlled. Qualified DDC users shall request through

_____."

If the report has been furnished to the Office of Technical Services, Department of Commerce, for sale to the public, indicate this fact and enter the price, if known.

11. SUPPLEMENTARY NOTES: Use for additional explanatory notes.

12. SPONSORING MILITARY ACTIVITY: Enter the name of the departmental project office or laboratory sponsoring *(paying for)* the research and development. Include address.

13. ABSTRACT: Enter an abstract giving a brief and factual summary of the document indicative of the report, even though it may also appear elsewhere in the body of the technical report. If additional space is required, a continuation sheet shall be attached.

It is highly desirable that the abstract of classified reports be unclassified. Each paragraph of the abstract shall end with an indication of the military security classification of the information in the paragraph, represented as *(TS), (S), (C), or (U).*

There is no limitation on the length of the abstract. However, the suggested length is from 150 to 225 words.

14. KEY WORDS: Key words are technically meaningful terms or short phrases that characterize a report and may be used as index entries for cataloging the report. Key words must be selected so that no security classification is required. Identifiers, such as equipment model designation, trade name, military project code name, geographic location, may be used as key words but will be followed by an indication of technical context. The assignment of links, rules, and weights is optional.

Security Classification